



**University of
Reading**

On Predicting the Opening of Arctic Sea Routes

A thesis submitted in part fulfilment of the degree of
Doctor of Philosophy

Nathanael Melia

Department of Meteorology

Supervised by: Professor K. Haines & Dr E. Hawkins

June 2016

Declaration

I confirm that this is my own work and the use of all material from other sources has been properly and fully acknowledged.

N. Melia

Nathanael Melia

Publications

Parts of the work in Chapter 4 of this thesis has appeared in Melia et al. (2015).

Melia, N., Haines, K., and Hawkins, E.: Improved Arctic sea ice thickness projections using bias-corrected CMIP5 simulations, *Cryosphere*, 9, 2237-2251, doi: 10.5194/tc-9-2237-2015, 2015.

Parts of the work in Chapter 6 of this thesis have been submitted as a publication.

Acknowledgements

First, I need to thank my supervisors, Ed Hawkins and Keith Haines for their patience, enthusiasm, support, and guidance. I really appreciate being treated as a colleague throughout my PhD, the confidence they both placed in me has led to the work you see before you. Ed, I blame you for the unhealthy obsession I now have with climate variability and creating nice data visualisations. I also have you to thank for the friends I have made through jetting around the world to conferences, meetings, and time spent on twitter! Keith, your wisdom has been invaluable over the course of my PhD, your knowledge and enthusiasm has been key to the work I have produced. I would also like to thank my Monitoring Committee, Ellie Highwood, and Danny Feltham. If it was not for Ellie's wisdom this PhD may have taken a while longer, if it was not for Danny's knowledge and robust questioning on all things sea ice I would not be aware of half of the sea ice processes that I am now. Thank you to Ross Reynolds and Keith Shine for support and dissertation supervision during my BSc and MSc degrees. Thank you also to Vikki Thompson for all the useful discussions on our PhD's, and for the hours I spent in gym classes.

In Chapter order, thank you Jon Robson and Dan Hodson for moving the HadGEM2-ES ensemble to Reading and providing formatting tools, used in Chapter 3. Thank you to Steffen Tietsche for the conversion of the PIOMAS data. Thanks to referees Gregory Flato and Francois Massonnet, and editor Julienne Stroeve for their quick and constructive suggestions for the paper presented in Chapter 4. Thanks to Robert Darby and the University of Reading Research Data Archive for hosting the MAVRIC data set. Thanks to Jonny Day and Steffen Tietsche for useful discussions on the work conducted in Chapter 7.

I wish to thank my parents for always believing in me and providing support through my PhD. Without my long-suffering wife Kelly, I would never have achieved many of the things I have in my life, let alone this thesis. Great credit goes to my PhD prayer group for their continued prayer, support, and friendship.

Principally, all glory to Jesus Christ: "For with God, nothing shall be impossible." (Luke 1:37, KJV).

Abstract

Satellite observations have revealed that the Arctic is undergoing rapid climate change. Climate model projections unanimously simulate that year-round reductions in Arctic sea ice will continue through the 21st century. The primary goal of this thesis is to investigate the implications of these changes for trans-Arctic shipping. Arctic routes offer a substantial distance saving over conventional routes, with potentially significant global economic implications. Shipping in Arctic waters is a hazardous endeavour and increases in shipping traffic heighten the need for robust projections of future shipping accessibility to assess the risks involved.

However, all global climate model (GCM) simulations contain intrinsic biases in their simulation of sea ice. This thesis has produced a calibration technique to constrain and reduce these biases. Applying this approach to a suite of state of the art GCMs reveals that the Arctic may become “ice-free” in the 2050s, a decade earlier than without the calibration technique. Projections of Arctic shipping are also made using data from these calibrated climate models, likely adding to their robustness. Using the calibrated multi-model ensemble reveals that, by mid-century, Arctic transit potential doubles for standard ‘open water’ vessels; most years become navigable for some period, irrespective of future emissions scenario, with the currently inaccessible Trans-polar Sea Route across the central Arctic becoming accessible for the first time. European routes to East Asia become 10 days faster on average than alternatives by mid-century, and 13 days faster by late-century, while North American routes become 4 days faster. Future greenhouse-gas emissions play a significant role by late-century; the shipping season reaching 8 months in RCP8.5, double that of RCP2.6 which exhibits substantial interannual variability. Moderately ice-strengthened vessels would enable fast and reliable trans-Arctic shipping, essentially year round, from mid-century.

Climate model projections reveal that sea ice will be present throughout the 21st century winter, regardless of future greenhouse gas emissions. This implies that Arctic sea routes will continue to open and close annually. This, combined with increased shipping in the region, highlights the need for improved seasonal predictions of conditions on the Arctic sea routes. The upper lead-time limit of predictability of the opening of Arctic sea routes is explored using ensembles of simulations in a ‘perfect model’ approach. Initial results indicate the skill of forecasts drops dramatically before May, indicating the presence of a predictability barrier.

Contents

Chapter 1 Introduction.....	1
1.1 Arctic sea ice decline: motivation for research	2
1.2 On the use of Global Climate Models (GCMs).....	5
1.3 Thesis aims.....	7
1.4 Thesis structure	8
References	11
Chapter 2 Scientific background.....	13
Summary.....	14
2.1 Arctic climate change.....	15
2.1.1 Sea ice lifecycle	15
2.1.2 Sea ice concentration (SIC)	17
2.1.3 Sea ice thickness (SIT) and volume (SIV).....	19
2.1.4 Uncertainty in sea ice observations	20
2.1.5 Seasonal cycle of Arctic sea ice.....	21
2.1.6 Historic Arctic sea ice observations.....	22
2.1.7 Trends	23
2.1.8 Future sea ice evolution	25
2.2 Climate model simulations of the Arctic	26
2.2.1 Advantages of modelling the climate	26
2.2.2 Modelling sea ice.....	27
2.2.3 GCM performance in simulating Arctic sea ice	28
2.2.4 Using GCMs to attribute changes to Arctic sea ice	30
2.2.5 Representative Concentration Pathways (RCP).....	30
2.2.6 Sea ice projections	31
2.3 Studies of future shipping.....	35
2.3.1 Economic feasibility	35

2.3.2 Future climatic viability for trans-Arctic shipping.....	36
2.3.3 Effects on the climate system.....	43
2.4 Discussion.....	45
References	47
Chapter 3 The Arctic early 20 th century warming.....	56
Summary.....	57
3.1 Past change	58
3.1.1 Past changes to Arctic Sea ice.....	59
3.2 Attribution of the Arctic early 20 th century warming	61
3.2.1 Internal variability	62
3.2.2 All forcings simulations.....	62
3.2.3 Natural only simulations.....	66
3.2.4 Greenhouse gas only simulations.....	67
3.2.5 Additional forcings.....	68
3.3 Fixed aerosol experiments	71
3.4 Spatial changes	74
3.4.1 Sea ice concentration.....	74
3.4.2 Sea ice thickness.....	77
3.4.3 Summary.....	80
3.5 Conclusions	82
References	83
Chapter 4 Improved Arctic sea ice thickness projections using bias corrected CMIP5 simulations	88
Summary.....	89
4.1 Introduction.....	90
4.2 Climate simulations and observations	92
4.2.1 PIOMAS.....	92
4.2.2 Global climate models.....	94

4.3 Bias correction methodology	97
4.3.1 Additive correction.....	99
4.3.2 Multiplicative correction	99
4.3.3 Mean multiplicative correction	99
4.3.4 Mean and variance correction	100
4.4 Bias-corrected sea ice thickness projections.....	102
4.4.1 MAVRIC validation	102
4.4.2 Temporal perspective example.....	105
4.4.3 Historical spatial perspective.....	106
4.4.4 CMIP5 subset multi-model sea ice thickness projections.....	107
4.4.5 Sources of uncertainty in projections of sea ice thickness.....	109
4.4.6 Further MAVRIC performance analysis.....	113
4.4.7 Reduced spread in timing of ice-free conditions	115
4.5 Summary and discussion	118
4.5.1 Summary.....	118
4.5.2 Discussion	118
References	121
Chapter 5 Arctic shipping background	126
5.1 Northern Sea Route	127
5.2 North West Passage.....	130
5.3 Maritime operations.....	132
5.3.1 Ships	132
5.3.2 Supplementary costs	133
5.4 Recent trends	134
References	139
Chapter 6 Faster 21 st century shipping using trans-Arctic routes	140
Summary.....	141
6.1 Introduction.....	142

6.2 Methods	144
6.2.1 GCM selection and bias-correction.....	144
6.2.2 Fastest route algorithm.....	145
6.2.3 Additional variables relevant to shipping.....	147
6.3 Faster September routes.....	149
6.3.1 Verification	151
6.3.2 21 st century multi-GCM ensemble projections.....	152
6.3.3 Separate GCMs.....	157
6.4 Variability and Extended season.....	163
6.4.1 Alternative algorithm.....	163
6.4.2 Inter-annual variability.....	164
6.4.3 Extended Season.....	172
6.5 Comparison with previous studies	175
6.5.1 Comparison with Smith and Stephenson (2013) (S&S).....	175
6.5.2 Comparison with Stephenson and Smith (2015)	178
6.6 Discussion and Summary	180
6.6.1 Summary.....	180
6.6.2 Discussion	181
References	183
Chapter 7 Seasonal to interannual predictability of Arctic shipping routes	186
Summary.....	187
7.1 Introduction.....	188
7.2 Potential predictability experiments	191
7.3 Predictability of the shipping season.....	193
7.3.1 1 st July first season predictability	193
7.3.2 1 st July 3-year predictability	195
7.3.3 1 st May 3-year predictability	196
7.3.4 1 st January 3-year predictability.....	198

7.4 Lead time skill dependence.....	200
7.5 Conclusions and future work	201
References	204
Chapter 8 Conclusions and future work	207
8.1 Summary of results.....	209
8.1.1 The Arctic early 20 th century warming	209
8.1.2 Improved Arctic sea ice thickness projections	210
8.1.3 Faster 21 st century shipping using trans-Arctic routes	210
8.1.4 Seasonal to interannual predictability of Arctic shipping routes.....	211
8.2 Conclusions	212
8.3 Will Arctic routes replace conventional routes?	213
8.4 Potential for future work	215
8.4.1 The Arctic early 20 th century warming	215
8.4.2 Improved Arctic sea ice thickness projections	216
8.4.3 Faster 21 st century shipping using trans-Arctic routes	217
8.4.4 Seasonal to interannual predictability of Arctic shipping routes.....	218
8.4.5 Summary.....	218
References	220

Chapter 1

Introduction

1.1 Arctic sea ice decline: motivation for research

Ever since satellites started to accurately measure the Arctic sea ice scientists have observed a rapid state of decline. The IPCC AR5 climate change report found it “very likely that the Arctic sea ice cover will continue to shrink and thin” (IPCC, 2013). The state of the art global climate models (GCMs) used in the comprehensive study unanimously simulates year-round reductions in Arctic sea ice by the end of the 21st century. The most accurate of which indicate, “a nearly ice-free Arctic Ocean in September is likely for RCP8.5 (high emissions scenario) by mid-century” (Massonnet et al., 2012; IPCC, 2013). This decline in Arctic sea ice extent has led to the opening of summer/autumn ice-free passages along the north coast of Russia and through the Canadian Archipelago; known as the Northern Sea Route (NSR) and North West Passage (NWP) respectively.

Arctic shipping peaked during the Cold War due to continuous investment in ports and icebreakers by the Soviet Union maintaining large shipping numbers on the NSR. Activity today is still mostly destination traffic, to and from ports within the Arctic; however, the reduction in summer Arctic sea ice has led to considerable transit shipping using the Arctic Ocean as a short cut between Pacific and Atlantic ports. The substantial distance and time savings compared with Suez and Panama Canal routes results in potentially substantial economic benefits due to reduced fuel consumption and increased trip frequency (Lasserre, 2014). This has led to major shipping nations such as China, Japan, Singapore, and South Korea requesting observer status to the Arctic Council (Bennett, 2014). Shorter shipping routes also have the potential to reduce global shipping emissions with a negligible increase in Arctic pollution, such as black carbon deposition (Browse et al., 2013).

Although passage through the Arctic has been the dream of many early trailblazers such as voyages by Franklin (1854), Nordenskjold (1879), Amundsen (1906), Glavsevmorput (1934), and Larsen (1942), it has not been until recently that the combination of the geo-political, economic, and the physical climate have led to serious speculation over trans-Arctic shipping. The geo-political groundwork was laid in a speech in 1987 by the then President of the Soviet Union, Mikhail Gorbachev, in the northern port city of Murmansk, who declared that the NSR was to be opened to international traffic, an agreement that was in force from 1990 (Granberg, 1998). It was not however until the

start of the 21st century and the remarkable ice minimum of 2007 that transit shipping numbers started to accelerate.

Figure 1.1 shows that a substantial proportion (27% in 2011) of the world's container shipping sails between the Far East and Europe on the established route via the Suez Canal. Although realistically Arctic routes will likely not replace traditional routes via the Suez and Panama Canals in the near future, it is certainly plausible that a niche market for trade via trans-Arctic routes could be established. The size of this market will likely depend on many factors such as fuel price, the global economic and geopolitical climate, as well as the length and reliability of the Arctic shipping season.

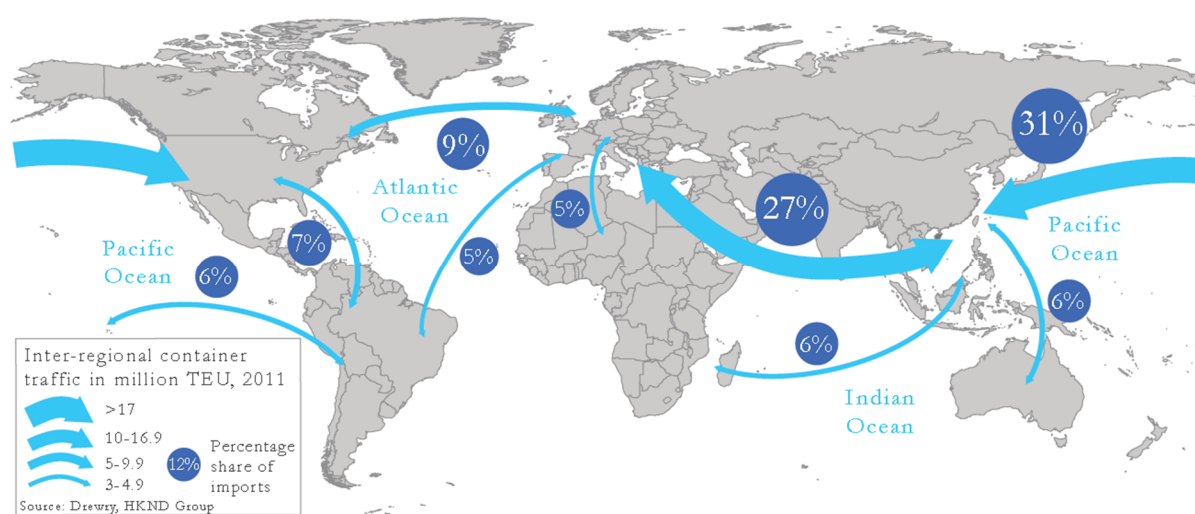


Figure 1.1 | Inter-continental container shipping, 2011. Europe – East Asia = 19 million TEU (twenty-foot equivalent units) (Humpert, 2013).

Many studies have looked at the potential for trans-Arctic shipping from different perspectives. One group assesses the potential from an economic perspective, assessing the economic models, ship owner's intentions, and legalistic and administrative considerations. Lasserre (2014) provides a review of much of this literature from 1991 – 2014 on the economic perspectives of trans-Arctic container shipping on both the NSR and NWP. Of the 26 studies, 13 find that Arctic routes are profitable over conventional routes via the Suez and Panama Canals, six are ambivalent or do not take a position, and seven conclude conditions are difficult for profitable exploitation of these routes.

The second group, of which this thesis forms a part of, examines the climatic potential for trans-Arctic shipping by assessing climate model simulations of the future. Stephenson et al. (2011) presents one of the first quantitative projections of changes to Arctic shipping finding the NSR will become accessible in the summer months by mid-

century but the NWP will remain impassable. This pioneering assessment only uses ensemble-mean—15-year-mean sea ice output from a single GCM. Rogers et al. (2013) used four GCMs to ascertain the prospects of a vessel capable of navigation in thin ice. They found that the Arctic would open rapidly throughout the century but with substantial variation in the timing between GCMs. Although this study benefits from multiple GCMs it only uses sea ice extent as a metric for accessibility rather than sea ice thickness as Stephenson et al. (2011) did which is a far more meaningful metric for shipping (Transport Canada, 1998; Tan et al., 2013). Smith and Stephenson (2013), in perhaps the most well-known study to date, make use of a ship routing algorithm combined with sea ice conditions from seven GCMs. They find that for moderately ice-strengthened vessels passage across the central Arctic Ocean, via the North Pole, is possible by mid-century. The study is limited by its use of ensemble mean projections and by assessing September only. All previous studies are limited by the fact that all GCMs contain substantial spatial biases in their sea ice distribution and thickness. For example, Smith and Stephenson (2013) find that with their methodology the NWP remains completely closed until at least mid-century, even for ice-strengthened vessels, despite the fact that satellite observations depict the NWP has been ice-free in the recent past. This model dependency is explored further in Stephenson and Smith (2015) where the same methodology of Smith and Stephenson (2013) is used by assessing the GCMs separately revealing contradictory results based on which model is used.

A study that incorporates all of the novel elements introduced by previous studies, but that lacks many of their limitations is required for accurate projections of the future of Arctic shipping. Specifically, this thesis will address the unanimous limitation of inter-model bias and develop a bias-correction technique to constrain the sea ice thickness simulated by GCMs by using observations (Melia et al., 2015). The sea ice thickness depicted by these calibrated GCMs have a realistic spatial distribution, temporal mean, and variance. This calibrated multi-model ensemble dataset (Melia, 2015) is used to find the fastest Arctic transit routes. Crucially, as the simulated sea ice conditions are more realistic and as multiple ensemble members are used, internal climate variability and hence uncertainty in the shipping projections can be robustly quantified. Although literature from all sources is utilised in this thesis, it is the climatic potential, specifically changes to sea ice, which is assessed in this thesis in the context of shipping.

1.2 On the use of Global Climate Models (GCMs)

A limitation of many previous studies is their use of multi-model and/or temporal mean projections. While the results from using these averaged projections provide insights into when regions of the Arctic may become accessible, it will miss substantial detail. The interannual variability of the ice pack is of vital importance to the reliability of the opening of Arctic sea routes. For example, high interannual variability in sea ice extent implies that one year a route could be open for months, while the next year the route is completely closed. This would be problematic for shipping operators looking to establish routine transit schedules through the Arctic; hence, a quantitative assessment of the uncertainty in the reliability of the shipping season as the Arctic continues to open throughout the 21st century is required.

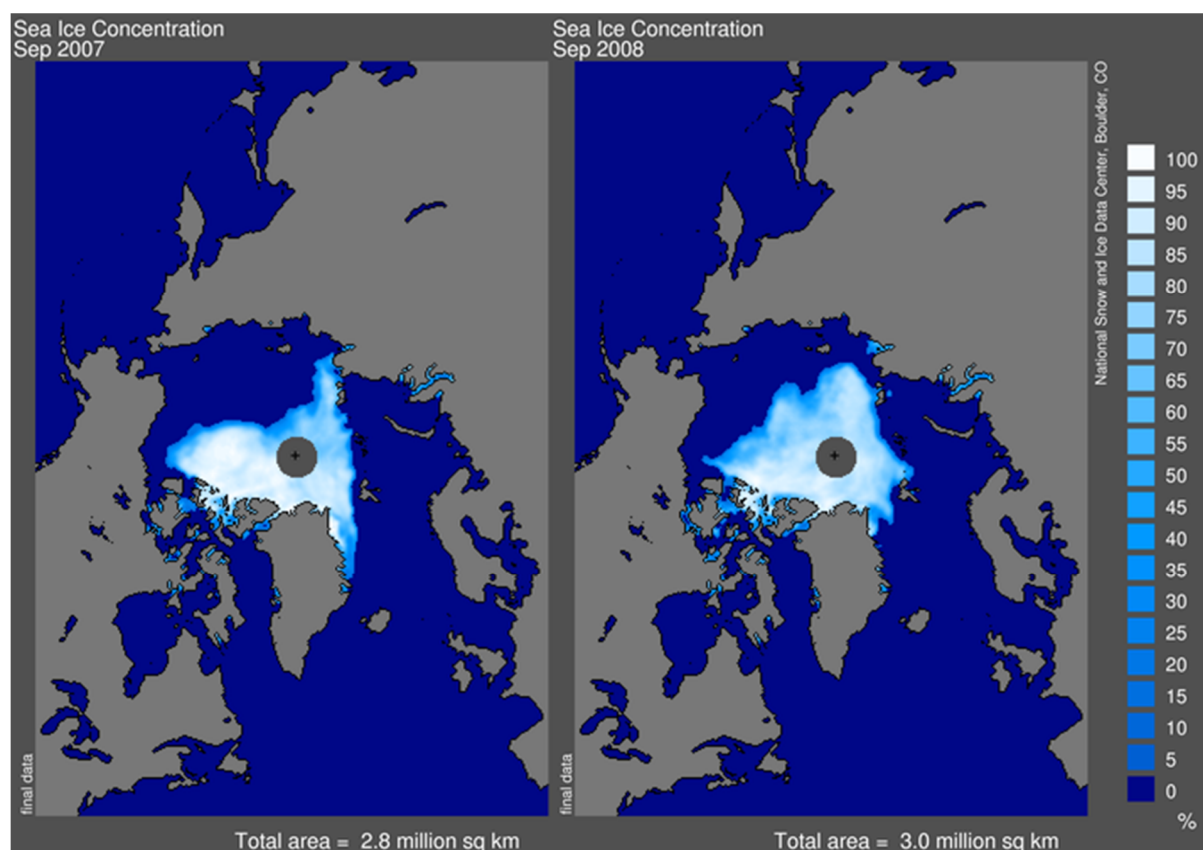


Figure 1.2 | Observed September 2007 and 2008 Arctic sea ice concentration from the National Snow and Ice Data Center (NSIDC).

Figure 1.2 shows the observed minimum sea ice concentration, which annually occurs in September, for the consecutive years 2007 and 2008. September 2007 saw a record breaking sea ice minimum of $2.8 \times 10^6 \text{ km}^2$, however despite this the NSR remained blocked by a tongue of ice extending from the main ice pack to the Russian coast.

However, in September 2008 the NSR was free of ice, despite an increase of $0.2 \times 10^6 \text{ km}^2$ over September 2007.

These observations highlight that to accurately project the openings of Arctic sea routes details of the ice pack must be considered beyond area integrated metrics such as total sea ice area. It also illustrates that individual years must be assessed explicitly and not by the use of multi-year and ensemble means, which are not an appropriate metric in such a spatially variable field such as the Arctic sea ice near its minimum extent.

The robust examination of future Arctic shipping accessibility requires the use of GCM simulations. It is important that the GCMs can accurately reproduce the climatic fluctuations observed in 2007 and 2008 if they are to be fit for purpose. Figure 1.3 shows the simulated sea ice concentration from a state-of-the-art GCM used in this thesis, for September 2016 and 2017. September 2016 has a remarkably high latitude open water passage across the Arctic Ocean, whereas September 2017 has ice extending all of the way to the Russian Coast. This illustrates that GCMs can indeed simulate the marked interannual spatial variability that the Arctic can display.

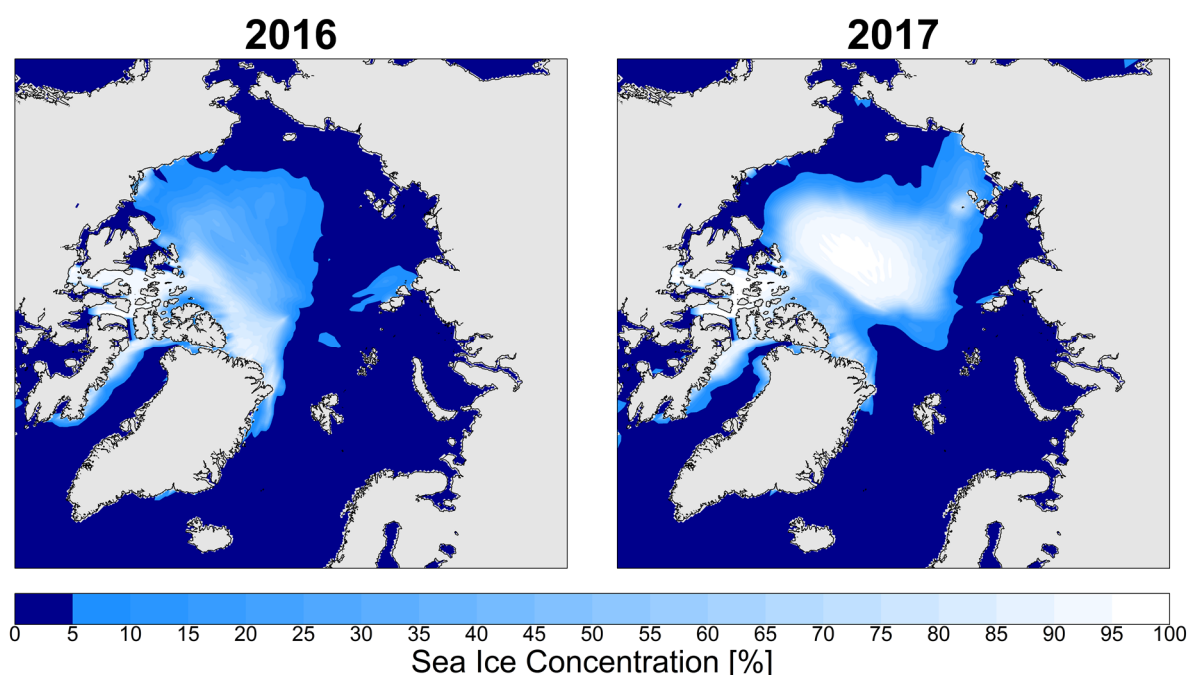


Figure 1.3 | September sea ice concentration as simulated by the UK Met Office’s HadGEM2-ES GCM. Output from the same ensemble member and emissions scenario.

1.3 Thesis aims

The future evolution of Arctic sea ice is uncertain, based on many unknown factors and complicated climate interactions. As Arctic sea ice is the biggest physical hazard to shipping in the Arctic, the future evolution of Arctic sea ice will have a profound influence on the future of Arctic shipping. This thesis aims to improve insight into the opportunities afforded to the shipping industry by the continued reduction in Arctic sea ice.

The principal questions this thesis will address are:

- 1. When will the Arctic display seasonally ice-free conditions?*
- 2. When will reliable trans-Arctic shipping be possible?*
- 3. How far in advance can predictions of Arctic sea route openings be made?*

To answer these questions a suite of GCMs will be used. It is important to understand that these GCMs themselves have limitations. Long-term simulations of the future are projections, these are distinct from predictions. Climate projections are inherently uncertain as they are composed of a number of factors which are either unknowable, like the magnitude of future anthropogenic greenhouse gases emissions; factors which are uncertain, like the temperature increase expected for a specified increase in forcing; or descriptions of processes which are only a basic representation of the real world.

However, GCMs are invaluable tools for simulating climate; their representation of the climate is well verified by simulating the past climate and comparing with observations. GCMs do accurately depict the behaviour of the climate on a range of spatial and temporal scales, from a realistic reproduction of the ocean circulation to the dip in global mean temperatures following a major volcanic eruption.

For Arctic sea ice the performance of GCMs has been well quantified, for example works by Stroeve et al. (2012) and (2014). One often cited limitation in the sea ice community is that over the last few decades the Arctic sea ice loss observed has been faster than simulated by GCMs e.g. Stroeve et al. (2007). However, the cause of the trend discrepancy is not well understood. It is possible that GCMs are missing a complete description of some important processes that are contributing to ice loss in the real world. However, it may be that the real world is in a natural state of internal variability

such that its ice loss trend is on the extreme end of the envelope as simulated by GCMs, Swart et al. (2015) finds some evidence for this.

1.4 Thesis structure

This thesis addresses a broad range of topics on both projections and predictions of Arctic shipping routes as well as more general topics on Arctic climate change.

The remainder of this thesis is structured as follows:

Chapter 2 Scientific background

Chapter 2 introduces the pertinent scientific principles used throughout the thesis by reviewing studies on observations and future projected changes to the Arctic climate. This is followed by a discussion of studies on the future of Arctic shipping and highlighting their limitations which this thesis aims to address.

Chapter 3 The Arctic early 20th century warming

Chapter 3 focuses on an intriguing period of warming that occurred towards the start of the 20th century in the Arctic and beyond. During this period sailors noted that Arctic Sea routes became open; a remarkable occurrence that has only been repeated in the last decade. This period is explored as the sea ice loss might contain similarities between the largescale warming that is ongoing. The total anthropogenic forcings in the early 20th century were far less than the current magnitude (Myhre et al., 2013). It is hence important to understand what caused the rapid early 20th century warming observed in the Arctic as a similar phenomenon could reoccur, potentially exacerbating future ice loss. The causes of the ice loss during the Arctic early 20th century warming are attributed by conducting forcing experiments using a state of the art climate model from the UK Met Office.

Chapter 4 Improved Arctic sea ice thickness projections

On analysing GCMs to ascertain future trans-Arctic shipping potential, it was discovered that the results were highly model dependant. The GCMs exhibit marked biases, so that the implications for future shipping, such as route choice, timing of route openings, and the prospects of different vessel classes, was uncertain due to the diversity of solutions given by different GCMs. In this chapter, a statistical bias-correction technique is developed that uses sea ice observations to constrain sea ice output in GCMs. This reduces the model bias and imparts greater confidence in using these improved projections.

Chapter 5 Arctic shipping background

Chapter 5 provides background information on Arctic shipping that is relevant for the following chapter where results for future trans-Arctic routes are presented. The major routes and passages through the Arctic Ocean are detailed, along with their navigability, climatic and geographic features. A brief background on maritime operations is provided including recent trends in Arctic shipping.

Chapter 6 Faster 21st century shipping using trans-Arctic routes

Chapter 6 presents some of the major findings of this thesis. The new calibrated multi-model GCM output from Ch. 4 is combined with a novel ship-routing algorithm to reveal that faster routes through the Arctic become possible through the 21st century. The algorithm is used to provide an assessment of the fastest trans-Arctic routes from East Asian to European and North American ports. The changes to the shipping season length and role of interannual variability are also quantified.

Chapter 7 Seasonal to interannual predictability of Arctic sea routes

This chapter examines ongoing work on the predictability of the opening of Arctic sea routes on seasonal to interannual time scales. With the combination of increasing activity and highly variable sea routes, the need for better sea ice forecasts for the opening of Arctic sea routes is larger than ever. The potential predictability of the opening of Arctic sea routes is explored using a ‘perfect model’ experiment, whereby a GCM ensemble is used to predict itself. Initial studies in the fledgling field of polar prediction show promise at producing skilful forecasts with increasing lead-times, however predictions on the opening of Arctic sea routes using this framework have not

been attempted before. These results provide an upper bound for the future skill of GCMs to predict the opening of Arctic sea routes.

Chapter 8 Conclusions and future work

This final chapter discusses the principal questions set out in the thesis aims. This thesis covers a broad spectrum of topics, each of which are likely to become more relevant with the combination of continued climate change in the Arctic and increase in human activity in the region. There are many opportunities for further advancement in each of the fields addressed in the chapters of this thesis. Future work is suggested for these topics, involving questions that arose during these investigations, but that were unfortunately beyond the scope of this thesis.

References

- Bennett, M. M.: North by Northeast: toward an Asian-Arctic region, *Eurasian Geography and Economics*, 55, 71-93, doi: 10.1080/15387216.2014.936480, 2014.
- Browse, J., Carslaw, K. S., Schmidt, A., and Corbett, J. J.: Impact of future Arctic shipping on high-latitude black carbon deposition, *Geophys. Res. Lett.*, 40, 4459-4463, doi: 10.1002/grl.50876, 2013.
- Granberg, A. G.: The northern sea route: trends and prospects of commercial use, *Ocean & Coastal Management*, 41, 175-207, doi: 10.1016/s0964-5691(98)00064-7, 1998.
- Humpert, M.: The Future of Arctic Shipping: A New Silk Road for China?, *The Arctic Institute*, 20, 2013.
- IPCC: Summary for Policymakers. In: *Climate Change 2013: The Physical Science Basis. Contribution of Working Group I to the Fifth Assessment Report of the Intergovernmental Panel on Climate Change*, edited by: Stocker, T. F., Qin, D., Plattner, G.-K., Tignor, M., Allen, S. K., Boschung, J., Nauels, A., Xia, Y., Bex, V., and Midgley, P. M., Cambridge University Press, Cambridge, United Kingdom and New York, NY, USA, 1–30, 2013, doi: 10.1017/CBO9781107415324.004.
- Lasserre, F.: Case studies of shipping along Arctic routes. Analysis and profitability perspectives for the container sector, *Transp. Res. Part A Policy Pract.*, 66, 144-161, doi: <http://dx.doi.org/10.1016/j.tra.2014.05.005>, 2014.
- Massonnet, F., Fichet, T., Goosse, H., Bitz, C. M., Philippon-Berthier, G., Holland, M. M., and Barriat, P. Y.: Constraining projections of summer Arctic sea ice, *Cryosphere*, 6, 1383-1394, doi: 10.5194/tc-6-1383-2012, 2012.
- Melia, N.: Improved Arctic sea ice thickness projections using bias corrected CMIP5 simulations. [Dataset]. University of Reading, doi: <http://dx.doi.org/10.17864/1947.9>, 2015.
- Melia, N., Haines, K., and Hawkins, E.: Improved Arctic sea ice thickness projections using bias-corrected CMIP5 simulations, *Cryosphere*, 9, 2237-2251, doi: 10.5194/tc-9-2237-2015, 2015.
- Myhre, G., Shindell, D., Bréon, F.-M., Collins, W., Fuglestedt, J., Huang, J., Koch, D., Lamarque, J.-F., Lee, D., Mendoza, B., Nakajima, T., Robock, A., Stephens, G., Takemura, T., and Zhang, H.: Anthropogenic and Natural Radiative Forcing. In: *Climate Change 2013: The Physical Science Basis. Contribution of Working Group I to the Fifth Assessment Report of the Intergovernmental Panel on Climate Change*, edited by: Stocker, T. F., Qin, D., Plattner, G.-K., Tignor, M., Allen, S. K., Boschung, J., Nauels, A., Xia, Y., Bex, V., and Midgley, P. M., Cambridge University Press, Cambridge, United Kingdom and New York, NY, USA, 659–740, 2013, doi: 10.1017/CBO9781107415324.018.
- Rogers, T., Walsh, J., Rupp, T., Brigham, L., and Sfraga, M.: Future Arctic marine access: analysis and evaluation of observations, models, and projections of sea ice, *Cryosphere*, 7, 321-332, 2013.

Smith, L. C. and Stephenson, S. R.: New Trans-Arctic shipping routes navigable by midcentury, *Proc. Natl. Acad. Sci. U.S.A.*, 110, E1191–E1195, doi: 10.1073/pnas.1214212110, 2013.

Stephenson, S. R. and Smith, L. C.: Influence of climate model variability on projected Arctic shipping futures, *Earth's Future*, 3, 331-343, doi: 10.1002/2015ef000317, 2015.

Stephenson, S. R., Smith, L. C., and Agnew, J. A.: Divergent long-term trajectories of human access to the Arctic, *Nature Clim. Change*, 1, 156-160, doi: 10.1038/nclimate1120, 2011.

Stroeve, J., Barrett, A., Serreze, M., and Schweiger, A.: Using records from submarine, aircraft and satellite to evaluate climate model simulations of Arctic sea ice thickness, *Cryosphere*, 8, 1839-1845, doi: 10.5194/tc-8-1839-2014, 2014.

Stroeve, J., Holland, M. M., Meier, W., Scambos, T., and Serreze, M.: Arctic sea ice decline: Faster than forecast, *Geophys. Res. Lett.*, 34, doi: 10.1029/2007GL029703, 2007.

Stroeve, J. C., Kattsov, V., Barrett, A., Serreze, M., Pavlova, T., Holland, M., and Meier, W. N.: Trends in Arctic sea ice extent from CMIP5, CMIP3 and observations, *Geophys. Res. Lett.*, 39, L16502, doi: 10.1029/2012gl052676, 2012.

Swart, N. C., Fyfe, J. C., Hawkins, E., Kay, J. E., and Jahn, A.: Influence of internal variability on Arctic sea-ice trends, *Nature Clim. Change*, 5, 86-89, doi: 10.1038/nclimate2483, 2015.

Tan, X., Su, B., Riska, K., and Moan, T.: A six-degrees-of-freedom numerical model for level ice–ship interaction, *Cold Reg. Sci. Technol.*, 92, 1-16, doi: <http://dx.doi.org/10.1016/j.coldregions.2013.03.006>, 2013.

Transport Canada: Arctic Ice Regime Shipping System (AIRSS), 1998.

Chapter 2

Scientific background

Summary

The Arctic is often noted as experiencing the effects of climate change the earliest, the climate's 'canary in the mine' perhaps. Satellite observations from 1979 reveal decreases to both sea ice extent and volume. This has in turn led to an increase in sea ice mobility and an increased melt season, with open-water prevalent for longer.

Climate models are an invaluable tool for providing projections of future climate change in addition to detection and attribution of changes. Modelling sea ice is complex and many of the processes are parameterised. The current generation of state-of-the-art climate models, such as those used in this thesis, have improved in many respects, and are starting to incorporate more realistic representations of sea ice processes. Climate model experiments of the historical period find that anthropogenic forcings are very likely to have contributed to Arctic sea ice loss since satellites started measurements in the 1970s. Simulations show that it is very likely that the Arctic ice cover will continue to shrink in the course of the 21st century as the global mean surface temperature rises. The exact rate and magnitude of this decline is difficult to state however due to uncertainty in future greenhouse gas and other forcings and model uncertainty.

Opinions vary on the economic viability of Arctic shipping as a rival to conventional routes. Simulating future shipping as derived from climate model projections is a relatively new field and studies have increased in complexity and applicability over the last decade. All such studies project that the Arctic will continue to open up through the 21st century with extensions to the shipping season. A notable finding is that a new route directly across the North Pole may become navigable by mid-century. The studies contain limitations to varying degrees but all rely on climate model projections that have known sea ice biases.

2.1 Arctic climate change

Arctic sea ice covers up to 3% of the Earth's surface and is a crucial component of the climate system. It is a physical barrier to the exchange of gases, heat, and momentum between the atmosphere and ocean. Sea ice contains salt and modifies the salinity of the ocean by ejecting salt on formation and releasing fresher water when melting, altering the ocean's density structure and affecting the Ocean circulation in the Arctic and beyond. Arctic sea ice is both affected by, and in turn affects, regional and global climate, through a variety of feedback mechanisms (Francis and Vavrus, 2012). Ecosystems in polar regions crucially depend on sea ice to provide habitats and food for a wide variety of plant and animal life.

Arctic sea ice extent is constrained by the geography of the Arctic Ocean basin. This land constraint is important as changes in climate that affect trends in the winter sea ice extent will be masked. This is one of the principal differences between the Arctic and Antarctic sea ice, where the situation is reversed with a continent covering the pole surrounded by ocean. The Arctic sea ice extent has exhibited a distinct decline over the past 30 years, whereas the Antarctic extent has shown a slight increase with large regional differences. Holland and Kwok (2012) report that changes to the wind patterns and hence ice drift may be responsible for this Antarctic growth.

Changes have occurred to all types of Arctic sea ice. Perennial ice (the summer minimum extent) has seen large changes and "very likely decreased by 9.4% – 13.6%", between 1979 – 2012 according to the IPCC AR5 report (Vaughan et al., 2013). High confidence is also assigned to the decrease in overall mean winter sea ice thickness, 3.64 m in 1980 which likely decreased by ~1.8 m in 2008. Changes to Arctic sea ice are important; however, they also have important implications for the future. Decreases in sea ice concentration and thickness reduces ice strength, making the ice more vulnerable to future melt and results in a more mobile ice pack increasing susceptibility to break-up and deformation.

2.1.1 Sea ice lifecycle

Saline ocean water is cooled to its freezing point and freezes during the winter months, the newly formed sea ice is then transported and deformed, if it has not reached sufficient thickness it will melt in the summer months; this subsection describes the major processes during the sea ice lifecycle.

The addition of salt lowers both the temperature at which the water reaches its maximum density and its freezing point. Polar oceans have a typical salinity of 35 ‰ and begin to freeze at -1.8°C . Convective overturning results in the presence of a mixed layer typically 10 m deep in the Arctic, this entire water mass needs to be cooled to the freezing point, any increase in the mixed layer depth will delay freeze up (Doronin and Kheisin, 1977).

Arctic sea ice becomes thicker through the winter months in addition to increasing its spatial extent. This thermodynamic process is limited however as thicker ice better insulates and reduces the rate of heat loss from the oceans. An additional layer of insulation is provided by snow covering the surface of the ice. The processes controlling the changes to sea ice can be split into thermodynamic and dynamic components. Thermodynamic processes melt or grow the ice in situ. Dynamic processes such as advection by wind and ocean currents redistribute this ice on a basin-wide scale via form drag (Tsamados et al., 2014) and locally increase or reduce ice thickness by deformation and the creation of open water.

The majority of Arctic sea ice is grouped together as pack ice. On smaller scales, ice can be separated into floes and is affected by wind and ocean currents. The dynamics can cause cracks in the ice called leads, which are roughly linear in nature with open water in-between the ice floes. Leads form important navigational channels for shipping and wildlife as well as affecting the local climatic conditions by exposing relatively warm ocean water. Where dynamical divergence occurs, areas of open water can be created called polynyas. These polynyas are important for the formation of sea ice at the start of the winter freeze up and are responsible for the formation of cold saline water, which is important in maintaining the Arctic Ocean halocline. Polynyas can form in the open ice pack, against the land, or against ice fastened to the land (called fast-ice). Fast-ice occurs in coastal regions and is usually grounded in shallow water with the seaward edge typically located between the 20 – 30 m isobaths (Mahoney et al., 2007). The locations of these polynyas and fast-ice massifs are well known and appear routinely in ice navigation charts.

Convergence on the other hand causes ice to deform and become thicker. Thin floes move easily and collisions result in rafting. When the ice is thicker, collisions are more energetic and ridging takes place. Ridges present a significant hazard to human activities on the ice as their thickness can exceed 2 m above the surface and greater than 10 m below.

Arctic summer air temperatures regularly exceed 0°C, which leads to widespread surface melting and formation of surface melt ponds, vastly reducing the surface albedo. The water in the melt ponds trickles through both the underlying porous ice and also flows into the open leads that are abundant during the melt season (Eicken et al., 2002), thus leading to a significant thinning of the sea ice during summer emanating from the surface of the sea ice. Despite their importance for determining the radiative properties of the Arctic Ocean during summer and the evolution of the melt season (Flocco et al., 2012; Schröder et al., 2014), the processes governing the development of the melt ponds are still an active area of research (Flocco and Feltham, 2007; Flocco et al., 2010). The melting of sea ice is complicated by the fact that sea ice is a mixture of freshwater ice and interstitial brine. The conservation of phase equilibrium in this mixture leads to there being no specific melting temperature for sea ice, it rather changes some of its freshwater ice into liquid upon heating (Notz, 2005). These internal phase changes act to dampen the rate of melting, this melt rate is not constant over time. Initially the melt rate increases slowly due to a decreased heat transfer into the ice interior. Upon peak rates being reached a decrease then occurs due to the remaining ice consisting higher levels of solid ice (Wiese et al., 2015).

2.1.2 Sea ice concentration (SIC)

Reliable sea ice observations are available from 1979 onwards via satellite multichannel passive microwave sensors (Figure 2.1). A number of procedures are used to convert the brightness temperature measured into the fractional area of ice coverage (e.g. Comiso and Nishio (2008) and Markus and Cavalieri (2000)). Sea ice extent is defined as the area of ice covered gridcells with a concentration of at least 15%.

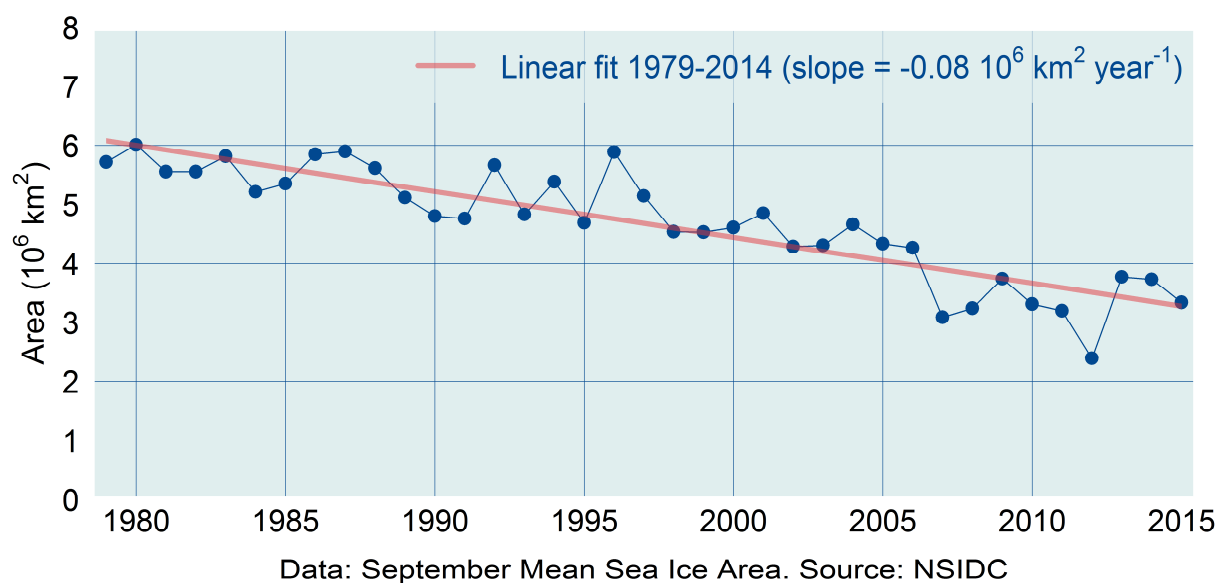


Figure 2.1 | Observed September mean sea ice area. Data from NSIDC. The inter-annual error is $0.02 - 0.03 \times 10^6 \text{ km}^2$; the absolute error is up to $1 \times 10^6 \text{ km}^2$.

Arctic sea ice cover varies seasonally from about $6 \times 10^6 \text{ km}^2$ to $15 \times 10^6 \text{ km}^2$ (Comiso and Nishio, 2008; Cavalieri and Parkinson, 2012; Meier et al., 2012), typically reaching its maximum extent in February/March and its minimum in September. The sea ice extent in Figure 2.2 shows this marked seasonal variability. Since 2000 the downward trend in the sea ice minimum has been larger compared to the trend in the maximum, and some have hinted that this could be a fundamental change in behaviour or a ‘tipping point’ (Lindsay and Zhang, 2005; Lenton et al., 2008; Stroeve et al., 2012a). However, observations since these studies show a near linear decline in the annual minimum (e.g. Figure 2.1) and therefore indicate that dips around these previous studies should be expected as a result of the internal variability of the climate system.

To examine changes to the vulnerability of sea ice to rapid future melt, changes to variance are examined. First, trends must be removed; there are two dominant trends, the seasonal cycle, and the forced response. On removing these, the detrended extent reveals a marked increase in the variance from 2007 (Figure 2.2) as also noted by Livina and Lenton (2013).

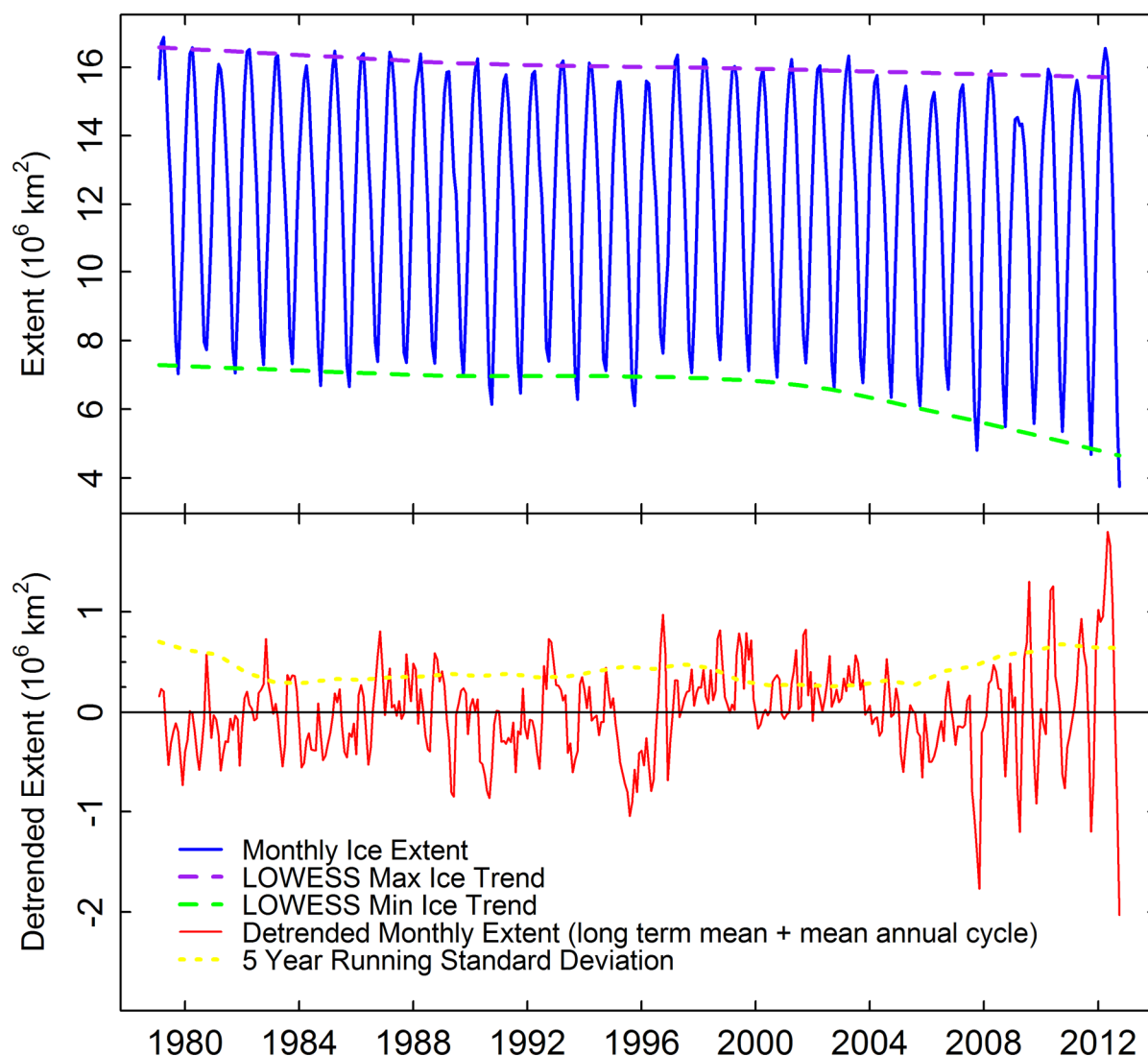


Figure 2.2 | HadISST observed monthly mean sea ice extent (top), and after detrending (bottom), with locally weighted smoothing lines (LOWESS).

2.1.3 Sea ice thickness (SIT) and volume (SIV)

In general, sea ice thickness (SIT) is harder to measure than concentration. Several techniques are used to estimate thickness including submarine sonars, satellite altimetry, and airborne electromagnetic sensing; these all provide strong evidence that the Arctic SIT is reducing. However, SIT observations have been relatively sparse, in both space and time, until recently.

The analysis of data collected by upward-looking sonar on submarines operating under the cover of the sea ice was pioneered by Wadhams (1983, 1990). Studies by Rothrock et al. (1999) and Wadhams and Davis (2000) indicate that since the middle of the last century the ice draft (submerged portion of sea ice) has decreased in thickness by 40%.

The prominent 2007 melt season that broke the sea ice extent record also saw large decreases in SIT (Giles et al., 2008). Recently, real-time data from Cryosat2 has been made available, which should provide a valuable resource for the science community and operations in the Arctic (Laxon et al., 2013; Tilling et al., 2015; Tilling et al., 2016).

Reanalysis products of SIT also exist which benefit from a continuous spatial and temporal record. This includes the Pan-Arctic Ice Ocean Model and Assimilation System (PIOMAS) (Zhang and Rothrock, 2003) which is introduced in detail in Ch. 4. The combination of SIT with SIC is used to calculate pan-Arctic sea ice volume (SIV); SIV is an integrated metric, and is simply the average sea ice thickness over the sea ice area.

2.1.4 Uncertainty in sea ice observations

The most common method to observe Arctic sea ice is by the use of satellites; passive microwave sensors are used to measure the SIC and radar altimetry to measure the SIT. Numerical techniques are required to convert the signal received by the sensors into SIC or SIT. These algorithms contain parameters for the physical properties of the ice and other factors which affect the signal, these include: ice roughness, ice freeboard height and atmospheric water vapour (Laxon et al., 2013; Ivanova et al., 2015). Ivanova et al. (2015) evaluates the skill of 30 of these algorithms for SIC, all of which give a quantitatively different answer for Arctic sea ice area at any given time. In calculating SIC Notz (2014) identifies four general sources of error to which the algorithms give differing solutions: (1) sensitivity to the temperature of the sea ice, (2) atmospheric effects, (3) melt ponds, and (4) thin ice. For calculating SIT the presence of melt ponds is a particular hindrance, the sensor cannot distinguish between the liquid water of the melt ponds on ice and that of open water. This problem is so acute that seasonally observations are halted from May to September each year (Tilling et al., 2016). This is particularly frustrating for the sea ice and seasonal prediction community as this is seasonally when the Arctic sea ice undergoes its most dramatic change. Typical absolute error magnitudes for SIT are 0.25 m, for sea ice area errors are up to 10% (Zygmuntowska et al., 2014).

The satellite sensors also have a finite lifetime, with discontinuities between new instrumentation. On real-time timescales, the satellites only have a specific footprint and are only able to measure a specific swath of the Arctic at a time, for a spatially complete picture of the Arctic many days swaths are required. When interpreting observational products of SIC and SIT, and computing sea ice area and volume, the

uncertainty between algorithms, discontinuities between sensors and gaps in the time series all need to be kept in mind.

2.1.5 Seasonal cycle of Arctic sea ice

In addition to significant observed changes in sea ice area and volume, strong regional changes are occurring in the seasonality of sea ice (Stammerjohn et al., 2012; Parkinson, 2014). Markus et al. (2009) find significant changes in almost every region of the Arctic, with changes to an earlier melt onset and a later freeze up. These changes are critical for indigenous communities, ecosystems, and operations in the region such as shipping. These changes are regional, affecting the seasonal ice regions found at the edges of the ice pack (Vaughan et al., 2013); these are exactly the regions where current Arctic shipping lanes are located. In these coastal regions, the open-water season is widely increasing by 10 – 30 days per decade, and in parts of the Barents Sea up to 70 days per decade averaged over 1979-2013 (Parkinson, 2014).

Changes to the melt season are also occurring in the Canadian Archipelago, shown by Figure 2.3. Sea ice fracture dates obtained from the Canadian Ice Service reveal that changes are greatest in Baffin Bay, with fracture dates advancing ~4 days per decade. The magnitude of this trend decreases through the Archipelago interior (~ 3.5 days earlier per decade) and is lowest in the Beaufort sea (< 2.5 days earlier per decade). Trends are significant in most of the stations; but sites around Lancaster Sound and Barrow Strait have very high inter-annual variability making trend reductions at these locations harder to determine.

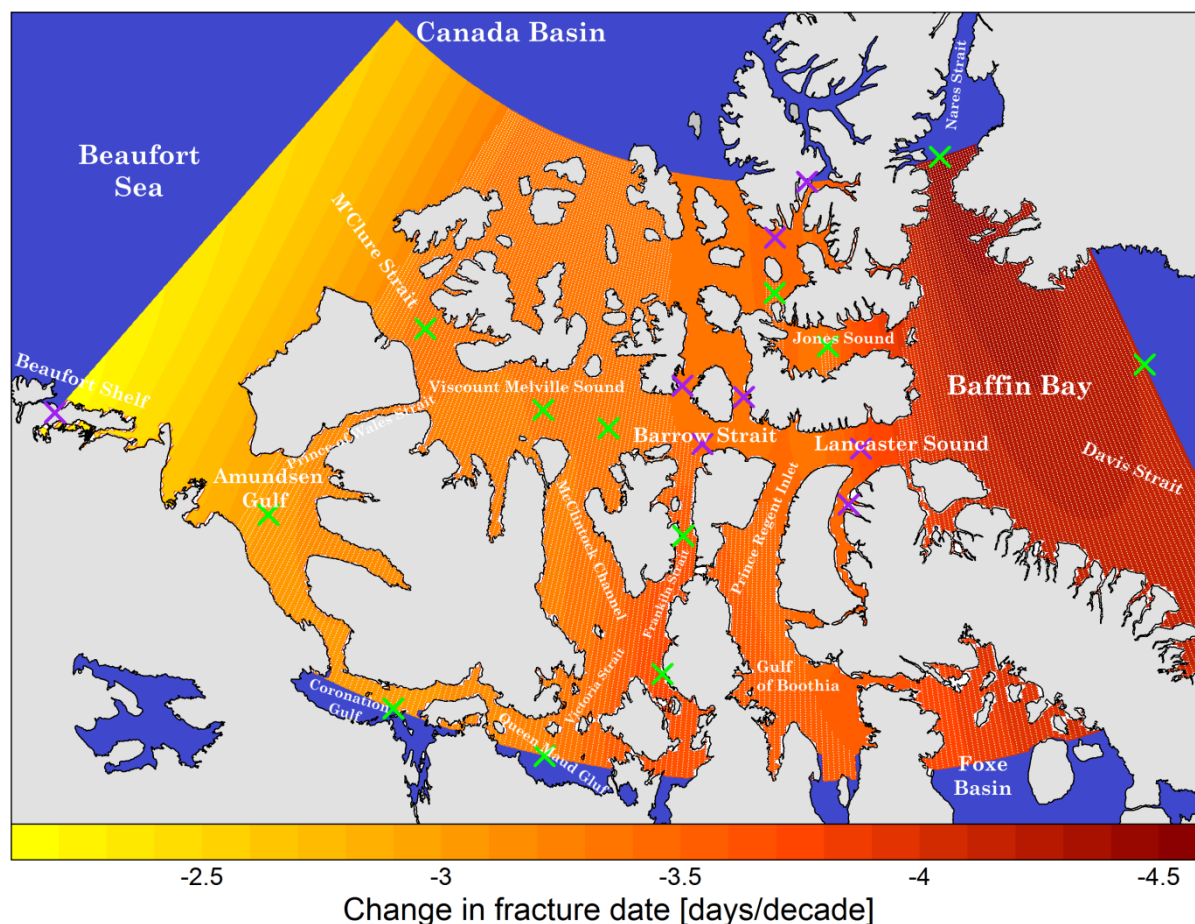


Figure 2.3 | 1968 – 2013 observed change in sea ice fracture date, data supplied by the Canadian Ice Service, plot by the author. Crosses show the 19 observation sites, trend significance determined by a linear trend at 2σ significance, green indicates significance, purple not. The yellow-red shading was filled using kriging and is for schematic purposes only; white stippling indicates significant trend regions.

2.1.6 Historic Arctic sea ice observations

Although satellite records since 1979 are long enough for somewhat robust conclusions to be drawn about the trends and variability for sea ice, the conditions prior to the satellite era are also of interest. Pre-satellite records are comprised of regional observations taken from ships or aircraft (Walsh and Chapman, 2001; Polyakov et al., 2003; Rayner et al., 2003). In the more distant past, they can be inferred from terrestrial proxies (Macias Fauria et al., 2009; Kinnard et al., 2011). Changes to sea ice prior to the satellite era are discussed in depth in Ch. 3.

2.1.7 Trends

Observations of Arctic sea ice during the satellite era show rapid changes in many metrics. Figure 2.4a shows a linear decrease in sea ice extent of -3.8 ± 0.3 % per decade, with seasonal and interannual variability superimposed (from Comiso and Nishio (2008) updated to 2012 (Vaughan et al., 2013)). This decrease has occurred mainly in the seasonal ice zone. Further into the interior of the ice pack decreases to multiyear ice coverage have also occurred (Figure 2.4b) (Kwok, 2009); multiyear ice is important as it is a particular hazard to shipping, and also provides a dampening effect helping to resist advection and melt. Observations of SIT are more problematic, however a consistent record is possible by combining records for the central Arctic region (Haas et al., 2008; Rothrock et al., 2008; Kwok and Rothrock, 2009). Figure 2.4c shows that combining these datasets over the central Arctic and North Pole region reveals a thinning of the sea ice of 0.62 m per decade. This reduction in concentration of all sea ice ages, and thinning of sea ice, creates a more mobile ice pack. The anomalies in buoy (Rampal et al., 2009) and satellite-derived sea ice drift speed (Sprenn et al., 2011) shown in Figure 2.4d reveal an increase of 0.55 ± 0.04 km day⁻¹ per decade. This anomaly is larger for the winter months, up to 0.94 ± 0.3 km day⁻¹ per decade. The seasonality of the Arctic sea ice is also undergoing significant lengthening of the melt season by 5.7 ± 0.9 days per decade, illustrated in Figure 2.4e updated from Markus et al. (2009) in Vaughan et al. (2013).

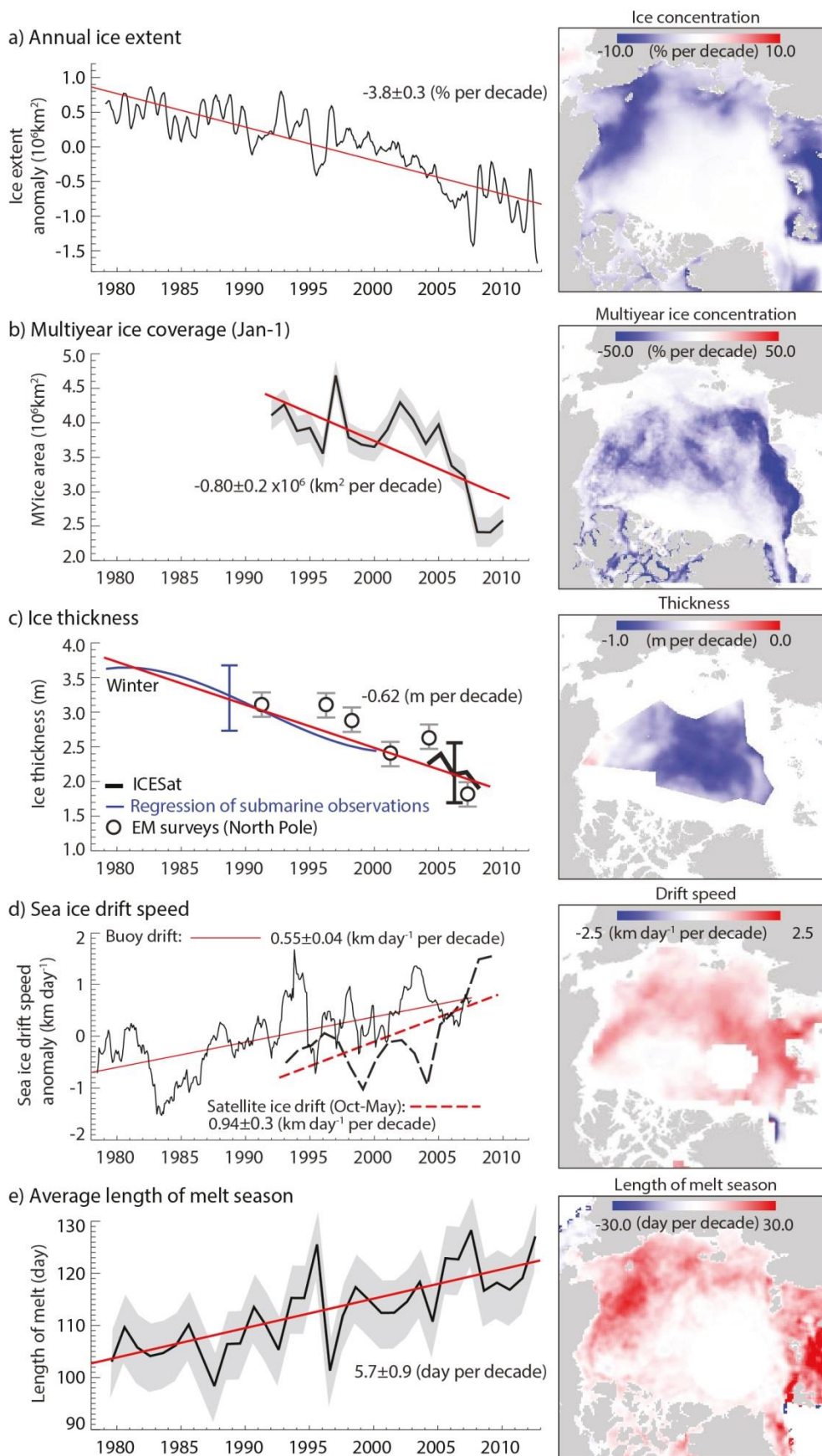


Figure 2.4 | Summary of linear trends in Arctic sea ice (AR5 Fig. 4.6) (Vaughan et al., 2013).

2.1.8 Future sea ice evolution

In a warming world, Arctic sea ice is expected to decrease in volume. There are however many processes that will become more important as the climate changes that will exacerbate the non-linear response of sea ice in a changing climate.

One of the key processes in the evolution of sea ice is the positive ice albedo feedback mechanism. Melt ponds are the leading order source of seasonal variability in sea ice albedo. In a warming world there will be a marked reduction in freezing degree days and hence an increase in melt ponds and a potentially accelerated melt.

Ocean waves or swell can act to break up the edge of the ice pack through mechanical processes. This effectively increases the size of the marginal ice zone, where sea ice exists in a loose and fractured state. The power of the ocean waves undergoes attenuation due to the damping effect of sea ice on the surface. The distance which these waves can propagate into the ice pack depends on the wave power, which is a function of the wave amplitude and period. The length of open water, or fetch which these waves form over is directly correlated to the wave power and hence the capability to enhance ice breakup. Uniquely the Arctic undergoes a seasonal cycle in wave fetch from zero in the winter months to hundreds of kilometres in the summer months. With the increasing amounts of open water due to climate change the fetch and hence wave power is increased (Thomson and Rogers, 2014). This combined with potential changes to storminess in high northern latitudes could lead to emergence of an additional positive feedback mechanism further enhancing ice loss in the Arctic.

Clouds are a principle varying component in the radiative transfer of the Arctic climate system (Curry et al., 1996). In the Arctic more clouds are observed in the summer months than the winter months. Taylor et al. (2015) finds the largest covariance between low cloud properties and sea ice around the sea ice minimum with significant changes to the boundary layer temperature structure at high SIC. These processes and the complex feedback mechanisms are likely to be important to the future evolution of the Arctic (Vavrus et al., 2008).

To quantify the future sea ice evolution requires complex climate model simulations, which should represent as many of these processes as possible. The next section outlines climate model simulations of Arctic sea ice.

2.2 Climate model simulations of the Arctic

Climate models are the primary tools for making climate predictions on seasonal to decadal time scales, and projections of future climate for the 21st century and beyond. Results from a series of coordinated experiments with the current generation of models are collected as part of the Coupled Model Intercomparison Project, phase5 (CMIP5) (Taylor et al., 2012). Climate models all contain separate components for the atmosphere, land surface, ocean, and sea ice. The current state-of-the-art models are called earth system models and additionally feature separate components for aerosol, atmospheric chemistry, land carbon, and ocean biogeochemistry processes. More generally, these models are termed Global Climate Models or General Circulation Models (GCMs); this thesis utilises CMIP5 GCMs in Chs. 3, 4, and 6.

The primary function of a GCM is to simulate the dynamics of the climate system, and in turn to make projections of future climate based on future emissions of greenhouse gases and other radiative forcings. The state-of-the-art GCMs analysed in Chs. 3, 4, and 6 of this thesis also include some of the processes qualifying them as earth system models. These include processes and feedbacks that are important for climate projections of several decades. The experiments conducted in Ch. 7 use the previous generation of GCMs which do not contain these extra components, making them useful for seasonal to decadal predictions where computational efficiency is of higher importance.

2.2.1 Advantages of modelling the climate

Observations provide a record of past climate and often provide the best insight into understanding what happened to the climate. Although the extent of observations is ever increasing, there remains a limit to how well sampled, both temporally and spatially the earth's climate is. For instance the daily Central England Temperature series (Parker et al., 1992), dates back to 1772, providing an invaluable record of climate change over two centuries. However, the data is for one region and provides little information about the climate at other locations. Variables from past and future GCM simulations are spatially and temporally complete.

Climate models provide the opportunity to test causes of past climate change and provide a simulated record of the historical climate. GCMs allow experiments to be carried out with a representation of the earth; these can be repeated multiple times with

varying initial, boundary and physical conditions to test hypotheses. This cannot be done with the real earth, although one could reason that a CO₂ ramping experiment is inadvertently taking place.

The unique advantage of GCMs however lies in the insight into the future that they provide. This is possible to some extent with observations with certain assumptions, and indeed statistical models do perform as well as GCMs for some predictions such as the Indian Monsoon and seasonal forecasts of ice minimum, e.g. Wu et al. (2009) and Stroeve et al. (2014b).

2.2.2 Modelling sea ice

Parameterisations are included in every component of a GCM as they are required to represent processes that occur on scales that are too fine to resolve. This is no different for the sea ice component of GCMs. In GCMs grid cells are 10 – 100 km, compared with 1 m – 1 km scales for typical ice floes. Despite this, the large scale thermodynamic and dynamic processes in GCMs are generally well represented (Hunke et al., 2010).

A basic goal of sea ice models is to predict the evolution of the ice thickness distribution. Many GCMs now include some representation of sub-grid scale thickness variations along with processes that can convert thin ice to thicker ice through deformation. Generally 5 – 20 thickness categories are utilised, with more thinner ice categories to calculate accurate growth during freeze-up (Hunke et al., 2010).

The thermodynamic processes are still treated with 1-D parameterisation schemes in GCMs, due to the dominance of the vertical interactions (Hunke et al., 2010). The sea-ice albedo is widely quoted as being a crucial aspect and potential positive feedback in the climate system. This is primarily because of the sensitive radiation response of sea ice and the large albedo contrast between sea ice and open water once ice is removed (Maykut and Perovich, 1987).

Melt ponds are an important aspect of the sea ice lifecycle. They change the surface albedo and the draining of melt ponds through the ice is important for the salinity of the underlying oceans. They also cause problems for satellite remote sensing instruments. There are several techniques for the treatment of melt ponds on sea ice in models. The simplest, and most widely used, is a surface albedo adjustment under warm conditions. A second method, as used in models such as CCSM4 (one of the GCMs utilised and introduced later in this thesis) is virtual melt ponds which can affect the radiative

equations but their melt water is flushed directly into the ocean (Hunke et al., 2010). The most complex method involves considering the finer points of a melt pond's evolution such as melting and re-freezing within the ponds (Flocco and Feltham, 2007).

Dynamical equations including those for momentum, rheology, transport, and deformation are also included to simulate ice movement. Ice can diverge easily because it exists in a somewhat fractured state. Convergence is harder as ice is essentially incompressible, but deformation can occur with the formation of ice ridges if the convergent forces are strong enough to overcome the ice strength.

Generally the sea ice models incorporated into many GCMs are relatively basic, however more advanced parameterisations are making their way into the ice model components (Flocco et al., 2012; Hunke et al., 2013).

2.2.3 GCM performance in simulating Arctic sea ice

To evaluate the performance of GCM simulations of sea ice, reliable observations are needed. The GCMs that comprise CMIP5 exhibit improvements over the previous generation of models (CMIP3). The multi-model mean error is within 10% of the observational estimates for all months (Flato et al., 2013). However in many GCMs the regional distribution of sea ice is poorly simulated (Figure 2.5) as shown for SIC by Stroeve et al. (2012b), and for SIT by Stroeve et al. (2014a). This is likely due to incorrect representation of winds and currents (Melsom et al., 2009; Koldunov et al., 2010); Ch. 4 discusses these biases in-depth and presents a novel solution (Melia et al., 2015).

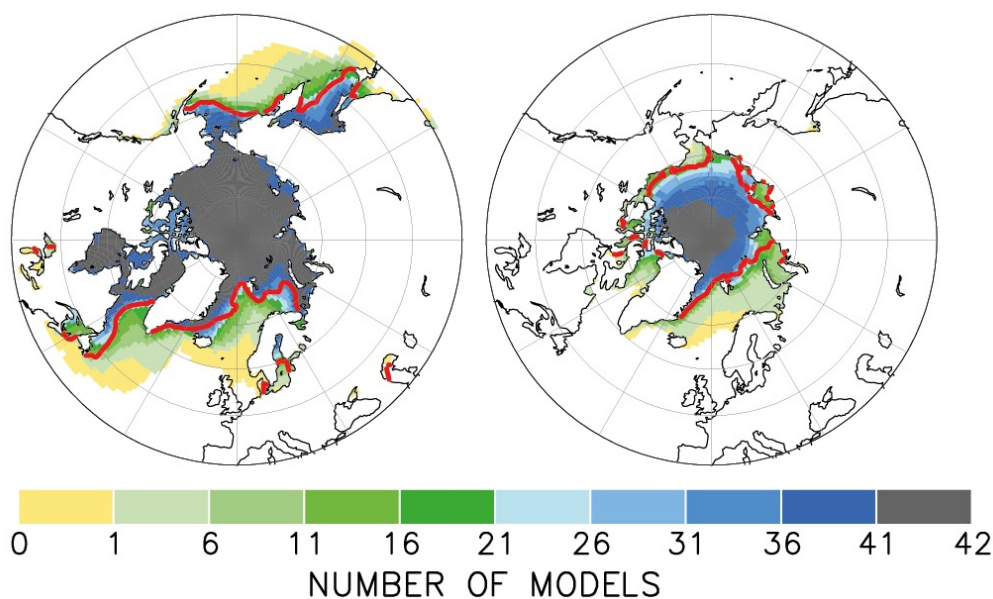


Figure 2.5 | Arctic sea ice distribution (1986 – 2005) for February (left) and September (right) as simulated by 42 CMIP5 GCMs. Single ensemble members from each GCM are used. This figure indicates for every grid cell the number of models that simulate a SIC of at least 15%. The observed 15% boundary (red) is from HadISST (Rayner et al., 2003). (Adapted from IPCC AR5 Fig. 9.23, Flato et al. (2013))

A systematic failure of most CMIP3 GCMs is a marked underestimation of the decline of September sea ice extent. Many reasons for this have been proposed in the literature including internal climate variability, model inadequacies, and observational uncertainties (e.g. Stroeve et al. (2007), Kay et al. (2011), and Day et al. (2012)) In comparison, CMIP5 GCMs better simulate this ice loss trend observed in the sea ice minimum. Stroeve et al. (2012b) suggests that this could be due to the incorporation of new sea ice albedo parameterisation schemes. However, Notz et al. (2013) cautions against directly comparing GCMs with observations unless the GCMs internal variability is carefully assessed. Using the MPI-ESM, Notz et al. (2013) find a range of simulated trends from 1979, some even positive, in a warming climate, due to internal climate variability.

Although improvements are seen in CMIP5 simulations, the multi-model mean trend in September Arctic sea ice extent over the satellite era is still underestimated compared to observations (Massonnet et al., 2012; Stroeve et al., 2012b; Wang and Overland, 2012; Overland and Wang, 2013). Although over the relatively short period that satellites observations are available for one would not expect the CMIP5 ensemble mean to match observations. Attributing the reasons for this disparity is difficult as the observational

period is relatively short, thus the influence of internal variability cannot be ruled out (Swart et al., 2015).

2.2.4 Using GCMs to attribute changes to Arctic sea ice

The IPCC AR5 report concludes that “Anthropogenic forcings are very likely to have contributed to Arctic sea ice loss since 1979” (Bindoff et al., 2013). This conclusion is drawn from the fact that the decline in Arctic sea ice is only seen in GCM simulations that include anthropogenic forcing.

The Arctic has undergone unprecedented change over the satellite record. The rate of sea ice loss has dramatically increased (Maslanik et al., 2007; Zhang et al., 2008; Comiso, 2012), and based on SIT estimates from satellites and reanalysis 75% of the SIV has been lost since the 1980s (Schweiger et al., 2011; Maslowski et al., 2012; Laxon et al., 2013; Overland and Wang, 2013). Seminal sea ice minima occurred in 2007 and 2012 that were 37% and 49% less than the 1979 – 2000 climatology respectively (Bindoff et al., 2013). The two minima are attributed to different causes, the 2007 minimum coincided with a shift in winds, whilst the minimum in 2012 was due to a more general thinning (Lindsay et al., 2009; Wang et al., 2009; Zhang et al., 2013).

The confidence in attributing these changes must come from multiple lines of enquiry, and as trends continue, the evidence becomes stronger. These lines of enquiry include the wider signs of change in the Arctic including additional variables such as, snow, permafrost, changes to ecosystems, as well as more obvious variables such as temperatures (Duarte et al., 2012). Modelling studies such as Min et al. (2008) compare the characteristics of the seasonal cycle finding a human influence on the change in sea ice extent since 1990. Kay et al. (2011), Schweiger et al. (2011) and Jahn et al. (2012) used the CCSM4 GCM to investigate the anthropogenic influence on the Arctic sea ice decline. They found that the internal variability exhibited by CCSM4 could not account for the magnitude of the trends observed in sea ice extent. At best, internal variability could account for a maximum of 50% of the observed decline 1979 – 2005.

2.2.5 Representative Concentration Pathways (RCP)

Climate change projections require information about future anthropogenic emissions of greenhouse gases, aerosols and other climate drivers. The future scenarios used to accomplish this in CMIP5 are denoted Representative Concentration Pathways (RCPs) (Van Vuuren et al., 2011). They are identified by their approximate change in radiative

forcing by the year 2100 relative to 1750, in Wm^{-2} . From low to high emissions, the scenarios are RCP2.6, RCP4.5, RCP6.0, and RCP8.5. The lowest, RCP2.6, represents a climate change mitigation scenario leading to the lowest simulated forcing with a peak and decline by 2100. RCP4.5 and RCP6.0 represent stabilisation scenarios where RCP4.5 stabilises by 2100. RCP8.5 represents essentially unabated greenhouse gas emissions. The RCPs specify land use changes, specific pollutants, greenhouse gas concentrations, and anthropogenic emissions up to 2100.

2.2.6 Sea ice projections

Most CMIP5 GCMs project a consistent ice-free Arctic (5 consecutive years $< 1 \times 10^6 \text{ km}^2$) by 2100 in RCP8.5 (Kirtman et al., 2013), with some reaching this threshold far sooner, e.g. 2040 (Holland et al., 2006). Some more radical projections have stated ice-free conditions could occur as early as 2016 (Maslowski et al., 2012). However their approach fails to take into account internal variability (Overland and Wang, 2013) and ignores negative feedback effects that become important as the ice thins (Notz, 2009). Mahlstein and Knutti (2012) estimate that for the ice to disappear the global mean surface warming threshold of 2°C above pre-industrial would have to be reached, a threshold which is widely quoted as leading to “dangerous” warming.

For the CMIP5 GCMs Massonnet et al. (2012) found high correlations between the timing of a seasonally ice-free Arctic ocean and its current sea ice extent and volume (Figure 2.6a,b). Boe et al. (2009), Collins et al. (2011), and Massonnet et al. (2012) found the timing of a seasonally ice-free Arctic to also be correlated with a GCM’s past trend in September Arctic sea ice extent and mean seasonal cycle amplitude (Figure 2.6c,d). These findings are pleasingly logical and indicate that the CMIP5 GCMs are capturing the correct climatic changes, but may suffer biases to varying degrees. Generally, trends and patterns of GCM behaviour in the past are likely to continue into the future. For example, one generally expects GCMs with smaller amounts of sea ice in the past to also have smaller amounts in the future, thus becoming ice-free sooner. Likewise, a faster ice-loss trend in the past should also continue into the future. The correlation in the amplitude of the seasonal cycle is a logical result as it indicates that models which display a larger seasonal cycle contain sea ice that is more sensitive to the changes in radiative forcing and temperature in the melt season, and therefore as the melt season extends in the future this behaviour is enhanced.

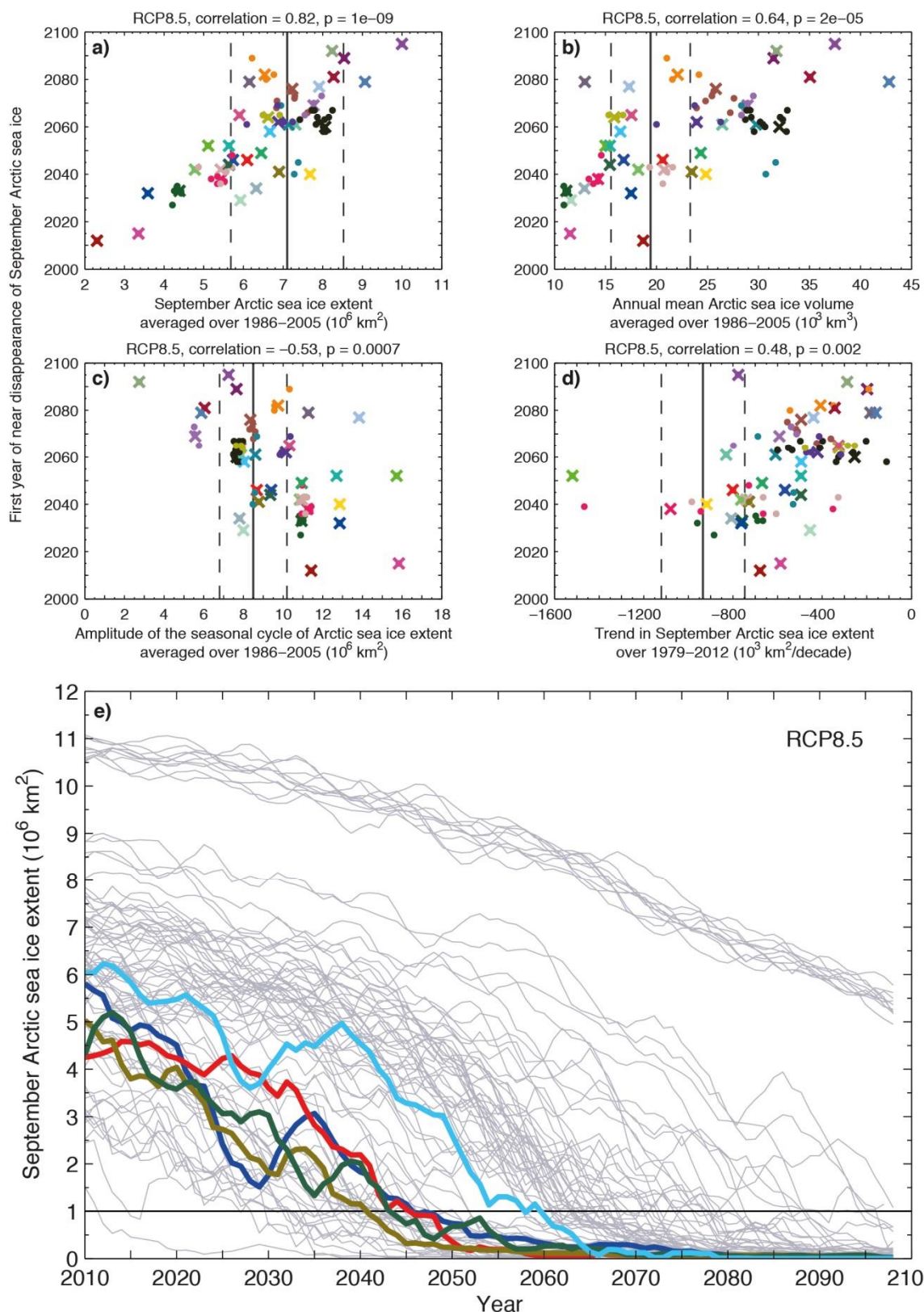


Figure 2.6 | Year of first ice-free September CMIP5 projections as a function of (a) past extent, (b) annual mean SIV, (c) past mean seasonal cycle amplitude, (d) past ice loss trend, solid lines represent observations. (e) 5 year running mean for all ensemble members (RCP8.5), colours represent Massonnet et al. (2012) selection. IPCC AR5 Fig. 12.31 (Collins et al., 2013).

The reduction in sea ice coverage is greatest in September. The CMIP5 multi-model mean projected reduction between 1986 – 2005 and 2081 – 2100 shown in Figure 2.7 ranges from 8% in RCP2.6 to 34% in RCP8.5 for February and 43% for RCP2.6 and 94% for RCP8.5 in September (Collins et al., 2013). However, the AR5 report only attaches medium confidence to these projections due to error in both simulated present day climate and large ranges in future projections between GCMs.

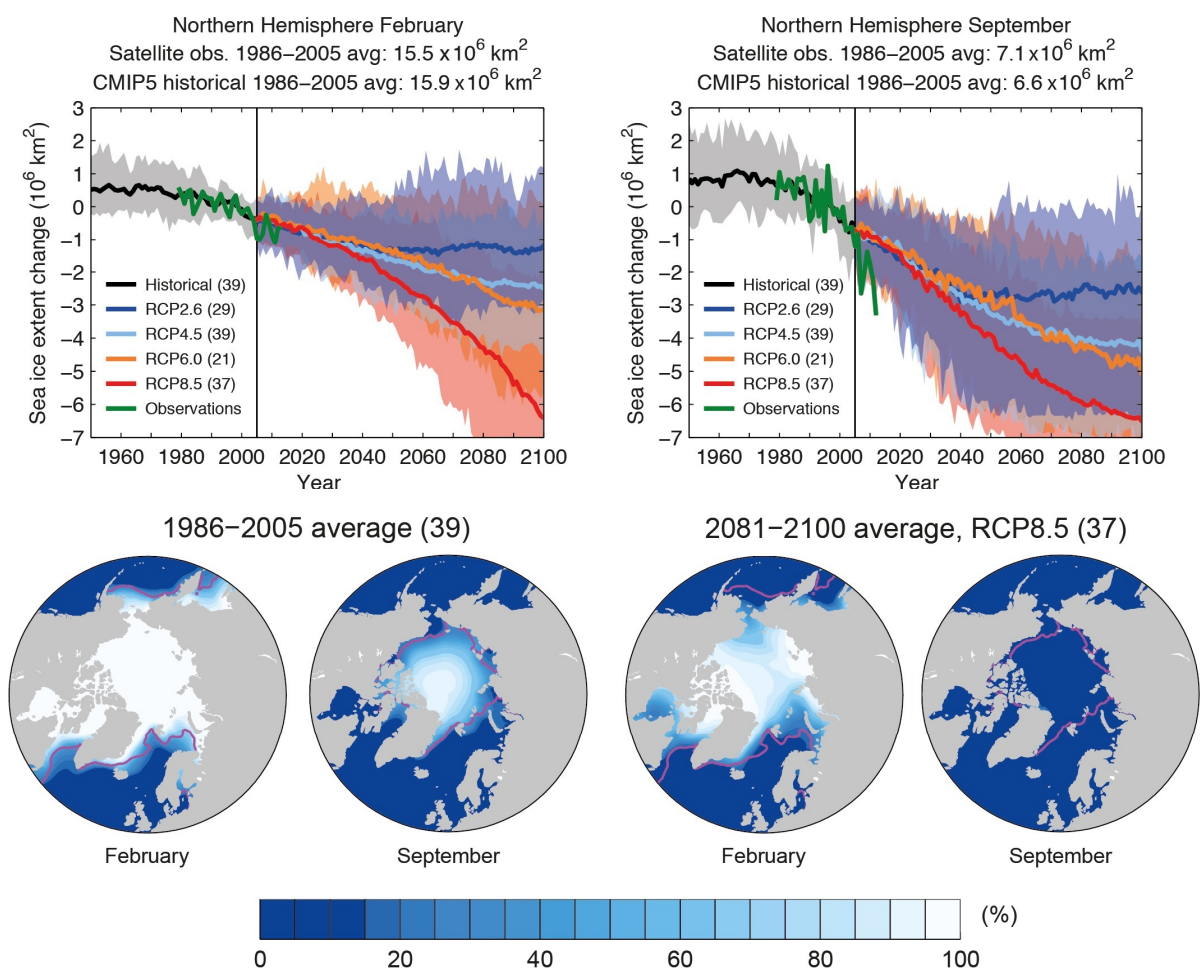


Figure 2.7 | Changes in February and September Arctic sea ice as simulated by CMIP5 GCMs; figure adapted from IPCC AR5 Figs. 12.28 and 12.29 (Collins et al., 2013). Time-series solid curves show the multi-model means and the shading denotes the 5 – 95% ensemble range, anomalies relative to 1986 – 2005. Colours denote RCPs with number of available models in brackets, green shows the satellite data updated from Comiso and Nishio (2008) over 1979 – 2012. Maps show multi-model mean SIC. The pink contour indicates the observed 15% SIC 1986 – 2005 from Comiso and Nishio (2008).

The IPCC AR5 report states that “it is very likely that the Arctic sea ice will continue to shrink and thin all year round during the 21st century as the annual mean global

surface temperature rises” (Kirtman et al., 2013). It also states with medium confidence, that it is “likely that the Arctic Ocean will become nearly ice-free in September before the middle of the century for high greenhouse gas emissions such as those corresponding to RCP8.5” (Kirtman et al., 2013).

2.3 Studies of future shipping

Over the past decade the idea of shipping in the Arctic and particularly the prospect of Arctic transit shipping, i.e. sailing through the Arctic Ocean as a short cut between the Pacific and Atlantic Oceans, has gained increasing attention in the scientific community (Vaughan et al., 2013), popular press (The Economist, 2012), industry (Hansen et al., 2016), and in government (House of Lords, 2015). The growth of shipping in the region also raises the question of the legal status of the North West Passage (NWP) and Northern Sea Route (NSR) (Byers, 2009; Lasserre and Pelletier, 2011). The United States and European Union claim the routes are international straits, Canada and Russia unsurprisingly claim that they are internal and thus subject to their sovereignty. But what of the status of the central Arctic, where the future trans-polar sea route (TSR) may open by mid-century, as Smith and Stephenson (2013) find. Will these waters continue to be classified as neutral in the light of recent continental shelf claims by several Arctic states? The development of Arctic shipping remains a controversial topic and expert analyses varies, e.g. Howell and Yackel (2004), Brigham (2010), and Lasserre and Pelletier (2011). However, with the continued thinning of Arctic sea ice and the use of powerful icebreakers, shipping in the Arctic is becoming more of a business problem. The question of whether normal ocean going “Open Water” vessels will be able to transit the Arctic Ocean, given the increasing prevalence of open water found in the Arctic now (Parkinson, 2014) that is projected to continue (Barnhart et al., 2015), remains uncertain.

This section analyses the state of knowledge on trans-Arctic shipping. The literature splits into three distinct groups. The first group looks at the economic feasibility of trans-Arctic shipping to assess if such a venture is an economically feasible and attractive endeavour for shipping companies. The second group assesses the viability of trans-Arctic shipping with regards to the changing physical climate, focusing mainly on changes to Arctic sea ice throughout the 21st century. As this is the group to which this thesis belongs, each study will be discussed in detail. A final group examines potential changes to the environment and climate system as a result of increased shipping in the Arctic.

2.3.1 Economic feasibility

Arctic transit shipping has undergone a rapid increase since 2007, coinciding with a period of reduced sea ice extent, which likely stimulated the increase. This includes the

peak of 71 vessels transiting the NSR in 2013, a year that also saw a coalbunker vessel and a passenger cruise ship with 508 passengers sailing the NWP. However, the peak in Arctic shipping still occurred under the Soviet Union before the effects of climate change drastically affected the Arctic sea ice pack on the scale seen in the last 20 years. This Soviet peak in shipping was only possible with huge investments in icebreakers, ports, and infrastructure, from the centrally planned Soviet economy that controlled the entire stretch of the eastern Arctic coast.

Studies into the economic feasibility of trans-Arctic shipping date back as early as Wergeland (1992), a year after the NSR became open to international traffic and just after the collapse of the Soviet Union. The study compared transits on the NSR verses using conventional alternative routes via the Suez and Panama Canals, and found NSR routes were more profitable. Lasserre (2014) compiled a comprehensive review of 26 such studies and finds that 13 studies conclude that Arctic routes can be profitable for commercial shipping, six are ambivalent or do not take a position, and seven conclude that conditions are too difficult to be profitable.

The Russian NSR administration advertise tariffs for transit along the NSR that make any routine use prohibitively expensive, however communications between Lasserre (2014) and the Managing Director of a large Arctic shipping company (Tschudi), reveal that these rates are negotiable so as to attract future business. Lasserre (2014) concludes from these 26 studies, and his own analysis, that the profitability of transits depends on destination, with north-eastern Asian ports like Yokohama (Japan) being more profitable than more south-eastern Asian ports like Shanghai (China) due to the smaller distance savings via the Arctic to the latter ports. A particularly interesting conclusion is that, rather than profitability primarily being a function of fuel cost, it is in fact average transit speed (and hence time) that is most important, as faster journeys allows a higher frequency of voyages. It is thus important that future studies aim to find the fastest routes through the Arctic and to assess the journey times, an aspect investigated explicitly in Ch. 6 of this thesis.

2.3.2 Future climatic viability for trans-Arctic shipping

Utilising GCMs to assess the potential for trans-Arctic shipping is a comparatively new idea. To the authors knowledge the first peer reviewed attempt was that of Mokhov et al. (2007), and new studies continue to be published on a near yearly basis. The studies have evolved in their complexity, with initial work looking for ice-free regions for a

single emission scenario in a single GCM, to later works pioneered by Smith and Stephenson (2013) that apply established ice navigation methodologies and route finding algorithms to a range of GCMs.

2.3.2.1 Mokhov et al. (2007)

In the first such study Mokhov et al. (2007) use the CMIP3 GCM MPI-ECHAM5, to examine the prospects for the NSR throughout the 21st century. They use the IPCC AR4 (AR5 precursor) SRES-A2 anthropogenic emission scenario; a high emissions scenario, with a similar trajectory, but with a radiative forcing slightly below that of RCP8.5 throughout the 21st century. The study is comparatively basic by only analysing one GCM and one future emission scenario for only the NSR. However, the use of the word “simulations” in their study when referring to the MPI-ECHAM5 GCM implies that they may have used more than one ensemble member, although the use of a single, multiple or an ensemble mean projection is not deducible from the manuscript. They assume that navigation through a grid cell is possible if the SIC is below 15%.

They find that the navigation season along the NSR increases throughout the 21st century. Before 2030, the season is 10 days, 2031 – 2060 one month, 2061 – 2090 three months. They also find spatial variations in future shipping seasons. The peripheral Barents and Chukchi seas have the largest extension to the season, while the internal Russian seas of the Laptev and East Siberian show little change in SIC until at least 2061.

2.3.2.2 Khon et al. (2010)

A thorough analysis by Khon et al. (2010) uses 21 CMIP3 GCMs and again assumes a 15% SIC navigation threshold. They focus on average changes to season length, analysing the simulated past in each GCM and comparing with observations. Their chosen projection is the initially high SRES-A1B scenario (with a total radiative forcing in-between RCP8.5 and SRES-A2 before starting to level off from 2060). The study mostly discusses GCM shipping projections in a multi-model mean sense.

They find an extension to the NSR and NWP navigation season of 40 and 30 days per 30 years respectively. They analyse the NWP by selecting nine of the 21 CMIP3 GCMs available, as the remaining GCMs do not contain a depiction of the channels in the NWP. Their GCMs predict a prolongation of the season of 3 to 6 months for the NSR and from 2 to 4 months for the NWP by the end of the 21st century. They also speculate on the economic implications by extrapolating global shipping trends and combining with

their GCM results leading to a bold claim that by the end of the 21st century the NSR may become more profitable than the Suez Canal even in the winter months.

2.3.2.3 Stephenson et al. (2011)

Stephenson et al. (2011) assess the changes to both maritime and land-based forms of transport until 2060, sectors that are likely to experience opposite accessibility changes. Their methodology is notable as the first shipping study to utilise SIT, important as vessels have explicit SIT thresholds based on their design (Transport Canada, 1998), whereas SIC is a more ambiguous variable in this regard. Their methodology is novel and reflects operational considerations more realistically than previous studies. However, the framework is only applied to output from the CMIP3 GCM — CCSM3. Results are further limited by the use of ensemble mean projections averaged over 15-year windows for just the SRES-A1B scenario.

By mid-century, they find that the NSR is fully accessible for July – September. The claim of ‘fully’ accessible is misleading as it implies accessibility all of the time, when the use of an ensemble-mean–time-mean does not allow for such a conclusion. They are the first study to analyse the viability of the TSR, which is also open July – September from mid-century. However, they find the NWP remains closed until beyond mid-century in CCSM3. This is because of a considerably high SIT bias in this region. This is a common feature in GCMs, likely exacerbated by constricted and ‘dead-end’ channels in the Canadian Archipelago causing sea ice to build up continually, highlighting limitations of relying on a single GCM output without bias-correction.

2.3.2.4 Rogers et al. (2013)

Rogers et al. (2013) assess observed pan-Arctic and regional sea ice trends. They rank 13 GCMs using three metrics, and the best performing four GCMs are then used to assess future Arctic shipping. The GCMs used are from the CMIP3 set and are forced with the A1B emission scenario. Their methodology uses 9-year means about the years 2030, 2060, and 2090; although they do admit that significant interannual variability exists and the results should be interpreted accordingly. They also note that observations show a faster sea ice loss trend than simulated by the CMIP3 GCMs, and note that this could be because of natural variability in the observations, rather than model inadequacies, a cause widely postulated in the Arctic sea ice community. These insights impart confidence for the remainder of the manuscript.

The study is unique in examining the prospects of a Polar Class 7 (PC7) ship, the least ice-strengthened of the Polar Classes but still more resilient than standard Open Water vessels. The Polar Classes have specific operational sea ice type, ice age and ice thickness thresholds (Transport Canada, 1998). However Rogers et al. (2013) only make use of SIC, they alleviate this limitation by assuming that a PC7 vessel would not navigate extensive segments of ocean were any ice present. They practically apply this rationale by seeking largely ice-free routes and define a route as being closed if at least two consecutive grid cells are ice covered (greater than 15% SIC). While this is a reasonable compromise given the restriction of SIC for this purpose, it must be noted that smaller passages and straits on the NSR and NWP often become blocked with ice and subsequent ice convergence may lead to SIT exceeding a PC7 vessels threshold.

They find that for typical conditions around 2030 only one GCM is open and only for one month for both the NSR and NWP. Strangely for the NSR this occurs in August not September indicating a slightly too high ice sensitivity to some seasonally varying forcings leading to the sea ice minimum occurring too early. In 2060, the NSR season is 3 months long in three GCMs and completely closed in the fourth highlighting substantial model uncertainty even in the 'best' performing CMIP3 GCMs.

2.3.2.5 Smith and Stephenson (2013)

Work by Smith and Stephenson (2013) is briefly introduced here and compared in-depth to results from this thesis in Ch. 6.5.1. Their study uses the same Arctic shipping accessibility methodology outlined in their previous study Stephenson et al. (2011) but updated to the CMIP5 GCMs. The novel aspect of Smith and Stephenson (2013) is their use of an algorithm to find the optimal navigation routes rather than relying on fixed routes. This methodology allows them to find a northerly migration of routes over the next few decades in September transitioning from the NSR to the TSR, which they find navigable for a moderately ice strengthened PC6 vessel by mid-century (Figure 2.8).

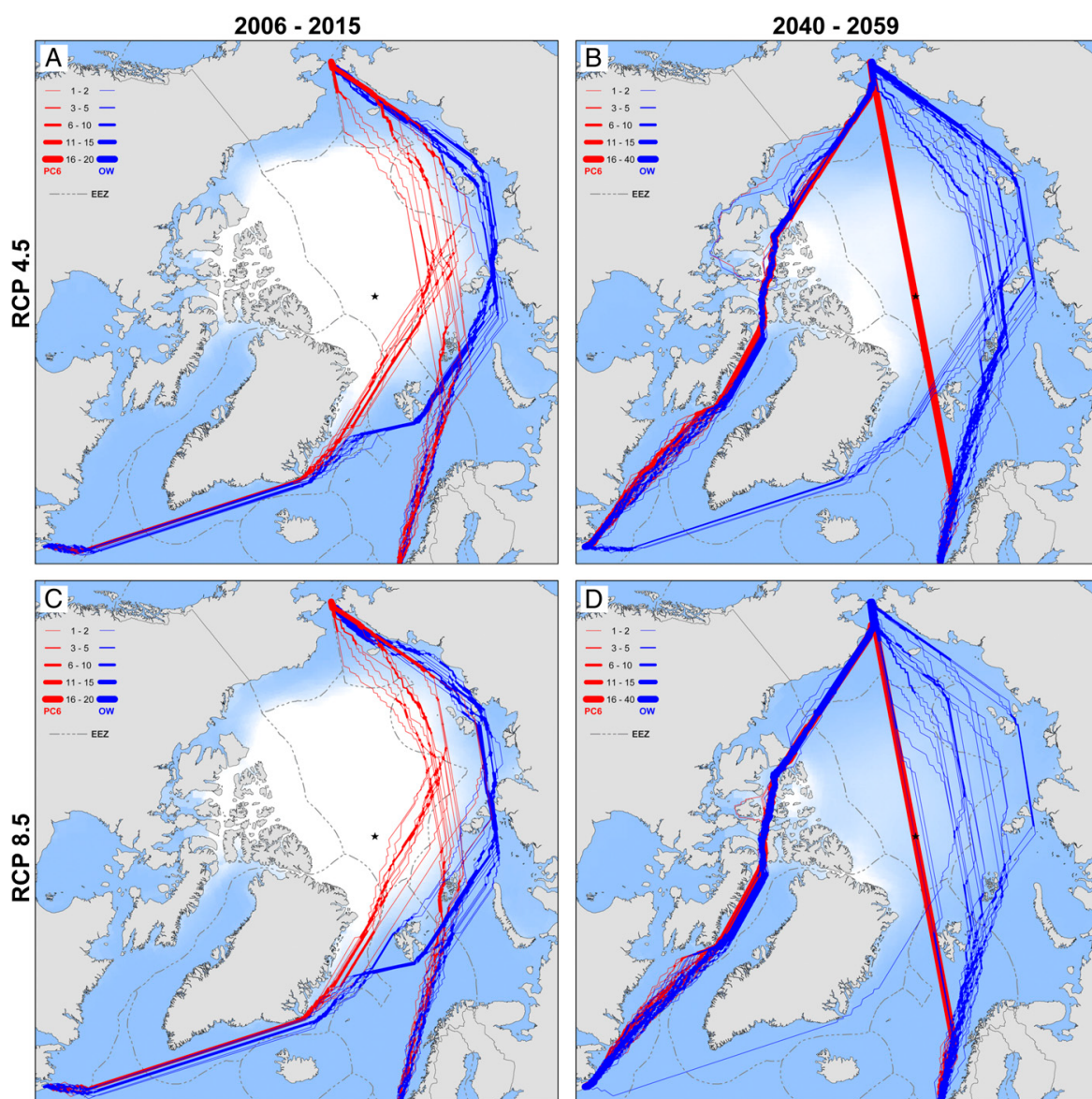


Figure 2.8 | Optimal September navigation routes for hypothetical ships crossing the Arctic Ocean as driven by multi-model-mean sea ice conditions. Reproduced from Smith and Stephenson (2013), Fig. 2.

Their study only looks at the prospects for September and their use of a multi-model mean as shown in Figure 2.8 leads to the NWP being completely inaccessible to even PC6 vessels 2006 – 2015, despite the fact that the satellite observations and real ship traffic data depicts that some past Septembers have been navigable.

2.3.2.6 Stephenson et al. (2013b)

The Stephenson et al. (2013b) study uses the same Arctic shipping accessibility methodology developed for Stephenson et al. (2011). The study is novel in that it assesses season length by using daily instead of monthly data and includes an ice-

breaking PC3 class vessel in addition to PC6 and OW classes. They do however make a few puzzling choices such as assessing RCP4.5, RCP6.0, and RCP 8.5 but not RCP2.6. They also only utilise ensemble #6 from the CCSM4, without specifying why this particular ensemble member was selected.

The study aims to quantify changes to the length of the shipping season in a spatial sense. They do this by examining winter (DJFM) and summer (JASO) seasons for three 20-year periods through the century. They calculate the change in accessible area, which shows an increase with time, although this metric is less relevant for transit shipping or many other uses as the locations of the newly opened regions are not given. The results also show negligible differences between similar RCP4.5 and RCP6.0 scenarios, even later in the century. Spatial maps of accessibility are shown for the early century period for the different seasons and vessel classes. They comment on the inter-annual variability of the shipping season, which is an important factor omitted in other studies by the use of averaging data across years and models. However, the variability in the shipping season is calculated as the standard deviation of the number of accessible days metric across different years, rather than on the sea ice data directly. The “number of accessible days” metric will not be normally distributed and hence standard deviations cannot be robustly used, as explained below. Their error is repeated in Stephenson et al. (2013a) where the implications are worse as the standard deviation is calculated every month as opposed to every season, discussion of which is continued in the next section.

2.3.2.7 Stephenson et al. (2013a)

The third paper by the Stephenson et al. group focuses on the NSR and benefits from discussing some finer aspects of navigating on the route with contributions from co-author Capt. Lawson Brigham who has extensive operational experience. The study uses the same accessibility methodology as Stephenson et al. (2013b) and again only assesses CCSM4 ensemble #6; uniquely they choose the RCP6.0 emission scenario, a medium scenario that was the least simulated of all the RCPs by the CMIP5 modelling centres, potentially because of its similarity to RCP4.5.

The study aims to characterise the future NSR season length and variability. Inter-annual variability is an important factor for reliable future shipping, one that is often overlooked. However to ascertain the variability the mean “days of accessibility” is calculated for each month for 2013 – 2027; this number ranges 0 – 30. The metric is always a positive integer, due to the 0 and 30 day bounding. The distribution is also very likely bimodal and skewed, as the most common results are likely to be completely

closed — 0 days, or completely open — 30 days; values in-between will be relatively far less common. Stephenson et al. (2013a) then calculate the variability as the standard deviation of these data, a metric that is only meaningful if the parent data is Gaussian. The manifestation of this error is that many of the uncertainty plumes suggest that above 100% of days are navigable. The plumes would also likely occupy space that would equate to negative days based on their trajectories, were they not limited by the plot region. The studies mean statistics can be trusted however, and by calculating accessibility with longitude through the Russian seas, implications for future destination shipping traffic can be drawn.

2.3.2.8 Stephenson and Smith (2015)

Stephenson and Smith (2015) is a particularly useful study whereby the explicit optimal route finding approach of Smith and Stephenson (2013) is used and results are presented for each GCM separately to reveal the climate model uncertainty in projections of Arctic shipping. These results are analysed and compared to comparable simulations conducted in this thesis in Ch.6.5.2.

Their major findings are that there is considerable model uncertainty in the future opening of Arctic routes, both in their timing and which routes are most popular. They find that the NSR is dominant in the near term and is slowly replaced by the TSR as the sea ice continues to retreat. They also note that in four of the ten GCMs used, the NWP is not navigable to PC6 vessels, a claim that this thesis will challenge and attribute to the considerable biases in the sea ice in GCMs.

2.3.2.9 Aksenov et al. (2015)

A study by Aksenov et al. (2015) addresses a slightly different aspect of Arctic shipping than those discussed previously. They discuss and present an example of a different approach to Arctic shipping simulations. They argue that higher resolution models are needed to resolve the intricacies of popular straits in the Arctic, and the marginal ice zone. They use an eddy-permitting ocean model (NEMO-ROAM025) with a considerably higher resolution than the GCMs in previous shipping studies. This high-resolution ocean model is forced with data from HadGEM2-ES RCP8.5. They present additional variables from their model that need to be considered for safe Arctic navigation such as wind speed, wave height, and ocean currents. They rightly highlight that future routing algorithms will need to consider all factors to combat multiple sea ice hazards. One omission however is that without bias-correction, the high-resolution projections will

generally just resolve the biases in finer detail. This is evident as the SIC depicts similar spatial biases to HadGEM2-ES.

The manuscript is a valuable addition to the literature and with the inclusion of appropriate bias-correction would give an exciting insight into the future direction of research in this field.

2.3.3 Effects on the climate system

A potential climatic benefit of the shorter trans-Arctic shipping routes is a reduction in global shipping emissions. This is plausible, as the shorter journeys would result in less total emissions for the same fuel efficiency; alternatively bulk-shipping journeys through the Arctic could be conducted at a relatively slower speed. As the power required is proportional to the cube of speed (Tan et al., 2013), this could lead to substantial reductions in the amount of fuel burned, hence further reducing emissions.

However, Browse et al. (2013) reveals the benefits to the climate system may not be as straight forward as that. Their study simulates the deposition of black carbon on snow released by additional Arctic shipping. They find that high-latitude black carbon deposition would indeed increase in the Arctic following increases in shipping by mid-century. However, the contribution by additional shipping is less than 1% of all Arctic black carbon deposition, although they note that regional effects are higher.

In a similar study, Granier et al. (2006) find that future shipping in the region will also increase concentrations of ozone. They show that in the summer months surface ozone concentrations could be enhanced by a factor of 2 – 3 and may become as high as values hitherto only observed in the industrialised regions of the northern hemisphere.

A study by Lindstad et al. (2016) assessed the influence of additional climate forcers that are emitted by shipping. They conclude that there are no climatic benefits to using the NSR compared to traditional routes as the emission of short-lived climate forcers into the climatically sensitive Arctic outweighs the benefits gained from shorter journeys.

Fuglestad et al. (2014) conducted an experiment whereby they simulated emissions from shipping traffic from Europe to Asia via the Suez Canal, and then compared this to a scenario whereby all this traffic sails the NSR instead. Although, given the current shipping situation it is very unlikely that Arctic routes would entirely replace the Suez Canal. They find a net radiative forcing increase of $+0.05$ to $+0.65 \text{ mWm}^{-2}$, with the

forcing components displaying a mixed response, e.g. black carbon provides a direct negative radiative forcing, but its semi-direct and snow/ice deposition effects result in a net positive radiative forcing.

Miller and Ruiz (2014) note that environmental concerns also need to be considered with a potential boom in Arctic shipping. The new routes offer the possibility of invasive species entering into Arctic waters, potentially affecting marine habitats and ecosystems. These species can be transported in ballast tanks or on the side of the ships themselves from other regions of the world and then released into a delicate foreign ecosystem. The newly ratified Polar Code (International Maritime Organization (IMO), 2015), has been partly designed with this threat in mind and contains legislation to ban the release of ballast water in the Arctic (except in an emergency) to try to mitigate this risk.

It is clear from these studies that the effects of increased shipping in the Arctic on the climate are mixed and somewhat conditional. It is hard to draw any robust conclusions, especially considering the potential advances in technology over the next 30 years. It is however clear that considering the implications of aerosols and short-lived greenhouse gases is important, in addition to the impact of increased shipping on the environment and on communities in the Arctic, is vital should Arctic shipping wish to flourish.

2.4 Discussion

Arctic sea ice is a crucial component of the earth's climate system and is changing rapidly because of anthropogenic climate change. The GCMs from CMIP5 show a marked improvement in their simulation of sea ice from their predecessors. Generally they do a reasonable job in capturing the seasonal cycle and past change to the sea ice. Although GCM performance varies across CMIP5 GCMs. This can be combatted by selecting the 'best' performing GCMs, akin to Massonnet et al. (2012), Rogers et al. (2013), and Snape and Forster (2014).

Studies on the economic attractiveness of Arctic shipping draw contrasting conclusions on its profitability based on the methods used, with roughly half of the literature finding Arctic shipping profitable over conventional routes. Studies which look at the environmental implications of Arctic shipping show equally ambivalent implications, although all warn of an increase in pollutants in the region. Some studies claim that these increases are negligible compared to increases from other sources further afield which impact the Arctic, while others argue that detailed consideration needs to be given to the regional changes that will occur as a result of increased shipping in the Arctic.

Simulating future shipping, as derived from GCM projections, is a relatively new field. Studies have increased in complexity and applicability over the last decade from single model studies assessing SIC to multi-model simulations with operational sea ice thresholds fed into explicit route finding algorithms. All such studies find an increase in the potential for Arctic shipping as the GCMs unanimously show year round reductions in Arctic sea ice.

As with all such studies, they each have their limitations. Some limitations are due to understandable limits to a single study's scope. All the studies presented here share a limitation however; their GCMs contain biases in their sea ice when compared to current observations. It is very likely that these biases remain into the future and as such, implications from such projections need to be revisited.

Despite these critiques, there has been a great deal of advancement in knowledge in this field over the last decade. This thesis will address their limitations by using multiple GCMs and ensemble members to robustly sample internal climate variability, and use multiple ship classes and emission scenarios to give a range of futures. Crucially a bias-

correction technique will be developed (Ch. 4) and implemented to find faster 21st century shipping routes through the Arctic (Ch. 6).

References

- Aksenov, Y., Popova, E. E., Yool, A., Nurser, A. J. G., Williams, T. D., Bertino, L., and Bergh, J.: On the future navigability of Arctic sea routes: High-resolution projections of the Arctic Ocean and sea ice, *Mar. Policy*, doi: <http://dx.doi.org/10.1016/j.marpol.2015.12.027>, 2015.
- Barnhart, K. R., Miller, C. R., Overeem, I., and Kay, J. E.: Mapping the future expansion of Arctic open water, *Nature Clim. Change*, doi: 10.1038/nclimate2848, 2015.
- Bindoff, N. L., Stott, P. A., AchutaRao, K. M., Allen, M. R., Gillett, N., Gutzler, D., Hansingo, K., Hegerl, G., Hu, Y., Jain, S., Mokhov, I. I., Overland, J., Perlwitz, J., Sebbari, R., and Zhang, X.: Detection and Attribution of Climate Change: from Global to Regional. In: *Climate Change 2013: The Physical Science Basis. Contribution of Working Group I to the Fifth Assessment Report of the Intergovernmental Panel on Climate Change*, edited by: Stocker, T. F., Qin, D., Plattner, G.-K., Tignor, M., Allen, S. K., Boschung, J., Nauels, A., Xia, Y., Bex, V., and Midgley, P. M., Cambridge University Press, Cambridge, United Kingdom and New York, NY, USA, 867–952, 2013, doi: 10.1017/CBO9781107415324.022.
- Boe, J., Hall, A., and Qu, X.: September sea-ice cover in the Arctic Ocean projected to vanish by 2100, *Nat. Geosci.*, 2, 341-343, doi: 10.1038/ngeo467, 2009.
- Brigham, L. W.: Think again: the Arctic, *Foreign Policy*, 71, 2010.
- Browse, J., Carslaw, K. S., Schmidt, A., and Corbett, J. J.: Impact of future Arctic shipping on high-latitude black carbon deposition, *Geophys. Res. Lett.*, 40, 4459-4463, doi: 10.1002/grl.50876, 2013.
- Byers, M.: Who owns the Arctic, *Understanding Sovereignty Disputes in the North*, 88-108, 2009.
- Cavalieri, D. J. and Parkinson, C. L.: Arctic sea ice variability and trends, 1979–2010, *Cryosphere*, 6, 881-889, doi: 10.5194/tc-6-881-2012, 2012.
- Collins, M., Booth, B. B. B., Bhaskaran, B., Harris, G. R., Murphy, J. M., Sexton, D. M. H., and Webb, M. J.: Climate model errors, feedbacks and forcings: a comparison of perturbed physics and multi-model ensembles, *Clim. Dyn.*, 36, 1737-1766, doi: 10.1007/s00382-010-0808-0, 2011.
- Collins, M., Knutti, R., Arblaster, J., Dufresne, J.-L., Fichet, T., Friedlingstein, P., Gao, X., Gutowski, W. J., Johns, T., Krinner, G., Shongwe, M., Tebaldi, C., Weaver, A. J., and Wehner, M.: Long-term Climate Change: Projections, Commitments and Irreversibility. In: *Climate Change 2013: The Physical Science Basis. Contribution of Working Group I to the Fifth Assessment Report of the Intergovernmental Panel on Climate Change*, edited by: Stocker, T. F., Qin, D., Plattner, G.-K., Tignor, M., Allen, S. K., Boschung, J., Nauels, A., Xia, Y., Bex, V., and Midgley, P. M., Cambridge University Press, Cambridge, United Kingdom and New York, NY, USA, 1029–1136, 2013, doi: 10.1017/CBO9781107415324.024.
- Comiso, J. C.: Large Decadal Decline of the Arctic Multiyear Ice Cover, *J. Clim.*, 25, 1176-1193, doi: 10.1175/jcli-d-11-00113.1, 2012.

Comiso, J. C. and Nishio, F.: Trends in the sea ice cover using enhanced and compatible AMSR-E, SSM/I, and SMMR data, *J. Geophys. Res. Oceans*, 113, doi: 10.1029/2007jc004257, 2008.

Curry, J. A., Schramm, J. L., Rossow, W. B., and Randall, D.: Overview of Arctic Cloud and Radiation Characteristics, *J. Clim.*, 9, 1731-1764, doi: doi:10.1175/1520-0442(1996)009<1731:OOACAR>2.0.CO;2, 1996.

Doronin, Y. P. and Kheisin, D. E.: *Sea ice*. Amerind Publishing Company Limited, 1977.

Duarte, C. M., Lenton, T. M., Wadhams, P., and Wassmann, P.: Abrupt climate change in the Arctic, *Nature Clim. Change*, 2, 60-62, doi: 10.1038/nclimate1386, 2012.

Eicken, H., Krouse, H. R., Kadko, D., and Perovich, D. K.: Tracer studies of pathways and rates of meltwater transport through Arctic summer sea ice, *J. Geophys. Res. Oceans*, 107, SHE 22-21-SHE 22-20, doi: 10.1029/2000jc000583, 2002.

Flato, G., Marotzke, J., Abiodun, B., Braconnot, P., Chou, S. C., Collins, W., Cox, P., Driouech, F., Emori, S., Eyring, V., Forest, C., Gleckler, P., Guilyardi, E., Jakob, C., Kattsov, V., Reason, C., and Rummukainen, M.: Evaluation of Climate Models. In: *Climate Change 2013: The Physical Science Basis. Contribution of Working Group I to the Fifth Assessment Report of the Intergovernmental Panel on Climate Change*, edited by: Stocker, T. F., Qin, D., Plattner, G.-K., Tignor, M., Allen, S. K., Boschung, J., Nauels, A., Xia, Y., Bex, V., and Midgley, P. M., Cambridge University Press, Cambridge, United Kingdom and New York, NY, USA, 741–866, 2013, doi: 10.1017/CBO9781107415324.020.

Flocco, D. and Feltham, D. L.: A continuum model of melt pond evolution on Arctic sea ice, *J. Geophys. Res. Oceans*, 112, doi: 10.1029/2006jc003836, 2007.

Flocco, D., Feltham, D. L., and Turner, A. K.: Incorporation of a physically based melt pond scheme into the sea ice component of a climate model, *J. Geophys. Res. Oceans*, 115, n/a-n/a, doi: 10.1029/2009jc005568, 2010.

Flocco, D., Schroeder, D., Feltham, D. L., and Hunke, E. C.: Impact of melt ponds on Arctic sea ice simulations from 1990 to 2007, *J. Geophys. Res. Oceans*, 117, doi: 10.1029/2012jc008195, 2012.

Francis, J. A. and Vavrus, S. J.: Evidence linking Arctic amplification to extreme weather in mid-latitudes, *Geophys. Res. Lett.*, 39, L06801, doi: 10.1029/2012gl051000, 2012.

Fuglestad, J. S., Dalsøren, S. B., Samset, B. H., Berntsen, T., Myhre, G., Hodnebrog, Ø., Eide, M. S., and Bergh, T. F.: Climate Penalty for Shifting Shipping to the Arctic, *Environmental Science & Technology*, 48, 13273-13279, doi: 10.1021/es502379d, 2014.

Giles, K. A., Laxon, S. W., and Ridout, A. L.: Circumpolar thinning of Arctic sea ice following the 2007 record ice extent minimum, *Geophys. Res. Lett.*, 35, doi: 10.1029/2008gl035710, 2008.

Granier, C., Niemeier, U., Jungclaus, J. H., Emmons, L., Hess, P., Lamarque, J.-F., Walters, S., and Brasseur, G. P.: Ozone pollution from future ship traffic in the Arctic northern passages, *Geophys. Res. Lett.*, 33, doi: 10.1029/2006gl026180, 2006.

- Haas, C., Pfaffling, A., Hendricks, S., Rabenstein, L., Etienne, J.-L., and Rigor, I.: Reduced ice thickness in Arctic Transpolar Drift favors rapid ice retreat, *Geophys. Res. Lett.*, **35**, doi: 10.1029/2008gl034457, 2008.
- Hansen, C., Grønsedt, P., Graversen, C., and Hendriksen, C.: Arctic Shipping Commercial Opportunities and Challenges, CBS Maritime, 2016.
- Holland, M. M., Bitz, C. M., and Tremblay, B.: Future abrupt reductions in the summer Arctic sea ice, *Geophys. Res. Lett.*, **33**, L23503, doi: 10.1029/2006gl028024, 2006.
- Holland, P. R. and Kwok, R.: Wind-driven trends in Antarctic sea-ice drift, *Nat. Geosci.*, **5**, 872-875, doi: 10.1038/ngeo1627 2012.
- House of Lords: Responding to a changing Arctic, 2015, <http://www.publications.parliament.uk/pa/ld201415/ldselect/ldarctic/118/118.pdf>.
- Howell, S. E. L. and Yackel, J. J.: A vessel transit assessment of sea ice variability in the Western Arctic, 1969–2002: implications for ship navigation, *Can. J. Remote Sens.*, **30**, 205-215, doi: 10.5589/m03-062, 2004.
- Hunke, E. C., Hebert, D. A., and Lecomte, O.: Level-ice melt ponds in the Los Alamos sea ice model, *CICE, Ocean Modell.*, **71**, 26-42, doi: <http://dx.doi.org/10.1016/j.ocemod.2012.11.008>, 2013.
- Hunke, E. C., Lipscomb, W. H., and Turner, A. K.: Sea-ice models for climate study: retrospective and new directions, *Journal of Glaciology*, **56**, 1162-1172, doi: 10.3189/002214311796406095, 2010.
- International Maritime Organization (IMO): <http://www.imo.org/en/MediaCentre/HotTopics/polar/>.
- Ivanova, N., Pedersen, L. T., Tonboe, R. T., Kern, S., Heygster, G., Lavergne, T., Sørensen, A., Saldo, R., Dybkjær, G., Brucker, L., and Shokr, M.: Inter-comparison and evaluation of sea ice algorithms: towards further identification of challenges and optimal approach using passive microwave observations, *Cryosphere*, **9**, 1797-1817, doi: 10.5194/tc-9-1797-2015, 2015.
- Jahn, A., Sterling, K., Holland, M. M., Kay, J. E., Maslanik, J. A., Bitz, C. M., Bailey, D. A., Stroeve, J., Hunke, E. C., Lipscomb, W. H., and Pollak, D. A.: Late-Twentieth-Century Simulation of Arctic Sea Ice and Ocean Properties in the CCSM4, *J. Clim.*, **25**, 1431-1452, doi: 10.1175/jcli-d-11-00201.1, 2012.
- Kay, J. E., Holland, M. M., and Jahn, A.: Inter-annual to multi-decadal Arctic sea ice extent trends in a warming world, *Geophys. Res. Lett.*, **38**, L15708, doi: 10.1029/2011gl048008, 2011.
- Khon, V. C., Mokhov, I. I., Latif, M., Semenov, V. A., and Park, W.: Perspectives of Northern Sea Route and Northwest Passage in the twenty-first century, *Clim. Change*, **100**, 757-768, doi: 10.1007/s10584-009-9683-2, 2010.
- Kinnard, C., Zdanowicz, C. M., Fisher, D. A., Isaksson, E., de Vernal, A., and Thompson, L. G.: Reconstructed changes in Arctic sea ice over the past 1,450 years, *Nature*, **479**, 509-512, doi: 10.1038/nature10581, 2011.

Kirtman, B., Power, S. B., Adedoyin, J. A., Boer, G. J., Bojariu, R., Camilloni, I., Doblaser-Reyes, F. J., Fiore, A. M., Kimoto, M., Meehl, G. A., Prather, M., Sarr, A., Schar, C., Sutton, R., van Oldenborgh, G. J., Vecchi, G., and Wang, H. J.: Near-term Climate Change: Projections and Predictability. In: *Climate Change 2013: The Physical Science Basis. Contribution of Working Group I to the Fifth Assessment Report of the Intergovernmental Panel on Climate Change*, edited by: Stocker, T. F., Qin, D., Plattner, G.-K., Tignor, M., Allen, S. K., Boschung, J., Nauels, A., Xia, Y., Bex, V., and Midgley, P. M., Cambridge University Press, Cambridge, United Kingdom and New York, NY, USA, 953–1028, 2013, doi: 10.1017/CBO9781107415324.023.

Koldunov, N. V., Stammer, D., and Marotzke, J.: Present-Day Arctic Sea Ice Variability in the Coupled ECHAM5/MPI-OM Model, *J. Clim.*, **23**, 2520-2543, doi: 10.1175/2009jcli3065.1, 2010.

Kwok, R.: Outflow of Arctic Ocean Sea Ice into the Greenland and Barents Seas: 1979–2007, *J. Clim.*, **22**, 2438-2457, doi: 10.1175/2008jcli2819.1, 2009.

Kwok, R. and Rothrock, D. A.: Decline in Arctic sea ice thickness from submarine and ICESat records: 1958–2008, *Geophys. Res. Lett.*, **36**, doi: 10.1029/2009gl039035, 2009.

Lasserre, F.: Case studies of shipping along Arctic routes. Analysis and profitability perspectives for the container sector, *Transp. Res. Part A Policy Pract.*, **66**, 144-161, doi: <http://dx.doi.org/10.1016/j.tra.2014.05.005>, 2014.

Lasserre, F. and Pelletier, S.: Polar super seaways? Maritime transport in the Arctic: an analysis of shipowners' intentions, *J. Transp. Geogr.*, **19**, 1465-1473, doi: 10.1016/j.jtrangeo.2011.08.006, 2011.

Laxon, S. W., Giles, K. A., Ridout, A. L., Wingham, D. J., Willatt, R., Cullen, R., Kwok, R., Schweiger, A., Zhang, J., Haas, C., Hendricks, S., Krishfield, R., Kurtz, N., Farrell, S., and Davidson, M.: CryoSat-2 estimates of Arctic sea ice thickness and volume, *Geophys. Res. Lett.*, **40**, 732-737, doi: 10.1002/Grl.50193, 2013.

Lenton, T. M., Held, H., Kriegler, E., Hall, J. W., Lucht, W., Rahmstorf, S., and Schellnhuber, H. J.: Tipping elements in the Earth's climate system, *Proc. Natl. Acad. Sci. U.S.A.*, **105**, 1786-1793, doi: 10.1073/pnas.0705414105, 2008.

Lindsay, R. W. and Zhang, J.: The Thinning of Arctic Sea Ice, 1988–2003: Have We Passed a Tipping Point?, *J. Clim.*, **18**, 4879-4894, doi: 10.1175/jcli3587.1, 2005.

Lindsay, R. W., Zhang, J., Schweiger, A., Steele, M., and Stern, H.: Arctic Sea Ice Retreat in 2007 Follows Thinning Trend, *J. Clim.*, **22**, 165-176, doi: 10.1175/2008jcli2521.1, 2009.

Livina, V. N. and Lenton, T. M.: A recent tipping point in the Arctic sea-ice cover: abrupt and persistent increase in the seasonal cycle since 2007, *Cryosphere*, **7**, 275-286, doi: 10.5194/tc-7-275-2013, 2013.

Macias Fauria, M., Grinsted, A., Helama, S., Moore, J., Timonen, M., Martma, T., Isaksson, E., and Eronen, M.: Unprecedented low twentieth century winter sea ice extent in the Western Nordic Seas since A.D. 1200, *Clim. Dyn.*, **34**, 781-795, doi: 10.1007/s00382-009-0610-z, 2009.

- Mahlstein, I. and Knutti, R.: September Arctic sea ice predicted to disappear near 2°C global warming above present, *J. Geophys. Res. Atmos.*, 117, D06104, doi: 10.1029/2011jd016709, 2012.
- Mahoney, A., Eicken, H., and Shapiro, L.: How fast is landfast sea ice? A study of the attachment and detachment of nearshore ice at Barrow, Alaska, *Cold Reg. Sci. Technol.*, 47, 233-255, doi: <http://dx.doi.org/10.1016/j.coldregions.2006.09.005>, 2007.
- Markus, T. and Cavalieri, D. J.: An enhancement of the NASA Team sea ice algorithm, *IEEE Transactions on Geoscience and Remote Sensing*, 38, 1387-1398, doi: 10.1109/36.843033, 2000.
- Markus, T., Stroeve, J. C., and Miller, J.: Recent changes in Arctic sea ice melt onset, freezeup, and melt season length, *J. Geophys. Res. Oceans*, 114, doi: 10.1029/2009jc005436, 2009.
- Maslanik, J. A., Fowler, C., Stroeve, J., Drobot, S., Zwally, J., Yi, D., and Emery, W.: A younger, thinner Arctic ice cover: increased potential for rapid, extensive sea-ice loss, *Geophys. Res. Lett.*, 34, L24501, doi: 10.1029/2007gl032043, 2007.
- Maslowski, W., Kinney, J. C., Higgins, M., and Roberts, A.: The Future of Arctic Sea Ice, *Annual Review of Earth and Planetary Sciences*, 40, 625-654, doi: doi:10.1146/annurev-earth-042711-105345, 2012.
- Massonnet, F., Fichfet, T., Goose, H., Bitz, C. M., Philippon-Berthier, G., Holland, M. M., and Barriat, P. Y.: Constraining projections of summer Arctic sea ice, *Cryosphere*, 6, 1383-1394, doi: 10.5194/tc-6-1383-2012, 2012.
- Maykut, G. A. and Perovich, D. K.: The role of shortwave radiation in the summer decay of a sea ice cover, *J. Geophys. Res. Oceans*, 92, 7032-7044, doi: 10.1029/JC092iC07p07032, 1987.
- Meier, W. N., Stroeve, J., Barrett, A., and Fetterer, F.: A simple approach to providing a more consistent Arctic sea ice extent time series from the 1950s to present, *Cryosphere*, 6, 1359-1368, doi: 10.5194/tc-6-1359-2012, 2012.
- Melia, N., Haines, K., and Hawkins, E.: Improved Arctic sea ice thickness projections using bias-corrected CMIP5 simulations, *Cryosphere*, 9, 2237-2251, doi: 10.5194/tc-9-2237-2015, 2015.
- Melsom, A., Lien, V. S., and Budgell, W. P.: Using the Regional Ocean Modeling System (ROMS) to improve the ocean circulation from a GCM 20th century simulation, *Ocean Dynamics*, 59, 969-981, doi: 10.1007/s10236-009-0222-5, 2009.
- Miller, A. W. and Ruiz, G. M.: Arctic shipping and marine invaders, *Nature Clim. Change*, 4, 413-416, doi: 10.1038/nclimate2244, 2014.
- Min, S.-K., Zhang, X., Zwiers, F. W., and Agnew, T.: Human influence on Arctic sea ice detectable from early 1990s onwards, *Geophys. Res. Lett.*, 35, doi: 10.1029/2008gl035725, 2008.

Mokhov, I., Khon, V. C., and Roeckner, E.: Variations in the ice cover of the Arctic Basin in the 21st century based on model simulations: Estimates of the perspectives of the Northern Sea Route, 2007, 759.

Notz, D.: Thermodynamic and fluid-dynamical processes in sea ice, PhD, University of Cambridge, 2005.

Notz, D.: The future of ice sheets and sea ice: Between reversible retreat and unstoppable loss, *Proc. Natl. Acad. Sci. U.S.A.*, 106, 20590-20595, doi: 10.1073/pnas.0902356106, 2009.

Notz, D.: Sea-ice extent and its trend provide limited metrics of model performance, *Cryosphere*, 8, 229-243, doi: 10.5194/tc-8-229-2014, 2014.

Notz, D., Haumann, F. A., Haak, H., Jungclaus, J. H., and Marotzke, J.: Arctic sea-ice evolution as modeled by Max Planck Institute for Meteorology's Earth system model, *Journal of Advances in Modeling Earth Systems*, 5, 173-194, doi: 10.1002/jame.20016, 2013.

Overland, J. E. and Wang, M.: When will the summer Arctic be nearly sea ice free?, *Geophys. Res. Lett.*, 40, 2097-2101, doi: 10.1002/grl.50316, 2013.

Parker, D. E., Legg, T. P., and Folland, C. K.: A new daily central England temperature series, 1772–1991, *International Journal of Climatology*, 12, 317-342, doi: 10.1002/joc.3370120402, 1992.

Parkinson, C. L.: Spatially mapped reductions in the length of the Arctic sea ice season, *Geophys. Res. Lett.*, 41, 4316-4322, doi: 10.1002/2014gl060434, 2014.

Polyakov, I. V., Alekseev, G. V., Bekryaev, R. V., Bhatt, U. S., Colony, R., Johnson, M. A., Karklin, V. P., Walsh, D., and Yulin, A. V.: Long-Term Ice Variability in Arctic Marginal Seas, *J. Clim.*, 16, 2078-2085, doi: 10.1175/1520-0442(2003)016<2078:liviam>2.0.co;2, 2003.

Rampal, P., Weiss, J., and Marsan, D.: Positive trend in the mean speed and deformation rate of Arctic sea ice, 1979–2007, *J. Geophys. Res. Oceans*, 114, doi: 10.1029/2008jc005066, 2009.

Rayner, N. A., Parker, D. E., Horton, E. B., Folland, C. K., Alexander, L. V., Rowell, D. P., Kent, E. C., and Kaplan, A.: Global analyses of sea surface temperature, sea ice, and night marine air temperature since the late nineteenth century, *Journal of Geophysical Research-Atmospheres*, 108, 4407, doi: 10.1029/2002jd002670, 2003.

Rogers, T., Walsh, J., Rupp, T., Brigham, L., and Sfraga, M.: Future Arctic marine access: analysis and evaluation of observations, models, and projections of sea ice, *Cryosphere*, 7, 321-332, doi: 10.5194/tc-7-321-2013, 2013.

Rothrock, D. A., Percival, D. B., and Wensnahan, M.: The decline in arctic sea-ice thickness: Separating the spatial, annual, and interannual variability in a quarter century of submarine data, *J. Geophys. Res.*, 113, C05003, doi: 10.1029/2007jc004252, 2008.

Schröder, D., Feltham, D. L., Flocco, D., and Tsamados, M.: September Arctic sea-ice minimum predicted by spring melt-pond fraction, *Nature Clim. Change*, 4, 353-357, doi: 10.1038/nclimate2203, 2014.

Schweiger, A., Lindsay, R., Zhang, J., Steele, M., Stern, H., and Kwok, R.: Uncertainty in modeled Arctic sea ice volume, *J. Geophys. Res. Oceans*, 116, C00D06, doi: 10.1029/2011jc007084, 2011.

Smith, L. C. and Stephenson, S. R.: New Trans-Arctic shipping routes navigable by midcentury, *Proc. Natl. Acad. Sci. U.S.A.*, 110, E1191–E1195, doi: 10.1073/pnas.1214212110, 2013.

Snape, T. J. and Forster, P. M.: Decline of Arctic sea ice: Evaluation and weighting of CMIP5 projections, *J. Geophys. Res. Atmos.*, 2013JD020593, doi: 10.1002/2013jd020593, 2014.

Sprenn, G., Kwok, R., and Menemenlis, D.: Trends in Arctic sea ice drift and role of wind forcing: 1992–2009, *Geophys. Res. Lett.*, 38, doi: 10.1029/2011gl048970, 2011.

Stammerjohn, S., Massom, R., Rind, D., and Martinson, D.: Regions of rapid sea ice change: An inter-hemispheric seasonal comparison, *Geophys. Res. Lett.*, 39, doi: 10.1029/2012gl050874, 2012.

Stephenson, S. R., Brigham, L. W., and Smith, L. C.: Marine accessibility along Russia's Northern Sea Route, *Polar Geogr.*, 1-23, doi: 10.1080/1088937x.2013.845859, 2013a.

Stephenson, S. R. and Smith, L. C.: Influence of climate model variability on projected Arctic shipping futures, *Earth's Future*, 3, 331-343, doi: 10.1002/2015ef000317, 2015.

Stephenson, S. R., Smith, L. C., and Agnew, J. A.: Divergent long-term trajectories of human access to the Arctic, *Nature Clim. Change*, 1, 156-160, doi: 10.1038/nclimate1120, 2011.

Stephenson, S. R., Smith, L. C., Brigham, L. W., and Agnew, J. A.: Projected 21st-century changes to Arctic marine access, *Clim. Change*, 118, 885-899, doi: 10.1007/s10584-012-0685-0, 2013b.

Stroeve, J., Barrett, A., Serreze, M., and Schweiger, A.: Using records from submarine, aircraft and satellite to evaluate climate model simulations of Arctic sea ice thickness, *Cryosphere*, 8, 1839-1845, doi: 10.5194/tc-8-1839-2014, 2014a.

Stroeve, J., Hamilton, L. C., Bitz, C. M., and Blanchard-Wrigglesworth, E.: Predicting September sea ice: Ensemble skill of the SEARCH Sea Ice Outlook 2008–2013, *Geophys. Res. Lett.*, 41, 2411-2418, doi: 10.1002/2014gl059388, 2014b.

Stroeve, J., Holland, M. M., Meier, W., Scambos, T., and Serreze, M.: Arctic sea ice decline: Faster than forecast, *Geophys. Res. Lett.*, 34, doi: 10.1029/2007GL029703, 2007.

Stroeve, J., Serreze, M., Holland, M., Kay, J., Malanik, J., and Barrett, A.: The Arctic's rapidly shrinking sea ice cover: a research synthesis, *Clim. Change*, 110, 1005-1027, doi: 10.1007/s10584-011-0101-1, 2012a.

Stroeve, J. C., Kattsov, V., Barrett, A., Serreze, M., Pavlova, T., Holland, M., and Meier, W. N.: Trends in Arctic sea ice extent from CMIP5, CMIP3 and observations, *Geophys. Res. Lett.*, 39, L16502, doi: 10.1029/2012gl052676, 2012b.

Swart, N. C., Fyfe, J. C., Hawkins, E., Kay, J. E., and Jahn, A.: Influence of internal variability on Arctic sea-ice trends, *Nature Clim. Change*, 5, 86-89, doi: 10.1038/nclimate2483, 2015.

Tan, X., Su, B., Riska, K., and Moan, T.: A six-degrees-of-freedom numerical model for level ice–ship interaction, *Cold Reg. Sci. Technol.*, 92, 1-16, doi: <http://dx.doi.org/10.1016/j.coldregions.2013.03.006>, 2013.

Taylor, K. E., Stouffer, R. J., and Meehl, G. A.: An overview of CMIP5 and the experiment design, *Bull. Am. Meteorol. Soc.*, 93, 485-498, doi: 10.1175/Bams-D-11-00094.1, 2012.

Taylor, P. C., Kato, S., Xu, K.-M., and Cai, M.: Covariance between Arctic sea ice and clouds within atmospheric state regimes at the satellite footprint level, *J. Geophys. Res. Atmos.*, 120, 12656-12678, doi: 10.1002/2015jd023520, 2015.

The Economist: Short and sharp, 2012, <http://www.economist.com/node/21556803>.

Thomson, J. and Rogers, W. E.: Swell and sea in the emerging Arctic Ocean, *Geophys. Res. Lett.*, 41, 3136-3140, doi: 10.1002/2014gl059983, 2014.

Tilling, R. L., Ridout, A., and Shepherd, A.: Near Real Time Arctic sea ice thickness and volume from CryoSat-2, *The Cryosphere Discuss.*, 2016, 1-15, doi: 10.5194/tc-2016-21, 2016.

Tilling, R. L., Ridout, A., Shepherd, A., and Wingham, D. J.: Increased Arctic sea ice volume after anomalously low melting in 2013, *Nat. Geosci.*, 8, 643-646, doi: 10.1038/ngeo2489, 2015.

Transport Canada: Arctic Ice Regime Shipping System (AIRSS) Standards, Transport Publication, 12259 E, 1998.

Tsamados, M., Feltham, D. L., Schroeder, D., Flocco, D., Farrell, S. L., Kurtz, N., Laxon, S. W., and Bacon, S.: Impact of Variable Atmospheric and Oceanic Form Drag on Simulations of Arctic Sea Ice, *Journal of Physical Oceanography*, 44, 1329-1353, doi: 10.1175/JPO-D-13-0215.1, 2014.

Van Vuuren, D. P., Edmonds, J., Kainuma, M., Riahi, K., Thomson, A., Hibbard, K., Hurtt, G. C., Kram, T., Krey, V., and Lamarque, J.-F.: The representative concentration pathways: an overview, *Clim. Change*, 109, 5-31, doi: 10.1007/s10584-011-0148-z, 2011.

Vaughan, D. G., Comiso, J. C., Allison, I., Carrasco, J., Kaser, G., Kwok, R., Mote, P., Murray, T., Paul, F., Ren, J., Rignot, E., Solomina, O., Steffen, K., and Zhang, T.: Observations: Cryosphere. In: *Climate Change 2013: The Physical Science Basis. Contribution of Working Group I to the Fifth Assessment Report of the Intergovernmental Panel on Climate Change*, edited by: Stocker, T. F., Qin, D., Plattner, G.-K., Tignor, M., Allen, S. K., Boschung, J., Nauels, A., Xia, Y., Bex, V., and Midgley, P. M., Cambridge University Press, Cambridge, United Kingdom and New York, NY, USA, 317–382, 2013, doi: 10.1017/CBO9781107415324.012.

- Vavrus, S., Waliser, D., Schweiger, A., and Francis, J.: Simulations of 20th and 21st century Arctic cloud amount in the global climate models assessed in the IPCC AR4, *Clim. Dyn.*, 33, 1099-1115, doi: 10.1007/s00382-008-0475-6, 2008.
- Wadhams, P.: Sea ice thickness distribution in Fram Strait, *Nature*, 305, 108-111, doi: 10.1038/305108a0, 1983.
- Wadhams, P.: Evidence for thinning of the Arctic ice cover north of Greenland, *Nature*, 345, 795-797, doi: 10.1038/345795a0, 1990.
- Wadhams, P. and Davis, N. R.: Further evidence of ice thinning in the Arctic Ocean, *Geophys. Res. Lett.*, 27, 3973-3975, doi: 10.1029/2000gl011802, 2000.
- Walsh, J. E. and Chapman, W. L.: 20th-century sea-ice variations from observational data, *Annals of Glaciology*, 33, 444-448, doi: 10.3189/172756401781818671, 2001.
- Wang, J., Zhang, J., Watanabe, E., Ikeda, M., Mizobata, K., Walsh, J. E., Bai, X., and Wu, B.: Is the Dipole Anomaly a major driver to record lows in Arctic summer sea ice extent?, *Geophys. Res. Lett.*, 36, doi: 10.1029/2008gl036706, 2009.
- Wang, M. and Overland, J. E.: A sea ice free summer Arctic within 30 years: An update from CMIP5 models, *Geophys. Res. Lett.*, 39, L18501, L18501, doi: 10.1029/2012gl052868, 2012.
- Wergeland, T.: The Northern Sea Route: rosy prospects for commercial shipping, *International Challenges*, 12, 43-57, 1992.
- Wiese, M., Griewank, P., and Notz, D.: On the thermodynamics of melting sea ice versus melting freshwater ice, *Annals of Glaciology*, 56, 191-199, 2015.
- Wu, Z., Wang, B., Li, J., and Jin, F.-F.: An empirical seasonal prediction model of the east Asian summer monsoon using ENSO and NAO, *J. Geophys. Res. Atmos.*, 114, doi: 10.1029/2009jd011733, 2009.
- Zhang, J., Lindsay, R., Schweiger, A., and Steele, M.: The impact of an intense summer cyclone on 2012 Arctic sea ice retreat, *Geophys. Res. Lett.*, doi: 10.1002/grl.50190, 2013.
- Zhang, J., Lindsay, R., Steele, M., and Schweiger, A.: What drove the dramatic retreat of arctic sea ice during summer 2007?, *Geophys. Res. Lett.*, 35, L11505, doi: 10.1029/2008gl034005, 2008.
- Zhang, J. and Rothrock, D.: Modeling global sea ice with a thickness and enthalpy distribution model in generalized curvilinear coordinates, *Mon. Weather Rev.*, 131, 845-861, doi: 10.1175/1520-0493(2003)131<0845:MGSIIWA>2.0.CO;2, 2003.
- Zygmuntowska, M., Rampal, P., Ivanova, N., and Smedsrud, L. H.: Uncertainties in Arctic sea ice thickness and volume: new estimates and implications for trends, *Cryosphere*, 8, 705-720, doi: 10.5194/tc-8-705-2014, 2014.

Chapter 3

The Arctic early 20th century warming

Summary

“The [Arctic early 20th century] warming is one of the most puzzling climate anomalies of the 20th century” (Bengtsson et al., 2004).

In addition to the current warming period, a large-scale acceleration in temperatures occurred during the early part of the 20th century, as recorded in observations and literature from the era. This warming caused reductions in the Arctic sea ice that was observed by sailors and scientists at the time. Simulations from the Met Office earth system model, HadGEM2-ES, also show a large decline in sea ice around this period when the historical forcings are used. The possible cause of the decline in sea ice is investigated by using HadGEM2-ES to simulate the historical climate with individual forcing constituents isolated in turn.

The individual forcing experiments reveal that both natural and anthropogenic greenhouse forcings were responsible for the sea ice decline 1915 – 1930, while aerosols likely continued and maintained the anomaly during the 1930s and 1940s. However, the individual impact of all these forcings (natural, anthropogenic greenhouse gas, and aerosol) do not entirely account for the magnitude of the trend simulated in the historical simulations. This implies that internal variability likely also contributed.

The spatial signature of modelled ice loss indicates that separate forcings were responsible for distinct regional changes in the sea ice; it is suggested that the complimentary combination of these individual forcings resulted in the pattern of ice loss observed. It is clear that future attribution work on the early 20th century warming should continue to use individual forcing simulations and focus on regional changes. For the effects of internal variability to be robustly quantified, an ensemble larger than the four-member ensemble used here is likely required.

3.1 Past change

The principal questions this chapter addresses are:

1. *Can a GCM reproduce the changes to sea ice observed in the Arctic during the early 20th century?*
2. *What different factors contributed to the Arctic sea ice loss?*

To understand better the current decline trend in Arctic sea ice, the past is examined to see if a similar event can be found. A similar question was asked by Serreze et al. (2007) who questioned whether the recent warming and ice loss seen in the Arctic was unique in the instrumental record. The rate of climate change depicts variability on time scales from decadal to millennial. This variability is found during the 20th century, and whilst much of the scope of this thesis uses global climate models (GCMs) to project the future, examining historical simulations has the distinct advantage of being able to compare to observations. There are two periods of accelerated warming since 1900, the recent 1975 – present period, and also a period in the first half of the century 1910 – 1940 where global temperature increased 0.5°C in 30 years (Figure 3.1). This period is known as the early 20th century warming (ETCW). Temperature anomalies in the Arctic during the 1930s were apparently as large as those in the 1990s and 2000s.

The first clue to the cause of the ETCW is to examine the signature it left on the climate system. According to Bindoff et al. (2013) and Brohan et al. (2006) signs of the ETCW are found in the northern hemisphere temperature record, however, Johannessen et al. (2004) and Wood and Overland (2010) find that it failed to materialise in the mid-latitudes and on the Pacific side of the Arctic respectively. This regional warming signature indicates that internal variability likely has significant role to play in the ETCW.

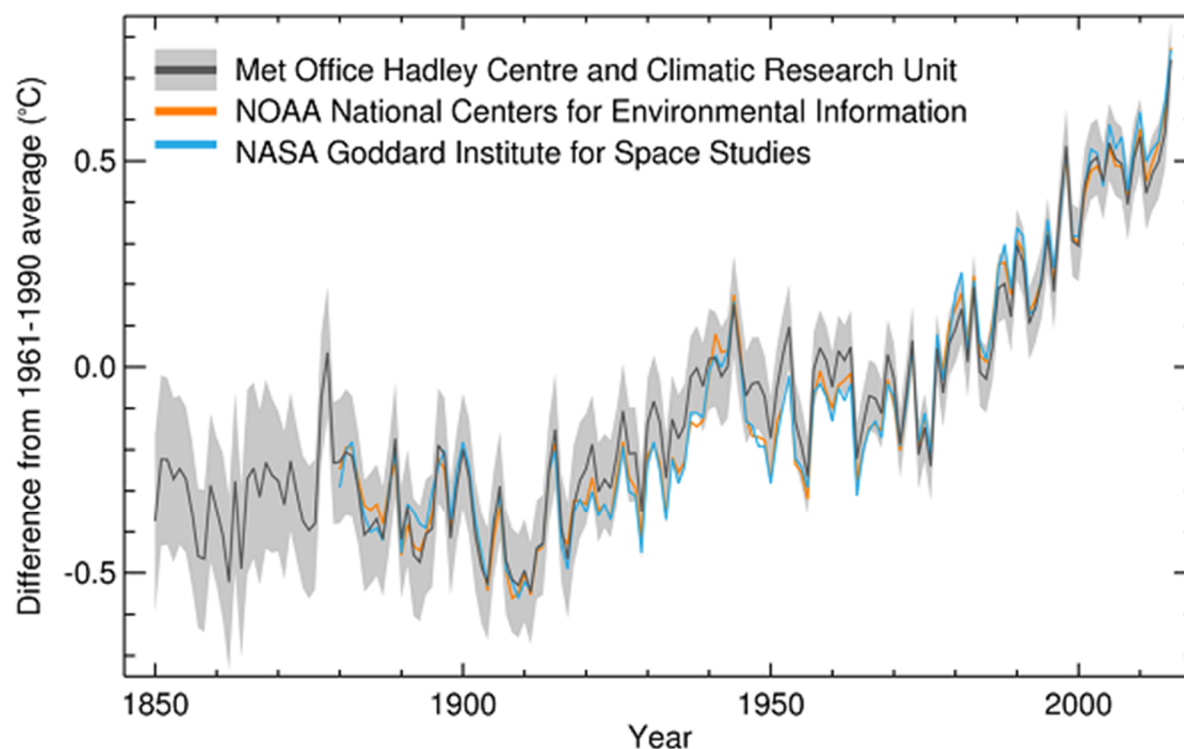


Figure 3.1 | Global average temperature anomaly from 1850 – 2015 relative to the 1961 – 1990 average. Met Office data (black) HadCRUT4 (Morice et al., 2012) (with 95% confidence range (grey). NOAA data (orange), MLOST (Peterson and Vose, 1997), and NASA data (blue), GISTEMP (Hansen et al., 2010). Figure source: Met Office, UK.

3.1.1 Past changes to Arctic Sea ice

Records of sea ice are available for the last few centuries but it is only since the introduction of satellite observations starting in the 1970's that records started to become spatially and temporally comprehensive. Past observations off the east coast of Iceland, show a decrease in sea ice from the 1900's through to 1940, with a subsequent recovery in the following 20 years (Koch, 1945; Kelly et al., 1987).

Historical direct and proxy records of shipping activity provide an invaluable insight into the sparsely visited Arctic Ocean. These are constrained however to locations near ports and on shipping lanes. Caution also needs to be applied when interpreting data though they certainly provide a useful qualitative tool.

One of the earliest records of the ETCW in the literature is from Ifft (1922), who reports on “radical change in climatic conditions, and hitherto un-heard-of high temperatures” in the eastern Arctic where fishermen, seal hunters, and explorers were sending back reports from. Ifft (1922) also reports that record sailing in open-water was possible as

far north as 81° 29' and a “very warm” Gulf Steam. Seasoned Arctic mariners reported that the landscape was completely unrecognisable and as early as 1924 the possibility of a navigable northern sea route was even considered by the Leningrad Arctic Institute (Ahlmann, 1946).

Early expeditions such as Nansen’s Fram, 1893 – 1896, used ice-hardened ships designed to be frozen into, and drift with the ice pack collecting climatic data en route. Their mission was repeated 40 years later (1937 – 1940) with the Russian Icebreaker Sedov (Ahlmann, 1946). The differences observed were stark. The annual mean temperature had increased by 6°C, and by 14°C for the winter months. Sea ice thickness (SIT) had decreased from 3.64 m to 2.18 m. The route was also completed in half the time of Fram’s, suggesting a faster ice drift and generally easier navigational conditions, though the more modern ship probably played a role when in transit under propulsion.

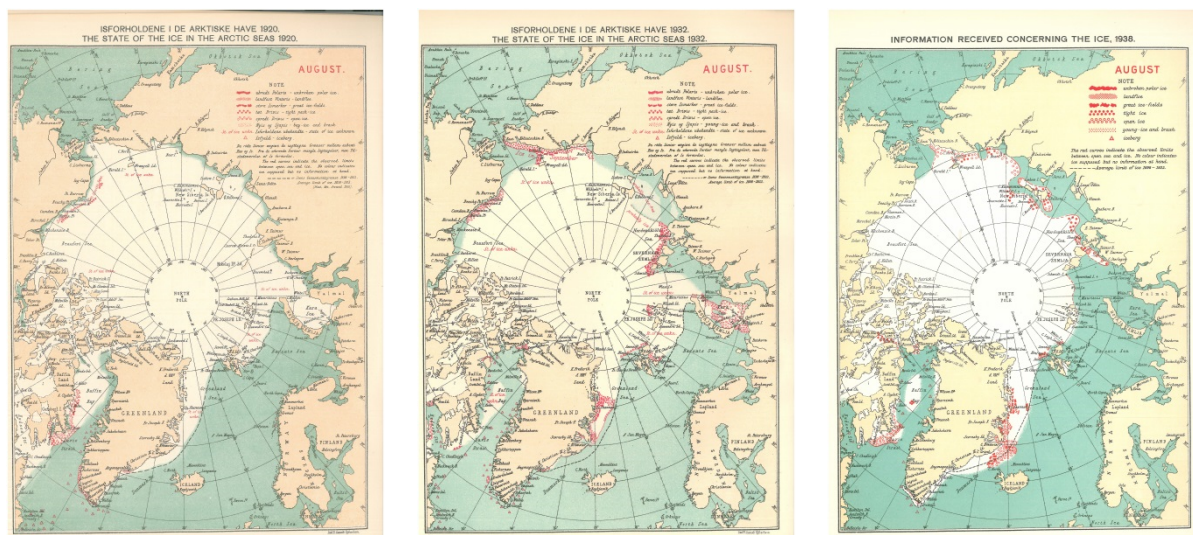


Figure 3.2 | Danish Meteorology Institute (DMI) sea ice extent charts, August 1920, 1932, 1938.

The Danish Meteorological Institute (DMI) has recently released digitised maps showing monthly Arctic ice extent. The charts show typical conditions before the ETCW (1920), a chart from 1932 when the Northern Sea Route was first navigated by the Russian ship Sibiriyakov and then the ETCW minimum around 1939 where large swaths of the Russian Arctic sea are ice-free.

3.2 Attribution of the Arctic early 20th century warming

Previous work on the ETCW has proposed a variety of principle causes: internal variability — Tett et al. (2002), Bengtsson et al. (2004), Bronnimann (2009), Grant et al. (2009), Wood and Overland (2010), and Jones et al. (2013); natural forcings — Karoly et al. (2003), Nozawa et al. (2005), and Shiogama et al. (2006); and anthropogenic forcings — Delworth and Knutson (2000) and Stott et al. (2001); while Polyakov et al. (2003) argues that air temperatures in the region undergo a 50 to 80 year natural cycle. It is likely that some combination of these forcings are responsible. The North Atlantic is often highlighted as a region of importance due to the rapid warming observed and relatively good observations. In fact, even today the North Atlantic remains an intriguing area with the anomalous North Atlantic cold pool obvious in analysis of global temperature anomalies in models and observations (Rahmstorf et al., 2015). The Arctic was (and to some extent remains) a sparsely observed area. Overpeck et al. (1997) states that the Arctic ETCW (AETCW) began earlier than other regions and was of a larger magnitude; Bengtsson et al. (2004) suggests natural variability as the cause.

The AETCW has implications outside of the Arctic, for example potentially causing an increase flux of freshwater into the North Atlantic. Schmith and Hansen (2003) found ice export through the Fram Strait decreased from 1900; however, models do not show a decrease until the 1920s. Several studies have proposed links between the Arctic and Atlantic meridional overturning circulation (AMOC). Frankcombe and Dijkstra (2011) found surface salinity changes in the Arctic caused changes to the AMOC in the GFDL GCM. However, Miles et al. (2014) found the opposite causation with the AMOC leading Arctic changes.

There remains considerable discussion over the temperature anomalies that caused the AETCW (Ahlmann, 1946; Hegerl et al., 2007) with internal variability a likely factor. This chapter aims to identify changes to the Arctic sea ice in the ETCW and potentially attribute this to forcings via the Hadley Centre Global Environmental Model version 2, Earth System model (HadGEM2-ES) historical forcings simulations, a full model description can be found in Collins et al. (2011) and The HadGEM2 Development Team et al. (2011). HadGEM2-ES is selected for this study as the model is notable for including a number of aerosol processes that are interactively calculated rather than specified in advance (Booth et al., 2012). It is important to be aware of the limitations of

attributions via a single GCM, as every model has its own biases and the literature illustrates that opposite signals can be found between models.

3.2.1 Internal variability

Internal variability is the natural fluctuations of the climate present without any induced changes via radiative forcing. These are intrinsic interactions between different components of the climate system that occur on a variety of spatial and temporal scales. Examples of this climate behaviour include the North Atlantic Oscillation (NAO) cycle, which occurs with no particular periodicity in North Atlantic atmospheric pressure and affects weather in Europe (see Hurrell (1995)). The El Niño Southern Oscillation (ENSO), an irregular cycle in the tropical Pacific winds and sea surface temperatures affecting global climate (see Trenberth (1997)). The Pacific Decadal Oscillation (PDO) an ENSO type pattern that can exist for decades (see Mantua et al. (1997) and Zhang et al. (1997)).

These can be thought of as the climate's personality, entirely natural ramifications of the redistribution of energy in the climate system. Simulations with GCMs should be able to robustly reproduce them; however, detecting climate cycles can be problematic, let alone attributing changes to them as they are often masked by other signals e.g. longer-term trends or shorter-term noise.

3.2.2 All forcings simulations

Simulations that are conducted including all forcings that are possible to model are termed all forcing simulations; they are the standard type of simulations run in CMIP5 for the past and future. Their aim is to accurately reproduce the past historical climate for when reliable observations and forcing records exist (1860 – 2005), and the future climate from 2006 with a set of assumed future forcing scenarios, i.e. the RCPs as discussed in Ch. 2. They contain all known significant forcings including human influenced well mixed greenhouse gases, aerosols, land use changes etc. in addition to natural forcings including changes to solar irradiance and volcanic eruptions. A summary of the components of the total radiative forcing is shown in Figure 3.3.

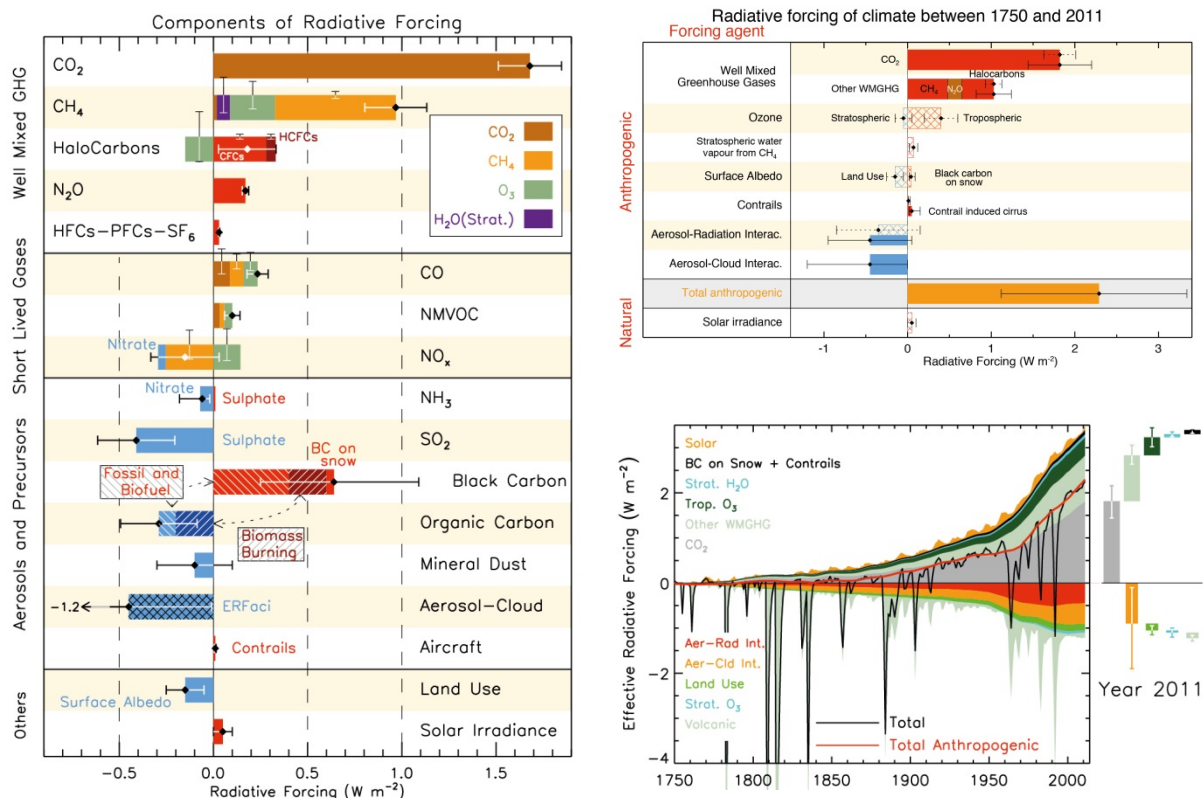


Figure 3.3 | Left: radiative forcing (RF) bar chart for the period 1750–2011 based on emitted compounds (gases, aerosols or aerosol precursors) or other changes. Top-right: Bar chart for RF (hatched) and effective-RF (ERF) (solid) for the period 1750–2011, where the total ERF is derived from Figure 8.16. Uncertainties (5 to 95% confidence range) are given for RF (dotted lines) and ERF (solid lines). Bottom-right: time evolution of forcing for anthropogenic and natural forcing mechanisms. (Myhre et al., 2013) (AR5 Figs. 8.17, 8.15, 8.18).

These historical runs can be used as a benchmark of a GCMs performance by comparing them with time series of observed variables. As GCMs often have biases this is often done in an anomaly framework where the ability of climate models to robustly capture the timing and magnitude of changes is prioritised over the absolute value of a particular variable.

Generally greenhouse gases, the concentration of which has and continues to increase from anthropogenic activity, causes an increase in radiative forcing and hence an increase in temperature. Aerosols generally have a negative radiative forcing, though the uncertainty here is far larger than for GHG. The one exception to this is black carbon, which can increase radiative forcing through albedo effects on snow and ice. Large volcanic eruptions have a very strong negative effective radiative forcing, though this effect is short lived and dependant on the particulars of the eruption.

The Climate Model Inter-comparison Project (CMIP5) experimental set-up states that historical runs are conducted from 1860-2005 with observed forcings, termed here as the ‘all forcings run’ (*All*). The oceanic component of HadGEM2-ES has a latitude-longitude grid, with a zonal resolution of 1° everywhere and a meridional resolution of 1° between the poles and 30° latitude (higher resolution in the tropics). Four separate ensemble members of HadGEM2-ES were utilised to sample internal variability. To try to reduce the effect of the small ensemble size the ensembles were initialised in 1860 from differing Atlantic Multidecadal Oscillation (AMO) states (Thompson, 2015).

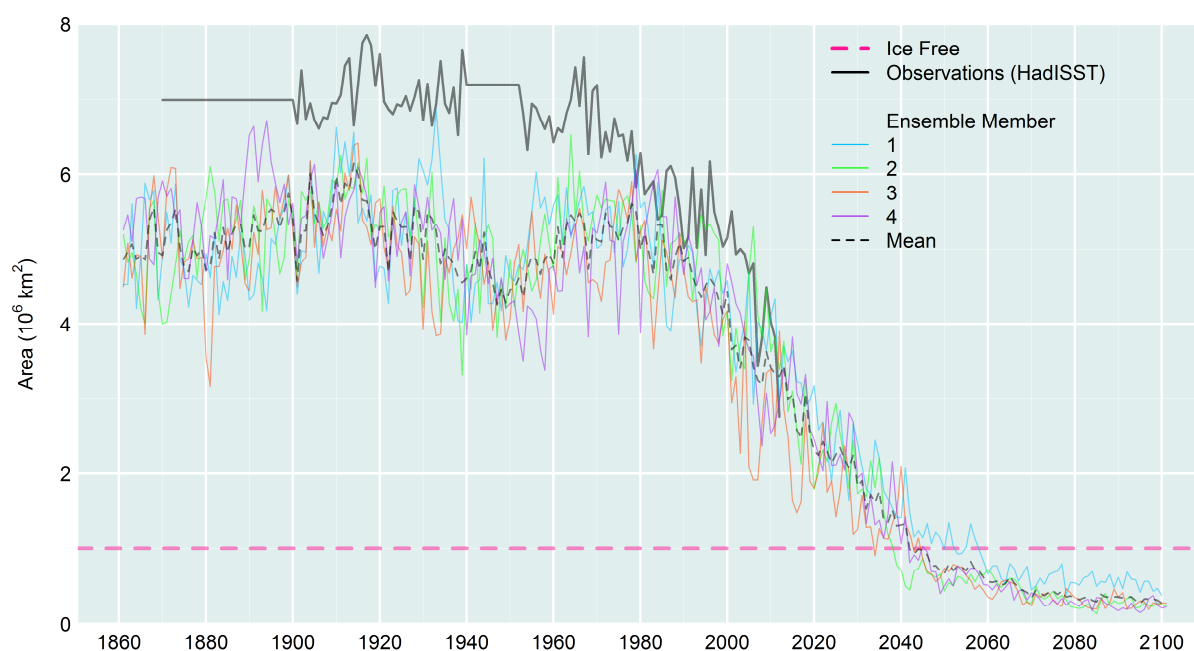


Figure 3.4 | HadISST and HadGEM2-ES historical and RCP4.5 September Arctic sea ice area.

Sea ice area is an integrated metric. The latitude dependant area of each grid cell is calculated and multiplied by that grid cell’s sea ice concentration (SIC). This is repeated for every grid cell giving the total sea ice area shown in Figure 3.4. The black line in Figure 3.4 represents the Hadley Centre Sea Ice and Sea Surface Temperature data set (HadISST1) (Rayner et al., 2003). Data from hand drawn ice charts is used pre 1978 and climatology assumed for years with no data (flat regions, pre ice charts and during and post-World War II). Passive microwave satellite observations are used from 1978. HadGEM2-ES simulates an area $2 \times 10^6 \text{ km}^2$ lower than HadISST1; the sea ice decline during the ECTW (1910 – 1940) also starts 5 – 10 years earlier in HadGEM2-ES than HadISST1. However, this is hard to determine in HadISST1 due to the limited spatial and temporal coverage of early data. The decrease in SIC coincides with the increase in high latitude temperature from about 1915 – 1940 (Johannessen et al., 2004). The sea

ice decline later in the century starts ~1950 in HadISST1 and ~1980 in HadGEM2-ES. The trend onset differences could be a result of HadGEM2-ES being an ensemble product where as HadISST1 contains just one climate. Ice-free is a term used in the sea ice community to mean “practically ice-free”, this widely adopted arbitrary value is a sea ice extent below $1 \times 10^6 \text{ km}^2$, repeated here for sea ice area. The HadGEM2-ES ensemble mean becomes ice-free in 2041 with an ensemble range of 2034 – 2058.

Sea ice volume (SIV) is an area integrated metric. The latitude dependent area of each grid cell is calculated and multiplied by its sea ice concentration (SIC) and its sea ice thickness (SIT). Repeating this for all grid cells provides the total SIV. All ensemble members show a decline during the ETCW (1910 – 1940), losing $\sim 3000 \text{ km}^3$, although around 1915 all members show remarkably similar positive SIV anomalies. Ensemble member #1 simulates a marked increase in SIV 1920 – 1930, hinting that any single forcing is not greater than the amplitude of possible internal variability, assuming no subtle interactions.

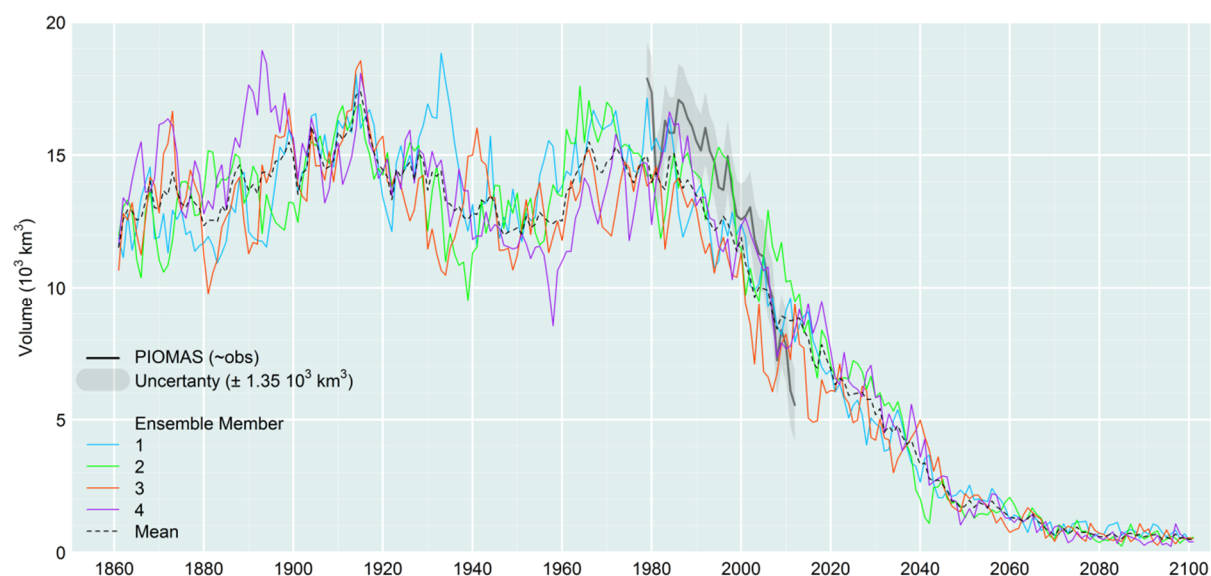


Figure 3.5 | PIOMAS and HadGEM2-ES historical and RCP4.5 Arctic October sea ice volume.

Later in the century HadGEM2-ES shows reasonable agreement in both trend and magnitude of SIV with the Pan-Arctic Ice-Ocean Modelling and Assimilation System (PIOMAS) (Zhang and Rothrock, 2003) discussed in depth in Ch. 4.

Can the *All* forcings simulation, and the AECTW being depicted within, be explained by a combination of greenhouse gas forcings and natural forcings? To investigate whether the AECTW signal can be attributed to either simulations are conducted with a ‘natural

forcing only’ simulation (*Nat*) (Figure 3.6) and a ‘greenhouse gas only’ simulation (*GHG*) (Figure 3.7).

3.2.3 Natural only simulations

Natural forcing only simulations include only volcanic and solar forcings; the climate is allowed to react to changes in these in addition to the internal variability that the climate model produces. Solar forcings vary with the seasons and solar activity; Milankovitch orbital cycles are negligible over such short time scales. Volcanic eruptions cause a rapid cooling followed by a slower recovery in temperatures, and the major volcanic eruptions are labelled in Figure 3.8. It is both the location and size of the volcanic eruption that is important. Generally, eruptions need to be large and tropical in latitude to inject aerosols high into the stratosphere so their effect can be relatively long lived (compared to fallout in the troposphere) and their impact felt over a large portion of the globe. However, it is possible that a high northern latitude eruption could have a significant regional impact on the Arctic.

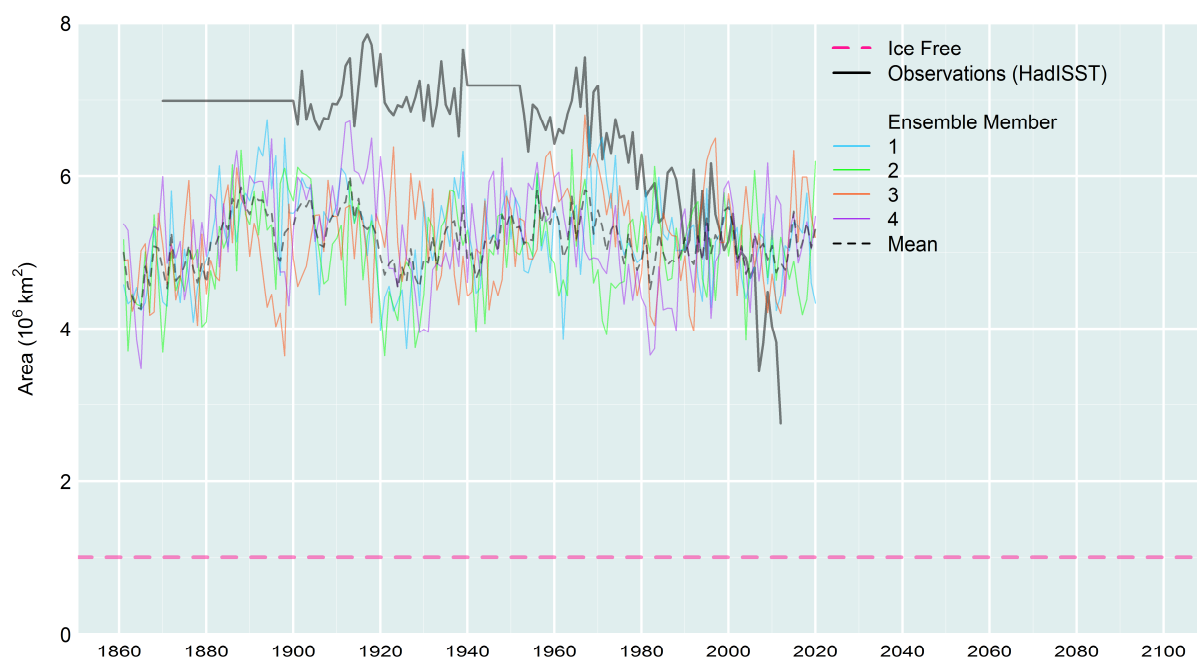


Figure 3.6 | HadGEM2-ES extended historical “natural forcings only” (*Nat*) simulations.

The *Nat* simulations are characterised by annual to multi-decadal variability with no overall trend (Figure 3.6). This is expected, as there is no anthropogenic increase in greenhouse gases in the *Nat* simulations. The ensemble mean does illustrate a reduction in SIA at about the correct time ~1910, however it is short lived and the sea ice recovers

to typical values by ~1930. Natural forcings are then a potential candidate for producing the AETCW but a signal from ~ 1930 – 1940 should be investigated from other sources.

The period before the ETCW is likely influenced by the fallout from the large volcanic eruptions of Krakatoa (1883), Santa Maria (1902), and Novarupta (1912) (Figure 3.8), whereas the ETCW period saw no climatically significant eruptions, likely causing changes to the aerosol forcings around this period. As an increase in aerosols generally causes cooling, a period of relatively high levels of aerosols from volcanoes prior to 1920, followed by a period where aerosol levels likely returned to levels that are more normal would have resulted in a warming effect in the transition into the ETCW period. Thompson (2015) suggests that the Santa Maria eruption had a delayed impact on the global climate through changes to ocean heat content in the Pacific and that the later Novarupta eruption may have forced summer NAO and European temperatures.

3.2.4 Greenhouse gas only simulations

The *GHG* simulations do not have the changes to solar irradiance or the volcanic forcings of the *Nat* simulations, but do include the anthropogenic changes in greenhouse gas concentrations. The ensemble mean sea ice area from the *GHG* simulations are characterised by a decrease throughout the time series with an acceleration after ~1960. Similar inter-annual – multi-decadal variability to *Nat* is superimposed on the trend. The *GHG* simulations become ice-free as early as 1999 (ensemble mean: 2007), approximately 30 years before the *All* forcing simulations. This implies that the sum of non-*GHG* forcings is moderating the impact of anthropogenic greenhouse gases; and that without this moderating effect of these other forcings the Arctic may have already become ice-free. This assumes HadGEM2-ES has a reasonable representation of the forced response, which compared to observations of sea ice area (Figure 3.4) and SIV (Figure 3.5) is not unreasonable.

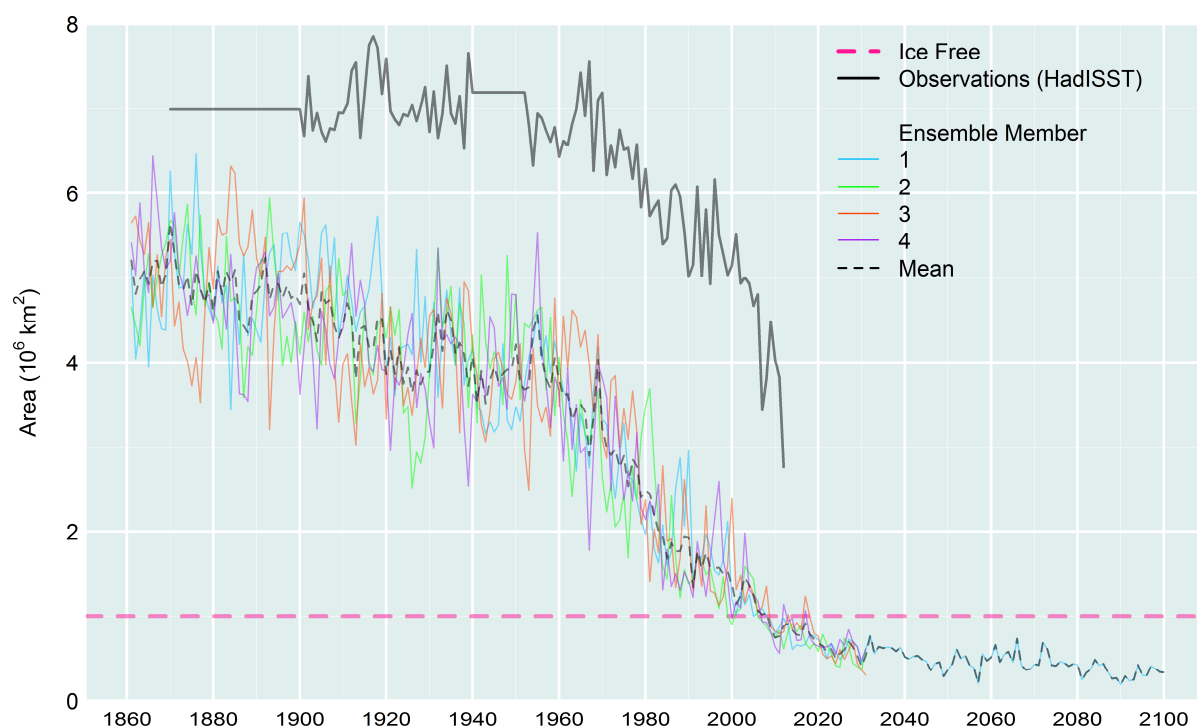


Figure 3.7 | HadGEM2-ES historical and RCP4.5 “greenhouse gas forcings only” (*GHG*) simulations.

The *GHG* simulations are also intriguing in the ETCW period. From 1920 – 1940 there is no robust trend in sea ice area, despite this period being superimposed on a longer declining trend. This implies that the *GHGs* may have been a factor from 1910 – 1920, but beyond that the forcings that sustained the decline to 1940 are not the combination found in the *GHG* simulations.

Upon analysing both the *Nat* and *GHG* simulations, it is found that the trends in the *GHG* and *Nat* simulations do not sufficiently explain the magnitude of the decline exhibited by the *All* simulations. It is hypothesised that aerosols could be a “hidden” but significant contributing factor.

3.2.5 Additional forcings

As neither of the *GHG* or *Nat* forcings can fully account for the sea ice loss in the AETCW the contribution of other anthropogenic forcings are examined. These additional forcings include, anthropogenic aerosols, black carbon (Bond et al., 2007) and land use changes (Hurtt et al., 2011) and are included in the historical *All* forcings runs. Additional detection can be investigated by examining the anomaly remaining after combining the simulations.

Assuming that aerosols (*Aerosols*) are the dominant effect then the following assumption can be made.

$$All' = Nat' + GHG' + Aerosols' \tag{3.1}$$

Where,

\overline{All} = 1860 to 1990 ensemble mean of the *All* simulations

$$All' = All - \overline{All}$$

$$Nat' = Nat - \overline{Nat}$$

$$GHG' = GHG - \overline{GHG}$$

Hence,

$$Aerosols' = All' - Nat' - GHG' \tag{3.2}$$

Using this approach, the perturbation due to *Aerosols* is shown in the bottom panel in Figure 3.8.

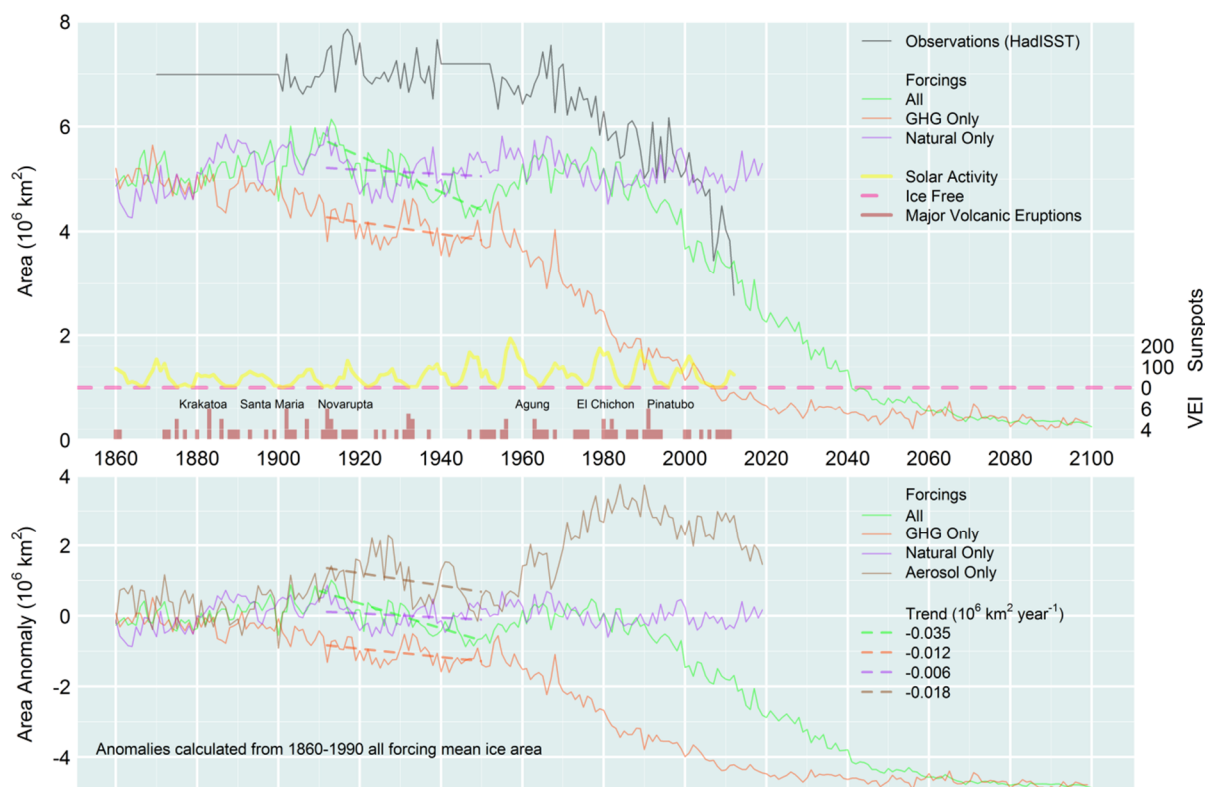


Figure 3.8 | HadGEM2-ES historical and RCP4.5 September Arctic sea ice area ensemble mean for multiple forcing runs (top), observations from HadISST (Rayner et al., 2003), solar activity (sunspots) and volcanic activity (Volcanic Explosively Index (VEI)).

Half of the 1910 – 1950 *All* trend is composed of contributions from *GHG* and *Nat* forcings, with *GHG* contributing twice as much as *Nat*. Half of the *All* trend then remains unexplained, although in Eq. (3.2) all remaining change is attributed to *Aerosols*. While this experiment has helped assign magnitudes the designation of all

unaccounted for forcing to *Aerosols* is not especially satisfactory. We explore this further in the next section

3.3 Fixed aerosol experiments

To better diagnose the impact of aerosols on the early 20th century decline in Arctic sea ice a new model simulation was conducted at the Met Office using constant anthropogenic aerosols, fixed at 1860 levels. Aerosols are known to alter global mean temperature trends over multi-decadal timescales; during the so-called big hiatus from the 1950s to the 1970s increased cooling from sulphate aerosols roughly offset the warming from increasing greenhouse gases (Fyfe et al., 2016). Wilcox et al. (2013) found an increase in global mean temperature in the 1930s from aerosols in a multi-model ensemble, which includes HadGEM2-ES as one of the five models used because of its thorough treatment of aerosol processes.

All remaining forcings, including solar, volcanic, greenhouse gas, and land use changes follow the historical time series described in Ch. 3.2. As the *All* simulation contains the effect of all forcings (including aerosols) and the constant aerosol simulation changes from all forcings excluding that which would have occurred had aerosols varied then the effect of the aerosols alone can be extracted.

The ‘Constant aerosol’ simulation can be approximated as:

$$\textit{Constant aerosol} = \textit{All forcings} - \textit{Aerosols forcings only}.$$

Hence, to calculate the perturbation caused by ‘Aerosols forcings only’ (*Aero*) is:

$$\textit{Aero}' = \textit{All} - \textit{Constant aerosol} \tag{3.3}$$

It is assumed *Aero'* results in the ice anomaly due to aerosols alone. To gain an estimate of the total ice area from this ice anomaly a baseline value must be added to this, for which the Arctic sea ice mean area from the *All* forcings simulation from 1860-1990 is used. It is also probable that internal climate variability is not adequately sampled in this experiment, as only four ensemble members are available.

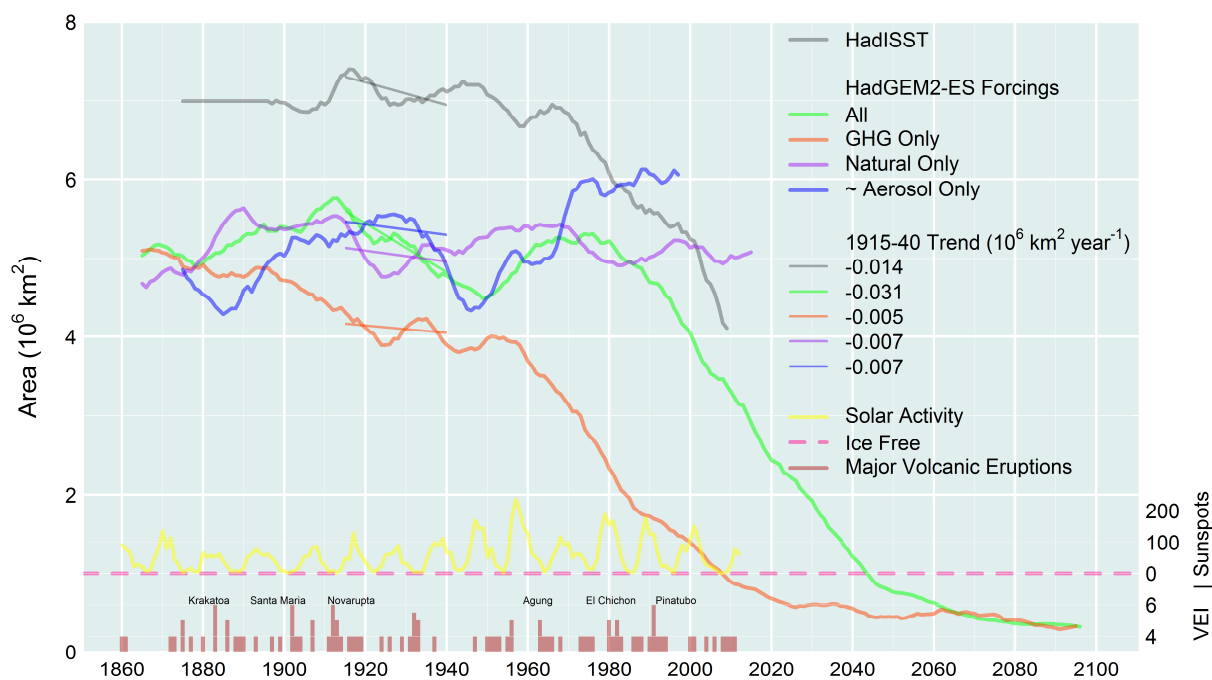


Figure 3.9 | HadGEM2-ES September Arctic sea ice area 10 year running ensemble mean for multiple forcing runs, 10 year mean observations from HadISST (Rayner et al., 2003), solar activity (sunspots) and volcanic activity (Volcanic Explosively Index (VEI)).

To attribute the forcings responsible for the decline seen in the *All* run between 1915 – 1940, linear trends are calculated over that period. The *Aero* and *Nat* individual forcing simulations each account for ~23% to the trend in the *All* forcings simulation. The *GHG* forcings account for a further ~16% leaving ~39% of the ice loss trend unaccounted for.

The individual forcing simulations have distinct temporal signatures, one hypothesis is that natural, and greenhouse gas forcings were the dominant cause of the AETCW from 1915 – 1930 while aerosols provide the missing component in the 1930s and 1940s. The trend analysis indicates the *Nat*, *GHG* and *Aero* forcing simulations do not entirely account for the magnitude of the trend in the *All* forcing simulation. However, this maybe an over estimate due to positive feedbacks such as the ice albedo feedback mechanism. The combination of *Nat* + *GHG* + *Aero* occurring simultaneously in the *All* simulation is possible larger than the sum of the individual forcing runs as the ice albedo feedback is positive.

Therefore either the combination of some or all the forcings results in a larger response — the whole is larger than the sum of the parts, or the contribution results from natural variability, as concluded Bengtsson et al. (2004). Fyfe et al. (2013) concluded that the warming in the Arctic over this period was a result of rising black carbon aerosol

emissions and natural variability (in the form of the AMO). Booth et al. (2012) used HadGEM2-ES to find that aerosols are the prime driver in North Atlantic multi-decadal SST variability. They too show that the ETCW period is captured well by HadGEM2-ES, with twice the warming of previous generation models, but note that HadGEM2-ES does not explain the entire observed trend in the North Atlantic.

As shown by Booth et al. (2012) for the North Atlantic the ETCW period showed strong regional trends. The next section explores the regional trends in Arctic sea ice during the AETCW.

3.4 Spatial changes

Bronnimann (2009) suggests that looking at the ETCW regionally is more informative than in a global sense. Having examined the area-integrated metrics the ice anomalies are next examined spatially, to see if for example the ice loss was mainly in the North Atlantic sector which would be complementary to the findings of Booth et al. (2012) and Fyfe et al. (2013).

To attribute the effect of the ETCW anomalies are calculated by differencing between the ice conditions just before and after the ETCW period. The September mean 1910 – 1915 is used as the period before and September mean 1945 – 1950 post ETCW. These trends are examined for the four ensemble members individually for the four different forcing experiments, for SIC (Figure 3.10) and SIT (Figure 3.11). The ensemble mean is used to show spatial consistency, ensemble standard deviation to show regions of inter-ensemble variations. The signal to noise ratio is calculated by *ensemble mean/standard deviation* (Leith, 1973), where a signal of ≥ 2 is used here to be indicative of areas where the change in ice is robust.

3.4.1 Sea ice concentration

The *All* forcings simulation displays a strong ice-loss signal; this is mostly around the edge of the ice pack in the marginal ice zone (MIZ). Ensemble member #1 shows most loss in the North-Atlantic sector, #2 in the Pacific sector, #3 and #4 lose most ice in the Laptev Sea. This spatial difference in the ensembles is interesting and the ensemble mean, unsurprisingly shows a robust ice loss signal in the entire MIZ from the Northern Barents Sea all the way round to the Beaufort Sea.

The *GHG* forcing signal extends further into the interior than the *All* forcings signal. The signal is also less consistent with an increase in SIC seen in areas where other members see a decrease in SIC, e.g. the Pacific sector #2 vs. #4 and the Fram Strait #1 vs #3, confirmed by ensemble standard deviations $\geq 20\%$. The trend is less spatially robust with significant signals limited to the central Arctic and Barrow Strait regions.

The *Nat* forcing signal is similarly mixed as expected by the lack of consistent trend seen in Figure 3.6. It is broadly similar to *GHG* with a consistent signal from reductions in SIC in the Beaufort Sea.

The *Aero* forcing signal (calculated using Eq. 3.3) is spatially mixed over the ensembles. For example, member #2 exhibits an increase in SIC of 20 – 40% in areas where other members show a reduction of 20%. The areas of largest reduction are in the coastal zones at the edges of the main ice pack, with robust SIC reductions in the Beaufort, Laptev, and Kara seas.

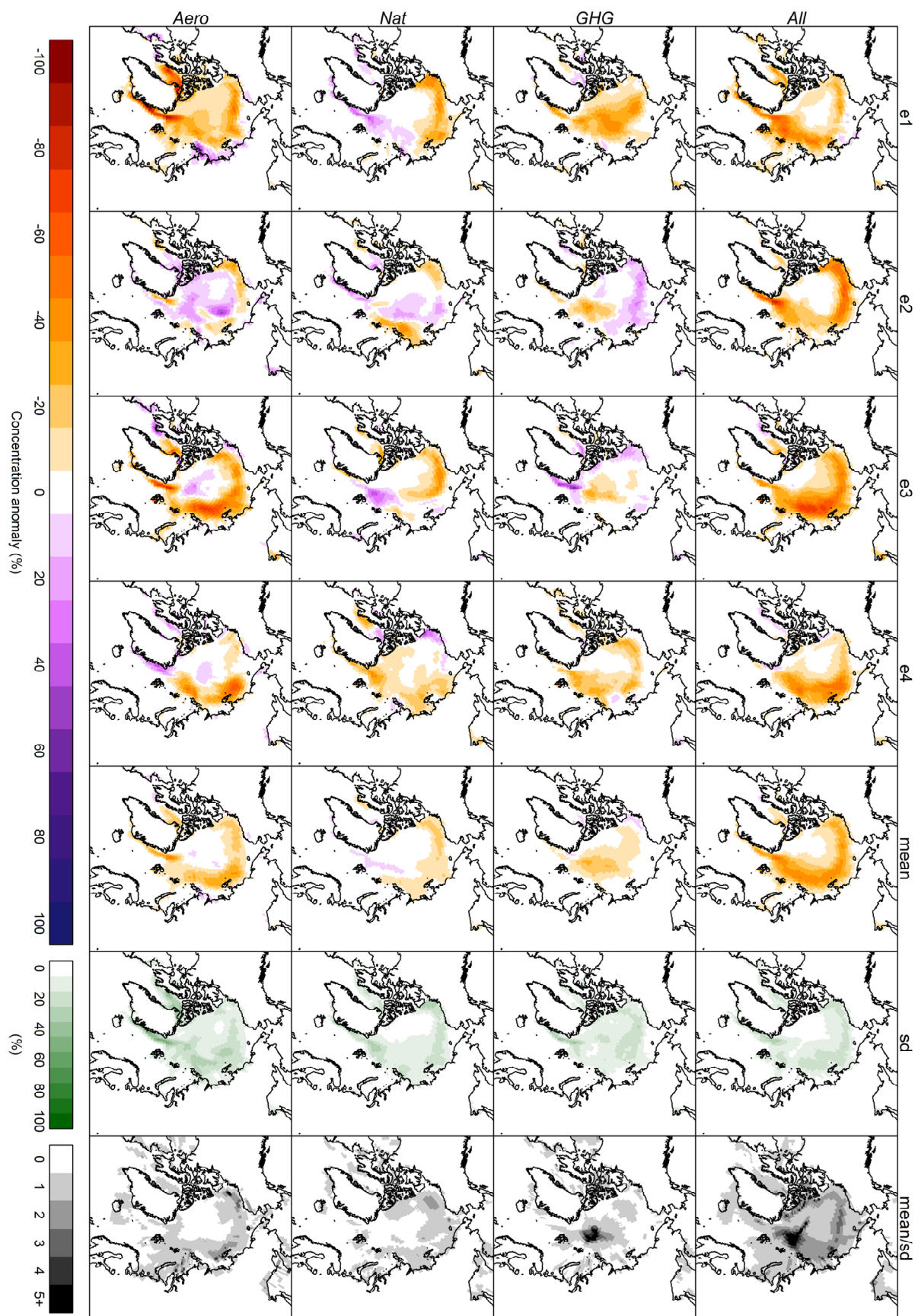


Figure 3.10 | HadGEM2-ES September SIC anomalies (mean 1945-50) — (mean 1910-15).

3.4.2 Sea ice thickness

It is also prudent to analyse changes to the SIT field in the ETCW period. This is important as local changes to the SIT can occur with no change to the SIC, particularly in regions that do not experience seasonal open water.

The *All* forcings simulations experience thinning of SIT in all Arctic Basin regions, ensemble member #1 mostly in the North Atlantic sector, #2 also in the North Atlantic sector in addition to the Pacific Sector, #3,4 have thinning in the central and Russian Arctic seas. The ensemble mean indicates thinning over the entire Arctic with MIZ regions robustly losing 0.5 – 1 m.

The *GHG* only members simulate a regional mix of SIT loss and gain: #1 has ~ 1 m loss from central Arctic regions, #2 simulates 0.25 – 0.75 m increase in SIT in the Beaufort Sea, #3,4 display a spatially inconsistent change in SIT with almost the opposite signal to each other. The ensemble mean reflects the ensemble diversity with robust loss occurring in a central arctic region to the Russian side of the pole.

Perhaps less surprising than the *GHG* forcing only simulation, the *Nat* forcing only simulations also shows no consistent robust regions of change in SIT. The ensemble mean indicates that it may have contributed to a reduction in SIT in the North American, Pacific and eastern Russian seas though the signal (~1m) and magnitude of SIT loss (~0.25m) is weak.

The SIT field from the *Aero* forcing only simulations reveal changes to the sea ice that is largely missing in the SIC field. This is plausible as a slight reduction in SIC leads to a more mobile ice pack, here advection by the wind and currents can more readily pile ice up on to land and fast-ice. The *Aero* simulations lead to the largest anomalies measured in any of the simulations. Ensemble member #1 and #2 simulates an increase in SIT >2 m in the Canadian Archipelago and east of Severnaya Zemlya; and #1 and #3 simulate losses >2 m in the Fram Strait, while #4 simulates SIT thickening of >2m in this region. The spatial inconsistency in changes mostly cancel each other out with robust signals of up to 0.75 m SIT thickening in the Canadian Archipelago and up to 0.5 m sea ice loss in the Laptev Sea and north of the Fram Strait remaining. Despite this less dramatic signal in the ensemble mean further investigation of the *Aero* ensemble is warranted to diagnose these trends. This is especially pertinent as the first action in climate change mitigation results in “cleaner” air from a reduction in aerosols, which inadvertently

could cause a short-term warming contribution as seen in some RCP2.6 simulations (Chalmers et al., 2012).

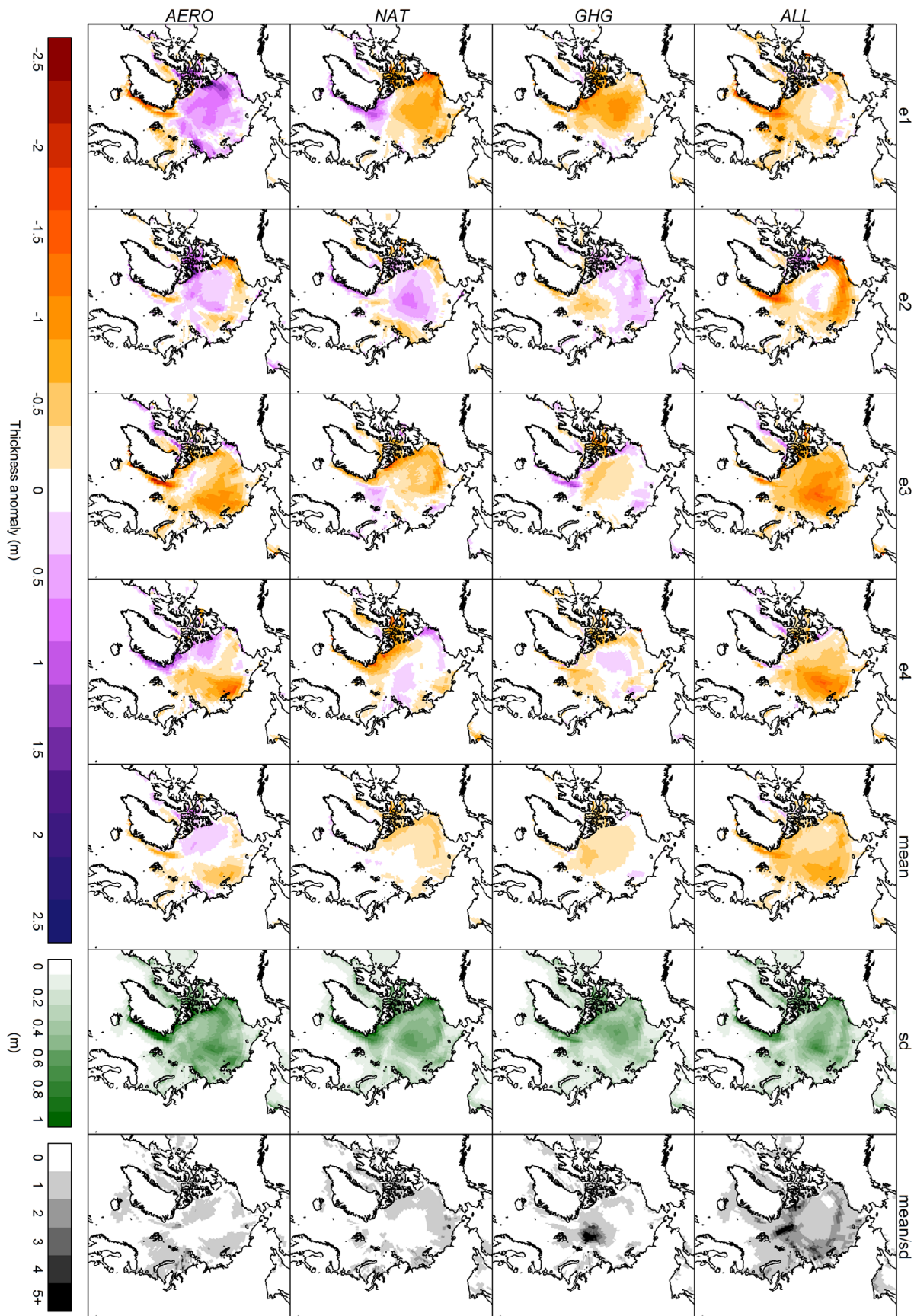


Figure 3.11 | HadGEM2-ES September SIT anomalies (mean 1945-50) — (mean 1910-15)

3.4.3 Summary

The fixed aerosol experiment indicated that up to 40% of the ice loss seen in the AETCW remains (the remnant, *Rem*) after accounting for natural, anthropogenic greenhouse gases, and aerosol contributions.

$$All' - (Nat' + GHG' + Aero') = Rem' \quad (3.4)$$

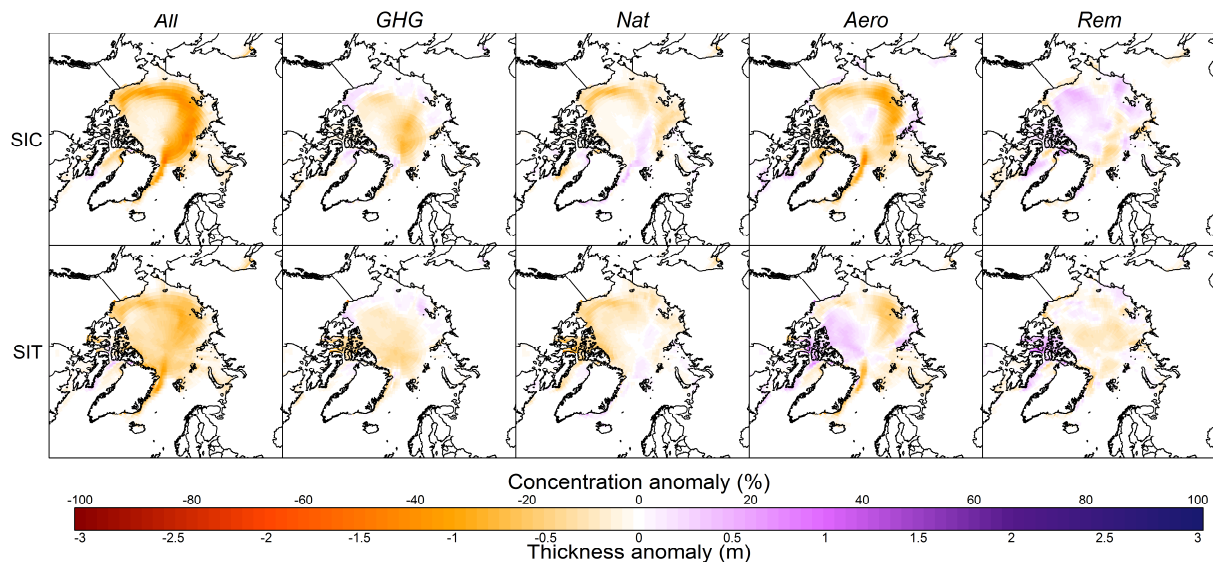


Figure 3.12 | HadGEM2-ES September ensemble mean SIC and SIC forcing anomalies as in Figure 3.10 and Figure 3.11. *Rem* is the remnant, changes in the *All* forcings simulations not accounted for by the *GHG*, *Nat*, and *Aero* simulations.

The spatial analysis of ice change in the separate forcing simulations are akin to jigsaw like contributions to the *All* forcing simulation. The *GHG* forcings accounted for sea ice loss in the central Arctic, *Nat* forcings account for sea ice loss in the Beaufort, Northern Chukchi Seas, the *Aero* forcings account for sea ice loss in the Fram Strait, Beaufort and all Russian Seas. The *Aero* simulation often has the opposite sign to the other simulations, showing an increase in ice in the thick-ice region in the central Arctic and in the Canadian Archipelago.

The *Rem* (Eq. 3.4) shows unaccounted for changes to sea ice. The *Rem* can include internal variability in separate forcing ensemble, non-linear interactions in the summation of the individual forcing simulations, or variables that contribute to forcings in the *All* forcing simulation that are not duplicated in the separate forcing simulations. The ice anomaly patterns seen in the *Rem* are less spatially consistent than any of the other simulations. This hints that the *Rem* is caused by non-linear forcing responses

rather than a missing forcing which would likely result in a more consistent ice anomaly.

3.5 Conclusions

The principal questions this chapter addressed are:

1. *Can a GCM reproduce the changes to sea ice observed in the Arctic during the early 20th century?*

The HadGEM2-ES GCM was used in this chapter to examine the Arctic sea ice loss observed in the early 20th century. Observed global mean surface temperatures indicate the ETCW occurred between 1910 – 1940. Observations of sea ice are limited in their spatial and temporal extent, and in their reliability due to the observation methods. They indicate that the ice loss started in ~1917 and continued low until ~1940. The sea ice from the HadGEM2-ES historical simulation indicates a period of ice loss starting slightly earlier ~1913 and lasting for longer, to ~1950, than the sea ice reanalysis.

2. *What different factors contributed to the Arctic sea ice loss?*

Simulations with HadGEM2-ES that isolate separate forcings indicate that many simultaneous factors may have contributed to the Arctic sea ice loss. Greenhouse gases caused a robust ice loss in the Pacific and North American sectors of the Arctic 1915 – 1930, while natural forcings caused a weaker and spatially mixed response. The effect from changing aerosols started around 1930 elongating the response to 1940. Internal variability also cannot be ruled out as the ensemble members show large diversity in their response and the sum of individual forcings is less than the decline simulated when the forcings are included together in the historical all forcing simulations.

It is likely that to robustly attribute the causes of the AETCW will require a large ensemble of individual forcing simulations. It is important to reiterate the limitations of attributions via a single GCM, as every model has its own response to forcings. Although attributions for the AETWC are suggested in this chapter, robust conclusions are limited due to the small ensemble size. The spatial maps reveal the contrasting response in different ensemble members. Future studies should repeat individual forcing simulations but with an adequate ensemble size to ascertain robust forcing responses.

References

- Ahlmann, H. W.: Researches on Snow and Ice, 1918-40, *The Geographical Journal*, 107, 11-25, doi: 10.2307/1789081, 1946.
- Bengtsson, L., Semenov, V. A., and Johannessen, O. M.: The Early Twentieth-Century Warming in the Arctic—A Possible Mechanism, *J. Clim.*, 17, 4045-4057, doi: 10.1175/1520-0442(2004)017<4045:tetwit>2.0.co;2, 2004.
- Bindoff, N. L., Stott, P. A., AchutaRao, K. M., Allen, M. R., Gillett, N., Gutzler, D., Hansingo, K., Hegerl, G., Hu, Y., Jain, S., Mokhov, I. I., Overland, J., Perlwitz, J., Sebbari, R., and Zhang, X.: Detection and Attribution of Climate Change: from Global to Regional. In: *Climate Change 2013: The Physical Science Basis. Contribution of Working Group I to the Fifth Assessment Report of the Intergovernmental Panel on Climate Change*, edited by: Stocker, T. F., Qin, D., Plattner, G.-K., Tignor, M., Allen, S. K., Boschung, J., Nauels, A., Xia, Y., Bex, V., and Midgley, P. M., Cambridge University Press, Cambridge, United Kingdom and New York, NY, USA, 867–952, 2013, doi: 10.1017/CBO9781107415324.022.
- Bond, T. C., Bhardwaj, E., Dong, R., Jogani, R., Jung, S., Roden, C., Streets, D. G., and Trautmann, N. M.: Historical emissions of black and organic carbon aerosol from energy-related combustion, 1850–2000, *Global Biogeochemical Cycles*, 21, doi: 10.1029/2006gb002840, 2007.
- Booth, B. B. B., Dunstone, N. J., Halloran, P. R., Andrews, T., and Bellouin, N.: Aerosols implicated as a prime driver of twentieth-century North Atlantic climate variability, *Nature*, 484, 228-U110, doi: 10.1038/nature10946, 2012.
- Brohan, P., Kennedy, J. J., Harris, I., Tett, S. F. B., and Jones, P. D.: Uncertainty estimates in regional and global observed temperature changes: A new data set from 1850, *J. Geophys. Res. Atmos.*, 111, doi: 10.1029/2005jd006548, 2006.
- Bronnimann, S.: Early twentieth-century warming, *Nat. Geosci.*, 2, 735-736, doi: 10.1038/ngeo670, 2009.
- Chalmers, N., Highwood, E. J., Hawkins, E., Sutton, R., and Wilcox, L. J.: Aerosol contribution to the rapid warming of near-term climate under RCP 2.6, *Geophys. Res. Lett.*, 39, doi: 10.1029/2012gl052848, 2012.
- Collins, W. J., Bellouin, N., Doutriaux-Boucher, M., Gedney, N., Halloran, P., Hinton, T., Hughes, J., Jones, C. D., Joshi, M., Liddicoat, S., Martin, G., O'Connor, F., Rae, J., Senior, C., Sitch, S., Totterdell, I., Wiltshire, A., and Woodward, S.: Development and evaluation of an Earth-System model – HadGEM2, *Geosci. Model Dev.*, 4, 1051-1075, doi: 10.5194/gmd-4-1051-2011, 2011.
- Delworth, T. L. and Knutson, T. R.: Simulation of Early 20th Century Global Warming, *Science*, 287, 2246-2250, doi: 10.1126/science.287.5461.2246, 2000.
- Frankcombe, L. M. and Dijkstra, H. A.: The role of Atlantic-Arctic exchange in North Atlantic multidecadal climate variability, *Geophys. Res. Lett.*, 38, doi: 10.1029/2011gl048158, 2011.

- Fyfe, J. C., Meehl, G. A., England, M. H., Mann, M. E., Santer, B. D., Flato, G. M., Hawkins, E., Gillett, N. P., Xie, S.-P., Kosaka, Y., and Swart, N. C.: Making sense of the early-2000s warming slowdown, *Nature Clim. Change*, 6, 224-228, doi: 10.1038/nclimate2938, 2016.
- Fyfe, J. C., von Salzen, K., Gillett, N. P., Arora, V. K., Flato, G. M., and McConnell, J. R.: One hundred years of Arctic surface temperature variation due to anthropogenic influence, *Sci. Rep.*, 3, doi: 10.1038/srep02645
- <http://www.nature.com/srep/2013/130912/srep02645/abs/srep02645.html#supplementary-information>, 2013.
- Grant, A. N., Brönnimann, S., Ewen, T., Griesser, T., and Stickler, A.: The early twentieth century warm period in the European Arctic, *Meteorologische Zeitschrift*, 18, 425-432, doi: 10.1127/0941-2948/2009/0391, 2009.
- Hansen, J., Ruedy, R., Sato, M., and Lo, K.: Global Surface Temperature Change, *Reviews of Geophysics*, 48, doi: 10.1029/2010rg000345, 2010.
- Hegerl, G. C., Crowley, T. J., Allen, M., Hyde, W. T., Pollack, H. N., Smerdon, J., and Zorita, E.: Detection of Human Influence on a New, Validated 1500-Year Temperature Reconstruction, *J. Clim.*, 20, 650-666, doi: doi:10.1175/JCLI4011.1, 2007.
- Hurrell, J. W.: Decadal Trends in the North Atlantic Oscillation: Regional Temperatures and Precipitation, *Science*, 269, 676-679, doi: 10.1126/science.269.5224.676, 1995.
- Hurt, G. C., Chini, L. P., Frohling, S., Betts, R. A., Feddema, J., Fischer, G., Fisk, J. P., Hibbard, K., Houghton, R. A., Janetos, A., Jones, C. D., Kindermann, G., Kinoshita, T., Klein Goldewijk, K., Riahi, K., Shevliakova, E., Smith, S., Stehfest, E., Thomson, A., Thornton, P., Vuuren, D. P., and Wang, Y. P.: Harmonization of land-use scenarios for the period 1500–2100: 600 years of global gridded annual land-use transitions, wood harvest, and resulting secondary lands, *Clim. Change*, 109, 117-161, doi: 10.1007/s10584-011-0153-2, 2011.
- Ifft, G. N.: The Changing Arctic, *Mon. Weather Rev.*, 50, 589-589, doi: 10.1175/1520-0493(1922)50<589a:TCA>2.0.CO;2, 1922.
- Johannessen, O. M., Bengtsson, L., Miles, M. W., Kuzmina, S. I., Semenov, V. A., Alekseev, G. V., Nagurnyi, A. P., Zakharov, V. F., Bobylev, L. P., and Pettersson, L. H.: Arctic climate change: Observed and modelled temperature and sea-ice variability, *Tellus A*, 56, 328-341, 2004.
- Jones, G. S., Stott, P. A., and Christidis, N.: Attribution of observed historical near-surface temperature variations to anthropogenic and natural causes using CMIP5 simulations, *J. Geophys. Res. Atmos.*, 118, 4001-4024, doi: 10.1002/jgrd.50239, 2013.
- Karoly, D. J., Braganza, K., Stott, P. A., Arblaster, J. M., Meehl, G. A., Broccoli, A. J., and Dixon, K. W.: Detection of a Human Influence on North American Climate, *Science*, 302, 1200-1203, doi: 10.1126/science.1089159, 2003.
- Kelly, P. M., Goodess, C. M., and Cherry, B. S. G.: The interpretation of the Icelandic sea ice record, *J. Geophys. Res. Oceans*, 92, 10835-10843, doi: 10.1029/JC092iC10p10835, 1987.

Koch, L.: The East Greenland ice, *Bianche Lunes*, 1945.

Leith, C. E.: The Standard Error of Time-Average Estimates of Climatic Means, *Journal of Applied Meteorology*, 12, 1066-1069, doi: 10.1175/1520-0450(1973)012<1066:tseota>2.0.co;2, 1973.

Mantua, N. J., Hare, S. R., Zhang, Y., Wallace, J. M., and Francis, R. C.: A Pacific Interdecadal Climate Oscillation with Impacts on Salmon Production, *Bull. Am. Meteorol. Soc.*, 78, 1069-1079, doi: 10.1175/1520-0477(1997)078<1069:apicow>2.0.co;2, 1997.

Miles, M. W., Divine, D. V., Furevik, T., Jansen, E., Moros, M., and Ogilvie, A. E. J.: A signal of persistent Atlantic multidecadal variability in Arctic sea ice, *Geophys. Res. Lett.*, 41, 463-469, doi: 10.1002/2013gl058084, 2014.

Morice, C. P., Kennedy, J. J., Rayner, N. A., and Jones, P. D.: Quantifying uncertainties in global and regional temperature change using an ensemble of observational estimates: The HadCRUT4 data set, *J. Geophys. Res. Atmos.*, 117, doi: 10.1029/2011jd017187, 2012.

Myhre, G., Shindell, D., Bréon, F.-M., Collins, W., Fuglestedt, J., Huang, J., Koch, D., Lamarque, J.-F., Lee, D., Mendoza, B., Nakajima, T., Robock, A., Stephens, G., Takemura, T., and Zhang, H.: Anthropogenic and Natural Radiative Forcing. In: *Climate Change 2013: The Physical Science Basis. Contribution of Working Group I to the Fifth Assessment Report of the Intergovernmental Panel on Climate Change*, edited by: Stocker, T. F., Qin, D., Plattner, G.-K., Tignor, M., Allen, S. K., Boschung, J., Nauels, A., Xia, Y., Bex, V., and Midgley, P. M., Cambridge University Press, Cambridge, United Kingdom and New York, NY, USA, 659–740, 2013, doi: 10.1017/CBO9781107415324.018.

Nozawa, T., Nagashima, T., Shiogama, H., and Crooks, S. A.: Detecting natural influence on surface air temperature change in the early twentieth century, *Geophys. Res. Lett.*, 32, doi: 10.1029/2005gl023540, 2005.

Overpeck, J., Hughen, K., Hardy, D., Bradley, R., Case, R., Douglas, M., Finney, B., Gajewski, K., Jacoby, G., Jennings, A., Lamoureux, S., Lasca, A., MacDonald, G., Moore, J., Retelle, M., Smith, S., Wolfe, A., and Zielinski, G.: Arctic Environmental Change of the Last Four Centuries, *Science*, 278, 1251-1256, doi: 10.1126/science.278.5341.1251, 1997.

Peterson, T. C. and Vose, R. S.: An Overview of the Global Historical Climatology Network Temperature Database, *Bull. Am. Meteorol. Soc.*, 78, 2837-2849, doi: 10.1175/1520-0477(1997)078<2837:aootgh>2.0.co;2, 1997.

Polyakov, I. V., Alekseev, G. V., Bekryaev, R. V., Bhatt, U. S., Colony, R., Johnson, M. A., Karklin, V. P., Walsh, D., and Yulin, A. V.: Long-Term Ice Variability in Arctic Marginal Seas, *J. Clim.*, 16, 2078-2085, doi: 10.1175/1520-0442(2003)016<2078:liviam>2.0.co;2, 2003.

Rahmstorf, S., Box, J. E., Feulner, G., Mann, M. E., Robinson, A., Rutherford, S., and Schaffernicht, E. J.: Exceptional twentieth-century slowdown in Atlantic Ocean overturning circulation, *Nature Clim. Change*, 5, 475-480, doi: 10.1038/nclimate2554, 2015.

Rayner, N. A., Parker, D. E., Horton, E. B., Folland, C. K., Alexander, L. V., Rowell, D. P., Kent, E. C., and Kaplan, A.: Global analyses of sea surface temperature, sea ice, and night marine air temperature since the late nineteenth century, *Journal of Geophysical Research-Atmospheres*, 108, 4407, doi: 10.1029/2002jd002670, 2003.

Schmith, T. and Hansen, C.: Fram Strait Ice Export during the Nineteenth and Twentieth Centuries Reconstructed from a Multiyear Sea Ice Index from Southwestern Greenland, *J. Clim.*, 16, 2782-2791, doi: 10.1175/1520-0442(2003)016<2782:fsiedt>2.0.co;2, 2003.

Serreze, M. C., Holland, M. M., and Stroeve, J.: Perspectives on the Arctic's Shrinking Sea-Ice Cover, *Science*, 315, 1533-1536, doi: 10.1126/science.1139426, 2007.

Shiogama, H., Nagashima, T., Yokohata, T., Crooks, S. A., and Nozawa, T.: Influence of volcanic activity and changes in solar irradiance on surface air temperatures in the early twentieth century, *Geophys. Res. Lett.*, 33, doi: 10.1029/2005gl025622, 2006.

Stott, A. P., Tett, B. S. F., Jones, S. G., Allen, R. M., Ingram, J. W., and Mitchell, B. J. F.: Attribution of twentieth century temperature change to natural and anthropogenic causes, *Clim. Dyn.*, 17, 1-21, doi: 10.1007/pl00007924, 2001.

Tett, S. F. B., Jones, G. S., Stott, P. A., Hill, D. C., Mitchell, J. F. B., Allen, M. R., Ingram, W. J., Johns, T. C., Johnson, C. E., Jones, A., Roberts, D. L., Sexton, D. M. H., and Woodage, M. J.: Estimation of natural and anthropogenic contributions to twentieth century temperature change, *J. Geophys. Res. Atmos.*, 107, ACL 10-11-ACL 10-24, doi: 10.1029/2000jd000028, 2002.

The HadGEM2 Development Team, Martin, G. M., Bellouin, N., Collins, W. J., Culverwell, I. D., Halloran, P. R., Hardiman, S. C., Hinton, T. J., Jones, C. D., McDonald, R. E., McLaren, A. J., O'Connor, F. M., Roberts, M. J., Rodriguez, J. M., Woodward, S., Best, M. J., Books, M. E., Brown, A. R., Butchart, N., Dearden, C., Derbyshire, S. H., Dharssi, I., Doutriaux-Boucher, M., Edwards, J. M., Falloon, P. D., Gedney, N., Grey, L. J., Hewitt, H. T., Hobson, M., Huddleston, M. R., Huges, J., Ineson, S., Ingram, W. J., James, P. M., Johns, T. C., Johnson, C. E., Jones, A., Jones, C. P., Joshi, M. M., Keen, A. B., Liddicoat, S., Lock, A. P., Maidens, A. V., Manners, J. C., Milton, S. F., Rae, J. G. L., Ridley, J. K., Sellar, A., Senior, C. A., Totterdell, I. J., Verhoef, A., Vidale, P. L., and Wiltshire, A.: The HadGEM2 family of Met Office Unified Model climate configurations, *Geosci. Model Dev.*, 4, 723-757, doi: 10.5194/gmd-4-723-2011, 2011.

Thompson, V.: *The Early Twentieth Century Warming*, Doctor of Philosophy, Department of Meteorology, University of Reading, 2015.

Trenberth, K. E.: The Definition of El Niño, *Bull. Am. Meteorol. Soc.*, 78, 2771-2777, doi: 10.1175/1520-0477(1997)078<2771:tdoen>2.0.co;2, 1997.

Wilcox, L., Highwood, E., and Dunstone, N.: The influence of anthropogenic aerosol on multi-decadal variations of historical global climate, *Environ. Res. Lett.*, 8, 024033, 2013.

Wood, K. R. and Overland, J. E.: Early 20th century Arctic warming in retrospect, *International Journal of Climatology*, 30, 1269-1279, doi: 10.1002/joc.1973, 2010.

Zhang, J. and Rothrock, D.: Modeling global sea ice with a thickness and enthalpy distribution model in generalized curvilinear coordinates, *Mon. Weather Rev.*, 131, 845-861, 2003.

Zhang, Y., Wallace, J. M., and Battisti, D. S.: ENSO-like Interdecadal Variability: 1900-93, *J. Clim.*, 10, 1004-1020, doi: 10.1175/1520-0442(1997)010<1004:eliv>2.0.co;2, 1997.

Chapter 4

**Improved Arctic sea ice thickness projections
using bias corrected CMIP5 simulations**

Summary

Projections of Arctic sea ice thickness (SIT) have the potential to inform stakeholders about accessibility to the region, but are currently rather uncertain. The latest suite of CMIP5 global climate models (GCMs) produce a wide range of simulated SIT in the historical period (1979 – 2014) and exhibit various biases when compared with the Pan-Arctic Ice-Ocean Modelling and Assimilation System (PIOMAS) sea ice reanalysis. A new method to constrain such GCM simulations of SIT via a statistical bias correction technique is described in this chapter.

The bias correction successfully constrains the spatial SIT distribution and temporal variability in the CMIP5 projections whilst retaining the climatic fluctuations from individual ensemble members. The bias correction acts to reduce the spread in projections of SIT and reveals the significant contributions of climate internal variability in the first half of the century and of scenario uncertainty from the mid-century onwards. The projected date of ice-free conditions in the Arctic under the RCP8.5 high emission scenario occurs in the 2050s, which is a decade earlier than without the bias correction, with potentially significant implications for stakeholders in the Arctic such as the shipping industry. This bias correction methodology developed here could be similarly applied to other variables to reduce spread in climate projections more generally.

Parts of the work in this Chapter has appeared in Melia et al. (2015):

Melia, N., Haines, K., and Hawkins, E.: Improved Arctic sea ice thickness projections using bias-corrected CMIP5 simulations, *Cryosphere*, 9, 2237-2251, doi: 10.5194/tc-9-2237-2015, 2015.

4.1 Introduction

Global climate models (GCMs) are the primary tool for making climate predictions on seasonal to decadal timescales, and climate projections over the next century (Flato et al., 2013). In a warming climate, changes to sea ice thickness (SIT) are expected to lead to significant implications for polar regions and beyond. A reduction in SIT will likely open up the Arctic Ocean to economic diversification including new marine shipping routes (Smith and Stephenson, 2013) and extraction of natural resources, as well as changes to the Arctic ecosystem and potential links to mid-latitude weather (Francis and Vavrus, 2012). Many of these economic opportunities may rely on SIT evolution, but current projections have considerable uncertainty. SIT is also much more informative than sea ice concentration (SIC), especially in the central Arctic, where future thinning can occur without major changes in the local SIC.

The GCMs from the Coupled Model Intercomparison Project, phase 5 (CMIP5) (Taylor et al., 2012) exhibit a large range in sea ice volume (SIV), spatial SIT distribution, and temporal SIT variability under present-day forcing conditions (e.g. Blanchard-Wrigglesworth and Bitz (2014)). For September sea ice extent, Swart et al. (2015) showed that the uncertainty in CMIP5 projections over the next few decades is dominated by these differences between models, termed “model uncertainty” by Hawkins and Sutton (2009, 2011). Uncertainty in climate projections arises from three distinct sources: (1) model uncertainty, (2) internal variability, and (3) scenario uncertainty, as discussed by Hawkins and Sutton (2009, 2011) for temperature and precipitation respectively. In contrast to projections of temperature where the anomalies are often used, the absolute value of SIT is important – for example, ships have critical SIT thresholds above which their use is not possible (Transport Canada, 1998; Stephenson et al., 2013).

Bias correction (BC) of GCM simulations has the potential to reduce the differences between models and hence potentially increase confidence in near-term climate projections. The importance of BC in impact-based climate change studies was described in a special report of the IPCC (Seneviratne et al., 2012), but BC has not previously been applied to projections of SIT; this chapter is novel in that it recalibrates SIT, and does it locally. There are many different types of proposed BC techniques (e.g. Christensen et al. (2008); Boe et al. (2009); Ho et al. (2011); Mahlstein and Knutti (2012); Watanabe et al. (2012); Vrac and Friederichs (2014), and references therein) which have mainly been

applied to temperature and precipitation. However, these existing methods need refining for sea ice as SIT is a particularly challenging variable. This is due to its positive semi-definite nature, and the spatial and temporal occurrence of zeros, in observations and projections of SIT.

This chapter addresses the development of a new BC technique that constrains both the mean and variance of SIT in GCMs to an estimate of the observed statistics. It is important to correct the mean as this corrects the spatial SIT distribution. Variability in SIT also has a significant impact on the simulated range of regional ice-free dates, something of great interest to stakeholders, and the CMIP5 GCMs exhibit a wide range in their SIT variability. The method can also utilise multiple ensemble members from the same model when performing the BC, something that is often not utilised in other studies. This is important as it enables an assessment of the role of internal variability in future projections to be made. The techniques described in this chapter are not limited to SIT, and would work for many climate variables. The exact implementation used in this chapter should also be calibrated to the user's needs based on factors such as the length of reliable observations and number of ensemble members.

In this chapter the Pan-Arctic Ice-Ocean Modelling and Assimilation System (PIOMAS) (Zhang and Rothrock, 2003) is used as a reanalysis-based estimate of recent SIT, along with climate projections from a subset of six GCMs from the CMIP5 archive (Ch. 4.2). The BC is developed in a 'toy model' environment to allow improvements from increasingly sophisticated methods to be easily quantified (Ch. 4.3).

The principal questions this chapter addresses are:

1. *Can a statistical bias correction technique be developed that corrects the SIT biases in GCMs?*
2. *Will the bias correction reduce the uncertainty in climate change projections of SIT?*
3. *When will the Arctic display seasonally ice-free conditions?*

4.2 Climate simulations and observations

4.2.1 PIOMAS

To represent observed SIT, estimates from the PIOMAS reanalysis are used. PIOMAS is a coupled ice-ocean model that is forced with the National Centers for Environmental Prediction (NCEP) atmospheric reanalysis, and assimilates satellite observed sea ice concentration (Lindsay and Zhang, 2006) and sea surface temperature (Schweiger et al., 2011). It does not however assimilate sea ice thickness (SIT), although this has been attempted using the NASA Operation IceBridge and SIZONet campaigns of 2012 (Lindsay et al., 2012).

As a reanalysis, PIOMAS is constrained by the quality of the assimilated observations. Lindsay et al. (2014) forced PIOMAS with four different atmospheric reanalysis products producing differing results. Schweiger et al. (2011) found biases in PIOMAS of 0.26 m in autumn and 0.1 m in spring when compared with ICESat (Zwally et al., 2002) although the spring bias is within the range of uncertainties found by Zygmuntowska et al. (2014). Larger differences are found in the areas of thickest ice, north of Greenland and the Canadian Archipelago, with ICESat retrievals around 0.7 m larger than PIOMAS. However in this region PIOMAS agrees better with in situ data (Schweiger et al., 2011). Zygmuntowska et al. (2014) suggest that this discrepancy is due to the choice of sea ice density in ICESat, and they support this explanation by finding lower discrepancies between PIOMAS and CryoSat-2 (Laxon et al., 2013) which utilises an alternative sea ice density value. Stroeve et al. (2014), in a comprehensive study of SIT across CMIP5 and observations, find that the spatial correlations in thickness between CMIP5 models and PIOMAS are generally higher than those between CMIP5 models and ICESat. It should be noted that these results will be sensitive to the data set chosen to represent observed SIT.

PIOMAS is selected to represent estimates of SIT as satellite observations are limited in their spatial and temporal range. For example, data from ICESat are only available between October and March 2003 – 2008 (Kwok et al., 2009). More recently CryoSat-2 has started producing real-time SIT data sets but only for the non-summer months (Tilling et al., 2015). This is also not ideal as it is the summer and autumn months when the ice is thinnest that is currently most relevant for potential shipping activity. The spatial consistency, temporal length, and completeness of the data are important considerations when computing climatological means and variances, as the longest

timeseries possible is needed to validate the statistics. It is primarily for this reason that PIOMAS is chosen to represent observations. Several studies (e.g. Lindsay and Zhang (2006), Schweiger et al. (2011), Laxon et al. (2013), and Stroeve et al. (2014)) have compared PIOMAS to satellite and in situ observations and models and find it a suitable estimate of observed SIT. PIOMAS is also deemed realistic enough to initialise numerical models for seasonal forecasts e.g., the Sea Ice Outlook (Blanchard-Wrigglesworth and Bitz, 2014) where the accuracy of the initial conditions is vital.

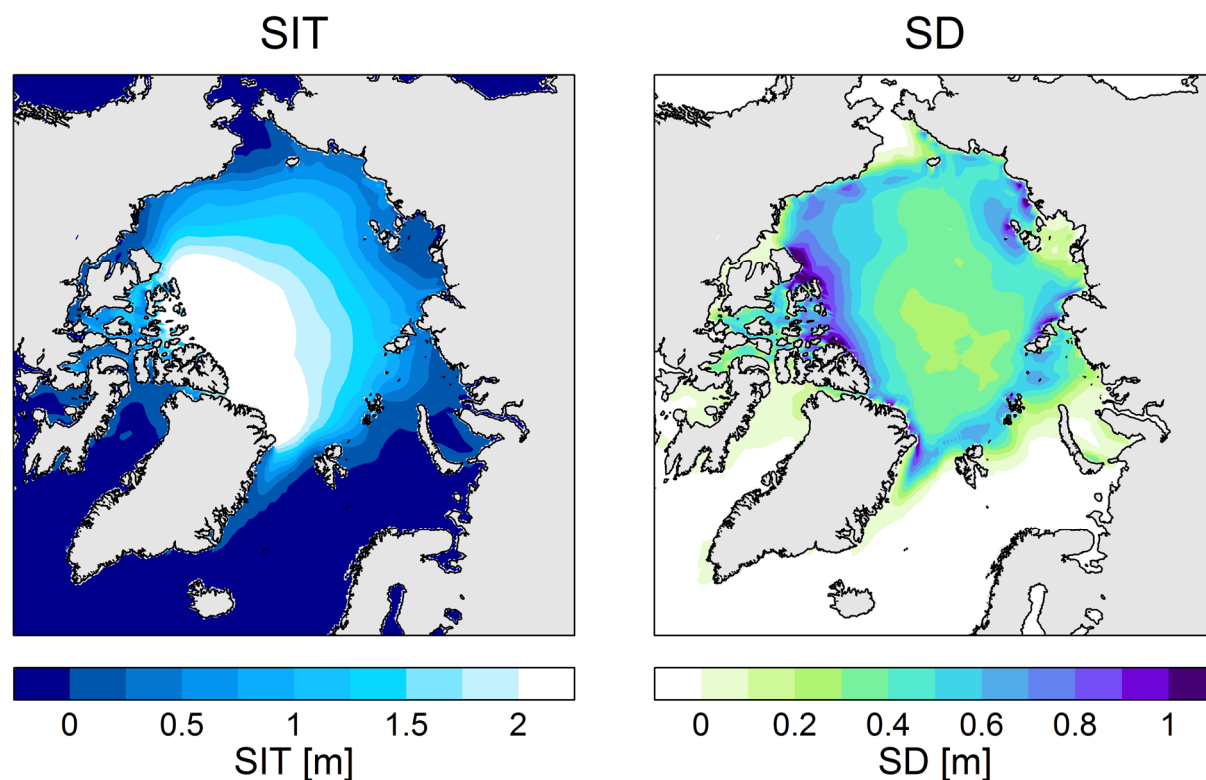


Figure 4.1 | September 1979 – 2014 mean SIT and standard deviation (SD) from the PIOMAS reanalysis. SD is calculated after removing the linear trend.

Figure 4.1 shows the mean September SIT and temporal standard deviation (SD) after linear detrending for PIOMAS over the satellite era (1979 – 2014). In the heart of the Canadian Archipelago, PIOMAS ice thickness is up to 1.5 m, which is reasonable when compared to Haas and Howell (2015) who measured ice along the Northwest Passage in May 2011 and April 2015 using airborne electromagnetic induction soundings, and to Tilling et al. (2015) who used CryoSat-2 for October and November 2010 – 2014. North of Greenland SIT exceeds 3.5 m, which is again comparable to CryoSat-2 for October and November 2010 – 2014 and is between 0 and 1 m along the north Russian coast. The SIT is most variable around the edge of the ice pack and especially near land. An effective

BC should ensure that the simulations replicate these patterns of mean SIT and SD over this recent period.

4.2.2 Global climate models

This chapter utilises a subset of six GCMs from CMIP5. Since a large part of this work assesses SIT variability, it is necessary for each GCM to have multiple ensemble simulations in the historical period and for each of the representative concentration pathways (RCPs) 2.6, 4.5 and 8.5 for future scenarios (Van Vuuren et al., 2011). In addition, the GCM mean spring thickness must fall within the 10th and 90th percentile of PIOMAS (Stroeve et al., 2014), have a reasonable spatial resolution, and a somewhat resolved Canadian Archipelago. A consistent spatial distribution of land is needed for realistic and spatially complete multi-model means. The six GCMs that comprise this CMIP5 subset are listed in Table 4.1.

For the CMIP5 subset the historical simulations are used for the period 1979 – 2005. In most of the analysis for the period post-2005 the RCP8.5 scenario is used, which ramps up the amount of greenhouse gases to have a cumulative effect of increasing the direct radiative forcing by 8.5 Wm⁻² (approximately 1370 ppm CO₂ equivalent) by 2100 (Van Vuuren et al., 2011). The impact of other scenarios is compared later in the analysis. Figure 4.2 shows the 1979 – 2014 ensemble-mean September SIT for the CMIP5 subset, highlighting the considerable differences between the model simulations, and indicating that model bias is likely to be the dominant uncertainty in near-term projections.

Table 4.1 | List of models used: the CMIP5 subset and observations.

Institution	Model name	Ensemble members ^a
Commonwealth Scientific and Industrial Research Organisation (CSIRO)	CSIRO Mark version 3.6.0: <i>CSIRO-Mk3.6.0</i> (Rotstayn et al., 2012)	10
Met Office Hadley Centre	Hadley Centre Global Environment Model version 2-Earth System: <i>HadGEM2-ES</i> (The HadGEM2 Development Team et al., 2011)	4
National Center for Atmospheric Research	Community Climate System Model, version 4: <i>CCSM4</i> (Gent et al., 2011)	6
National Center for Atmospheric Research	Community Earth System Model, Community Atmosphere Model, version 5: <i>CESM1-CAM5</i> (Meehl et al., 2013)	3
Model for Interdisciplinary Research on Climate (MIROC)	MIROC version 5: <i>MIROC5</i> (Watanabe et al., 2010)	3
Max Plank Institute for Meteorology (MPI)	MPI Earth System Model, low resolution: <i>MPI-ESM-LR</i> (Jungclaus et al., 2006)	3
Applied Physics Laboratory (University of Washington)	Pan-Arctic Ice-Ocean Modelling and Assimilation System: <i>PIOMAS</i> ^b (Zhang and Rothrock, 2003)	1

^amulti-model statistics are calculated using the first 3 ensemble members (Ch. 4.4.4 onwards).

^bused as observations.

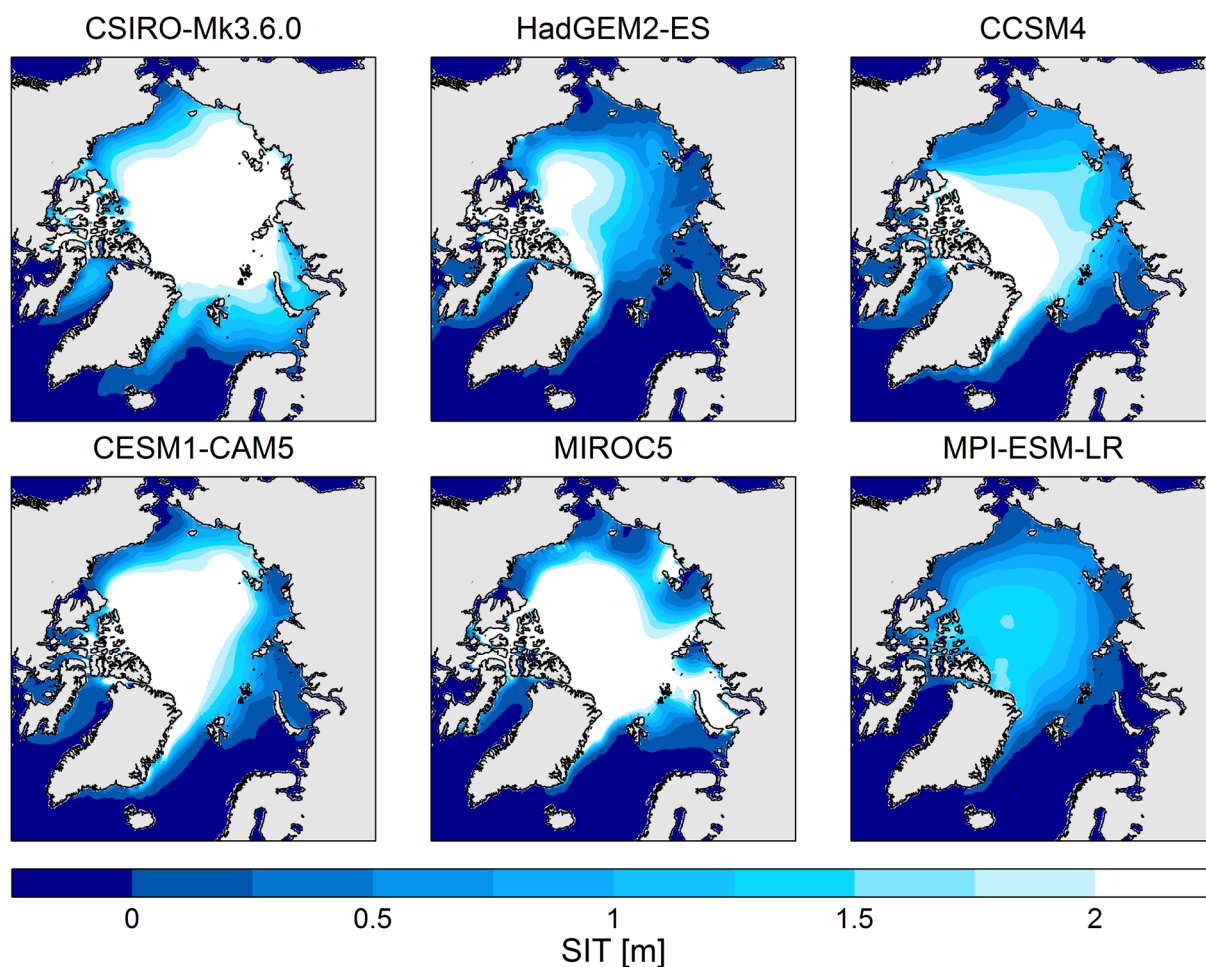


Figure 4.2 | Mean September SIT for each of the six GCMs considered, averaged over the period 1979 – 2014.

The aim of the SIT BC outlined in this chapter is to correct the mean and variance in the CMIP5 subset shown in Figure 4.2 to the PIOMAS statistics. Although this should improve short-term predictions, a caveat to this approach is that PIOMAS only yields one realisation of the past (see Lindsay et al. (2014) for discussion of PIOMAS forced with alternative atmospheric forcings). It has to be assumed that the relatively short period over which there are observations (36 years) captures a representative sample of the behaviour exhibited in the climate system. In the short term, this is probably a reasonable assumption, as the GCMs will not have evolved far from their corrected state of the recent past; this assumption is explored further in Ch. 4.4.

4.3 Bias correction methodology

Bias correction methods effectively aim to reduce model uncertainty by constraining GCMs to observations. There are two components to model uncertainty: the overall mean difference (or bias), and differences in the amplitude of response to specified forcings. The simulated ice loss trend is deliberately not corrected to that which PIOMAS depicts. The rationale is to keep this as prescribed by the different GCMs because the response of the SIT to future warming is unknown, likely non-linear, and the GCMs are designed to give an estimate of this. It is also doubtful how well the forced current trend can be determined from 36 years of data given the high noise to signal ratio for trends, especially on grid point scales. It is also uncertain how much of the recent ice loss seen in the observations can be attributed to changes in external forcing as opposed to internal variability, although previous studies have attempted this including Kay et al. (2011), Day et al. (2012), Notz and Marotzke (2012), Stroeve et al. (2012), Notz (2015), Swart et al. (2015) and Zhang (2015). Caution is also given to overfitting; applying a trend correction will potentially result in an over-confident projection.

To test the performance of different possible BC methods a toy model is used as proxy ensemble timeseries (representing SIT at a single grid point for the same month each year for the period 1979 – 2100). The timeseries are shown in Figure 4.3a for a high-mean–high-variance model (blue) and a low-mean–low-variance model (red), where the black line shows the “truth” observations with one realisation over the historical period only. The timeseries were all produced using a first-order auto-regressive (with an AR(1) parameter of 0.3 chosen to be representative of CMIP5 SIT auto-correlation) model imposed on a declining linear trend with negative numbers reset to zero. Each model has five separate model ensemble members (thin coloured lines); the thick lines represent the ensemble-means. The statistics in all the legends are calculated over the observation window (1979 – 2014). ‘Ice-free’ in Figure 4.3 is here defined as the first occurrence of an ensemble member below 0.15 m. Shown is the ice-free ensemble range, i.e. the year of the first ensemble member to be ice-free to the last ensemble member to be ice-free. A successful BC method should transform the individual ensemble members (thin red and blue lines) to match the mean and variance of the observations (black line), producing matched statistics. Various approaches for such a bias correction are explored. The mathematical notation for the following equations is in Table 4.2.

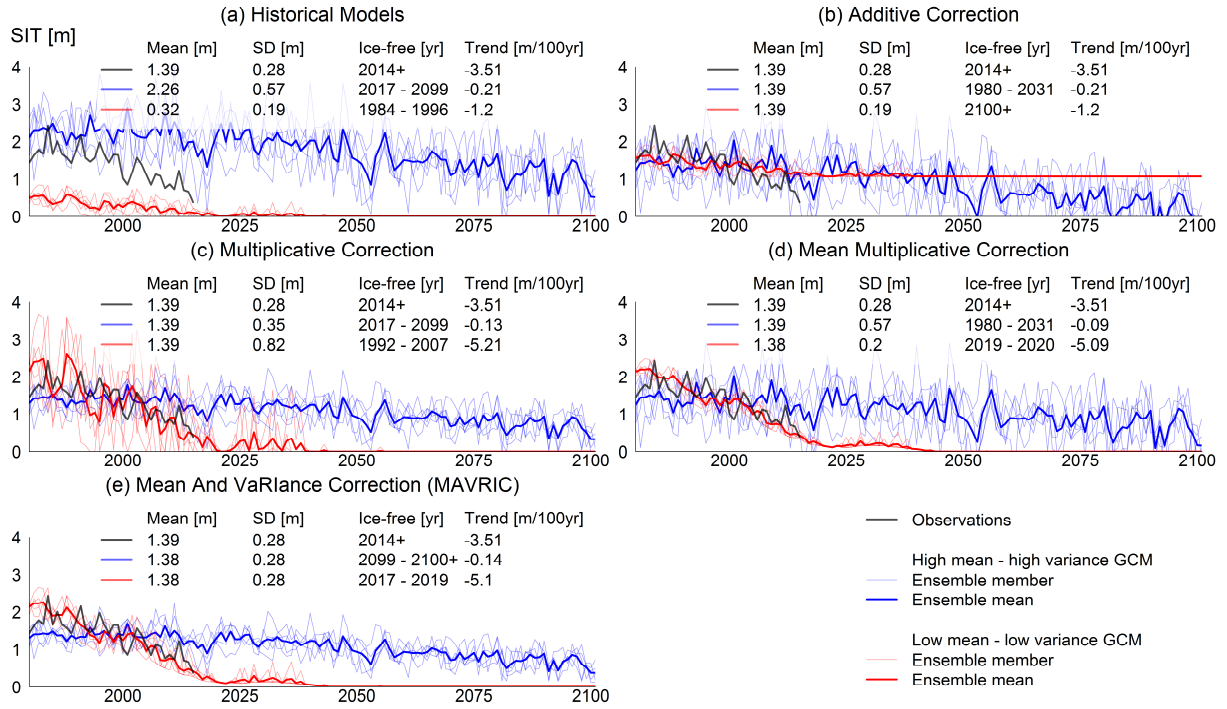


Figure 4.3 | Performance of different SIT BCs for one particular month at a hypothetical grid point in a toy model. Mean, SD (detrended) and trend legend statistics are calculated over the observation period (1979 - 2014). ‘Ice-free’ is defined as the first occurrence of any ensemble member below 0.15 m. The ice-free ensemble range is shown, i.e. the year of the first ensemble member to be ice-free to the last ensemble member to be ice-free. The black line represents ‘observations’; the blue and red lines represent high and low ice models respectively. The thin coloured lines represent ensemble members, and the thick lines represent the ensemble-mean.

Table 4.2 | Notation key.

Notation	Description
M	Model
O_h	Observations
x_h	x over the historical period (1979 – 2014)
\bar{x}	Time mean of x over historical period
$\langle x \rangle$	Ensemble-mean of x
\tilde{x}	Running time-mean (11 years) of x
\hat{x}	Temporally detrended x over the historical period
σ	Standard deviation

4.3.1 Additive correction

A basic additive correction, which has previously been used for temperature projections, is shown in Figure 4.3b. This approach simply corrects the time-mean by subtracting the difference between the historical model ensemble-mean–time-mean, $\langle \overline{M}_h \rangle$, and observation time-mean, \overline{O}_h , from each of the model ensemble members, M .

$$\text{Additive corrected thickness} = M - (\langle \overline{M}_h \rangle - \overline{O}_h) \quad (4.1)$$

However, as the low ice model is adjusted up by the addition of a constant, it equilibrates at a positive value in the future rather than zero. Likewise the high ice model equilibrates at negative values. Neither of these properties are sensible.

This chapter makes use of multiple ensemble members from the same model, raising the question of how to treat ensemble member statistics when calculating a particular GCM's bias. For calculating the mean SIT, each GCM's ensemble-mean is used because it is the GCM's mean bias that is necessary to correct. This is important because a particular ensemble member's deviation from the ensemble-mean is retained; it allows an individual ensemble member's time-mean to be different to the observations over the historical period, but not the ensemble-mean. The treatment of ensemble members for the SD calculation is described in Ch. 4.3.4.

4.3.2 Multiplicative correction

If a multiplicative correction is used (Figure 4.3c), where the ratio of the observed time-mean and model ensemble-mean–time-mean, $\overline{O}_h / \langle \overline{M}_h \rangle$, is multiplied as a factor to the model ensemble members, M , then the corrected thickness is as follows.

$$\text{Multiplicative corrected thickness} = M \frac{\overline{O}_h}{\langle \overline{M}_h \rangle} \quad (4.2)$$

Multiplicative methods effectively preserve the future zero ice year, which is potentially an important value for a wide range of stakeholders. However, when applied as above this approach has the undesired effect of distorting the variances by the same factor as the mean correction, as visible in Figure 4.3c.

4.3.3 Mean multiplicative correction

To avoid altering the variances, the mean multiplicative correction can be introduced (Figure 4.3d), where the multiplicative mean correction, $\overline{O}_h / \langle \overline{M}_h \rangle$, is applied only to the 11-year-centred–running-mean–ensemble-mean, $\langle \tilde{M} \rangle$. This corrects the model mean

evolution without corrupting the sub-decadal variance as $\langle \tilde{M} \rangle$ is smoothed. The model anomalies for each ensemble member, $M - \langle \tilde{M} \rangle$, are then added back to the corrected mean evolution.

$$\text{Mean multiplicative corrected thickness} = (M - \langle \tilde{M} \rangle) + \langle \tilde{M} \rangle \frac{\overline{O_h}}{\langle \overline{M_h} \rangle} \quad (4.3)$$

This works to correct the mean SIT and does not suffer from any peculiarities of the previous two methods. The model variance now remains unchanged but the approach opens up the possibility of correcting the variance towards that observed in the historical period. Note that by using the ensemble-mean, $\langle \overline{M_h} \rangle$, for all these corrections it ensures that each ensemble member is corrected in the same way, thus preserving certain ensemble properties into the future.

4.3.4 Mean and variance correction

The GCMs from CMIP5 show a large range in SIT variance, and the magnitude of these variations is a significant factor determining when regions of the Arctic may first become accessible (when one ensemble member may first become ice-free). Therefore a variance correction is incorporated into Eq. (4.3) by taking the ratio of the temporal standard deviation of the detrended observations, $\sigma_{\widehat{O_h}}$, to the square root of the ensemble-mean of the variance of the detrended model ensembles, $\langle \sigma_{\overline{M_h}} \rangle$ (detrended mean ensemble SD), over the historical period. The detrending in the models is calculated using each model's ensemble-mean linear trend. This has some similarities to the approach of Ho et al. (2011) in application to temperature projections for Europe. See also Ch. 4.4 details further discussion of the choices made.

To incorporate the variance correction, the mean multiplicative correction (Eq. (4.3)) is first de-trended, the variance correction applied, and the trend re-applied. This creates the Mean And VaRIance Correction (MAVRIC), shown in Eq. (4.4).

$$\text{MAVRIC} = (M - \langle \tilde{M} \rangle) \frac{\sigma_{\widehat{O_h}}}{\langle \sigma_{\overline{M_h}} \rangle} + \langle \tilde{M} \rangle \frac{\overline{O_h}}{\langle \overline{M_h} \rangle} \quad (4.4)$$

Figure 4.3e shows the MAVRIC does a near-perfect job of correcting both the mean and variance to the observed statistics while still retaining the individual ensemble members' own climate fluctuations, but being fractionally scaled by the variance ratio.

Comparing the ensemble range in projected ice-free date between the correction methods, it is apparent that although the shapes of time series have qualitatively

changed this does not always result in a different range in projected ice-free date. For example the difference evident on comparing the high-mean–high-variance GCM (blue) between (a) to (c) and (b) to (d) is partly coincidence and partly due to how the four correction methods shown manipulate the timeseries. The MAVRIC method (e) results in a unique set of ice-free dates. This is an important attribute that the MAVRIC method displays, as the ice-free date is of vital importance to stakeholders in the Arctic and more basic methods of bias correction fail to appropriately adjust this parameter.

4.4 Bias-corrected sea ice thickness projections

4.4.1 MAVRIC validation

Figure 4.3e illustrates that the MAVRIC successfully corrects the mean and variance in a toy model environment. Before proceeding to investigate the impact of the MAVRIC on SIT projections, it is prudent to test whether the MAVRIC can improve GCM performance by validating with PIOMAS; CSIRO-Mk3.6.0 (CSIRO) is the GCM used to test. The ice in CSIRO generally has too much areal coverage and too little variability and is a CMIP5 outlier model with regards to SIT (Stroeve et al., 2014). However, CSIRO benefits from having 10 ensemble members, increasing the robustness of the statistics. For these two reasons, it is considered a thorough test of the MAVRIC's performance within a real GCM.

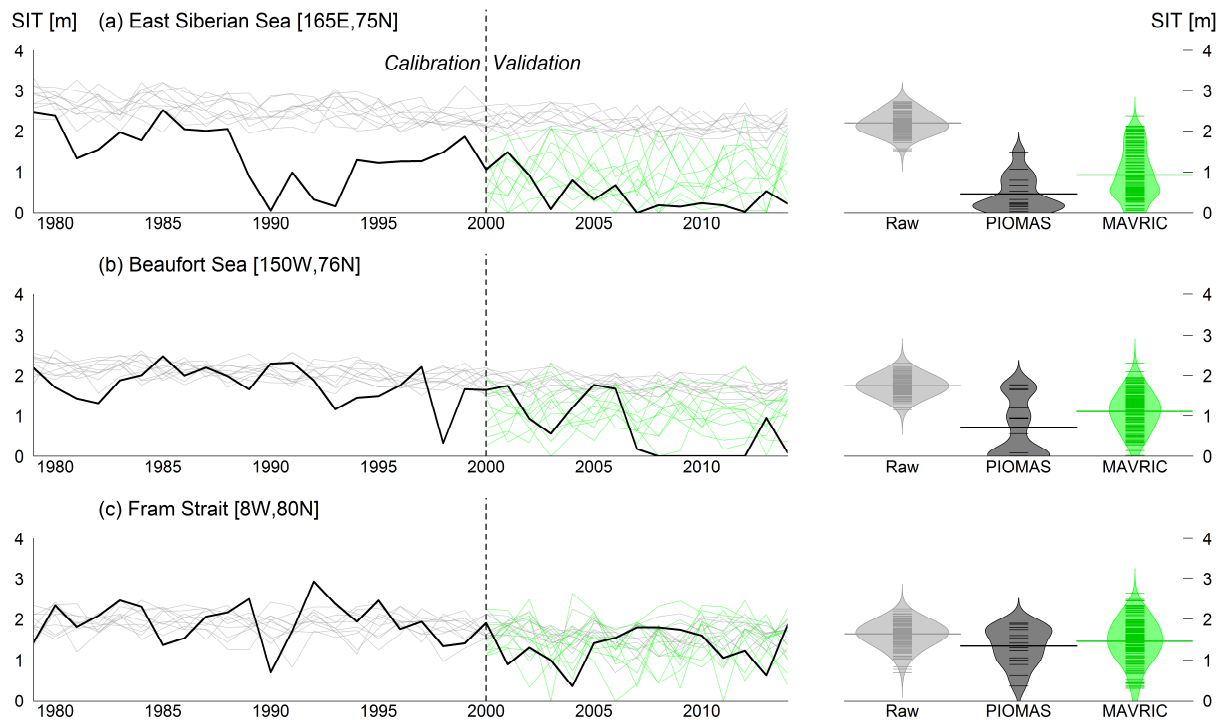


Figure 4.4 | September SIT at three grid point locations in the Arctic, from PIOMAS (black) and CSIRO-Mk3.6.0 historical (1979 – 2005) and RCP8.5 (2006 – 2014) raw output (grey) and post-MAVRIC (green). The raw CSIRO ensembles (grey) are bias-corrected via the MAVRIC using the PIOMAS observations (black) over the calibration window, producing the MAVRIC ensembles (green) for the validation window. Bean plots (right) show the distribution of the SIT for the validation period. The small horizontal lines show every SIT value, the frequency of which is illustrated by the width of the shaded region. The thick horizontal line depicts the mean.

The test uses a data denial method where MAVRIC is trained the on a subset of PIOMAS observations, 1979 – 1999, termed the “calibration window”. From this, the MAVRIC predicts the observations for 2000 – 2014, termed the “validation window”.

A limitation of this method is the length of observations: the period over which the MAVRIC calibration takes place must be long enough to capture a robust measure of the observed statistics. The validation period must also be long enough to be able to draw robust conclusions. It is not clear whether either the 21-year calibration or the 15-year validation windows are long enough for robust method calibration and results verification, but the test is limited by the data available. An additional limitation to this method is that the calibration and validation periods are very close to each other.

Figure 4.4 shows the performance of the MAVRIC at three grid points for September. The raw CSIRO ensembles (grey) are bias-corrected via the MAVRIC using the PIOMAS observations (black) over the calibration window, producing the MAVRIC corrected ensembles (green) for the validation window. If the MAVRIC can produce plausible predictions, the characteristics of PIOMAS should be indistinguishable from individual corrected ensemble members in the validation window. It is clear from the validation bean plots (right), that the distribution from the corrected ensembles resembles PIOMAS much more closely than the raw distribution, e.g. non-zero probability of zero ice. The distribution from PIOMAS is not expected to match the corrected distribution perfectly as PIOMAS only has one realisation (15 data points) while CSIRO has 10 realisations. It can be tentatively accepted that this test demonstrates the validity of the MAVRIC approach.

A concern with calibrating GCMs to the PIOMAS reanalysis is that as PIOMAS is a model product its statistics are potentially already similar to the statistics of the GCMs. Pure observational products such as satellite or submarine measurements of SIT may have fundamentally different characteristics to PIOMAS and the GCMs. Work by Wadhams (1983, 1990), Wadhams and Davis (2000), Kwok and Rothrock (2009) and other submarine voyages contains unprecedented measurements of SIT, the MAVRIC could be calibrated to these to test applicability. These measurements are however, limited temporally and spatially as they are only transects along the submarines path in space and time. More spatially and temporally complete products such as ICESat (Zwally et al., 2002) and CryoSat-2 (Laxon et al., 2013) add further ‘direct’ observational products with which to test the MAVRIC. This is planned as future work and it is hoped

will add to the robustness and verification of the MAVRIC on datasets with a variety of statistical characteristics.

In the following sections the MAVRIC is applied to the CMIP5 subset of six GCMs used in this study (Table 4.1). PIOMAS estimates of Arctic SIT are available from 1979 to 2014. This 36-year window is the period over which statistics are calculated in the observations, and in the CMIP5 subset (using historical runs for 1979 – 2005 and RCP8.5 for 2006 – 2014). Each model, month, and grid point has its own specific correction which is applied to all years (1979 – 2100). However, separate ensemble members from the same GCM are treated with the same correction, thus correcting the model bias and retaining the ensemble spread. Results are shown for September, initially only for CSIRO and later for all six models combined to form the CMIP5 subset used for this study.

For model biases to be calculated a common grid is needed, therefore all MAVRIC calculations took place on the CMIP5 model's native grid. This means that PIOMAS was converted to the CMIP5 model grid for each GCM's bias calculations. This choice was made as it only involves interpolating one of the two fields each time and generally it is PIOMAS that has the higher resolution. The BC shown in Eq. (4.4) contains two terms for the representation of the variance in both observations $\sigma_{\hat{o}_h}$ and models $\langle \sigma_{\hat{M}_h} \rangle$. Over the 36 year period of observations the magnitude of the ice loss trend can be significant. To accurately calculate variances this externally forced trend should first be removed to leave the variance due to internal variability. Here a choice needs to be made about how best to remove the externally forced trend. For the PIOMAS observations a linearly detrending the monthly data is chosen. A smoothed detrending was considered, however this might remove longer timescale variability which is undesirable. Using similar reasoning it is possible that the linear detrending removes some variability on the multi-decadal timescale. This is assumed to be significantly less than variability on smaller timescales, and much of the trend is attributed to be externally forced over the 36 years, hence should not be included as internal variability. The performance of a smoothed detrend was tested in a theoretical framework and resulted in a 10 % loss of accuracy in the variance correction due to attributing variance as trend.

The calculation of variance in the models is more complicated due to the fact that there is more than one realisation. It is obvious that the appropriate variance should be that calculated from the individual ensemble members rather than the ensemble-mean. The

variance should be calculated in each ensemble member and then the mean taken. There is another choice to make, i.e. whether each ensemble member should be detrended with its own trend, or whether the ensemble-mean trend should be used. It was decided that the ensemble-mean trend should be used as this is the models response to the changes in forcings. The model detrended ensemble-mean–standard-deviation, $\langle\sigma_{\tilde{M}_h}\rangle$, was calculated by calculating the detrended ensemble variances, then taking the square root of their mean.

The running mean for the future model correction term $\langle\tilde{M}\rangle$ is calculated over an 11-year period of the ensemble-mean, this window hence starts at 1975 for the historical calculations. The chosen period must be long enough to adequately smooth the timeseries, whilst still being able to capture variations in the sea ice decline trend. This was also tested and found to outperform a 21-year period.

4.4.2 Temporal perspective example

Figure 4.5 shows the impact of the MAVRIC in September in CSIRO at the same three grid points as Figure 4.4 but for the entire calibration window (1979 – 2014). The East Siberian Sea in CSIRO has about double the SIT and half the SD of PIOMAS (Figure 4.5a). The correction therefore reduces the mean SIT whilst increasing the variance. This brings forward the range of first year ice-free conditions (the first occurrence in each ensemble member of a SIT below 0.15 m) from after 2100 to 1981 – 2032. Similarly in the Beaufort Sea (Figure 4.5b) the SD needs to be almost tripled, and the correction results in the first ice-free year occurring over 100 years earlier. In the Fram Strait (Figure 4.5c) CSIRO and PIOMAS have similar SIT, requiring only a small mean adjustment; however CSIRO requires a big increase in variance. The MAVRIC moves the first possible ice-free date about 30 years earlier and increases the ensemble range from 32 to 63 years. It is worth noting that the dominant cause of this shift to an earlier ice-free date at this location is due to the variance correction term in the MAVRIC rather than the mean correction term. This highlights the importance of correcting the variance in addition to the mean. Figure 4.5 demonstrates that the MAVRIC can lead to simulations that look significantly more like reality in the historical period and have an impact on regional ice-free projections.

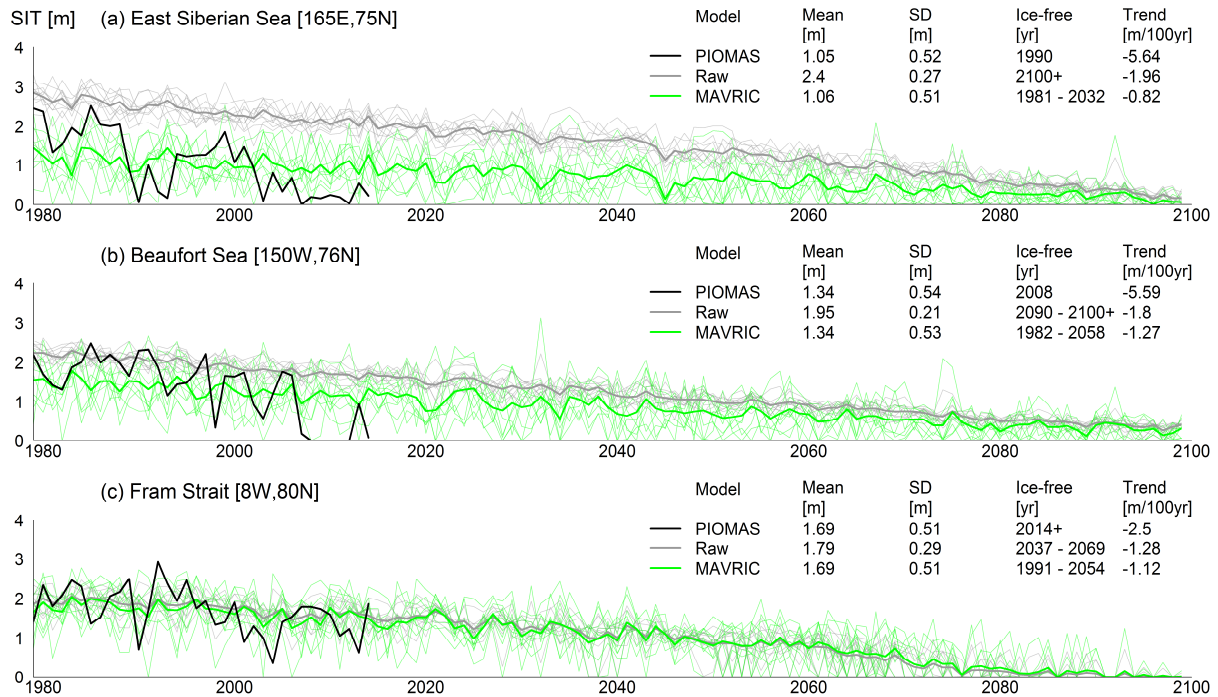


Figure 4.5 | September SIT at three grid point locations in the Arctic, from PIOMAS (black) and CSIRO-Mk3.6.0 historical (1979 – 2005) and RCP8.5 (2006 – 2100) raw output (grey) and post-MAVRIC (green). Thin lines show individual ensemble members; thick lines show the ensemble-means. Mean, SD, and trend legend statistics are calculated over the period of observations (1979 – 2014). The SD is the detrended mean ensemble SD. The range of the first occurrence of the first and last ensemble member below 0.15 m is considered to be ice-free.

4.4.3 Historical spatial perspective

In addition to examining the MAVRIC in a temporal sense, it is important to evaluate the results spatially to see where the MAVRIC is having the most effect and if it works at all locations. Figure 4.6 shows that the mean September SIT distribution is very different in HadGEM2-ES and CSIRO. After the MAVRIC is applied, the mean SIT fields are almost identical for the historical period (Figure 4.6). It is important to note there are still differences when considering individual years and ensemble members i.e. the year-to-year variability and ensemble spread is preserved (although adjusted by the MAVRIC).

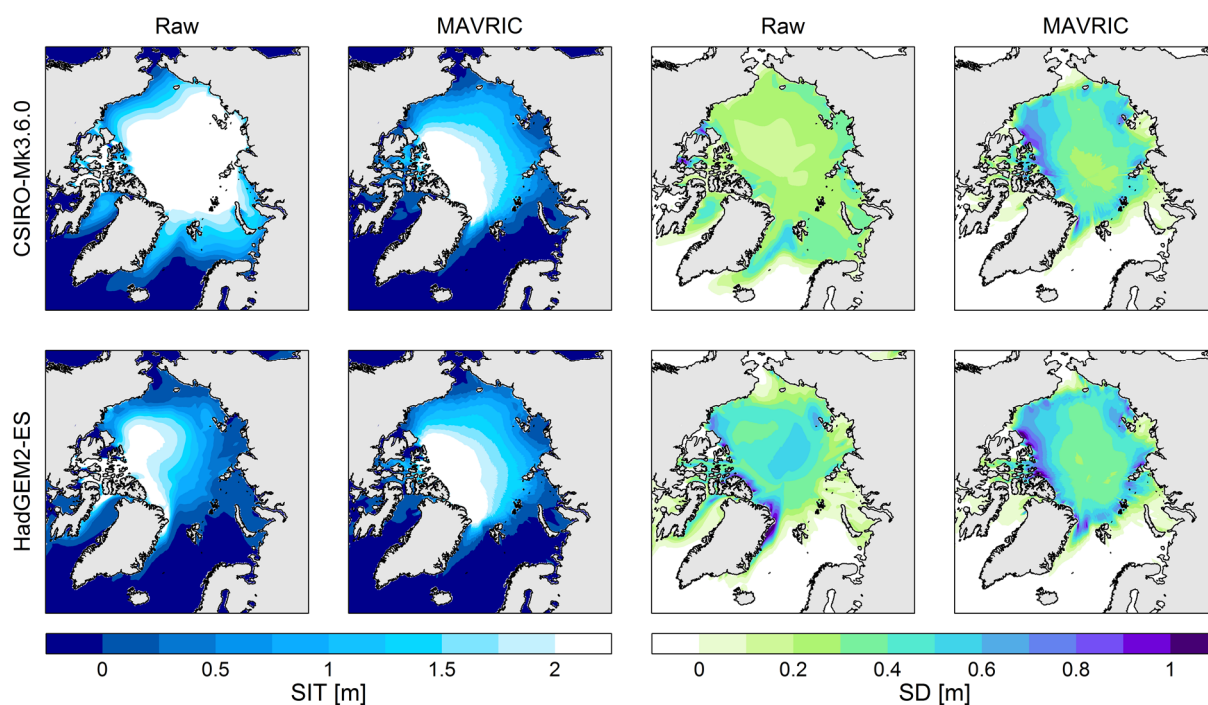


Figure 4.6 | CSIRO-Mk3.6.0 and HadGEM2-ES, September 1979 – 2014 ensemble-mean SIT and SD (detrended). The raw columns are the model solutions as found in the CMIP5 archive. The MAVRIC columns show the distribution after the MAVRIC has been applied. PIOMAS SIT fields are shown in Figure 4.1.

Figure 4.6 also shows the SD before and after the MAVRIC. The SD shown is the detrended mean ensemble SD as before. CSIRO has a variability that is too low in the majority of locations, although it correctly places the maximum SD near the edges of the ice pack similarly to PIOMAS. HadGEM2-ES exhibits about the same magnitude of variability as the observations but the variability is too high in the centre of the ice pack and too low at the edges. After the correction the SD fields in both GCMs now look more similar to each other with the highest variability located at the edge of the ice pack and at coastal locations. They are now also both similar to the estimate from PIOMAS (Figure 4.1).

4.4.4 CMIP5 subset multi-model sea ice thickness projections

The bias-corrected SIT from each GCM can be brought together to form the multi-model mean CMIP5 subset, computed using three ensemble members (the maximum available across all models) from each of the six GCMs for the historical and future decadal periods (Figure 4.7). It is remarkable how the raw multi-model mean product for the historical period is not too different from PIOMAS in Figure 4.1, showing that the location and magnitude of model biases cancel out to a considerable degree, at least with

this subset of models. This agrees with the CMIP5 multi-model mean error which is within 10% of the observational estimates for all months (Flato et al., 2013). Given this result it is not so surprising that the raw and corrected fields are fairly similar for the future projections also.

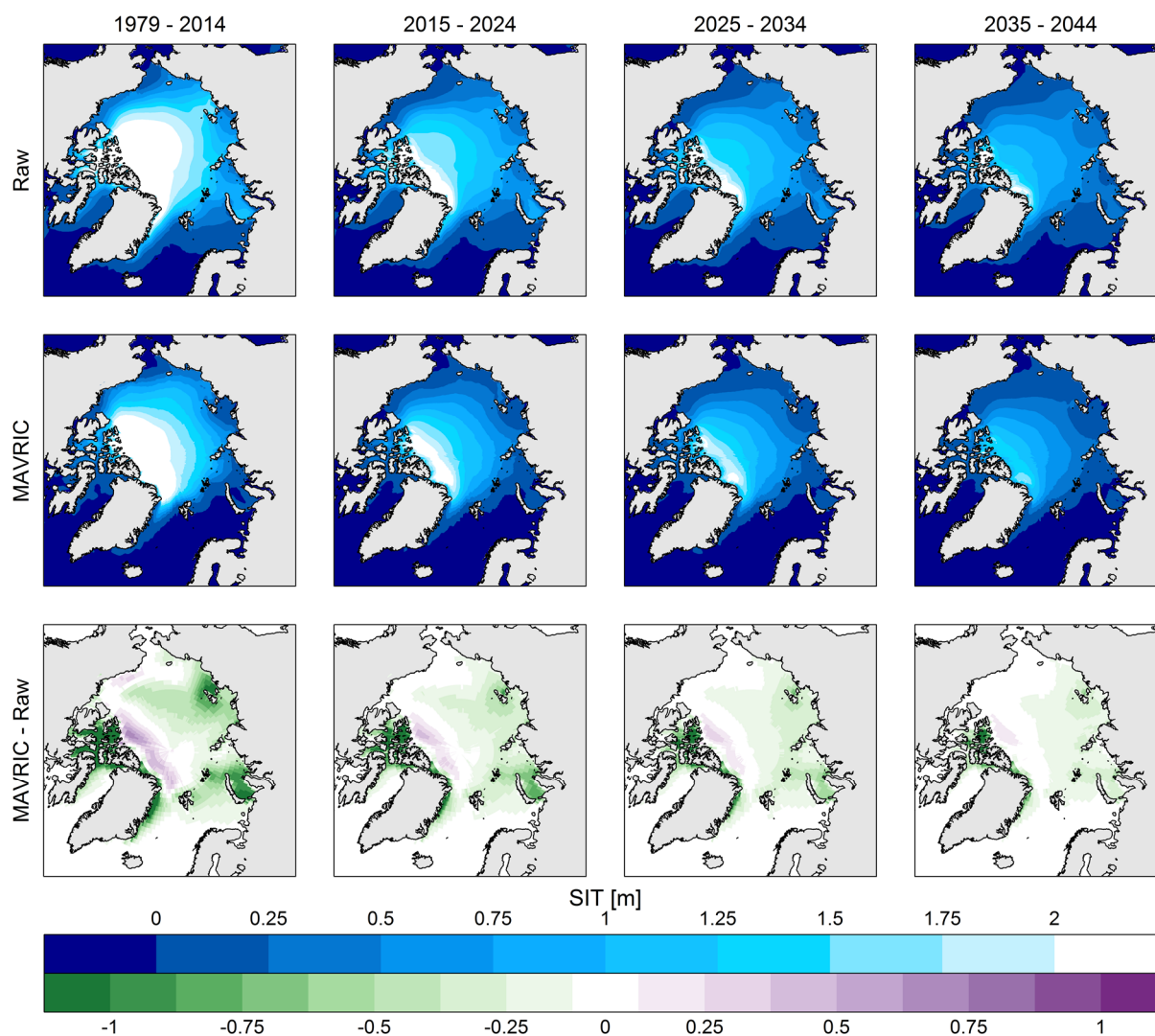


Figure 4.7 | September multi-model-ensemble-mean (three members from each model) mean SIT from the CMIP5 subset, using the raw data (top row) and post-MAVRIC (middle row). The bottom row shows (MAVRIC – raw) ; hence green areas are where MAVRIC has reduced SIT and purple areas are where MAVRIC has increased SIT.

Nevertheless, even in this multi-model multi-ensemble framework the MAVRIC is still making some discernible differences. These differences are most apparent in the Canadian archipelago and the Russian Arctic seas, where the correction leads to a reduction in SIT of approximately 1 m in both regions. Both the raw and bias-corrected fields predict a SIT loss of about 0.25 m per decade.

The fact that the MAVRIC is still making a significant difference on the regional scale is critical, e.g. for ship route availability. Currently, studies that assess the future opening of Arctic shipping routes, which critically depend on the absolute value of SIT, do not yet account for such factors and will need to be reassessed.

4.4.5 Sources of uncertainty in projections of sea ice thickness

The uncertainty in climate projections can be partitioned into three distinct sources: (1) model uncertainty: for the same radiative forcing, different models simulate different mean distributions and temporal changes; (2) internal variability: the natural fluctuations of the climate present with or without any anthropogenic induced changes to radiative forcing; (3) scenario uncertainty: uncertainty in future radiative forcing resulting from unknown future emissions. Hawkins and Sutton (2009, 2011) assessed these sources of uncertainty in global and regional temperature and precipitation projections. Here the sources of uncertainty in SIT are quantified by utilising the CMIP5 subset multi-model ensemble. Crucially the absolute values of SIT are used rather than considering anomalies as is often done for other climate variables. An additional source of uncertainty that is neglected here is the PIOMAS calibration uncertainty emerging from the choice of atmospheric reanalysis and model tuning. This could be assessed by sampling the different versions of the PIOMAS reanalysis described in Lindsay et al. (2014). They find the different versions are broadly similar and can be accounted for by appropriate tuning of the ice model component. This bias in PIOMAS itself will introduce systematic biases to the MAVRIC projections. This bias is not a flaw in the MAVRIC however, but a limitation intrinsic to the observational dataset one is correcting to.

Here the sources of uncertainty are calculated for each decadal period (2005 – 2014, 2015 – 2024, etc.) separately as follows. Three ensemble members from each of the six GCMs are utilised for three different emission scenarios (RCP2.6, 4.5, and 8.5). This results in each decade having $6(\text{GCMs}) \times 3(\text{ensemble members}) \times 3(\text{scenarios}) \times 10(\text{years}) = 540(\text{fields})$.

- The total uncertainty is the SD calculated across all 540 fields.
- The internal variability is calculated similarly to the total variability except instead of the absolute values, the anomalies from the models' decadal-mean–ensemble-mean for each scenario are used.

- To calculate the model uncertainty, each of the six models' decadal-mean–ensemble-mean is calculated, resulting in six fields. The variance is then calculated across these six fields, and repeated for all three scenarios separately (to eliminate differential model dependent responses to the different emission scenarios). The model uncertainty is the square root of the mean of these three fields.
- The scenario uncertainty is calculated in a similar way. For each model, each of the three scenarios decadal-mean–ensemble-means are calculated resulting in three (scenario-dependant) decadal-mean–ensemble-means for each of the six models. The variance is then calculated through these three scenario mean fields for each of the six models, resulting in six fields of the variance in each model. The square root of the mean of the six models scenario uncertainty is the scenario uncertainty.

The MAVRIC method outlined in this study acts to eliminate the model bias in the MAVRIC calibration period (1979 – 2014). After this period the model uncertainty grows due to the GCM's differing responses to changes in external forcing. The sources of uncertainty for SIT for the decade 2015 – 2024, immediately following the MAVRIC calibration period, are shown in Figure 4.8. The total uncertainty in the corrected CMIP5 subset is strikingly lower than in the raw CMIP5 subset. Closer analysis reveals that this is due to the substantial reduction in model uncertainty owing to the MAVRIC. The other sources of uncertainty do not change as much.

The temporal evolution of these sources of uncertainty is shown in Figure 4.9a by taking the median variance from each of the panels in Figure 4.8 for this and other periods. There are three competing factors for how the uncertainty will change with time. First, the SIT is decreasing, and this will reduce the uncertainty as the range of values of which the SIT can occupy shrinks. Second, the separate GCM's simulated SIT responses due to external forcing will differ from each other, causing GCMs to drift apart over time. Thirdly, sea ice at the grid point scale becomes more mobile and vulnerable to external factors as it thins. This will increase variability, initially at least (Sou and Flato, 2009). All of these factors are involved in the evolution of the uncertainties.

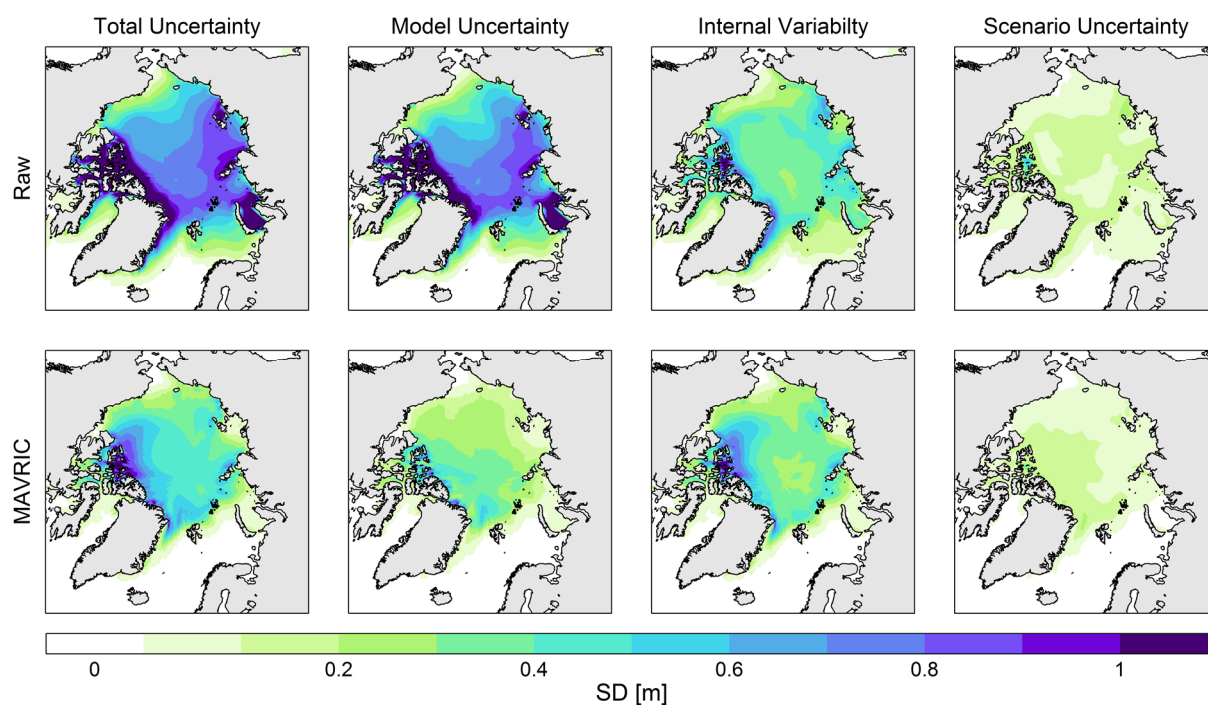


Figure 4.8 | September 2015-2024 sources of SIT uncertainty from the CMIP5 subset (SD of the detrended SIT). The multi-model–ensemble-mean (three members from each) is shown when comparing raw output (top row) and post-MAVRIC (bottom row).

The raw CMIP5 subset exhibits a decrease in total uncertainty with time (dashed black in Figure 4.9a). This is primarily due to the reduction in model uncertainty (dashed blue), likely because the mean SIT is reducing. The corrected total uncertainty is lower than the raw uncertainty until at least the end of the century. This means that the MAVRIC can reduce the model spread (or bias) and so may potentially increase confidence in climate projections of SIT throughout this period. The corrected model uncertainty increases for the first 3 decades, as the models start from a similar state and subsequently diverge because of differing responses to the changes in external forcing. Later the corrected model uncertainty reduces as the mean SIT decreases towards zero.

The total uncertainty is the sum of model uncertainty, internal variability, and scenario uncertainty. The other panels in Figure 4.9 illustrate the relative importance of these sources of uncertainty in terms of the percentage total variance explained, for the raw data, and after the MAVRIC.

To create Figure 4.9b and c it is assumed that the total variance (total uncertainty, T^2) is the sum of the variance due to model uncertainty (M^2), internal variability (I^2), and scenario uncertainty (S^2), formally:

$$T^2 = M^2 + I^2 + S^2 \tag{4.5}$$

It should be noted that the variances calculated above do not always sum exactly in this way due to small interaction terms (approximately 10%) which is ignored.

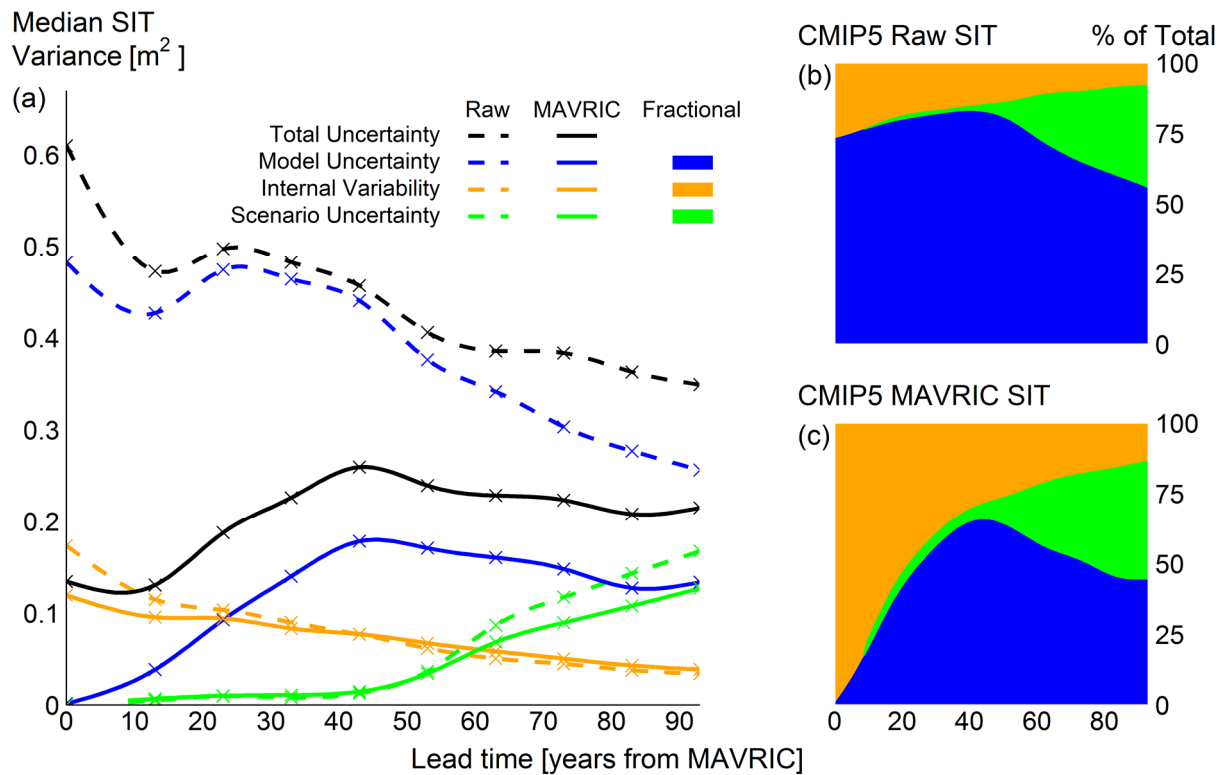


Figure 4.9 | The evolution of the sources of September SIT uncertainty in the CMIP5 sub-set with lead time. Year zero is the MAVRIC window mid-point (1997) and the emission scenarios (RCPs) start in 2006. Panel (a) shows the change in magnitude of the different sources of uncertainty. The uncertainty shown is the median SIT variance and hence the lines scale additively. The dashed lines are for the raw model output and solid lines are for post-MAVRIC. Contributions of model uncertainty, internal variability, and scenario uncertainty as a fraction of total uncertainty are shown for the raw output (b) and post-MAVRIC (c).

Figure 4.9b illustrates that in the raw projections, model uncertainty remains the dominant (> 50 %) source of uncertainty until at least 2100, whereas it only becomes dominant for a few decades mid-century after the MAVRIC (Figure 4.9c). The absolute magnitude of internal variability, and its contribution to the total uncertainty, decreases

with time because SIT also decreases with time. In the corrected projections, the internal variability is the major contributor to the total uncertainty for the first 25 years, compared to a maximum contribution of only 26 % in the raw projections. This highlights the importance of correcting the variance to realistic magnitudes and also the key role of natural variations in predicting the near-future evolution of sea ice. The scenario uncertainty accounts for less than 10 % of the total uncertainty for the first 50+ years. Further analysis metrics on the performance of the MAVRIC method are discussed in the next section (Ch. 4.4.6).

Although demonstrated here, the MAVRIC method reduces the model uncertainty, as seen by the reduction in spread of projected SIT with this selection of GCMs, this may not necessarily correspond to a reduction in uncertainty in the real world.

4.4.6 Further MAVRIC performance analysis

To highlight whether the estimated uncertainties are reliable, the errors in the projections are examined by considering one member as ‘truth’. As all ensemble members are constrained by PIOMAS, one individual ensemble member out of sample should fall within the distribution of the remaining ensemble members. This principle should hold true for all ensemble members out of sample in turn.

The root-mean-square error (RMSE) is calculated using Eq. (4.6):

$$\text{RMSE} = \sqrt{\frac{1}{18} \sum_{n=1}^{18} (E_n - \overline{E_{15}})^2}, \quad (4.6)$$

where E_n is the ensemble member between 1 and 18; $\overline{E_{15}}$ is the mean of the 15 ensemble members from the models of which E_n is not a member.

Figure 4.10 shows the advantage of the MAVRIC method in this out of sample RMSE test. A decreasing RMSE means that the models are initially biased though are converging to a common value (as is expected in this case as the models trend towards being ice-free). An increasing RMSE means that the models are diverging as they have different ice loss trends.

The MAVRIC ensemble trained on every individual ensemble member within MAVRIC results in a RMSE of 0.1 m initially and up to a maximum RMSE of 0.5 m. The fact that the raw RMSE decreases (as opposed to increases) highlights that the models have

biases. The 0.1 m in the MAVRIC RMSE indicates that initially the MAVRIC ensemble members differ only in internal variability. The RMSE then grows due to differing ice loss trends which is expected as there is no attempt to correct the trends in this study.

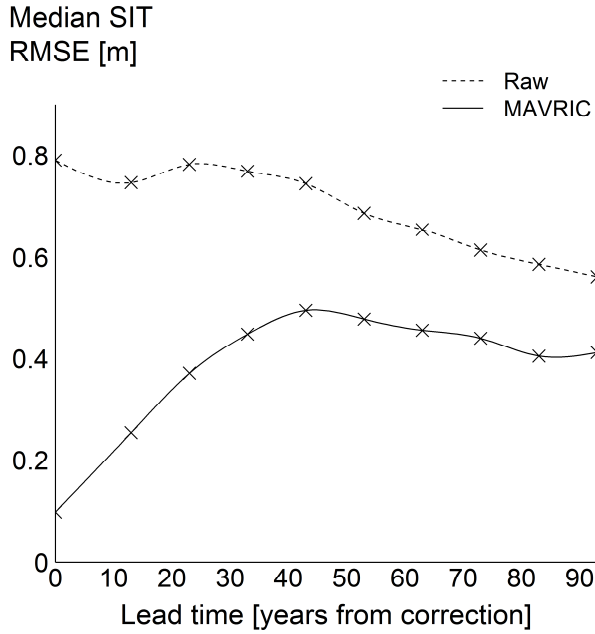


Figure 4.10 | Multi-model ensemble out of sample September median SIT RMSE.

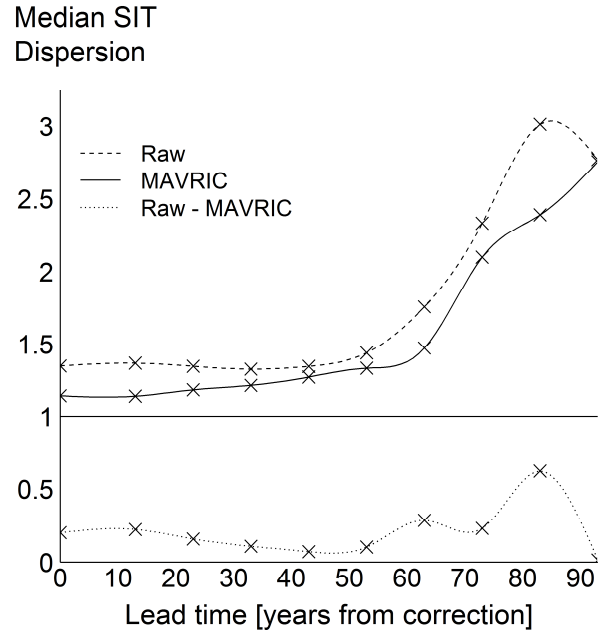


Figure 4.11 | Multi-model ensemble out of sample September median SIT dispersion.

To find the dispersion of the MAVRIC multi-model ensemble this style of experiment repeated with the standard error (SE) metric, using Eq. (4.7)

$$SE = \frac{E_n - \overline{E_{15}}}{\sigma_{15}}, \tag{4.7}$$

where E_n is the ensemble member between 1 and 18; $\overline{E_{15}}$ is the mean of the 15 ensemble members from the models of which E_n is not a member, and σ_{15} is the standard deviation of the 15 ensemble members of which E_n is not a member. This is repeated for all 18 ensemble members, giving 18 SEs of how different each ensemble member is to the rest of the multi-model ensemble set. The SD across these 18 SEs is the dispersion of the multi-model ensemble. A perfectly dispersed ensemble set will have a dispersion of 1. Numbers less than 1 mean the ensemble set is under-dispersed and hence predictions/projections from that set will be under-confident as the SD is too large. Values greater than 1 indicate that the system is over-dispersive and hence over-confident.

The results of the dispersion calculation are shown in Figure 4.11. The MAVRIC ensemble is approximately 15 % – 30 % over-dispersed for lead times of up to 60 years. This means that the ensemble is slightly over-confident and thus has slightly too little overall variance. The rapid increase in dispersion from 60 years is solely due to the CSIRO GCM, specifically its comparatively slow ice loss trend. This was tested by repeating the dispersion experiment omitting CSIRO (not shown). At this lead time many models are starting to be ice-free in September while CSIRO retains ice. It is to the merit of MAVRIC that it is less over-dispersed than the raw output, hence more reliance can be placed on MAVRIC than the raw output as it's ensemble distribution is more representative.

4.4.7 Reduced spread in timing of ice-free conditions

By reducing the model spread the range of possible outcomes has been reduced, this potentially leads to greater confidence in SIT projections. Figure 4.12 shows the raw and corrected CMIP5 subset SIV* projections until 2100 using the 18 multi-model ensemble members in each scenario as before (* calculated here does not consider spatial SIC as it is not bias-corrected). To find a representative SIC for the SIV* calculation the September SIC in CCSM4 RCP8.5 is used, it simulates a mean (of the non-zero grid cells) SIC of approximately 50% for 2006-2100.

The thick coloured lines show the multi-model scenario mean and the coloured regions represent the 16 – 84 percentiles (equivalent to 1σ around the mean of a Gaussian distribution) of the ensemble members. To account for the large range in SIT at any particular time in the CMIP5 subset, a method similar to that of Massonnet et al. (2012) is used to calculate first ice-free conditions. A SIV for ice-free conditions of $1 \times 10^3 \text{ km}^3$ is postulated, which is in agreement with previous studies calculating first ice-free dates (e.g. Massonnet et al. (2012) and Overland and Wang (2013)), and is equivalent to 1 m thick ice for an ice extent of 10^6 km^2 .

The MAVRIC reduces the total SIV, but the relative magnitude of this reduction decreases as SIV declines. The 16 – 84 % range has also been vastly reduced, particularly for the near future. For example, in 2025 the MAVRIC has reduced the 16 – 84 % range from $6 \times 10^3 \text{ km}^3$ to $2.5 \times 10^3 \text{ km}^3$. It is this reduction in the plausible range of SIV that leads to potential increased confidence in projections of SIT and SIV. To assess when the Arctic will first display ice-free conditions RCP8.5, the most realistic scenario from the last 10 years (Fuss et al., 2014), is used. The cumulative number of

ensemble members having satisfied the ice-free criterion as a function of time is shown in Figure 4.12c. If the range in this parameter has reduced, this will be shown by the gradient of the line increasing post-MAVRIC, and this is clearly seen. Figure 4.12d further illustrates the spread reduction with box plots, where the internal line represents the median (9th) ensemble member to go ice-free. This occurs in 2052 with the MAVRIC, 9 years earlier than before. The box represents 16 – 84 % of the ensemble members. This range has been reduced by about 20 years; dates after 2085 can now be eliminated.

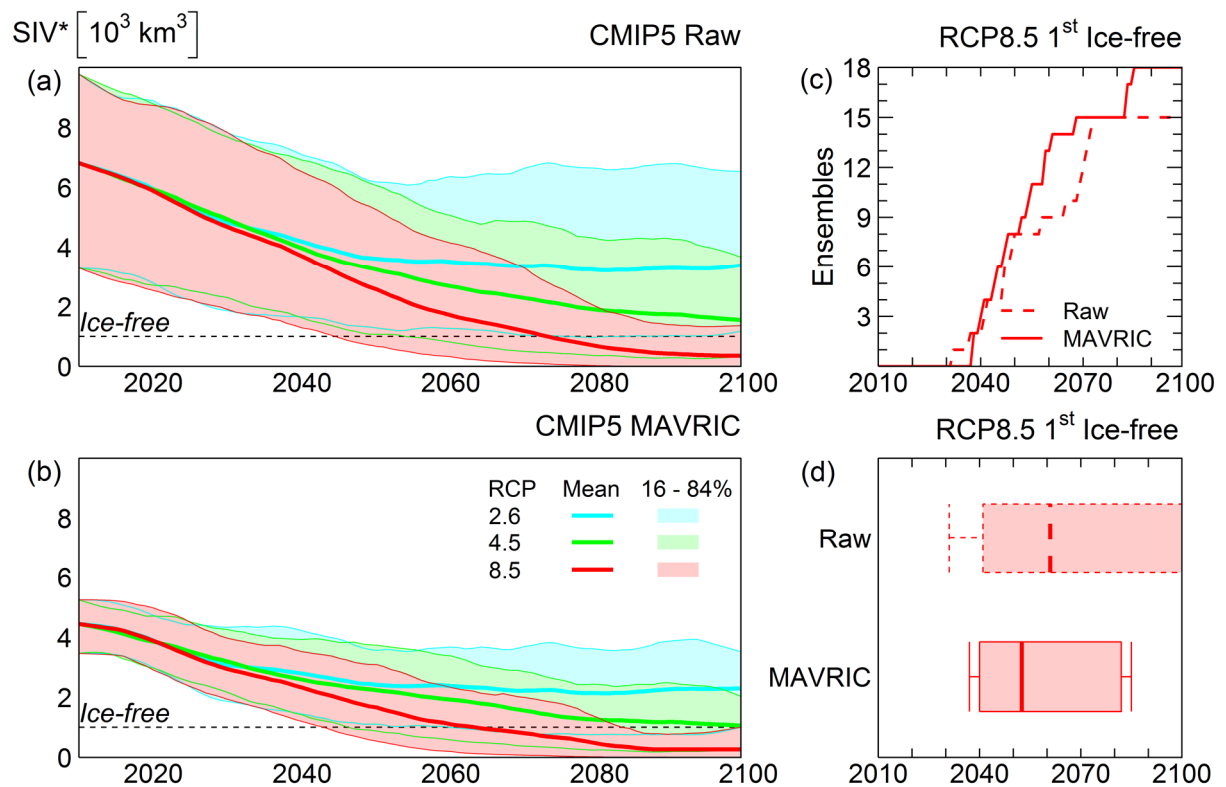


Figure 4.12 | CMIP5 subset sea ice volume (SIV*) projections and first ice-free conditions. Panels (a, b) show the projected SIV* from all six models (18 ensemble members total) in both the raw and corrected GCMs (11-year running mean), and shaded regions are the 16th – 84th percentiles. Panel (c) shows the number of ensemble members having passed the ice-free threshold. Panel (d) shows the statistics of (c), with the whiskers representing the range (1st and 18th ensemble member ice-free), the box capturing the 16th – 84th percentiles, and the bold line showing the median (9th ensemble member). Ice-free is defined as the first year the pan-Arctic SIV* dips below $1 \times 10^3 \text{ km}^3$ for a particular ensemble member. *Volume (SIV*) is calculated using a constant 50 % SIC throughout.

Corrected results from the other emission scenarios show similar features but with later ice-free dates, as expected for lower emissions, and some ensemble members fail to

become ice-free by 2100. For RCP4.5 the MAVRIC makes a profound difference with the median ice-free date occurring 35 years earlier in 2060. For RCP2.6 there is spread reduction mid-century but the CMIP5 subsets before and after the MAVRIC are in good agreement by the end of the century, with projected ice-free dates around 2090.

4.5 Summary and discussion

4.5.1 Summary

In this chapter a bias-correction methodology for simulations of sea ice thickness (SIT) has been developed. By constraining CMIP5 simulations with the PIOMAS reanalysis the following has been demonstrated.

1. *Can a statistical bias correction technique be developed that corrects the SIT biases in GCMs?*

GCMs simulate a wide range of SIT in the historical period and exhibit various spatial and temporal biases when compared with the PIOMAS reanalysis. This model uncertainty (or bias) is the dominant source of uncertainty in CMIP5 future climate projections of SIT. The Mean And VaRIance Correction (MAVRIC) technique outlined in this chapter robustly corrects these biases to the PIOMAS reanalysis.

2. *Will the bias correction reduce the uncertainty in climate change projections of SIT?*

The MAVRIC significantly reduces the total uncertainty in future projections of SIT to at-least 2100 by reducing model uncertainty. Correcting both mean and variance of models is found to be critical for improving the robustness of the projections. The MAVRIC results in internal variability being the dominant source of uncertainty until 2022, and model uncertainty is dominant thereafter. From the mid-century onwards, scenario uncertainty becomes increasingly important and as influential as model uncertainty by 2100.

3. *When will the Arctic display seasonally ice-free conditions?*

Using the SIV* metric and the ice-free criterion described in Ch. 4.4.7, the MAVRIC results in projected September ice-free conditions in the Arctic under RCP8.5 occurring in the 2050s, up to 10 years earlier than without the correction, and with a considerably narrower range, e.g. excluding post-2085 dates. Under RCP4.5, ice-free conditions are likely delayed to the turn of the century; RCP2.6 most likely avoids consistent September ice-free conditions altogether.

4.5.2 Discussion

Without the MAVRIC, the true magnitude of the internal variability and scenario uncertainty in projections of SIT is concealed by the dominant model uncertainty. This

demonstrates that time invested in running many ensemble members to sample internal variability in SIT may be more beneficial than running many future emission scenarios for near-term projections. These findings implicate that there is room for improvement in GCMs at least for 50-year projections where the scenario differences are negligible. However, for projections at the end of the century, the scenarios become more important.

The MAVRIC bias correction technique developed in this study results in a significant improvement in model simulations of SIT with respect to observations. In future projections, the MAVRIC results in a substantial reduction in the range of SIT, potentially leading to increased confidence in climate projections. As absolute values of SIT are utilised, this reduction in spread potentially has important implications for stakeholder sectors operating in Arctic waters such as the shipping industry. The application of the bias correction results in a 60% reduction in the likely range (16 – 84 percentiles) of sea ice volume in September 2025.

There are a number of caveats to these findings. No attempt is made to constrain the trend in the GCMs. This would be difficult because of the short timescale over which observations are available, raising serious questions about the robustness of calculated historical trends. However, future studies could consider this further and assess the feasibility of a trend correction to GCMs. In addition, it is important to recognise that PIOMAS, used here to represent observations, will also have errors. It would be possible to reduce the multiplicative weightings in Eq. (4) to reflect some uncertainty in the historical data. Other temporally and spatially complete sea ice reanalyses could also be used in future to address this issue.

The simulations tend to show an increase in variance as the sea ice thins, before subsequently declining as the thickness approaches zero (Goosse et al., 2009). Blanchard-Wrigglesworth and Bitz (2014) assessed the relationship of this mean state-dependant variance in 19 GCMs, including five of the six used in this study, in addition to PIOMAS. They find a relationship between mean thickness variability and mean thickness in models; i.e. models with thicker SIT depict more variable SIT. In the 19 GCMs assessed, PIOMAS sits on the trend line for the correlation between mean thickness variability and mean thickness. However, in the MAVRIC, the change in variance is effectively decoupled from the change to the mean state. This aspect could be further developed, but only by making additional assumptions about future changes in SIT variability.

Studies should make use of the MAVRIC in assessing the impact on potential stakeholders sensitive to SIT. Chapter 6 utilises GCMs calibrated with the MAVRIC to investigate the opening of the Arctic sea routes. The bias corrected SIT fields are freely available online for further investigations at (Melia, 2015):

Melia, N.: Improved Arctic sea ice thickness projections using bias corrected CMIP5 simulations. [Dataset]. University of Reading, doi: <http://dx.doi.org/10.17864/1947.9>, 2015.

References

- Blanchard-Wrigglesworth, E. and Bitz, C. M.: Characteristics of Arctic Sea-Ice Thickness Variability in GCMs, *J. Clim.*, 27, 8244-8258, doi: 10.1175/Jcli-D-14-00345.1, 2014.
- Boe, J., Hall, A., and Qu, X.: September sea-ice cover in the Arctic Ocean projected to vanish by 2100, *Nat. Geosci.*, 2, 341-343, doi: 10.1038/ngeo467, 2009.
- Christensen, J. H., Boberg, F., Christensen, O. B., and Lucas-Picher, P.: On the need for bias correction of regional climate change projections of temperature and precipitation, *Geophys. Res. Lett.*, 35, L20709, doi: 10.1029/2008gl035694, 2008.
- Day, J. J., Hargreaves, J. C., Annan, J. D., and Abe-Ouchi, A.: Sources of multi-decadal variability in Arctic sea ice extent, *Environ. Res. Lett.*, 7, 034011, doi: 10.1088/1748-9326/7/3/034011, 2012.
- Flato, G., Marotzke, J., Abiodun, B., Braconnot, P., Chou, S. C., Collins, W., Cox, P., Driouech, F., Emori, S., Eyring, V., Forest, C., Gleckler, P., Guilyardi, E., Jakob, C., Kattsov, V., Reason, C., and Rummukainen, M.: Evaluation of Climate Models. In: *Climate Change 2013: The Physical Science Basis. Contribution of Working Group I to the Fifth Assessment Report of the Intergovernmental Panel on Climate Change*, edited by: Stocker, T. F., Qin, D., Plattner, G.-K., Tignor, M., Allen, S. K., Boschung, J., Nauels, A., Xia, Y., Bex, V., and Midgley, P. M., Cambridge University Press, Cambridge, United Kingdom and New York, NY, USA, 741–866, 2013, doi: 10.1017/CBO9781107415324.020.
- Francis, J. A. and Vavrus, S. J.: Evidence linking Arctic amplification to extreme weather in mid-latitudes, *Geophys. Res. Lett.*, 39, L06801, doi: 10.1029/2012gl051000, 2012.
- Fuss, S., Canadell, J. G., Peters, G. P., Tavoni, M., Andrew, R. M., Ciais, P., Jackson, R. B., Jones, C. D., Kraxner, F., Nakicenovic, N., Le Quere, C., Raupach, M. R., Sharifi, A., Smith, P., and Yamagata, Y.: Betting on negative emissions, *Nature Clim. Change*, 4, 850-853, doi: 10.1038/nclimate2392, 2014.
- Gent, P. R., Danabasoglu, G., Donner, L. J., Holland, M. M., Hunke, E. C., Jayne, S. R., Lawrence, D. M., Neale, R. B., Rasch, P. J., and Vertenstein, M.: The community climate system model version 4, *J. Clim.*, 24, 4973-4991, doi: 10.1175/2011JCLI4083.1, 2011.
- Goosse, H., Arzel, O., Bitz, C. M., de Montety, A., and Vancoppenolle, M.: Increased variability of the Arctic summer ice extent in a warmer climate, *Geophys. Res. Lett.*, 36, L23702, doi: 10.1029/2009gl040546, 2009.
- Haas, C. and Howell, S. E. L.: Ice thickness in the Northwest Passage, *Geophys. Res. Lett.*, 42, 7673-7680, doi: 10.1002/2015gl065704, 2015.
- Hawkins, E. and Sutton, R.: The Potential to Narrow Uncertainty in Regional Climate Predictions, *Bull. Am. Meteorol. Soc.*, 90, 1095-1107, doi: 10.1175/2009bams2607.1, 2009.

Hawkins, E. and Sutton, R.: The potential to narrow uncertainty in projections of regional precipitation change, *Clim. Dyn.*, 37, 407-418, doi: 10.1007/s00382-010-0810-6, 2011.

Ho, C. K., Stephenson, D. B., Collins, M., Ferro, C. A. T., and Brown, S. J.: Calibration Strategies: A Source of Additional Uncertainty in Climate Change Projections, *Bull. Am. Meteorol. Soc.*, 93, 21-26, doi: 10.1175/2011bams3110.1, 2011.

Jungclaus, J., Keenlyside, N., Botzet, M., Haak, H., Luo, J.-J., Latif, M., Marotzke, J., Mikolajewicz, U., and Roeckner, E.: Ocean circulation and tropical variability in the coupled model ECHAM5/MPI-OM, *J. Clim.*, 19, 3952-3972, doi: 10.1175/JCLI3827.1, 2006.

Kay, J. E., Holland, M. M., and Jahn, A.: Inter-annual to multi-decadal Arctic sea ice extent trends in a warming world, *Geophys. Res. Lett.*, 38, L15708, doi: 10.1029/2011gl048008, 2011.

Kwok, R., Cunningham, G. F., Wensnahan, M., Rigor, I., Zwally, H. J., and Yi, D.: Thinning and volume loss of the Arctic Ocean sea ice cover: 2003-2008, *J. Geophys. Res. Oceans*, 114, C07005, doi: 10.1029/2009jc005312, 2009.

Kwok, R. and Rothrock, D. A.: Decline in Arctic sea ice thickness from submarine and ICESat records: 1958–2008, *Geophys. Res. Lett.*, 36, doi: 10.1029/2009gl039035, 2009.

Laxon, S. W., Giles, K. A., Ridout, A. L., Wingham, D. J., Willatt, R., Cullen, R., Kwok, R., Schweiger, A., Zhang, J., Haas, C., Hendricks, S., Krishfield, R., Kurtz, N., Farrell, S., and Davidson, M.: CryoSat-2 estimates of Arctic sea ice thickness and volume, *Geophys. Res. Lett.*, 40, 732-737, doi: 10.1002/Grl.50193, 2013.

Lindsay, R. W., Haas, C., Hendricks, S., Hunkeler, P., Kurtz, N., Paden, J., Panzer, B., Sonntag, J., Yungel, J., and Zhang, J.: Seasonal forecasts of Arctic sea ice initialized with observations of ice thickness, *Geophys. Res. Lett.*, 39, L21502, doi: 10.1029/2012gl053576, 2012.

Lindsay, R., Wensnahan, M., Schweiger, A., and Zhang, J.: Evaluation of Seven Different Atmospheric Reanalysis Products in the Arctic*, *J. Clim.*, 27, 2588-2606, doi: 10.1175/jcli-d-13-00014.1, 2014.

Lindsay, R. W. and Zhang, J.: Assimilation of Ice Concentration in an Ice–Ocean Model, *J. Atmos. Oceanic Technol.*, 23, L21502, doi: 10.1029/2012gl053576, 2006.

Mahlstein, I. and Knutti, R.: September Arctic sea ice predicted to disappear near 2°C global warming above present, *J. Geophys. Res. Atmos.*, 117, D06104, doi: 10.1029/2011jd016709, 2012.

Massonnet, F., Fichefet, T., Goosse, H., Bitz, C. M., Philippon-Berthier, G., Holland, M. M., and Barriat, P. Y.: Constraining projections of summer Arctic sea ice, *Cryosphere*, 6, 1383-1394, doi: 10.5194/tc-6-1383-2012, 2012.

Meehl, G. A., Washington, W. M., Arblaster, J. M., Hu, A., Teng, H., Kay, J. E., Gettelman, A., Lawrence, D. M., Sanderson, B. M., and Strand, W. G.: Climate change projections in CESM1 (CAM5) compared to CCSM4, *J. Clim.*, 26, 6287-6308, doi: 10.1175/JCLI-D-12-00572.1, 2013.

Melia, N.: Improved Arctic sea ice thickness projections using bias corrected CMIP5 simulations. [Dataset]. University of Reading, doi: <http://dx.doi.org/10.17864/1947.9>, 2015.

Melia, N., Haines, K., and Hawkins, E.: Improved Arctic sea ice thickness projections using bias-corrected CMIP5 simulations, *Cryosphere*, 9, 2237-2251, doi: 10.5194/tc-9-2237-2015, 2015.

Notz, D.: How well must climate models agree with observations?, *Philosophical Transactions of the Royal Society of London A: Mathematical, Physical and Engineering Sciences*, 373, 2052, doi: 10.1098/rsta.2014.0164, 2015.

Notz, D. and Marotzke, J.: Observations reveal external driver for Arctic sea-ice retreat, *Geophys. Res. Lett.*, 39, L08502, doi: 10.1029/2012gl051094, 2012.

Overland, J. E. and Wang, M.: When will the summer Arctic be nearly sea ice free?, *Geophys. Res. Lett.*, 40, 2097-2101, doi: 10.1002/grl.50316, 2013.

Rotstayn, L., Jeffrey, S., Collier, M., Dravitzki, S., Hirst, A., Syktus, J., and Wong, K.: Aerosol-and greenhouse gas-induced changes in summer rainfall and circulation in the Australasian region: a study using single-forcing climate simulations, *Atmos. Chem. Phys.*, 12, 6377-6404, doi: 10.5194/acp-12-6377-2012, 2012.

Schweiger, A., Lindsay, R., Zhang, J., Steele, M., Stern, H., and Kwok, R.: Uncertainty in modeled Arctic sea ice volume, *J. Geophys. Res. Oceans*, 116, C00D06, doi: 10.1029/2011jc007084, 2011.

Seneviratne, S. I., Nicholls, N., Easterling, D., Goodess, C. M., Kanae, S., Kossin, J., Luo, Y., Marengo, J., McInnes, K., and Rahimi, M.: Changes in climate extremes and their impacts on the natural physical environment. In: *Managing the risks of extreme events and disasters to advance climate change adaptation*, edited by: Field, C. B., Barros, V., Stocker, T. F., Qin, D., Dokken, D. J., Ebi, K. L., Mastrandrea, M. D., Mach, K. J., Plattner, G. K., K., A. S., Tignor, M., and M., M. P., A Special Report of Working Groups I and II of the Intergovernmental Panel on Climate Change (IPCC), Cambridge University Press, Cambridge, UK, and New York, NY, USA, 109-230, 2012.

Smith, L. C. and Stephenson, S. R.: New Trans-Arctic shipping routes navigable by midcentury, *Proc. Natl. Acad. Sci. U.S.A.*, 110, E1191–E1195, doi: 10.1073/pnas.1214212110, 2013.

Sou, T. and Flato, G.: Sea Ice in the Canadian Arctic Archipelago: Modeling the Past (1950–2004) and the Future (2041–60), *J. Clim.*, 22, 2181-2198, doi: 10.1175/2008jcli2335.1, 2009.

Stephenson, S. R., Smith, L. C., Brigham, L. W., and Agnew, J. A.: Projected 21st-century changes to Arctic marine access, *Clim. Change*, 118, 885-899, doi: 10.1007/s10584-012-0685-0, 2013.

Stroeve, J., Barrett, A., Serreze, M., and Schweiger, A.: Using records from submarine, aircraft and satellite to evaluate climate model simulations of Arctic sea ice thickness, *Cryosphere*, 8, 1839-1845, doi: 10.5194/tc-8-1839-2014, 2014.

Stroeve, J., Serreze, M., Holland, M., Kay, J., Malanik, J., and Barrett, A.: The Arctic's rapidly shrinking sea ice cover: a research synthesis, *Clim. Change*, 110, 1005-1027, doi: 10.1007/s10584-011-0101-1, 2012.

Swart, N. C., Fyfe, J. C., Hawkins, E., Kay, J. E., and Jahn, A.: Influence of internal variability on Arctic sea-ice trends, *Nature Clim. Change*, 5, 86-89, doi: 10.1038/nclimate2483, 2015.

Taylor, K. E., Stouffer, R. J., and Meehl, G. A.: An overview of CMIP5 and the experiment design, *Bull. Am. Meteorol. Soc.*, 93, 485-498, doi: 10.1175/Bams-D-11-00094.1, 2012.

The HadGEM2 Development Team, Martin, G. M., Bellouin, N., Collins, W. J., Culverwell, I. D., Halloran, P. R., Hardiman, S. C., Hinton, T. J., Jones, C. D., McDonald, R. E., McLaren, A. J., O'Connor, F. M., Roberts, M. J., Rodriguez, J. M., Woodward, S., Best, M. J., Books, M. E., Brown, A. R., Butchart, N., Dearden, C., Derbyshire, S. H., Dharssi, I., Doutriaux-Boucher, M., Edwards, J. M., Falloon, P. D., Gedney, N., Grey, L. J., Hewitt, H. T., Hobson, M., Huddleston, M. R., Huges, J., Ineson, S., Ingram, W. J., James, P. M., Johns, T. C., Johnson, C. E., Jones, A., Jones, C. P., Joshi, M. M., Keen, A. B., Liddicoat, S., Lock, A. P., Maidens, A. V., Manners, J. C., Milton, S. F., Rae, J. G. L., Ridley, J. K., Sellar, A., Senior, C. A., Totterdell, I. J., Verhoef, A., Vidale, P. L., and Wiltshire, A.: The HadGEM2 family of Met Office Unified Model climate configurations, *Geosci. Model Dev.*, 4, 723-757, doi: 10.5194/gmd-4-723-2011, 2011.

Tilling, R. L., Ridout, A., Shepherd, A., and Wingham, D. J.: Increased Arctic sea ice volume after anomalously low melting in 2013, *Nat. Geosci.*, 8, 643-646, doi: 10.1038/ngeo2489, 2015.

Transport Canada: Arctic Ice Regime Shipping System (AIRSS) Standards, Transport Publication, 12259 E, 1998.

Van Vuuren, D. P., Edmonds, J., Kainuma, M., Riahi, K., Thomson, A., Hibbard, K., Hurtt, G. C., Kram, T., Krey, V., and Lamarque, J.-F.: The representative concentration pathways: an overview, *Clim. Change*, 109, 5-31, doi: 10.1007/s10584-011-0148-z, 2011.

Vrac, M. and Friederichs, P.: Multivariate—Intervariable, Spatial, and Temporal—Bias Correction, *J. Clim.*, 28, 218-237, doi: 10.1175/jcli-d-14-00059.1, 2014.

Wadhams, P.: Sea ice thickness distribution in Fram Strait, *Nature*, 305, 108-111, doi: 10.1038/305108a0, 1983.

Wadhams, P.: Evidence for thinning of the Arctic ice cover north of Greenland, *Nature*, 345, 795-797, doi: 10.1038/345795a0, 1990.

Wadhams, P. and Davis, N. R.: Further evidence of ice thinning in the Arctic Ocean, *Geophys. Res. Lett.*, 27, 3973-3975, doi: 10.1029/2000gl011802, 2000.

Watanabe, M., Suzuki, T., O'ishi, R., Komuro, Y., Watanabe, S., Emori, S., Takemura, T., Chikira, M., Ogura, T., and Sekiguchi, M.: Improved climate simulation by MIROC5: mean states, variability, and climate sensitivity, *J. Clim.*, 23, 6312-6335, doi: 10.1175/2010jcli3679.1, 2010.

Watanabe, S., Kanae, S., Seto, S., Yeh, P. J. F., Hirabayashi, Y., and Oki, T.: Intercomparison of bias-correction methods for monthly temperature and precipitation simulated by multiple climate models, *J. Geophys. Res. Atmos.*, 117, D23114, doi: 10.1029/2012jd018192, 2012.

Zhang, J. and Rothrock, D.: Modeling global sea ice with a thickness and enthalpy distribution model in generalized curvilinear coordinates, *Mon. Weather Rev.*, 131, 845-861, doi: 10.1175/1520-0493(2003)131<0845:MGSIWA>2.0.CO;2, 2003.

Zhang, R.: Mechanisms for low-frequency variability of summer Arctic sea ice extent, *Proc. Natl. Acad. Sci. U.S.A.*, 112, 4570-4575, doi: 10.1073/pnas.1422296112, 2015.

Zwally, H. J., Schutz, B., Abdalati, W., Abshire, J., Bentley, C., Brenner, A., Bufton, J., Dezio, J., Hancock, D., Harding, D., Herring, T., Minster, B., Quinn, K., Palm, S., Spinhirne, J., and Thomas, R.: ICESat's laser measurements of polar ice, atmosphere, ocean, and land, *Journal of Geodynamics*, 34, 405-445, doi: 10.1016/S0264-3707(02)00042-X, 2002.

Zygmuntowska, M., Rampal, P., Ivanova, N., and Smedsrud, L. H.: Uncertainties in Arctic sea ice thickness and volume: new estimates and implications for trends, *Cryosphere*, 8, 705-720, doi: 10.5194/tc-8-705-2014, 2014.

Chapter 5

Arctic shipping background

This chapter provides background information on Arctic shipping that is relevant for the following chapter where results for future trans-Arctic routes are presented. The major routes and passages through the Arctic Ocean are detailed, along with their navigability characteristics. A brief background on maritime operations is provided and finally a discussion of recent trends.

5.1 Northern Sea Route

The Northern Sea Route (NSR) encompasses multiple navigation corridors through the Russian Arctic seas; west – east: Barents, Kara, Laptev, East Siberian, and Chukchi. They are all marginal seas almost entirely located within the Arctic shelf and lie north of the Arctic Circle; the Russian coast is to their south and they freely mix with the Arctic Ocean to their north. The seas are separated by channels between the Russian coast and the archipelagos of Novaya Zemlya, Severnaya Zemlya, New Siberian Islands, and Wrangel Island (Figure 5.1). These channels present navigational waypoints and all the seas are shallow (up to 200 m), with the Sannikov Strait (the northern-most and primary channel between the New Siberian Islands and Russian mainland) being particularly shallow. The draught of a ship describes the vertical distance between the water line and bottom of the hull (keel). The Sannikov Strait is too shallow for the current largest class of vessels.

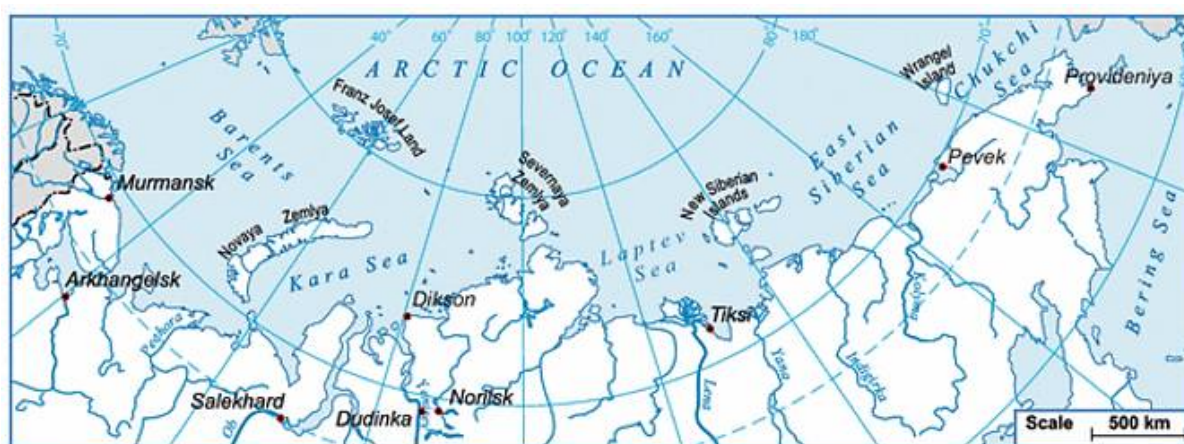


Figure 5.1 | Russian Arctic seas (Marchenko, 2012).

Arctic seas are characterised by the lack of solar heating and the extremely harsh climate that results. The ice conditions on the NSR are variable both spatially along its length, and temporally, with large seasonal and interannual variability. The Barents' sea ice is unique among the Russian Seas in that it is never completely ice covered,

reaching only a maximum of 50% in the winter months. The Kara and Chukchi Seas are affected by cyclonic weather systems from the Atlantic and Pacific Oceans respectively. However large oceanic waves are not often found here due to the dampening effect of the sea ice and small fetch, although this may change in the future with a reduction in the extent of sea ice (Thomson and Rogers, 2014). The hazard does not necessarily come from the waves themselves but from “icing”, where ocean spray instantly freezes onto the ships superstructure adding dangerous destabilising weight to a ship. The interior seas of the East Siberian and Laptev seas are often associated with anti-cyclonic weather, which makes fog a notable hazard. Shipping in the Arctic therefore requires experienced crews operating specially designed vessels with a plethora of upgrades and technologies to combat the unique hazards encountered in polar waters.

In the winter the Kara sea ice constitutes close-drift-ice with fast-ice (ice “fastened” to the land) covering the coastal regions. The Kara is seasonally ice covered, sea ice thickness (SIT) reaches up to 1.5 m in the winter months and usually entirely melts to reveal open water in the summer months. Two ice massifs (large areas of accumulated pack ice found in the same location each summer) are located in the western region of the Kara Sea, compared to five in the eastern Russian Seas (Marchenko, 2012). The Kara gate is the main shipping lane between the Barents and Kara Seas; it has a minimum depth of 21 m with separated shipping lanes, and is a popular route for ports like Murmansk. European traffic using the NSR would benefit from a short cut from the coast of Norway to the north of Novaya Zemlya, towards Severnaya Zemlya, when ice conditions permit.

The Laptev Sea contains one of the largest expanses of fast-ice in the world from January to June reaching up to 2 m thick (Marchenko, 2012). The Vilkitsky Strait linking the Laptev to the Kara Sea presents a challenge to navigation throughout the year. This is due to the presence of ice rather than draft restrictions. The Shokalsky Strait is an alternative just north of Vilkitsky, however the Vilkitsky is more reliably open and the Shokalsky is only ~10 miles wide so it is not resolved by the current generation of climate models, and so is not considered in the simulations here.

There are two major straits linking the East Siberian and Laptev seas. The southern is the Dmitri Laptev and the northern is the Sannikov Strait; they are a barrier to large vessels as they have a minimum depth of 10 m and 13 m respectively. Navigating to the north of the New Siberian Islands is necessary for larger vessels when ice conditions allow, with likely increasing frequency in the future. The East Siberian Sea is

characterised as the shallowest of a Eurasian seas with the continental shelf extending 500 km out into the Arctic Ocean. The winter prevailing wind direction is southerly producing favourable ice navigation conditions (for ice-hardened vessels) in leads and polynyas on the edge of the fast-ice. However, this trend is reversed in the summer with northerly winds helping to maintain the ice frozen over the winter months.

The Chukchi Sea is characterised by usually becoming ice-free early in the season, and for having large seasonal variations in sea ice due to advection of relatively warm water from the Bering Strait. However, the Beaufort Gyre regularly transports old ice from the central Arctic to this region creating a serious hazard to navigation.

Sea ice, present year round in the Arctic seas, is the most important factor in terms of navigation. Of particular interest are the growth and thawing of pack ice, and the formation and destruction of pack ice. The presence of land significantly affects these processes with the creation of ice massifs and polynyas.

5.2 North West Passage

The North West Passage (NWP) is the collective term for multiple routes through the Canadian Archipelago (Figure 5.2). It is located to the north of Canada from Baffin Bay to the Beaufort Sea and stretches for 2,400 km from east to west, encompassing an area about the size of Greenland. Although the land archipelago serves as a major obstacle to shipping from Atlantic to Pacific oceans, the passages are many and provide many route options. Collectively they make up the much-famed NWP, which held the attention of European explorers for at least 400 years. Famed Norwegian explorer, Roald Amundsen, was the first to complete a transit of the NWP 1903 – 1906. In general, the shipping season is relatively short on the NWP from late-July to mid-October (for ice-hardened vessels).

Table 5.1 | Description of the different NWP channels (Figure 5.2) categorised in southern (S.) and northern (N.) options. Top half used in this Thesis, bottom half too small to be resolved by climate models. Adapted from Ostreng et al. (2013).

Route	Routing	Of note
N.NWP(a)	Lancaster Sound – Barrow Strait – Viscount Melville Sound – M'Clure Strait	Icebreaker Kapitan Khlebnikov 2001
S.NWP(a)	Lancaster Sound – Barrow Strait – Peel Sound – Franklin Strait – Larsen Sound – Victoria Strait – Queen Maud Gulf – Dease Strait – Coronation Gulf – Dolphin ad Union Strait – Amundsen Gulf	Considered best of the southern NWP routes but 10 m draft
S.NWP(b)	As S.NWP(a) but routing the west of Prince of Wales Island on the M'Clintock Channel instead of Peel Sound – Franklin Strait	Longer alternative if Peel Sound blocked
N.NWP(b)	Lancaster Sound – Barrow Strait – Viscount Melville Sound – Prince of Wales Strait – Amundsen Gulf	Deep, St. Roch 1944, SS Manhattan 1969
S.NWP(c)	As S.NWP(a) but James Ross Strait- Rae Strait – Simpson Strait instead of Victoria Strait	Route of Roald Amundsen
S.NWP(d)	Hudson Strait – Foxe Channel – Foxe Basin – Fury and Heda Strait – Gulf of Boothia – Bellot Strait – Franklin Strait As S.NWP(a)	Not a commercial passage due to draft restrictions.

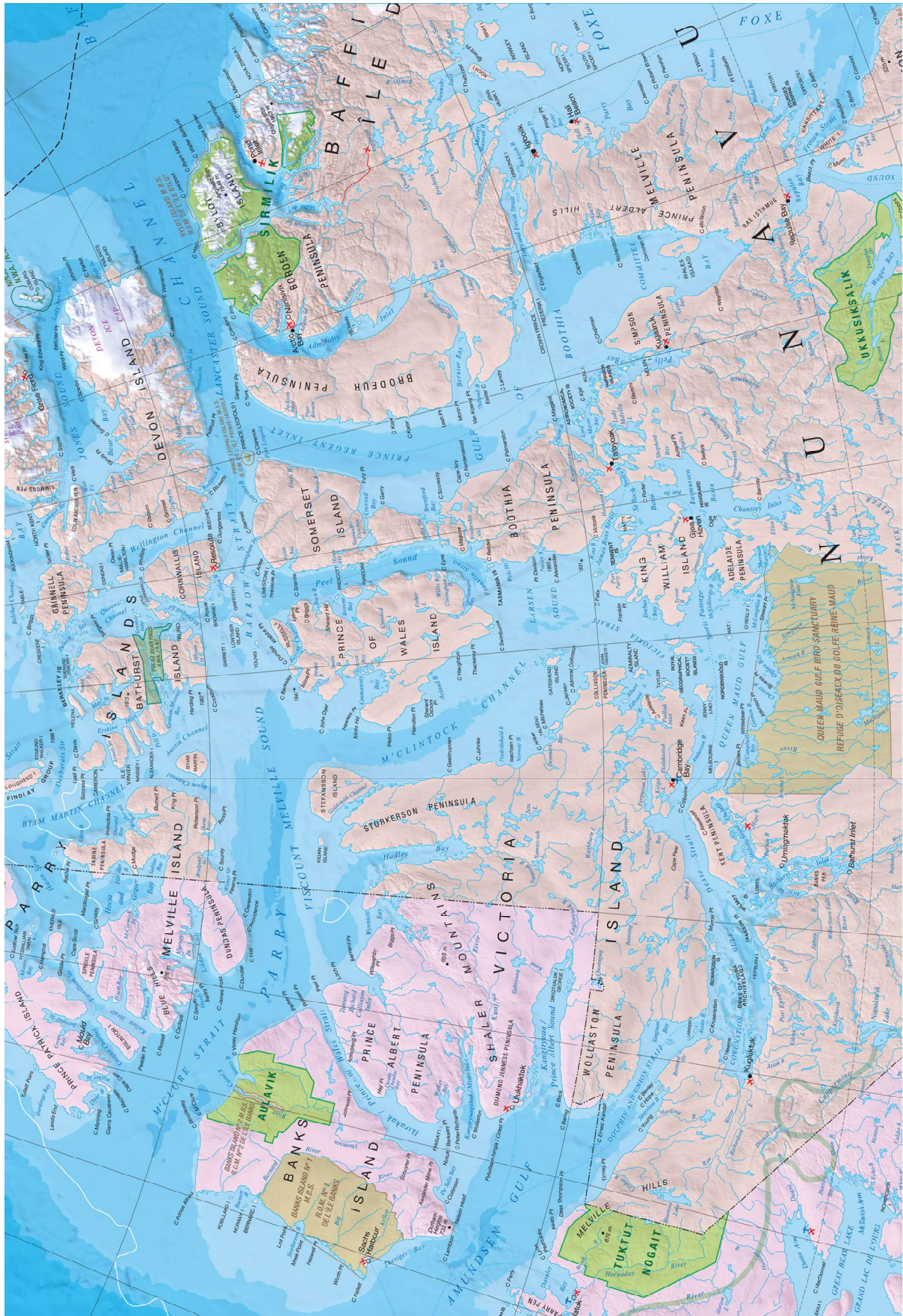


Figure 5.2 | Atlas of the Canadian Archipelago (Government of Canada, 2012).

The sea ice conditions on the NWP are far more complex than the NSR. Observations reveal large inter-annual variability in the ice conditions (explaining why robust trends are impossible to calculate for some stations (purple) in Fig. 2.3). Conditions on the NWP in any given year are not correlated with the NSR, illustrating the large spatial variability found across the Arctic. Knowledge of future ice conditions along the NWP is difficult, as global climate models simply do not possess high enough resolution to realistically simulate all the passages. Predicting the changes to an already complex system is also problematic. In general, warmer temperatures should lead to less ice on the NWP due to a longer and more intense melting season. However, the transition is very complicated. For example, channels in the northern regions of the archipelago are blocked, often year-round, with ice-plugs. Increased temperatures cause these plugs to fail more often, which then allows the back-log of thick multi-year ice to be advected through the passages from the north, invading the major NWP shipping channels.

There are multiple combinations of routes through the Canadian Archipelago; the top three in Table 5.1 are assessed in this thesis, as GCMs include sea ice information for these channels. The bottom three are regular shipping routes, but use channels too small to be represented by climate models, and so are not considered in future shipping projections in Ch. 6. The NWP routes are classed into northern versions (N.NWP, via M'Clure Strait) and southern versions (S.NWP, via Amundsen Gulf). The N.NWP is the shortest NWP route, however thick multi-year ice is often found in the M'Clure strait advected from the Beaufort Gyre. The S.NWP is a longer but more popular route; ice conditions are more favourable with open water not uncommon in summer.

5.3 Maritime operations

5.3.1 Ships

The same international maritime regulatory regime applies in the Arctic as for other oceans. The most important international convention concerning the safety of merchant ships is the international convention for the Safety Of Life At Sea (SOLAS) 1974, which specifies minimum standards for construction and equipment of ships. All Arctic states have ratified the SOLAS agreement; however, it is the responsibility of the Flag State to certify a ships requirement. In 2015 the Polar Code was ratified which adds additional polar-specific considerations and will come into effect in 2017. It covers aspects such as:

ship design, construction, equipment, operations, training, search and rescue, and measures protect to the polar environment.

Ships built for operation in ice-covered waters are built to a specific ice-class. These requirements include a strengthened hull, rudder, and propulsion systems. Icebreakers are furthered enhanced and are ships whose primary purpose is to break ice. The Polar Classes contain seven levels of strengthening, where PC7 is the least capable and PC1 the most, in terms of year round operations in all Arctic waters.

5.3.2 Supplementary costs

The general optimism behind trans-Arctic shipping is that routes become shorter/faster, and hence costs are reduced. However, for this to be assessed accurately the extra costs of operating in Arctic waters must be taken into account. Concerning this, the bureaucracy is very different between the NSR and NWP.

The northern sea route administration details a list of requirements, and charges to operate on the NSR (Arctic Logistics Information Office, 2015), however dialogue with ship owners has revealed that some of these are negotiable (Lasserre, 2014). To transit the NSR, a ship operator must apply for a permit between 120 – 15 days in advance of the estimated arrival in the NSR water area. The application must contain a detailed list of vessel specifications. After preliminary approval, a representative must then inspect the ship for ice-navigation-worthiness. If these requirements are met a date for passage is scheduled, and pilotage, icebreaker support, meteorological and satellite communications are arranged. There is no standard fee, as it is dependent on many variables for example ship size/cargo, ship crew, ice conditions, and presumably negotiation skills. Lasserre (2014), in a review paper on the costs of Arctic shipping, collates a number of studies that have found that these costs are high enough to negate any cost savings from the shortened route, though there are just as many studies finding the route cheaper. The main cost to shipping is the price of bunker fuel (the relatively unrefined fuel ships use); cheaper prices mean that trans-Arctic routes become less attractive. Incredibly the price dropped so much in 2015 (from ~\$400 to \$150) that some bulk cargo ships even shunned the Suez Canal for routes via Cape of Good Hope (Baraniuk, 2016).

The NWP currently has no fee system and the Canadian government will most likely not introduce fees, as it would discourage the economic viability of the route. However, insurance premiums vary widely; they are currently higher for the NWP than the NSR.

The NSR is currently the most attractive of the three major route choices because of the favourable ice conditions. Currently Russia plays a powerful role in controlling the waters of the NSR. With future reduction in Arctic sea ice, trans-polar routes via the North Pole may become a more attractive prospect and the current influence of the Russian government could diminish.

5.4 Recent trends

The number of transits in any given year on the NSR is influenced by the sea ice conditions and non-climatic factors such as bunker fuel price. The number of commercial ships making a trans-Arctic journey from the Pacific to the Atlantic (or vice versa) along the NSR was 4 in 2010, 41 in 2011, 46 in 2012, 71 in 2013, and 53 in 2014 (Northern Sea Route Information Office 2013a). Statistics for 2015 indicate that this dropped to just 18 vessels, likely due to the crash in the price of bunker fuel, meaning alternative routes (e.g. via the Suez Canal) are more attractive.

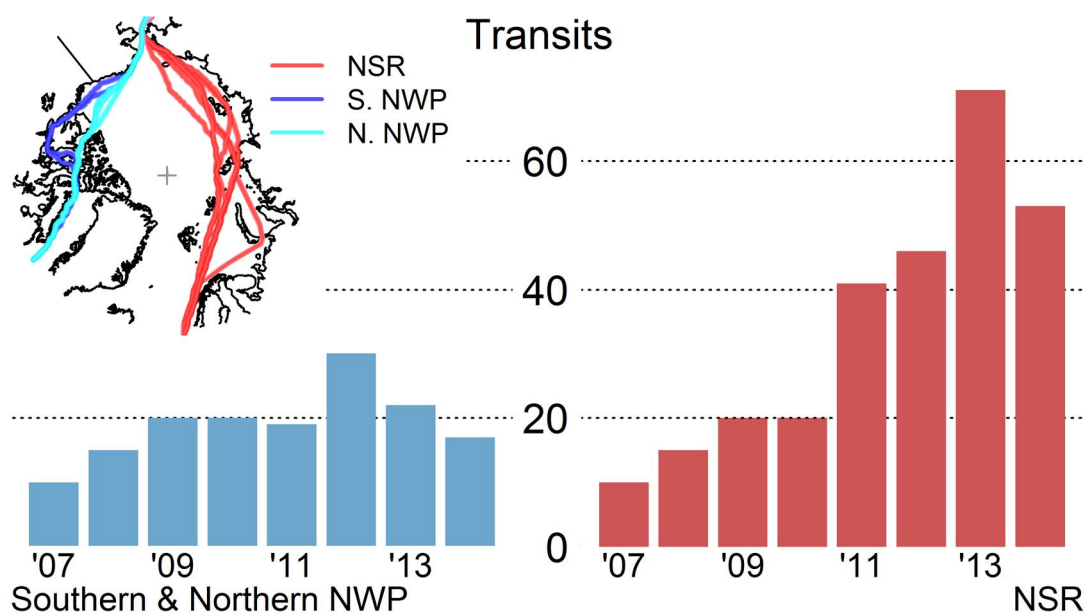


Figure 5.3 | Completed transits of the NWP and NSR. Map insert illustrates the different route versions.

Currently the majority of shipping in the Arctic is still destination shipping; i.e. trips are to and from ports within the Arctic rather than Arctic-transit shipping. Figure 5.4 shows the total number of ships in each region for a single month in August 2011. Note that this data is for all ships, not just commercial. The majority of routes inside the

Arctic are along the Eurasian coastlines on the NSR, at the sea ice edge between Spitzbergen and Greenland, and Canadian Archipelago.

The data also reveals voyages in the Arctic Ocean interior. This track belongs to the research icebreaker Polarstern of the German Alfred-Wegener-Institut for Polar and Marine Research (AWI) reaching the North Pole on August 22nd en route to the Canadian Arctic. The voyage included 55 scientists from six countries with the mission called: “TransArc – Trans-Arctic survey of the Arctic Ocean in transition”. One of the notable findings of the trip was a modal ice thickness of 0.9 m; they note this is identical to findings in 2007 before the notorious ice minimum (Alfred-Wegener-Institut, 2011). The ship-track data also reveals an absence of activity in the Barrow Strait. Consulting the sea ice concentration map shows that ice was present in this portion of the Parry Channel and that may have discouraged navigation in that region.

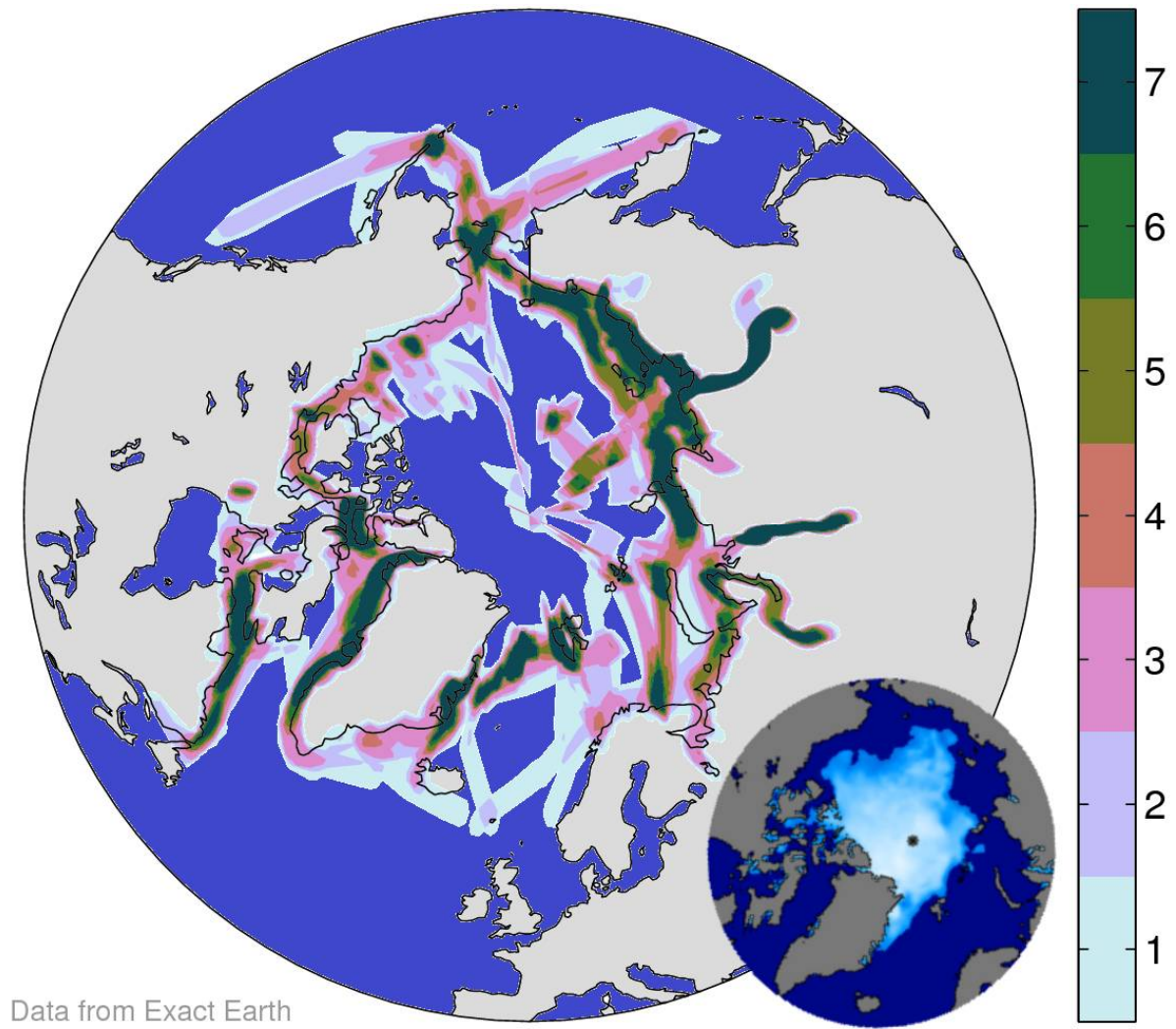


Figure 5.4 | Ship track density in August 2011 in the Arctic. Colours denote numbers of ships passing through that region. Data supplied by exactEarth (2013). Inset: NSIDC Sea ice concentration August 2011.

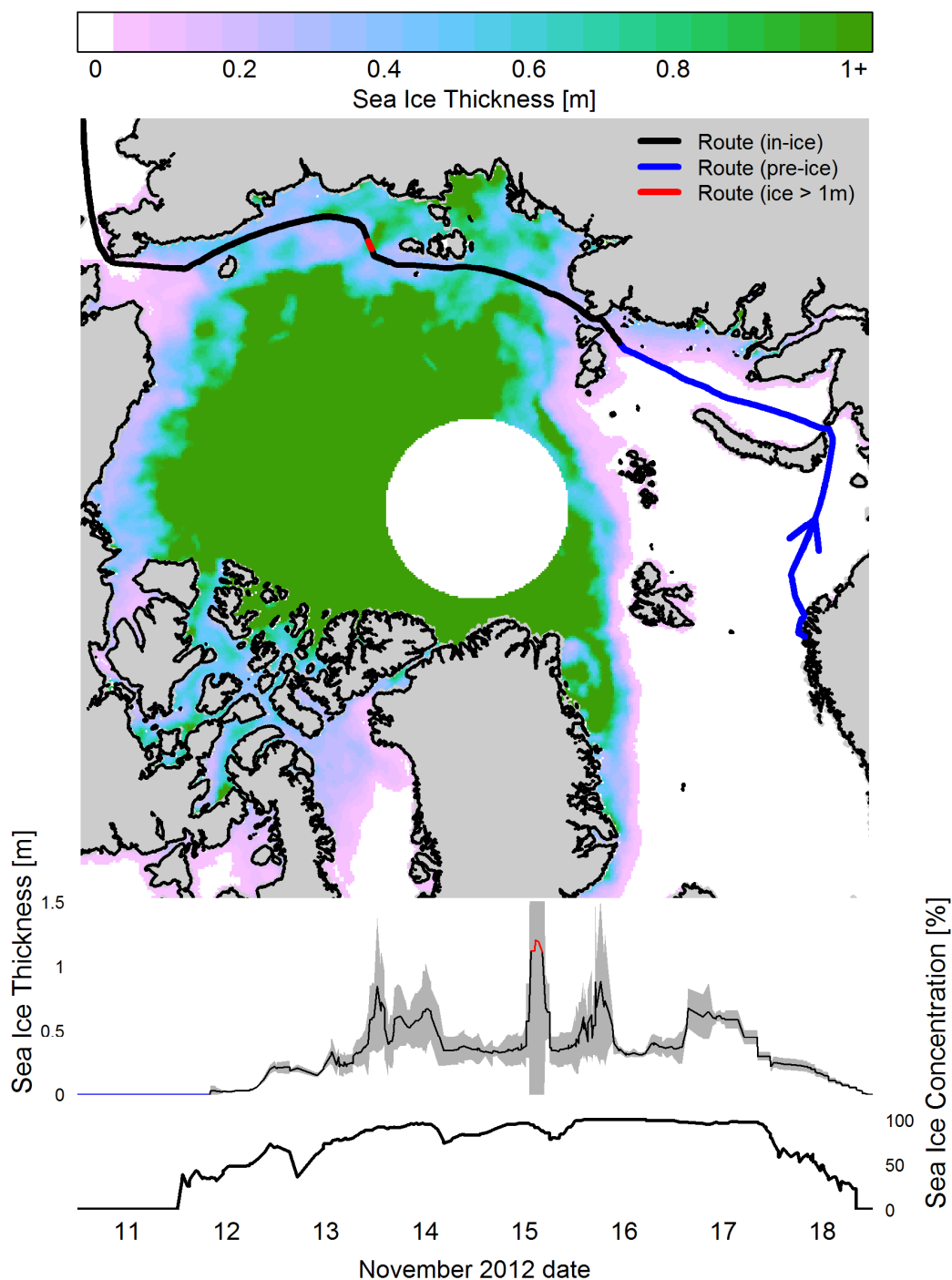


Figure 5.5 | The transit of the *Ob River* along the Northern Sea Route from 7th to 27th November 2012. The map shows the mean sea-ice thickness from the SMOS satellite from 12th to 18th November (Tian-Kunze et al., 2013). The blue line represents the route taken before any ice is encountered, and black thereafter, with red for the part of the route with thickness greater than 1m. The top timeseries is the sea ice thickness [m] along the route, according to the SMOS satellite, with grey shading representing the uncertainty. The lower timeseries represents the sea ice concentration [%] along the route according to the Reynolds dataset (Reynolds et al., 2007).

In November 2012, the first liquid natural gas tanker, the *Ob River*, sailed the NSR, creating a lot of media interest. Figure 5.5 shows the route of the *Ob River* tanker along the NSR (data supplied by exactEarth (2013)). It set sail on 7th November from Hammerfest in the north of Norway to Japan, escorted by the Russian nuclear icebreaker *Let Pobody* for much of the journey along the NSR. Figure 5.5 also shows a map of the mean sea-ice thickness for the duration of the voyage using data from the SMOS satellite (Tian-Kunze et al., 2013). The time-series of the ice thickness at the same time and space locations as the *Ob River* and sea ice concentration from the Reynolds et al. (2007) dataset are also shown. The SMOS satellite used is sensitive to thin ice, especially in the re-freeze season, which makes it well suited for this scenario in November. However, the accuracy of the instrument starts to degrade for thicknesses above 0.5m (Kaleschke et al., 2012). Although the sea-ice concentration was close to 100% for several days of the voyage, it is the sea ice thickness, which is the limiting factor for ship transit planning. The sea ice thickness along the route chosen by the *Ob River* shows large variations, but the transit generally used the thinner ice regions. Most of the journey experienced thicknesses less than 1m, but there is one period of thicker ice encountered in the East Siberian Sea (red line), according to the SMOS data. The observations also indicate that a slightly different route may have experienced thinner ice, highlighting the potential value for Arctic sea-ice forecasts.

References

Alfred-Wegener-Institut: Press Release: Research Vessel Polarstern at North Pole, 2011, <https://www.awi.de/en/about-us/service/press/archive/research-vessel-polarstern-at-north-pole.html>.

Arctic Logistics Information Office: Northern Sea Route Information Office Transit Statistics, Center for High North Logistics, 2015.

Baraniuk, C.: Cheap oil is taking shipping back to the 1800s. BBC Worldwide, 2016.

exactEarth: <http://www.exactearth.com/products/exactais-arctic-archive/>, last access: 13/05/13 2013.

Government of Canada; Natural Resources Canada; Earth Sciences Sector; Canada Centre for Mapping and Earth Observation: Atlas of Canada, 2012.

Kaleschke, L., Tian-Kunze, X., Maaß, N., Mäkynen, M., and Drusch, M.: Sea ice thickness retrieval from SMOS brightness temperatures during the Arctic freeze-up period, *Geophys. Res. Lett.*, 39, L05501, doi: 10.1029/2012gl050916, 2012.

Lasserre, F.: Case studies of shipping along Arctic routes. Analysis and profitability perspectives for the container sector, *Transp. Res. Part A Policy Pract.*, 66, 144-161, doi: <http://dx.doi.org/10.1016/j.tra.2014.05.005>, 2014.

Marchenko, N.: Russian Arctic Seas, Navigational conditions and accidents Springer Berlin Heidelberg, 2012.

Ostreg, W., Eger, K., Flostad, B., Jorgensen-Dahl, A., Lothe, L., Mejlaender-Larsen, M., and Wergeland, T.: Shipping in Arctic Waters: A comparison of the Northeast, Northwest and Trans-Polar Passages, Springer Praxis Books, Berlin, 2013.

Reynolds, R. W., Smith, T. M., Liu, C., Chelton, D. B., Casey, K. S., and Schlax, M. G.: Daily high-resolution-blended analyses for sea surface temperature, *J. Clim.*, 20, 5473-5496, 2007.

Thomson, J. and Rogers, W. E.: Swell and sea in the emerging Arctic Ocean, *Geophys. Res. Lett.*, 41, 3136-3140, doi: 10.1002/2014gl059983, 2014.

Tian-Kunze, X., Kaleschke, L., and Maass, N.: SMOS Daily sea ice thickness, 12th - 18th November 2012. University of Hamburg, 2013.

Chapter 6

**Faster 21st century shipping using
trans-Arctic routes**

Summary

Over the last few decades, the Arctic has experienced a rapid decline in both the extent and volume of sea ice. This decline is projected to continue and opens shorter trade routes across the Arctic Ocean, potentially leading to significant global economic benefits. Sea ice is the single biggest barrier to Arctic shipping, so reductions in sea ice thickness, and the increasing occurrence of open water, will reduce this primary hazard. Here, how the projected sea ice loss will increase opportunities for Arctic-transit shipping is quantified by using CMIP5 global climate models calibrated to remove spatial biases. By mid-century for standard Open Water (OW) vessels, transit potential doubles with most years navigable irrespective of emissions scenario, with the currently inaccessible Trans-polar Sea Route across the central Arctic being used for the first time. European routes to East Asia become 10 days faster on average than alternatives by mid-century and 13 days faster by late-century, while North American routes become 4 days faster. Future greenhouse-gas emissions play a significant role by late-century; the shipping season reaching 8 months in RCP8.5, double that of RCP2.6, with substantial interannual variability. Moderately ice-strengthened vessels enable fast and reliable trans-Arctic shipping, essentially year round, from mid-century.

6.1 Introduction

The principal questions this chapter addresses are:

1. *When will trans-Arctic shipping be possible?*
2. *What are the preferred routes to/from East Asia?*
3. *What are the time savings for open water vessels using trans-Arctic, opposed to conventional routes?*

Sailing from Europe to East Asia currently takes 30 days via the Suez Canal; voyages from North America via the Panama Canal take 25 days. This chapter examines how voyages from East Asian ports to European and North American ports may change over the 21st century by utilising trans-Arctic routes whenever possible. Many operational factors affect route choice (e.g. cargo type, fuel price, insurance premiums, and draft restrictions); this chapter focuses solely on the sea ice, the biggest physical hazard for Arctic shipping. This is achieved by utilising several global climate models (GCMs), each with multiple ensemble members, from the Coupled Model Intercomparison Project, phase 5 (CMIP5) (Taylor et al., 2012) that have each undergone bias-correction to calibrate them against recent SIT data (Zhang and Rothrock, 2003; Melia et al., 2015). This calibration is crucial as all GCMs contain biases in the spatial distribution and interannual variability of SIT, which strongly influence regional ice patterns along sea routes. Previous Arctic shipping studies have not used such calibration and therefore produce projections that are primarily model dependent (Stephenson and Smith, 2015), masking the roles of interannual variability and future emission scenarios. The calibration approach used here reduces inter-model variations of future sea ice (see Ch. 4 analysis and Melia et al. (2015)). Interannual variability is sampled using multiple ensemble members from each calibrated GCM, allowing uncertainty to be better quantified than only using single simulations, multi-model means, and multi-annual means used previously (Rogers et al., 2013; Stephenson et al., 2013; Aksenov et al., 2015). In addition the entire seasonal cycle is considered throughout the 21st century, capturing the future lengthening of the shipping season.

Future climate change scenarios are denoted by representative (greenhouse gas) concentration pathways (RCPs) that diverge after 2006 (Van Vuuren et al., 2011). RCP8.5 is the highest emission pathway, roughly equivalent to a global mean temperature increase of $4.3 \pm 0.7^\circ\text{C}$ from pre-industrial by 2100; RCP2.6 is the lowest

emission pathway with global mean temperatures stabilising at $\sim 1.6 \pm 0.4^\circ\text{C}$ above pre-industrial, consistent with the recent United Nations Paris (COP21) targets (IPCC, 2013; Hulme, 2016). Results from RCP4.5 ($\sim 2.4 \pm 0.5^\circ\text{C}$) are also presented. The prospects for two vessel classes are assessed: OW vessels with no specific ice strengthening, capable of navigation in SIT < 0.15 m, and polar class six (PC6) vessels with a 20% capital cost premium (Lasserre, 2014), but capable of operation in medium first-year ice, equivalent to SIT < 1.2 m (Transport Canada, 1998). A ship-routing algorithm with an empirical SIT – vessel speed relationship (Tan et al., 2013) is introduced to find the fastest Arctic route allowing statistics of transit time savings to be presented.

6.2 Methods

6.2.1 GCM selection and bias-correction

Only GCMs with multiple ensemble simulations in the historical period and for each of the representative concentration pathways (RCPs) 2.6, 4.5, and 8.5 for future scenarios have been selected (Van Vuuren et al., 2011). In addition, the GCM must have a reasonable spatial resolution (discounting CanESM2 and CSIRO-Mk3.6.0), and a somewhat resolved Canadian Archipelago for accurate ship routing through the NWP (discounting IPSL-CM5A-LR). The five qualifying GCMs (Figure 6.1 and Table 6.1) are bias-corrected to the SIT statistics of the PIOMAS reanalysis (Zhang and Rothrock, 2003) from the period 1995 – 2014 and utilise three ensemble members from each model in accordance with work from Melia et al. (2015) presented in Ch. 4.

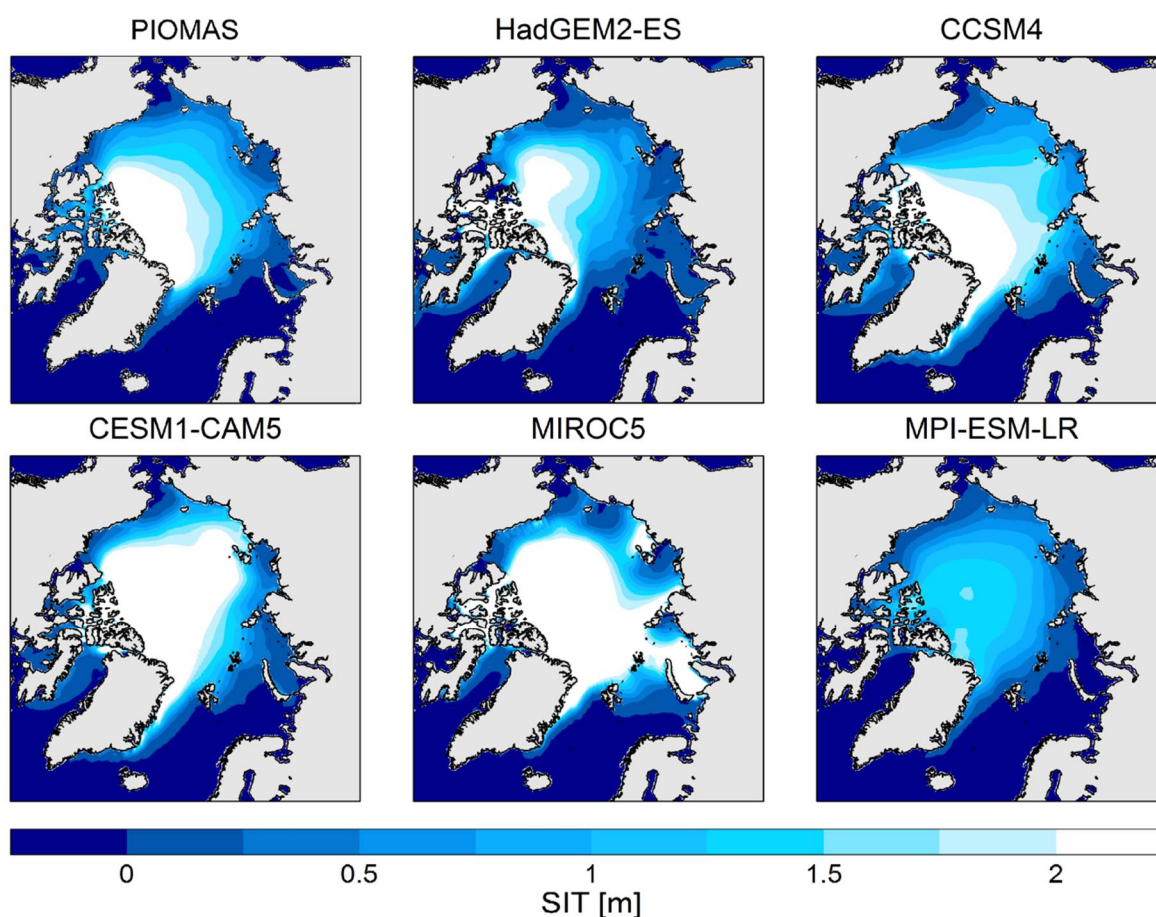


Figure 6.1 | September mean SIT over the satellite era (1979-2014) from the PIOMAS reanalysis (used to represent observed SIT) and the five uncalibrated GCMs.

The bias-correction accounts for the considerable biases in the spatial distribution of SIT (Figure 6.1) and SIT variability that have led to considerable inter-model spread in previous studies of future Arctic shipping potential as analysed in-depth by Stephenson and Smith (2015). By design, the calibration does not attempt to correct the sea ice loss trend to that depicted by the reanalysis. This is because it is currently not clear how to robustly decouple the externally forced trend from internal variability given the short time scales over which satellite observations (assimilated into the reanalysis) exist (for further discussion refer to Ch. 4.3). GCMs are designed to project future ice loss given changes to radiative forcing, and so the calibration effectively preserves the year at which a GCM becomes ice-free.

Table 6.1 | List of GCMs qualifying for analysis of future shipping.

Institution	GCM name
Met Office Hadley Centre	Hadley Centre Global Environment Model version 2-Earth System: <i>HadGEM2-ES</i> (The HadGEM2 Development Team et al., 2011)
National Center for Atmospheric Research	Community Climate System Model, version 4: <i>CCSM4</i> (Gent et al., 2011)
National Center for Atmospheric Research	Community Earth System Model, Community Atmosphere Model, version 5: <i>CESM1-CAM5</i> (Meehl et al., 2013)
Model for Interdisciplinary Research on Climate (MIROC)	MIROC version 5: <i>MIROC5</i> (Watanabe et al., 2010)
Max Plank Institute for Meteorology (MPI)	MPI Earth System Model, low resolution: <i>MPI-ESM-LR</i> (Jungclaus et al., 2006)
Applied Physics Laboratory (University of Washington)	Pan-Arctic Ice Ocean Modelling and Assimilation System: <i>PIOMAS*</i> (Zhang and Rothrock, 2003)

*Only used as reanalysis for GCM calibration.

6.2.2 Fastest route algorithm

The European route assumed is Rotterdam to Yokohama (NSR: 6930 nmi ~18 days, Suez: 11580 nmi ~30 days), and the North American Route is New York to Yokohama (NWP: 7480 nmi ~21 days, Panama: 9720 nmi ~25 days). Sailing times are calculated using 16 knots in open-water and slower in ice as detailed below. The canal voyage times omit delays and extra time required to navigate the canals, which can be

considerable. Current sailing times quoted via the NWP and NSR are averages and take into account recent ice conditions (see Figure 6.4). The speed of ice-class vessels through sea ice is inversely proportional to the sea ice thickness (SIT). To take this into account an empirical speed – SIT relationship that is based on full-scale field data and corroborated by numerical simulations from Tan et al. (2013) (Figure 6.2) is used.

The ship is equivalent to Polar Class 6 (PC6) according to the Canadian Arctic Ice Regime Shipping System (AIRSS) (Transport Canada, 1998), which is incapable of navigation in SIT greater than 1.2 m. This system is one of the few outlined in the new International Maritime Organisation’s Polar Code, designed to be used by operators to demonstrate adequate measures have been met to operate in Arctic waters (International Maritime Organization (IMO), 2015). The safe ice regime taken from AIRSS in Figure 6.2 shows SIT thresholds used for ice navigation charts; when the number is negative, navigation in this SIT is dangerous or impossible. No speed – SIT relationships exist (to the authors knowledge) for OW vessels. The same speed – SIT curve for PC6 vessels is assumed for OW vessels, only scaled down to the 0.15 m SIT threshold for OW vessels given by AIRSS, shown by the secondary y-axis in Figure 6.2.

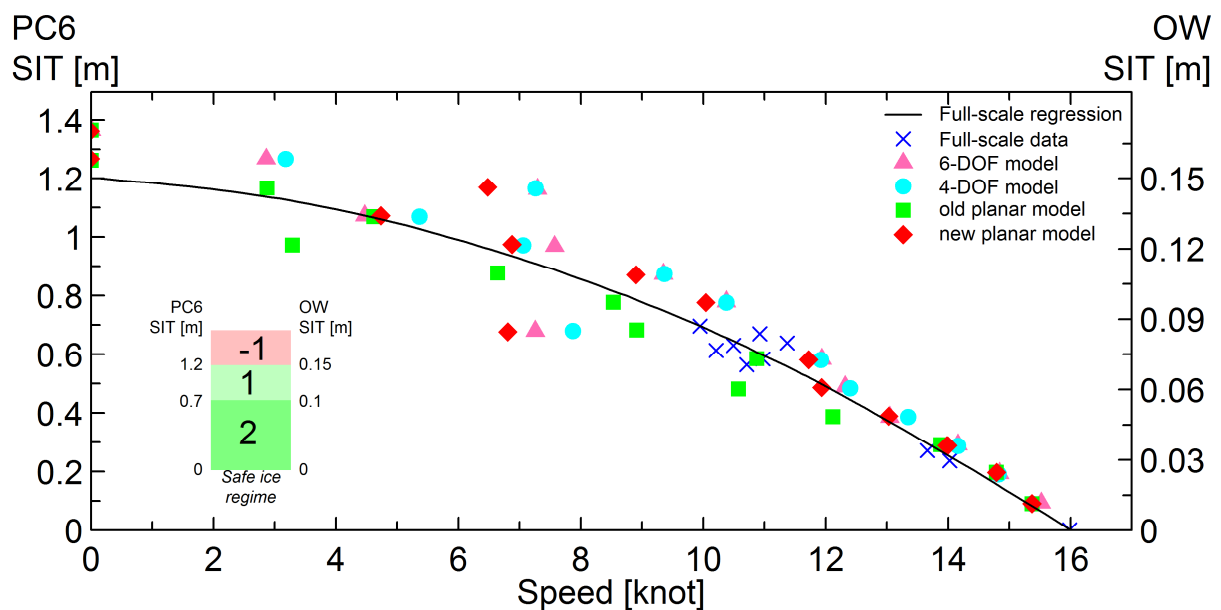


Figure 6.2 | Speed – SIT relationship from full-scale field data and numerical models. Figure adapted from Tan et al. (2013) and assumes the same relationship for Polar Class 6 (PC6) vessels scaled to a lower SIT threshold for Open Water (OW) vessels. Insert: safe ice regime threshold comparison taken from AIRSS; negative numbers indicate an unsafe regime.

The Speed – SIT relationship outlined in Figure 6.2 is incorporated into a ‘fastest route algorithm’, the detailed implementation of which is detailed in the next paragraph and

summarised here. The algorithm finds the absolute fastest route between two locations. It takes into account both the physical geographic distance and the vessel speed through grid cells of varying SIT. Given typical ice conditions, the fastest route is rarely the geographically shortest route, as the presence of high SIT will obstruct or significantly slow the vessel's progress. Routes that avoid ice entirely will have the highest average speed (16 knots) but will involve greater distance to be travelled. The algorithm takes all of these factors into account and finds the optimum route, which because the algorithm accounts for varying speed and distance, is the route that takes the least time. As the algorithm has perfect knowledge of the entire sea ice field it is able to pick a route based on pan-Arctic ice conditions (e.g. whether to use the NWP or NSR) rather than only having local knowledge of neighbouring gridcells. This perfect knowledge will not be available to a ship captain, due to lack of data and transient sea ice conditions, so the routes presented in this chapter are a best-case scenario.

Each GCM ensemble simulation of SIT is regridded to the National Snow and Ice Data Center (NSIDC) equal area stereographic grid, which benefits from extended coverage to include northern European and Pacific waters, required for accurate start/finish locations. The SIT is converted to an effective ice resistance for the respective vessel class. Ice resistances are the reciprocal of the vessel speed through that grid cell's SIT. The resistance fields on the NSIDC projection are then converted to raster grids from which geo-corrected transition matrices can be calculated. The transition matrix assigns a resistance to transiting from a grid box to its four orthogonal and diagonal neighbours. A least resistance path algorithm is then implemented, using work by Dijkstra (1959) and Van Etten (2015), adapted by the thesis author, to calculate the route between two points that accumulates the lowest total resistance, which because of the SIT – speed substitution is the fastest route. A similar approach has estimated trans-Atlantic flight times under predicted changes in the atmospheric jet stream (Williams, 2016).

6.2.3 Additional variables relevant to shipping

Although SIT is the most important climatic variable for Arctic shipping, the effects of other variables are also important, but are beyond the scope of this chapter. Local sea ice concentration (SIC) is relevant for shipping as ice navigators actively seek out open-water and 'leads' (natural linear breaks in ice flows revealing open-water) for efficient progress; however, these decisions are made on scales far finer than are resolved by GCMs. The speed – SIT relationship of Tan et al. (2013) is for continuous ice-breaking, i.e. 100% SIC. This effectively means that the SIT fields used in this study assume 100%

SIC for non-zero values of SIT, which is a conservative influence on our accessibility results. It is also worth noting that in both models and observations, low values of SIT (relevant for the <0.15 m SIT OW vessel threshold) imply that SIC is often below 100%.

Other climatic parameters that are beyond the scope of this study include maritime fog, wave heights, icing (the freezing of ocean spray on a ship's superstructure), ocean currents, and sea ice motion. Sea ice motion is particularly important as convergence can create pressure ridges, where ice floes collide, drastically increasing the local SIT; these are particularly hazardous to shipping. These can occur regularly between fast ice (ice fastened to the coastline) and the drifting ice pack, highlighting the importance of experienced Arctic ship crews and accurate observations/forecasts. Ice age is also an important variable to shipping as older ice is harder due to brine secretion occurring in the summer melt season (Walsh and Zwally, 1990). Ice age is presented alongside SIT in AIRSS to define a vessel class' safe operating threshold, but since ice age is not a standard CMIP5 output variable the effect of future ice age distribution on shipping accessibility is not currently possible.

6.3 Faster September routes

Currently, the fastest available routes for OW vessels are along the NSR and North West Passage (NWP) (Figure 6.3a, Figure 6.4). Transit statistics for the NSR and NWP show increasing traffic (Figure 6.3c) with considerable interannual variability from years when the NWP is open, but not the NSR, and vice-versa (Figure 6.3a). For example, 2007 had the second lowest ice extent on record, however the NSR was blocked by ice protruding from the main ice pack towards Russia; illustrating that reduced sea ice extent does not necessarily guarantee open routes. As the NSR is within the Exclusive Economic Zone (EEZ, a 200 nmi zone prescribed by the United Nations Convention on the Law of the Sea) of Russia, fees can be charged.

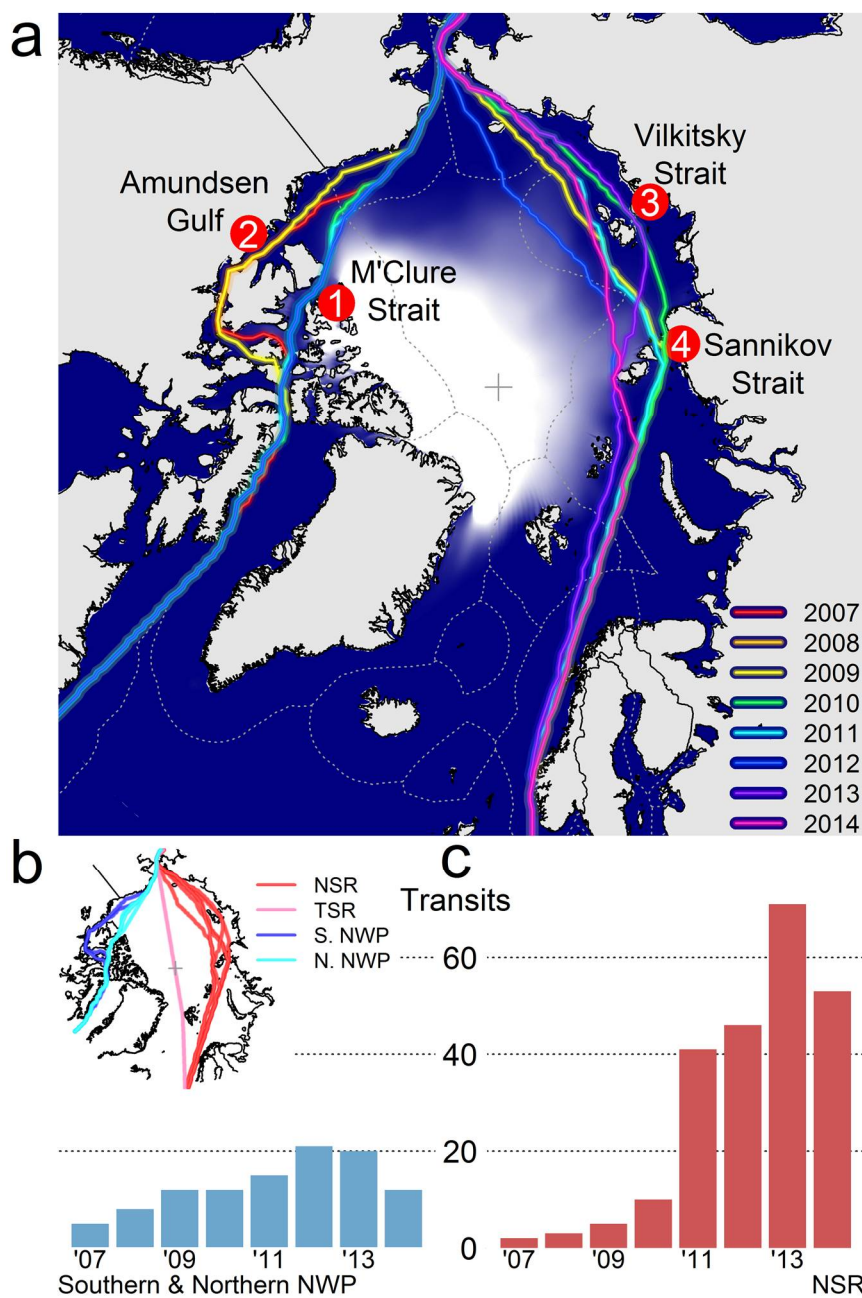


Figure 6.3 | Fastest possible September open water vessel routes from observations and transit statistics. a, Hypothetical Open Water vessel routes sailing through the September sea ice thickness field for 8 recent years from the PIOMAS reanalysis (Zhang and Rothrock, 2003). Routes only plotted when Arctic transits are possible. 1: The M'Clure Strait – the shortest North American route, the 'northern-NWP'. 2: Amundsen Gulf – the longer 'southern-NWP'. 3: Sannikov Strait. 4: Vilkitsky Strait. b, Main Arctic transit options. c, Recent total observed transits each year through the North West Passage (NWP) (Canadian Coast Guard, 2015) and Northern Sea Route (NSR) (Arctic Logistics Information Office, 2015); statistics for all voyages including ice class vessels and ice-breaker escorts.

6.3.1 Verification

The bias-correction method successfully corrects the historical mean and variance of SIT on a grid point scale (Ch. 4 and Melia et al. (2015)). It is however prudent to verify the calibration when applied to shipping routes. The “fastest route algorithm” is used to find the fastest September trans-Arctic routes in each GCM and the PIOMAS reanalysis for the calibration period (1995-2015). The only difference is in the number of simulated transits possible; PIOMAS has one realisation available, so only 20 simulated September voyages on North American and European routes. The GCM simulations use historical forcings (1995 – 2005) and RCP8.5 forcings (2006 – 2015). There are five GCMs, each with three ensemble members, hence 300 simulated September transits. However the route choices are very similar with the same channels and straits utilised in the simulations and the reanalysis (Figure 6.4). The SIT field shown is the mean of all the Septembers, and these are now very similar, compared to the differences seen in Figure 6.1. Note that the calibrated GCMs have a lower OW success rate, simulations — 16%, PIOMAS reanalysis — 35%, but for PC6 vessels the simulations have a higher success rate, simulations — 75%, Reanalysis — 65%. Routes are not open until 2007 in the reanalysis (Figure 6.3), but the calibrated simulations contain open routes throughout. There are two plausible mechanisms for this difference: firstly, the GCM simulations contain a total of 15 realisations (ensemble members) whereas only one realisation of the past is available for the reanalysis. It is possible that the last 20 years of observations were slightly unusual in terms of natural climatic fluctuations. Secondly, the reanalysis could have had a higher 1995 – 2015 ice loss trend, although the mechanism behind this signal is difficult to attribute to internal variability or an externally forced response (or likely some combination). This would explain the consistency in open routes post-2007 in the reanalysis, while openings are spaced more evenly throughout the 1995 – 2015 simulations.

An important distinction between Figure 6.3 and Figure 6.4 is that European and North American voyages are allowed to use ‘switch-transits’ if their own route is blocked. For example, the shortest North American route is via the NWP. If however, for a particular September the NWP is impassable due to too high SIT then vessels can sail round the southern tip of Greenland and utilise the NSR (or TSR) if open. The same switch is possible for European routes when the NSR is blocked and the NWP can be used if open.

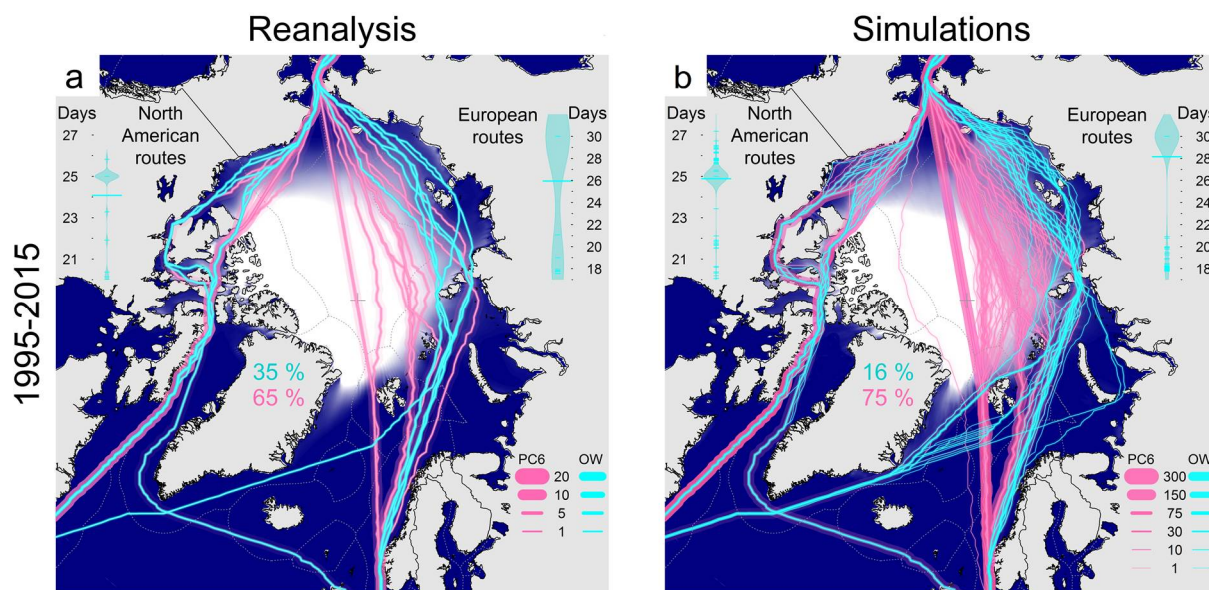


Figure 6.4 | Fastest available September trans-Arctic routes, 1995 – 2015, in reanalysis (PIOMAS) and simulations. The reanalysis period contains 20 consecutive Septembers while the simulations contain five GCMs, each with three ensemble members, hence over the 20 consecutive Septembers there are 300 simulated transits on the North American and European routes. Cyan lines represent Open Water vessels (OW) and pink lines represent Polar Class 6 vessels (PC6), line weight indicates the number of vessels using the same route. The percentages shown above Greenland represent the trans-Arctic potential for each vessel class respectively. East Asia transit time distributions are shown for North American routes and European routes. When Arctic routes are closed, the routes through Panama (25 days) and Suez (30 days) Canals respectively are used (red labels). Small lines indicate each individual voyage and large lines show the mean of all voyages, with individual route time distribution indicated by density shape.

6.3.2 21st century multi-GCM ensemble projections

Early-century projections (2015 – 2030, Figure 6.5 a-c) show Arctic transits are possible for 28 – 39% of Septembers. It is unlikely that the scenario differences are significant as the scenario signal accounts for <5% of the total variance (see Fig. 4.9c). However, Fig. 4.9c is concerned with an area averaged metric whereas the variations in OW vessel statistics are only due to changes to SIT around 0.15 m, hence the results in Figure 6.5 a-c will be more sensitive than Fig. 4.9c, and the early-century higher success rate from RCP8.5 could be robust.

European routes take only 18 – 19 days to East Asia using the NSR (Figure 6.6 a-c), with ‘switch-transits’ (i.e. when the NSR is blocked and the NWP is utilised instead), taking 20–22 days. North American voyages utilising the fastest ‘northern-NWP’ route (through the M’Clure Strait, see Figure 6.3) take 21 days, while the longer ‘southern-

NWP' (through the Amundsen Gulf) take 22 days, and switch-transits via the NSR take 25 days. Early-century switch-transits comprise ~50% of trans-Arctic routes, illustrating the considerable spatial variability in ice conditions that can exist across the Arctic.

PC6 vessels have an early-century transit potential of 90% (Figure 6.5 a – c), due to their higher SIT threshold. The inter-scenario difference here is only 3% compared to 11% for OW vessels. This is expected as the PC6 vessels are affected by SIT similarly to the metrics used in Fig. 4.9c. They can also take advantage of shorter routes impassable to OW vessels, with the majority of simulated European voyages using variations of the TSR; the majority of North American voyages use the shorter, northern-NWP. In addition to the increased trip frequency, the range in PC6 Arctic voyage times is less than one day, compared with a range of 7 days for OW vessels. This consistency is advantageous as ports and shipping companies operate 'just-in-time' schedules.

By mid-century (2045 – 2060, Figure 6.5 d – f), irrespective of RCP, the September OW transit potential is projected to double. The TSR is available for the first time and is 1 – 2 days faster than the NSR. The most common European route is a shorter version of the NSR, omitting the Vilkitsky and Sannikov Straits (see Figure 6.3); this is potentially advantageous as the Sannikov Strait contains depth restrictions preventing its use for larger ships. North American routes prefer the shorter northern-NWP over the southern-NWP, saving a day. In addition to greater potential utilisation, there is also increased diversity in routing choices with large swathes of the Arctic now ice-free in September. From mid-century, PC6 vessels favour the shortest routes along the TSR (European, ~17 days) and the northern-NWP (North American, ~20 days), for practically all Septembers.

Late-century (2075 – 2090) sees reliable September OW transits across a practically ice-free Arctic for RCP8.5 (Figure 6.5i). European voyages favour the TSR taking only 17 days; North American voyages favour the northern-NWP taking only 20 days. Under RCP2.6 (g) European and North American routes are open 68% of the time in September, and take on average 18 and 21 days respectively, with switch transits and all versions of the NWP and NSR still regularly needed.



Figure 6.5 | Projected fastest available September trans-Arctic routes. Routes for RCP2.6 (left), RCP4.5 (middle) and RCP8.5 (right) split into three periods (rows), each containing 15 consecutive Septembers, from five GCMs, with three ensemble members, equating to 225 simulations per panel. Cyan lines represent Open Water vessels (OW), pink lines represent Polar Class 6 vessels (PC6), and line weight indicates the number of vessels using the same route. The percentages shown above Greenland represent the trans-Arctic potential for each vessel class respectively. East Asia transit time distributions are shown for North American routes and European routes. When Arctic routes are closed, the routes through Panama (25 days) and Suez (30 days) Canals respectively are used (red labels). Small lines indicate each individual voyage and large lines show the mean of all voyages, with individual route time distribution indicated by density shape.

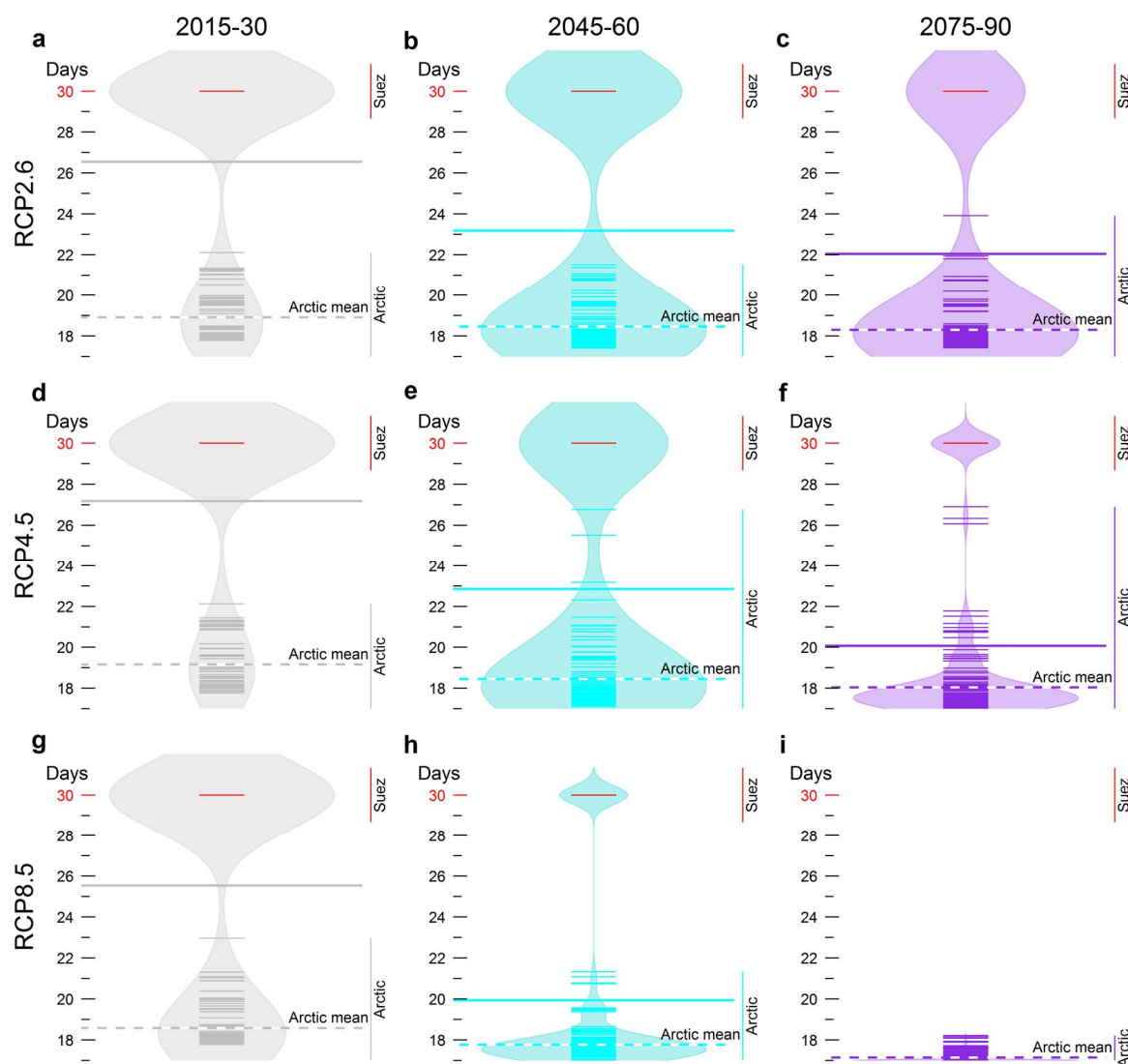


Figure 6.6 | Expanded East Asia transit time distributions for European routes as in Figure 6.5. When Arctic routes are closed, the route through Suez Canal (30 days) is used (indicated in red). Small lines indicate each individual voyage times, the large solid line shows the mean of all routes, the dashed line shows the mean of Arctic only routes, and individual route time distributions are indicated by density shape. Note row – column layout is swapped from Figure 6.5 to aid comparison of mean transit times through the 21st century.

Figures 6.6 and 6.7 show enlarged transit time distributions from Figure 6.5. Additionally they include a separate mean line for Arctic only routes. It is clear that through the century average transit times become faster.

By utilising the Arctic routes shown in Figure 6.5 when available, and using traditional European routes via Suez (30 days) otherwise, average journey times to East Asia can be dramatically reduced. Savings are achieved as Arctic routes become more available and more direct and ice-free through the century. In early-century, the average for all

European (Arctic + Suez) voyages using open water vessels is 26 days, which becomes 20 days by mid-century and 17 days by late century under RCP8.5. Under RCP2.6 the journey times are 23 days by mid-century and 22 days by late century. Savings are less striking for North America because the route via Panama is only 25 days (Figure 6.7). Sailing the NWP from North America to East Asia takes 20–22 days depending on channel choice and ice conditions, and when the NWP is impassable using alternative Arctic routes via the NSR or TSR takes at least 24 days.

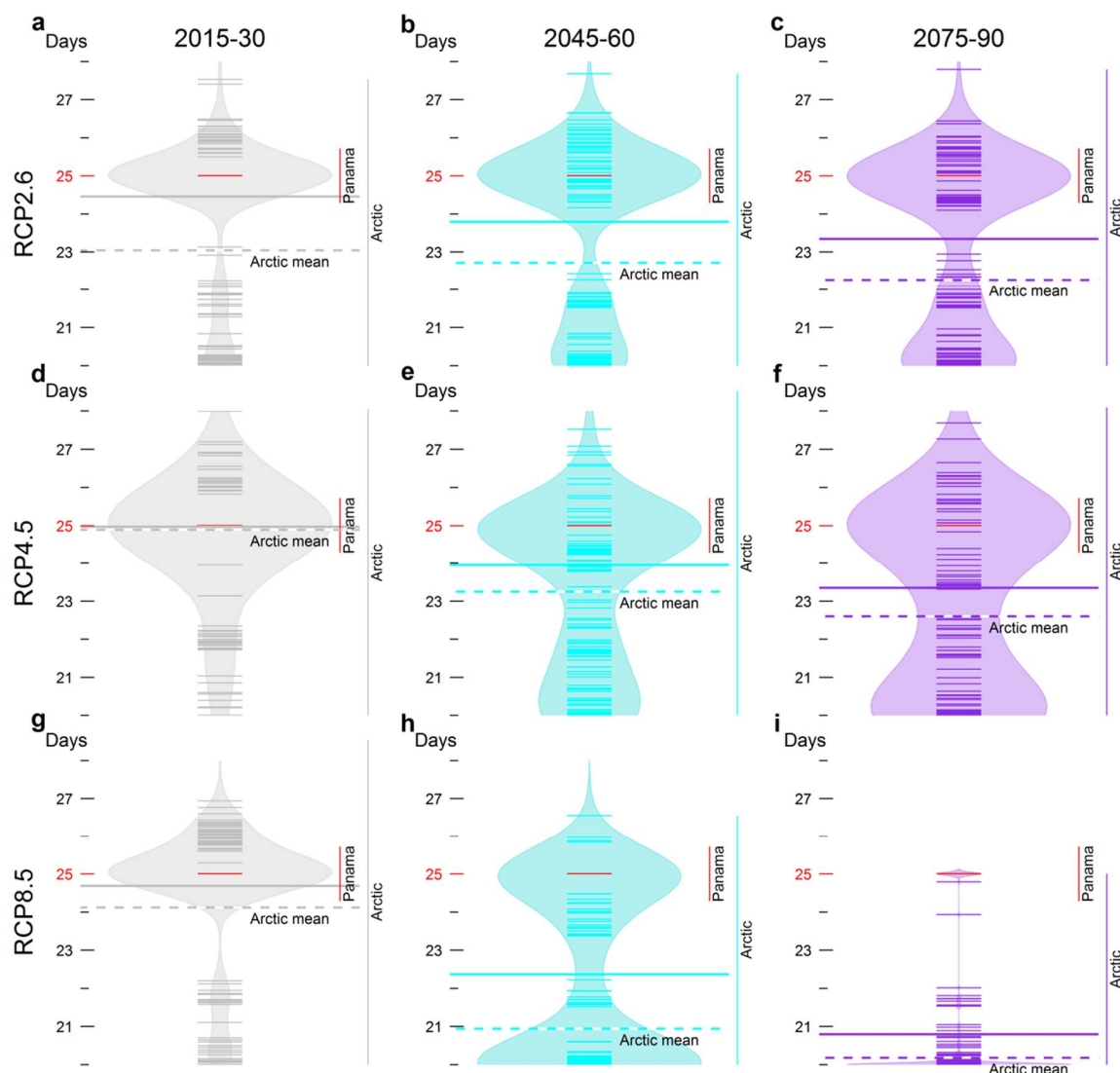


Figure 6.7 | Expanded East Asia transit time distributions for North American routes as in Figure 6.6 and Figure 6.5. When Arctic routes are closed, the route through Panama Canal (25 days) is used (indicated in red).

These transit times are the potential average savings a shipping company would experience if they were to utilise trans-Arctic routes at every possible opportunity. The

results have different implications depending on the destination port. For European voyages, trans-Arctic routes should always be utilised when available as even using switch transit routes are always considerably faster than traditional routes via Suez. For North American traffic however, switch-transits using the NSR actually take longer than traditional routes via Panama. Assuming efficient passage and short queues through the Canal, shipping would prefer to stick to the traditional route, as the hazards are likely less. To make this decision however requires detailed knowledge of the SIT at least a week in advance. Products like CryoSat-2 Near Real Time (NRT) SIT, typically available 1 – 3 days after satellite acquisition (Tilling et al., 2016), should help with forecasts at shorter lead times.

6.3.3 Separate GCMs

The calibrated GCMs have a SIT distribution and variability that is now considerably more realistic when compared to the PIOMAS reanalysis (see Fig. 4.6 for example). However the individual GCMs will still produce different routes and statistics. This is expected as each GCM only contains three ensemble members, not enough to fully sample internal variability. The GCMs grid point ice loss trend will also play an important role. Although the SIT distribution is now consistent with PIOMAS, the grid point ice loss trend will vary from model to model. The following Figs. 6.8 – 6.12 show the routes from the individual GCMs. In this way it is similar to Stephenson and Smith (2015) which presents accessibility from individual GCMs (the same as Smith and Stephenson (2013), with the addition of MIROC5 and MIROC-ESM-CHEM). They use a single ensemble member from 10 GCMs, whereas the results presented here are from three ensemble members from five GCMs. They also use the same methods as S&S. Crucially their SIT is not calibrated to reanalysis data, as two of the GCMs they use are the same, CCSM4 and MIROC5 a comment on the impact of the calibration may be possible at this stage, though as the methods used are different this will need to be taken into account.

6.3.3.1 CCSM4

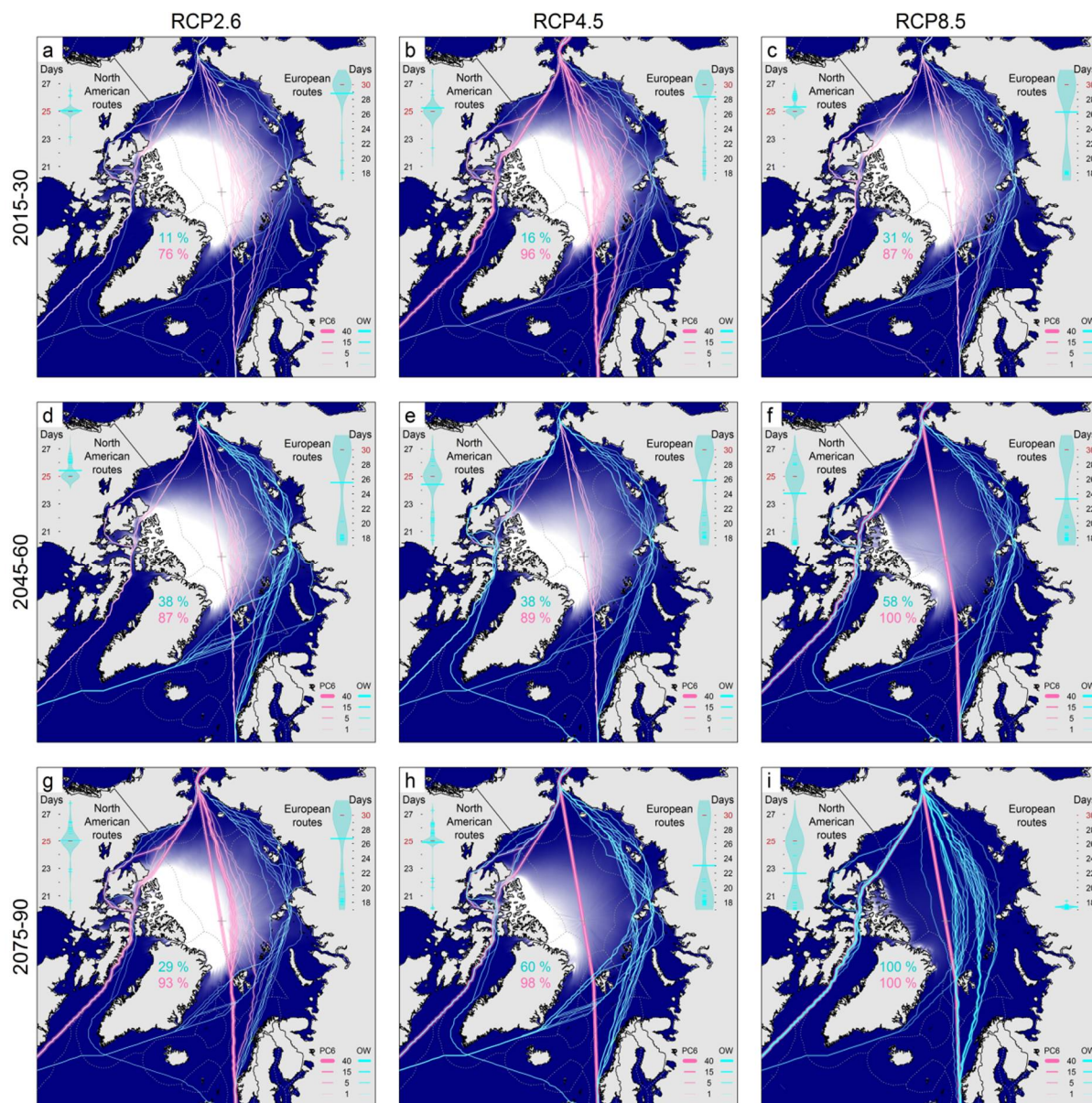


Figure 6.8 | As Figure 6.5 for CCSM4 only with 45 simulated Septembers per panel.

CCSM4 has a relatively small sea ice loss trend with a ~16% reduced Arctic amplification compared to its predecessor CCSM3 (Vavrus et al., 2012). The smaller trend particularly affects the NWP causing low usage early century. The OW vessels never sail the fastest European route.

6.3.3.2 CESM1-CAM5

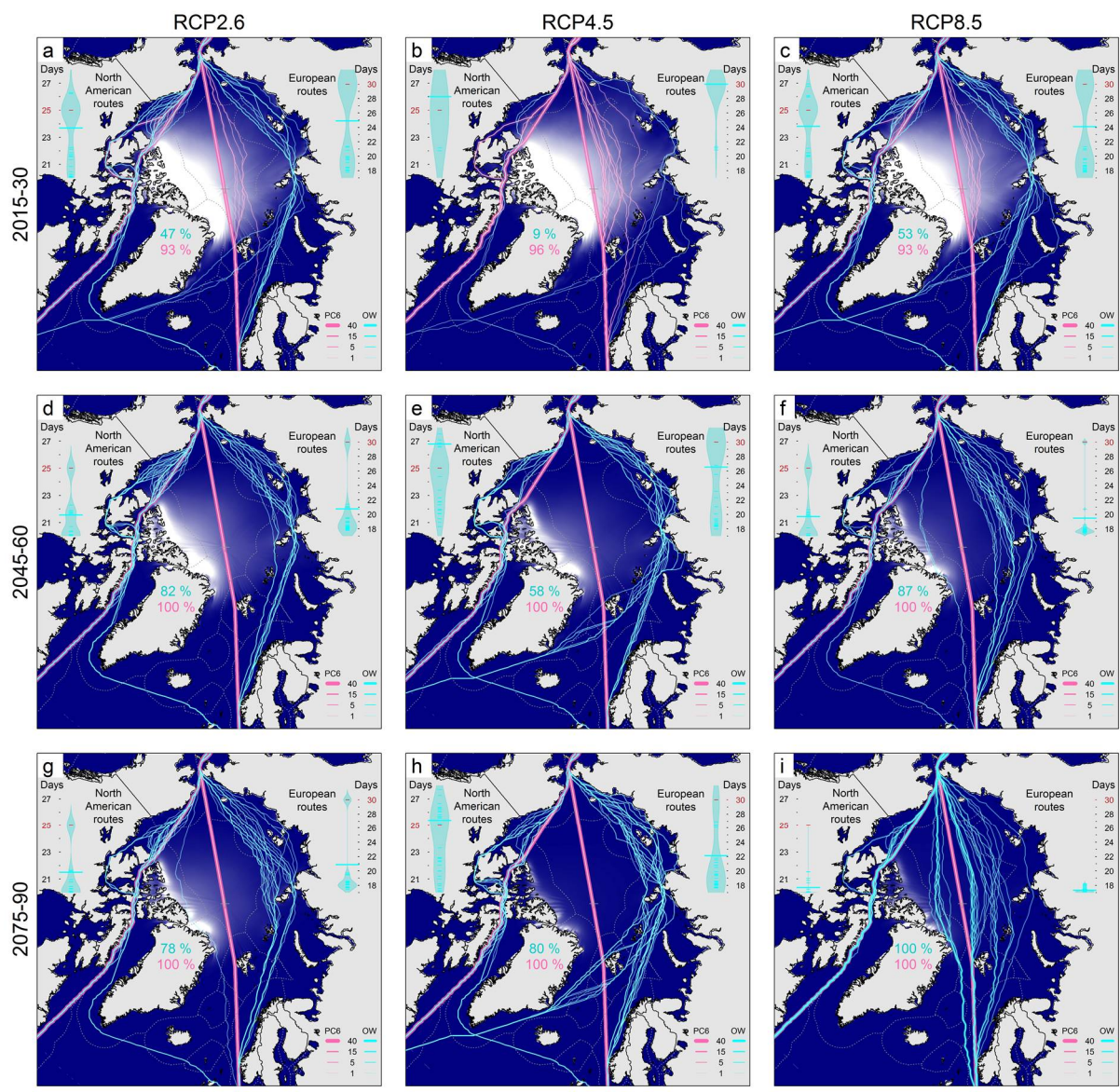


Figure 6.9 | As Figure 6.5 for CESM1-CAM5 only with 45 simulated Septembers per panel.

CESM1-CAM5 has fairly typical route opening frequencies. One striking feature however is the relatively low transit potential for OW vessels in RCP4.5 of 16%, ~40% lower than RCP2.6 or RCP8.5. This is puzzling as the SIT field look very similar, this even more intriguing given the fact that the PC6 transit potential is 3% higher in RCP4.5.

6.3.3.3 HadGEM2-ES



Figure 6.10 | As Figure 6.5 for HadGEM2-ES only with 45 simulated Septembers per panel.

HaGEM2-ES has a relatively slow ice loss trend in the Canadian Archipelago. The southern NWP is only used twice in the 135 simulated early-century Septembers. The main choke point seems to be around the M'Clure Strait, and in RCP2.6 this plug is broken by mid-century but is re-established late-century. This contrasts with a fast ice loss trend in the central Arctic. This results in the TSR quickly becoming the dominant route for all European and North American traffic by mid-century in RCP4.5 and RCP8.5.

6.3.3.4 MIROC5

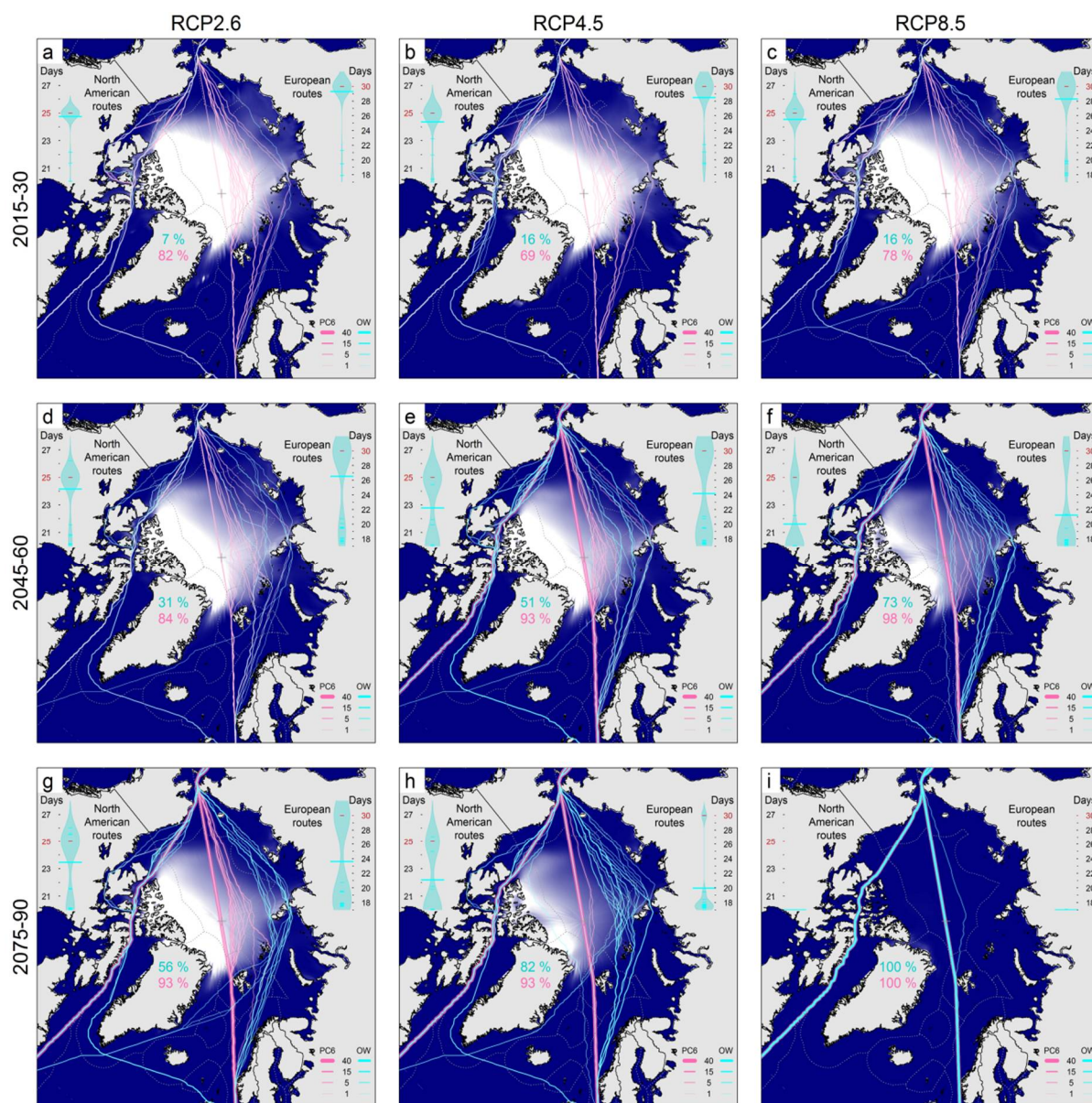


Figure 6.11 | As Figure 6.5 for MIROC5 only with 45 simulated Septembers per panel.

Early-century MIROC5 is unusual in that the NWP is more popular than the NSR. This is due to a relatively slow ice loss trend around and northwards of the Sannikov Strait. By mid-century, access along the NSR has improved, this means that some European routes are a straight route to the Sannikov Strait and then another straight route to the Bering Strait. This also means that switch-transits are far more common for European routes than North American routes.

6.3.3.5 MPI-ESM-LR

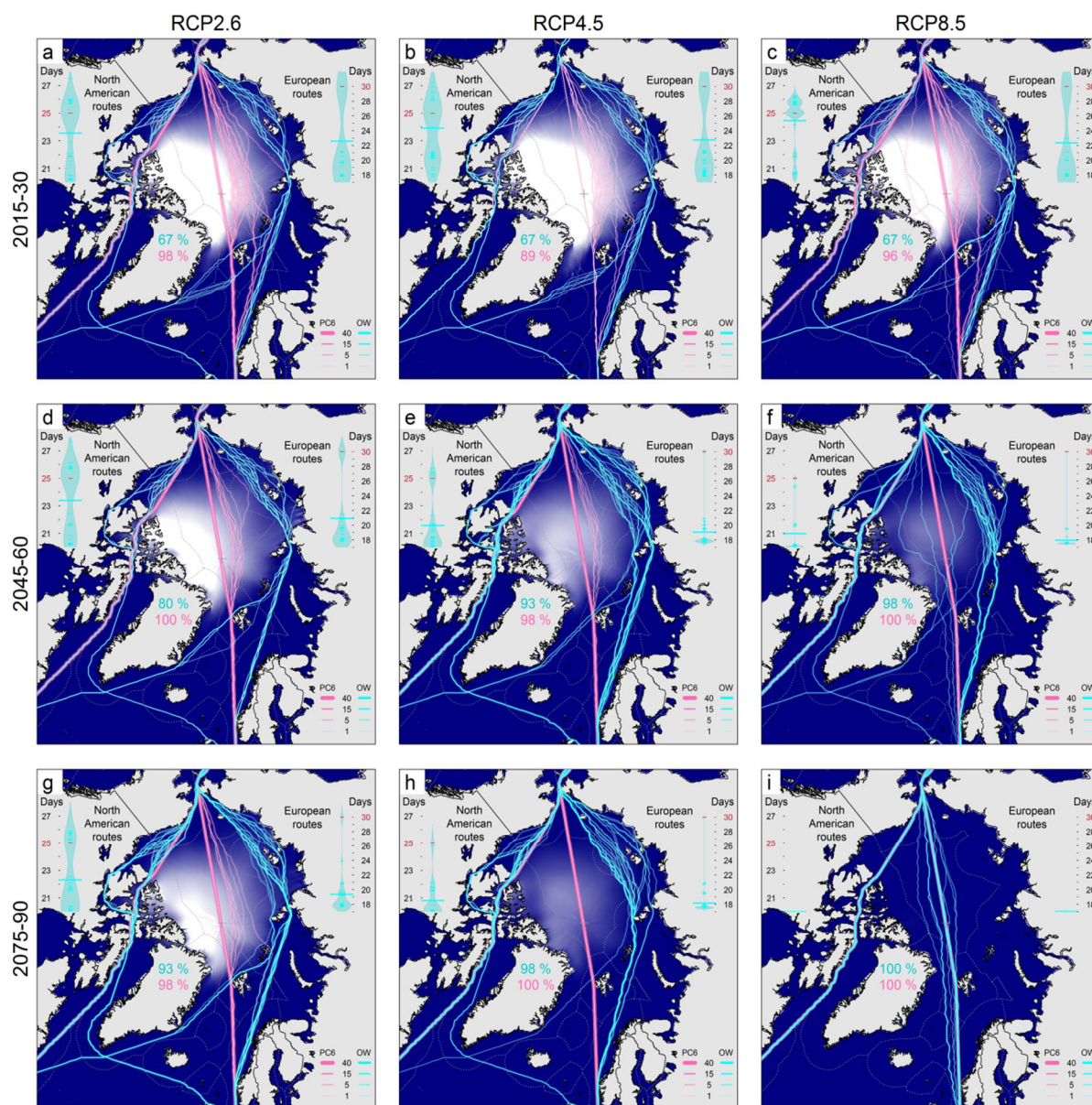


Figure 6.12 | As Figure 6.5 for MPI-ESM-LR only with 45 simulated Septembers per panel.

MPI-ESM-LR has the fastest ice loss trend of all the GCMs used here. The early-century OW transit potential is 67%; remarkably this is identical for every emission scenario, however as the PC6 statistics are different across the scenarios this is likely a coincidence. The transit potential is also very similar to the last decade in the reanalysis (Figure 6.3 and Figure 6.4). Therefore, in the short term perhaps MPI-ESM-LR provides the most likely projection of Arctic shipping. The NSR and NWP are used equally frequently, and the TSR is only a consistent option late-century in RCP8.5.

6.4 Variability and Extended season

6.4.1 Alternative algorithm

The methodology used in Ch. 6.3 (Figs. 6.3 – 6.12) calculates the fastest possible route across the Arctic. This algorithm essentially has to calculate every possible grid cell to grid cell transition and as such is computationally expensive. Although transit conditions remain optimal around September the prospects for all months needs to be considered if trans-Arctic shipping is to become useful to the wider shipping industry.

To calculate if Arctic routes are open or closed more generally a less computationally expensive algorithm can be used; the efficiency saving is made by basing the algorithm on fixed routes akin to Khon et al. (2010). As introduced previously, there are three broad route choices for trans-Arctic shipping, the Northern Sea Route (NSR), Trans-polar Sea Route (TSR), and North West Passage (NWP). The fixed route algorithm contains six paths per route that explores the different options available (Figure 6.13). The routes are designed around the EEZs, which allows certain implications to be considered in future route choices, e.g. the NSR stays within the Russian EEZ and the TSR avoids the Russian EEZ. If the SIT on any of the six possible paths never exceeds the OW vessel (0.15 m) or PC6 vessel (1.2 m) SIT thresholds then the route (NSR, TSR, and NWP) is considered open.

The limitation of the fixed route algorithm is that it will occasionally consider some months closed that are open for the fastest route algorithm. This is because the fastest route algorithm is route finding and will find a path, however complex, if one exists. These extra routes that the fastest route algorithm finds are spatially complex and occur in marginal conditions. The performance of the fixed route algorithm was verified by running both algorithms through the PIOMAS reanalysis; the fixed route algorithm had a miss rate of 6%, i.e. the two algorithms agree for 94% of cases, and for 6% of months a possible route exists that is not one of the 18 possible routes in the fixed route algorithm.

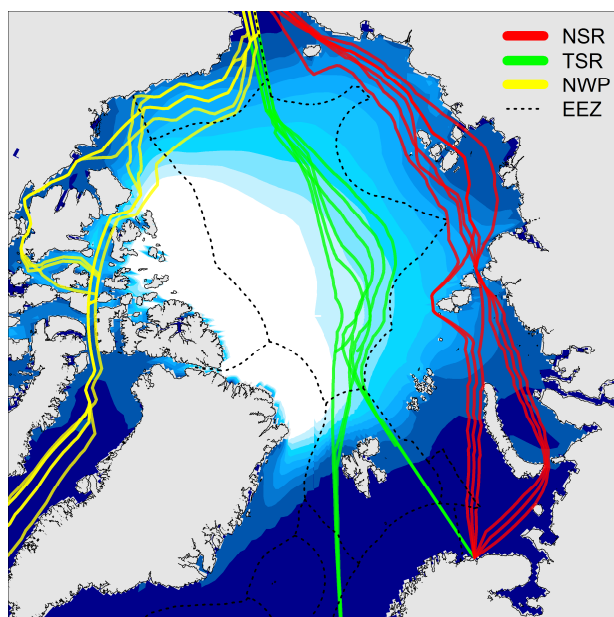


Figure 6.13 | Fixed Arctic route algorithm.

6.4.2 Inter-annual variability

Transit conditions always remain optimal around September but for trans-Arctic shipping to be viable, a longer Arctic shipping season is essential. By the end of the century the majority of the Arctic Ocean is expected to be open water for half the year (Barnhart et al., 2015). However, GCMs project that the transition to a mostly ice-free Arctic may be nonlinear, with substantial interannual variability (Swart et al., 2015). Figure 6.14 shows, for all months, the probability of the three trans-Arctic routes (Figure 6.13) being open for OW vessels in RCP2.6 (a), RCP4.5 (b), and RCP8.5 (c). The different routes are shown in three horizontal bands within each panel. Each route further splits into 12 rows representing each month, starting in April at the top, through to the minimum ice months in the middle, to the maximum ice month of March at the bottom of each band. The colours represent the ensemble consensus or simply the number of ensemble members indicating an open route, out of the 15 calibrated members available each year (3 members x 5 models). In current conditions, the NSR is the most open route, followed by the NWP, while the TSR is inaccessible until the 2030s at the earliest. The broadening of the plumes with time illustrates the lengthening of the OW shipping season. The NSR and NWP are only tentatively open August through October in early-century, with the addition of November by mid-century. Under RCP8.5 (Figure 6.14c) the TSR opens rapidly during mid-century and by late-century is open for up to 8 months of the year, consistently so from August through November. As the TSR is the fastest and shortest route and avoids the NSR fees, it would become an attractive

alternative. The substantial interannual variability indicates that not every year will be open, and highlights the potential value of skilful seasonal and interannual predictions of sea ice (Eicken, 2013; Hawkins et al., 2015).

The fixed route algorithm is also used on the “raw” (un-calibrated) GCMs for OW and PC6 vessels; these results are shown in Figs. 6.16 and 6.17, respectively. The impact of the calibration is illustrated by the difference plots (Figs. 6.18 and 6.19) for OW and PC6 vessels respectively. Here the number of open ensemble members from the raw GCMs is subtracted from the number of open ensemble members from the calibrated GCMs. For OW vessels (Figure 6.18) the effect of the calibration is route dependant with the NWP changing the most, and the differences across the scenarios reflect the greater number of months open in higher emission scenarios. The NSR is generally open less early-century. The calibration effect is also seasonal, and the potential shipping season shifts to be open earlier (August) and more closed later (November). These effects on the shipping season are explored further in the next section (Ch. 6.4.3). The raw models capture the extent of the OW shipping season on the NWP (August – September before mid-century) robustly, however they substantially under-estimate the frequency of accessibility to the passage. The NWP is closed too often in the raw GCMs, and the relatively detailed representation of ice in the Canadian Archipelago in PIOMAS compared to GCMs has a significant impact on the calibrated GCMs. The calibrated accessibility to the TSR shows no systematic difference to the raw GCMs through most of the 21st century, though the calibration does suggest that the TSR is first open 5 – 10 years later to OW vessels.

The calibration has had a far larger effect for PC6 vessels with the vast majority of months more likely to be open due to the calibration. As with OW vessels, prospective PC6 sailings along the NWP benefit most from the correction. The only recognisable systematic over-estimate in accessibility for PC6 vessels is the last month of the season on the NWP.

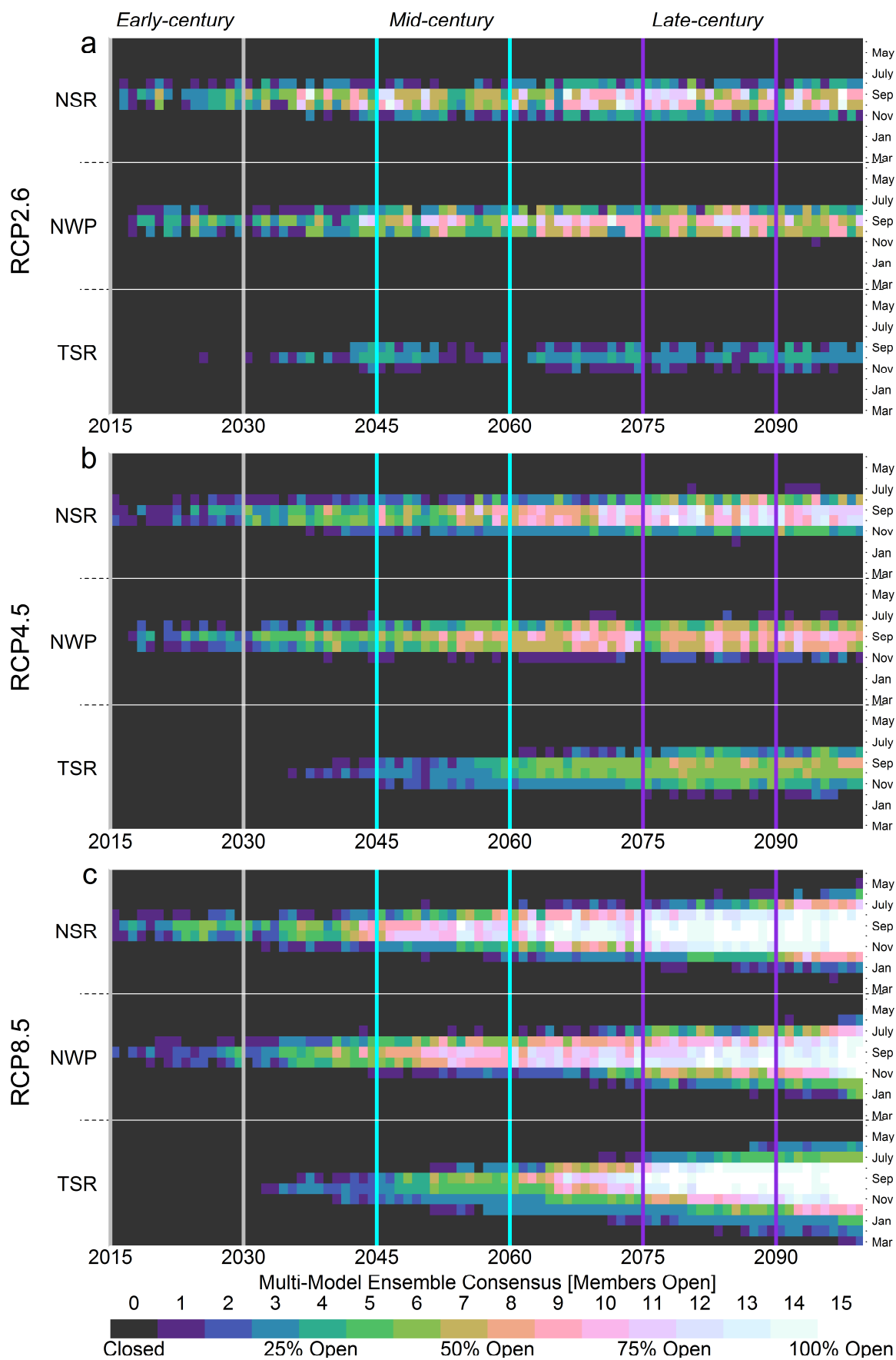


Figure 6.14 | Year-round trans-Arctic projections for open water vessels.

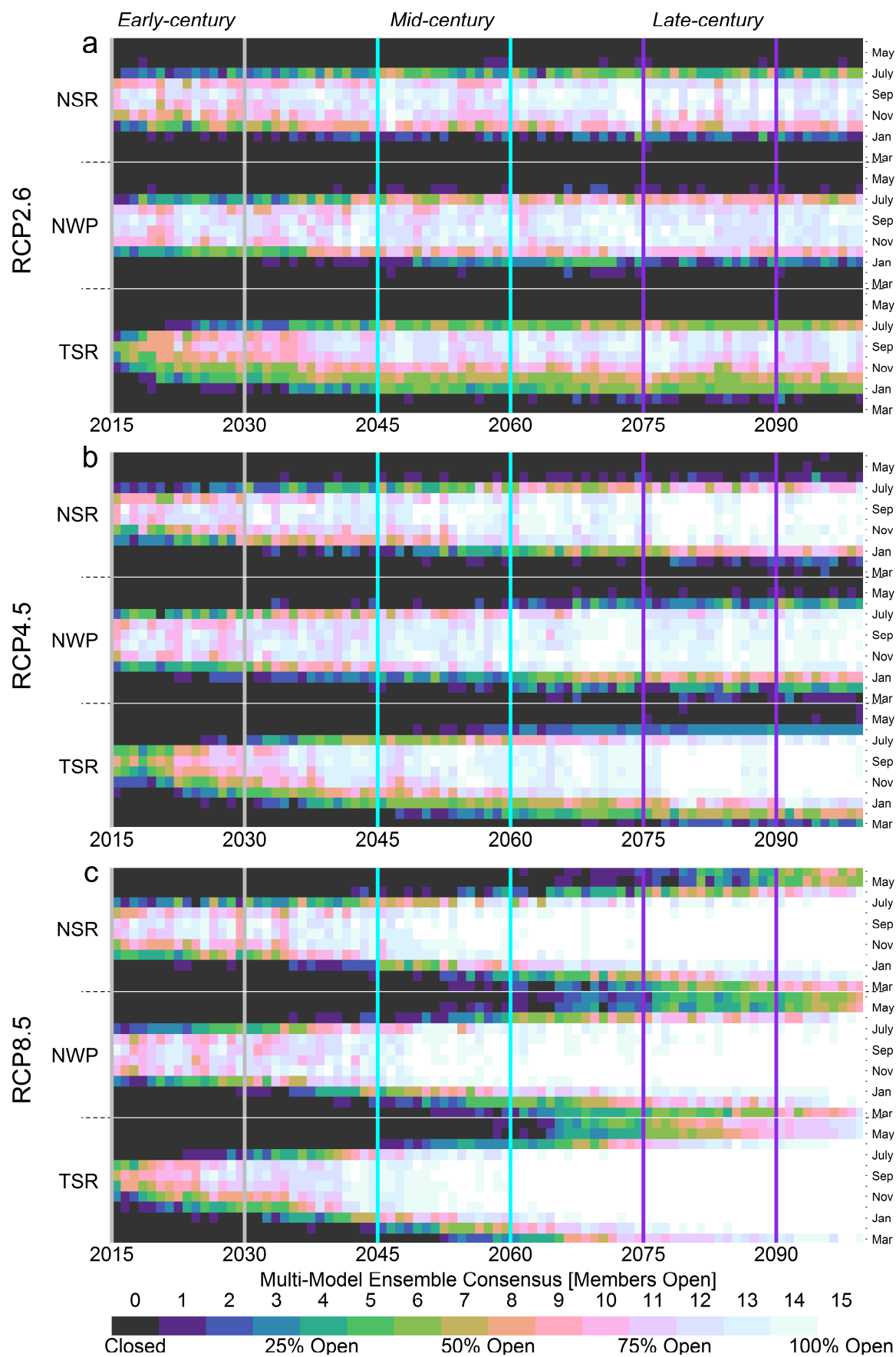


Figure 6.15 | As Figure 6.14 but for PC6 vessels.

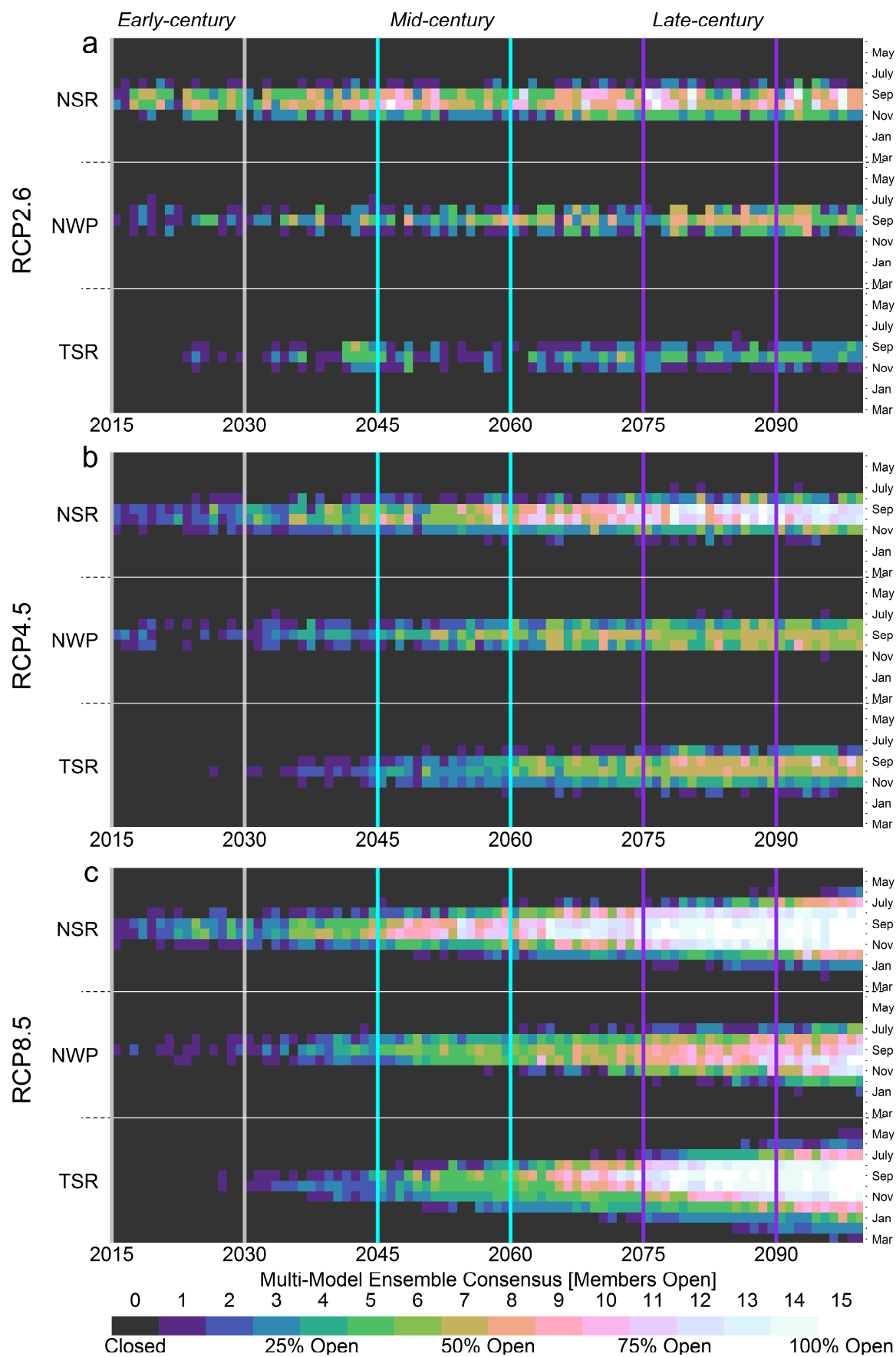


Figure 6.16 | As Figure 6.14 (OW vessels) but for “raw” (un-calibrated) GCMs.

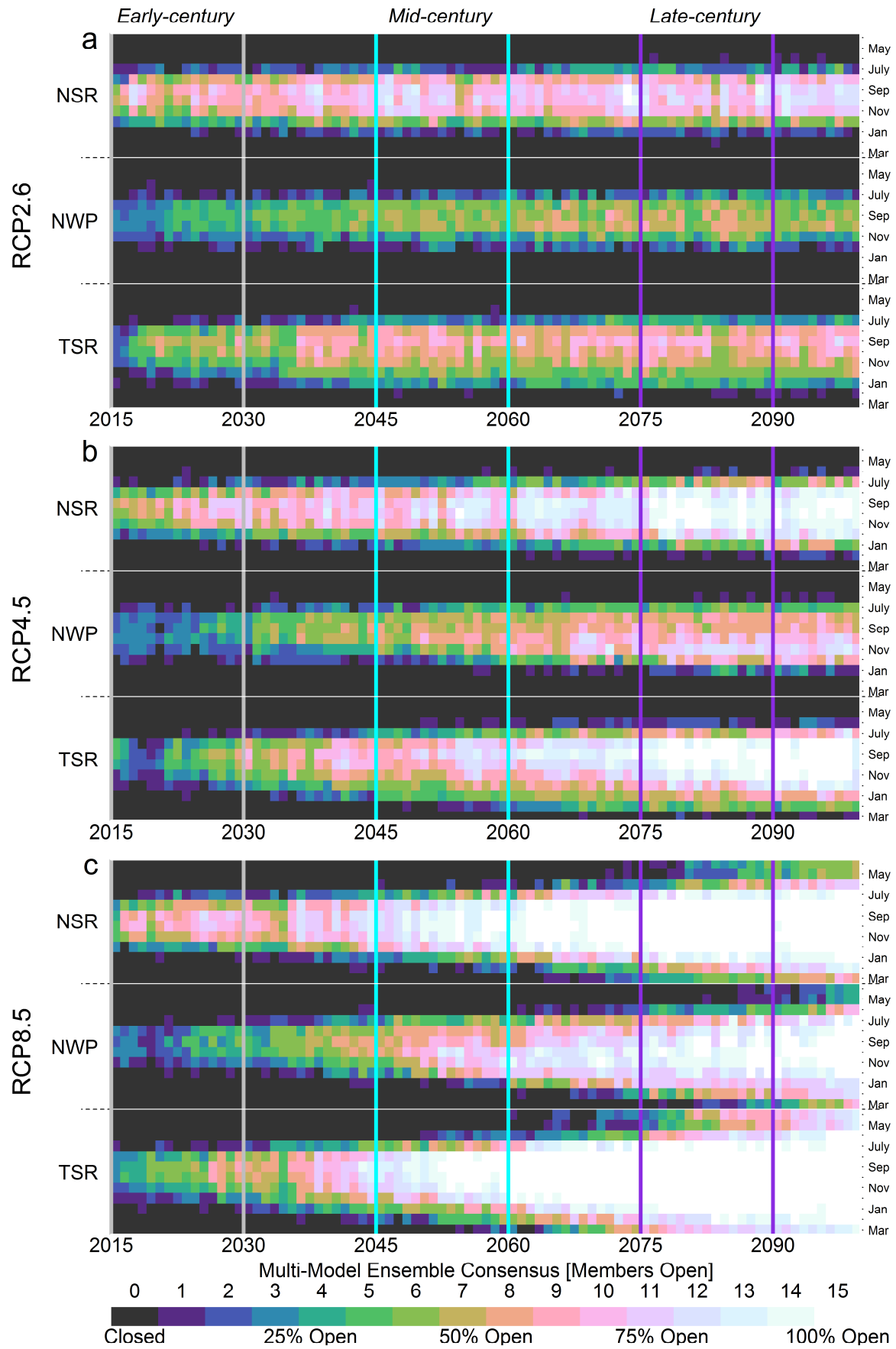


Figure 6.17 | As Figure 6.14 but for PC6 vessels using “raw” (un-calibrated) GCMs.

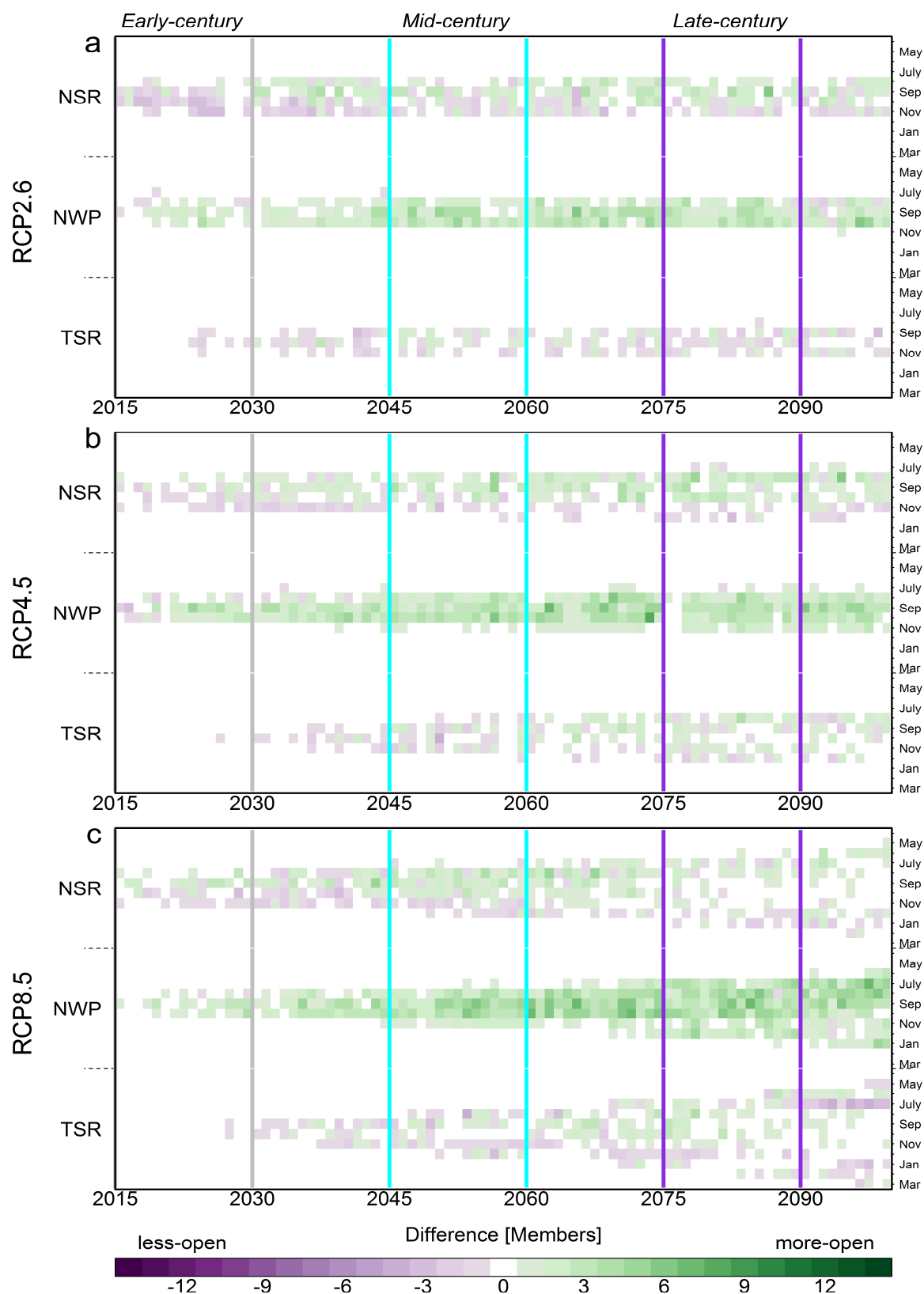


Figure 6.18 | Accessibility Difference, shown by the difference in number of members (calibrated – raw GCMs), i.e. Figure 6.14 minus Figure 6.16. Purple (green) indicates that the calibration has reduced (increased) accessibility.

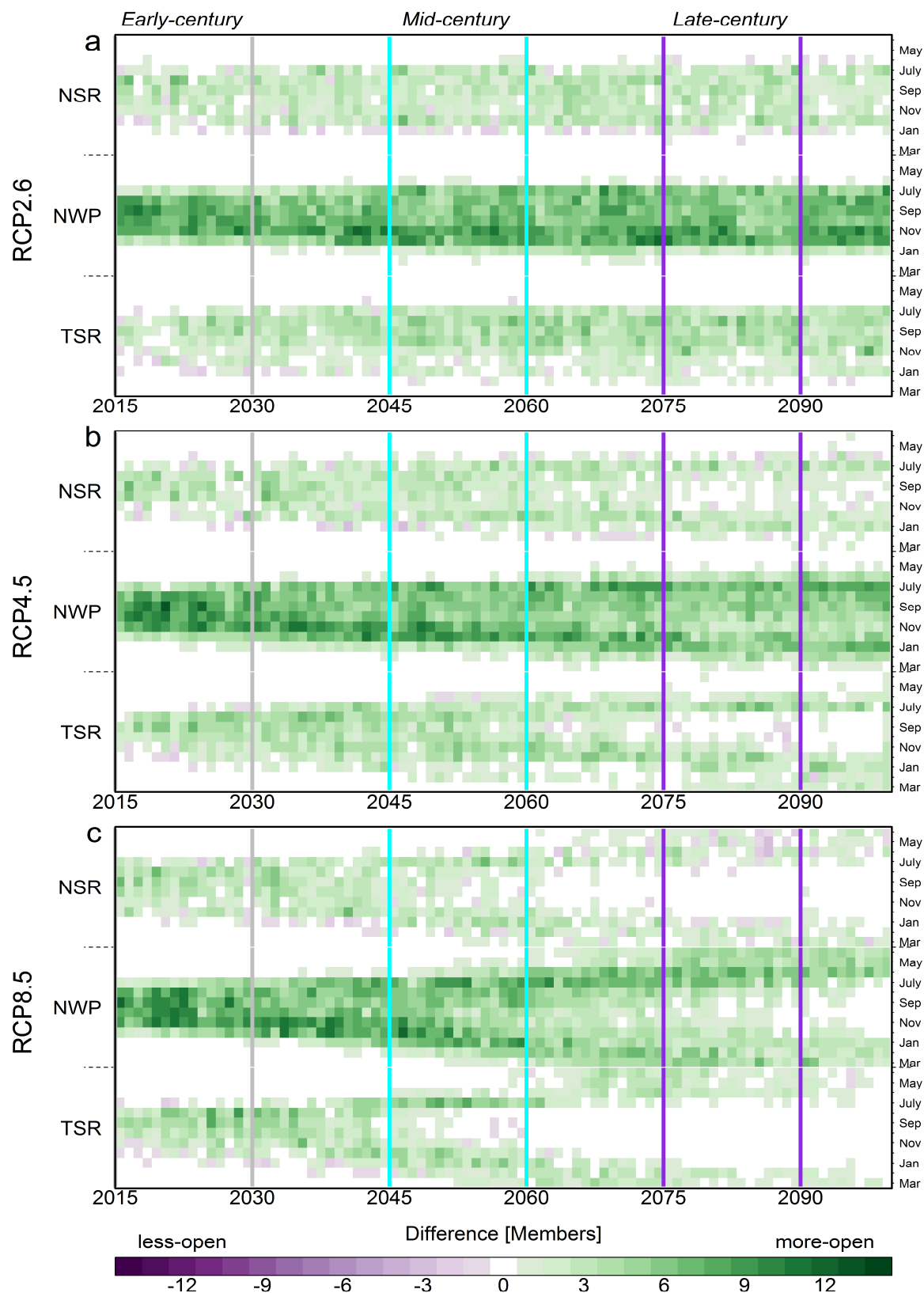


Figure 6.19 | As Figure 6.18 but for PC6 Vessels

6.4.3 Extended Season

The peak of the shipping season shifts with route choice and later into the century (Figure 6.20). The peak is mid-September, for the NWP, late-September for the NSR and October for the TSR. However, the shipping season curves are skewed with longer tails (later season voyages) towards the end of the century; this is most evident for the TSR in RCP8.5 (Figure 6.20i).

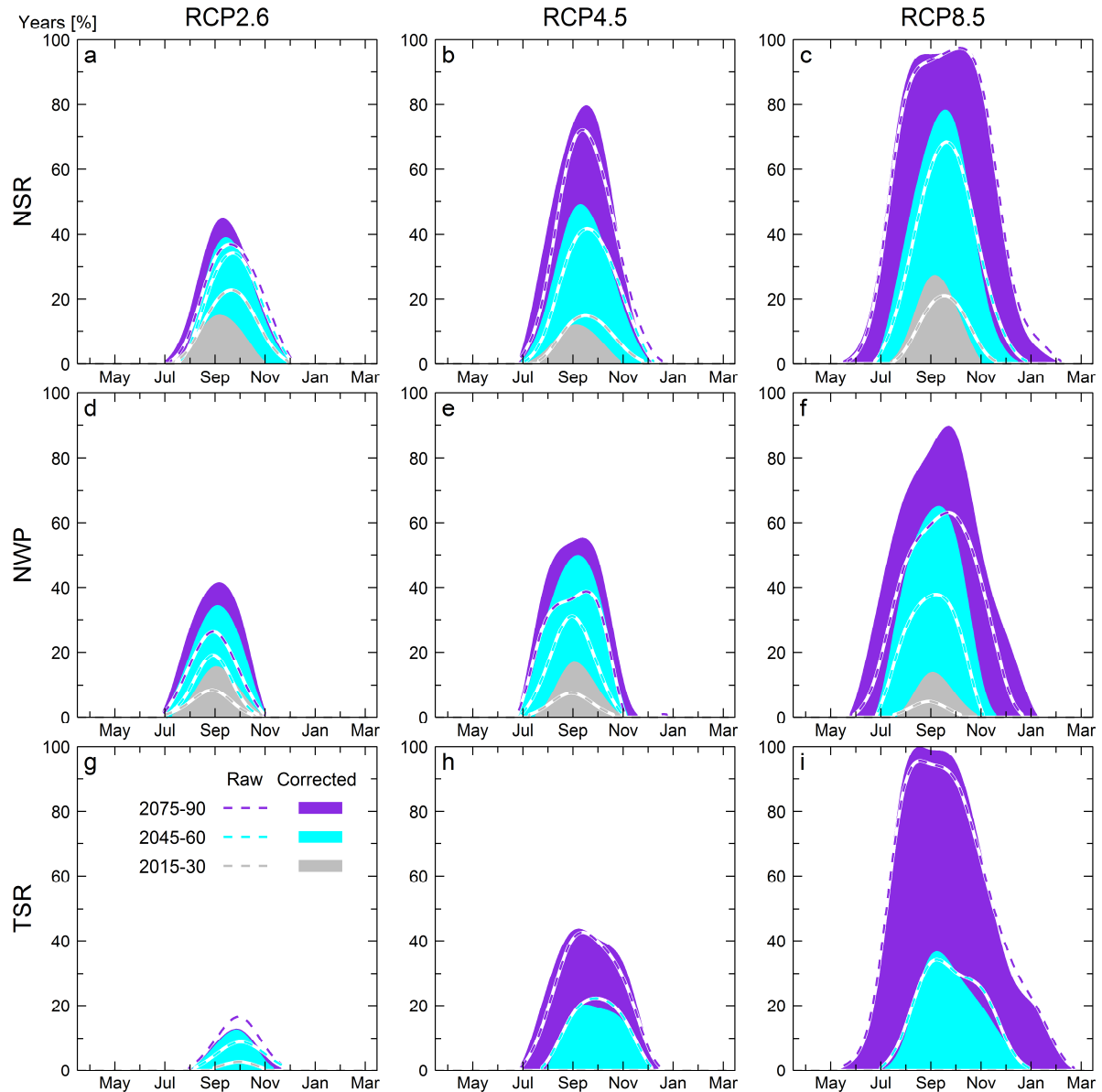


Figure 6.20 | Open water vessel season length simulated by raw and corrected GCMs for RCP2.6, 4.5, and 8.5 scenarios. For the early, mid, and late century periods the ensemble consensus (% probability of Arctic transit) is shown monthly. The season for the corrected GCMs (shaded regions) has shifted from the raw (un-calibrated) GCMs (dashed lines). Month tick marks represent the middle of the month. A smoothed fit is applied to the monthly data.

Early-century September conditions are equivalent to late-century July/December conditions in RCP8.5 (RCP2.6, August/November). The medium emissions RCP4.5 shipping season lies between RCP2.6 and 8.5. Figure 6.20 also shows the impact of the calibration; the “raw” (un-calibrated) GCMs clearly underestimate the number of years open by up to 30%. The calibration also shifts the peak of the shipping season to earlier in the year.

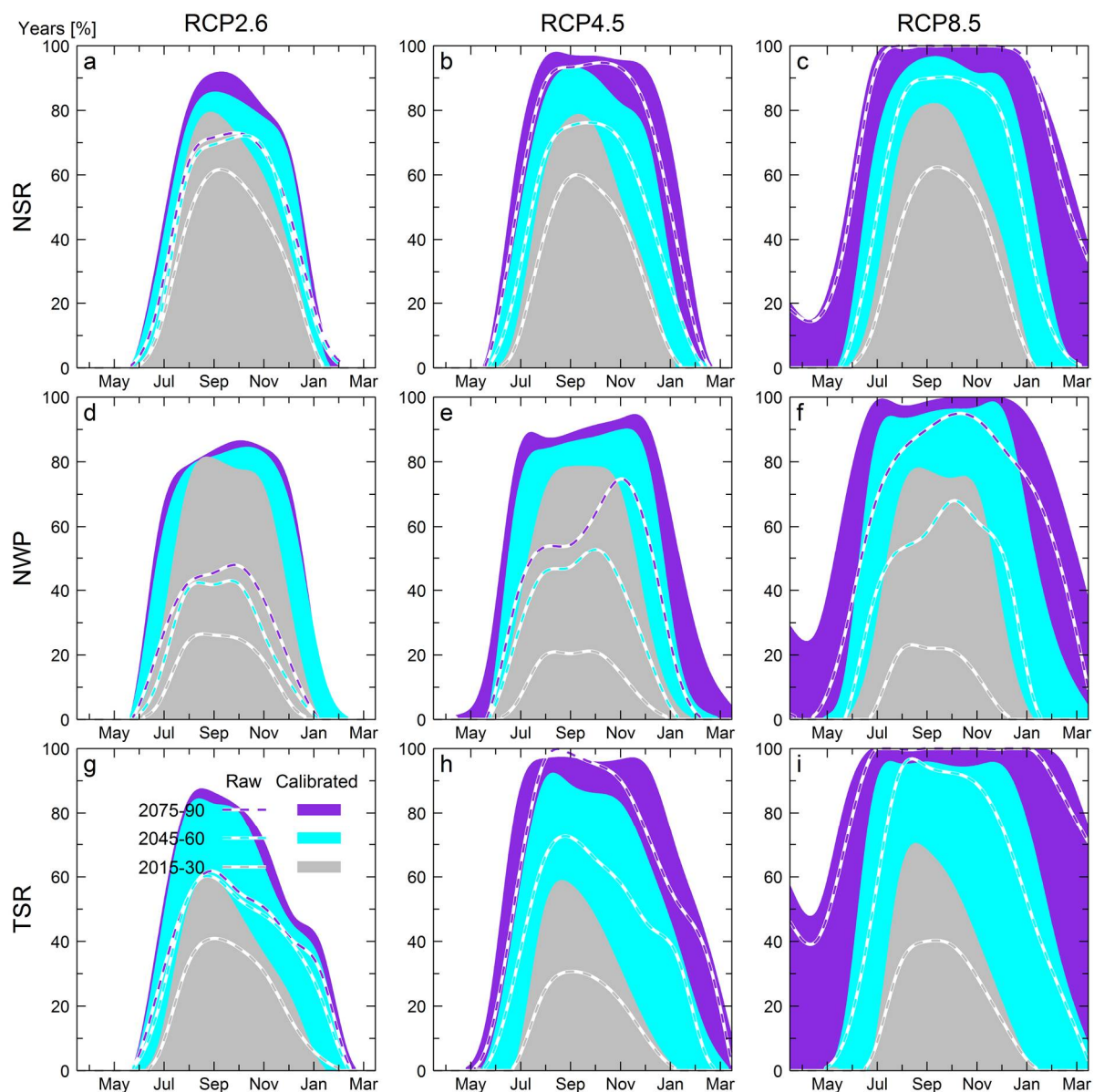


Figure 6.21 | As Fig.3 but for PC6 vessels.

The projected use of trans-Arctic routes early-century by PC6 vessels has generally increased by 20% – 60% as a result of the calibration. Early-century, the increase is ~20% on the NSR (Figure 6.21 a-c), with the length of the shipping season remaining

unchanged but the peak shifts from late to mid-September. September conditions in the raw GCMs are now typical of August/November on the NSR.

The calibration has increased PC6 transit potential early-century on the NWP by up to 60% (Figure 6.21 d-f). The NWP shows a constant shipping season with August – November being the peak months in terms of accessibility, this is extended to July – December mid/late-century. For the RCP2.6 and 4.5 scenarios the calibrated early-century conditions exceed that of the late-century conditions simulated by the raw GCMs. On the TSR, the calibration has increased PC6 transit potential by 20% – 30% early century, with a defined peak in accessibility early-September.

Typically, for all routes in RCP2.6 there is little difference between conditions from mid to late-century. RCP4.5 extends the shipping season by one month with a consistent increase in transit potential throughout the century. The defining feature of RCP8.5 at around mid-century, is that transits on any route are essentially guaranteed between July – December; by late-century on the TSR the minimum potential is ~50% in April. This means that for half of the years from 2075 the TSR, the shortest route across the central Arctic Ocean, is navigable year-round.

6.5 Comparison with previous studies

6.5.1 Comparison with Smith and Stephenson (2013) (S&S)

The Smith and Stephenson (2013) (S&S) maps shown in Figure 6.22 are the fastest routes through ensemble averaged data. They also report transit success rates taken from running their algorithm through the individual ensemble members, arising from sea ice conditions exceeding the vessel limitations (Table 6.2). The data and methods of S&S produce a higher transit potential for all scenarios and route except the NWP in RCP8.5 for mid-century.

Table 6.2 | Transit potential comparison to Smith and Stephenson (2013) (S&S). The double percentages refer to RCP4.5 / RCP8.5 respectively.

S&S	Any	NWP	Ch. 6	Any	NWP
1979 – 2005	~40%	15%	1995 – 2015	16%	6%
2006 – 2015	71% / 61%	17% / 27%	2015 – 2030	28% / 39%	14% / 14%
2040 – 2059	94% / 98%	53% / 60%	2045 – 2060	64% / 82%	49% / 63%

For the S&S summary maps (Figure 6.22A,C) it appears that the fastest route are plotted for each of the 2006 – 2015 (10 year) and 2040 – 2059 (20 year) periods for every September for each destination. Since there are 10 and 20 routes in panels A and C respectively per destination, either their multi-model mean is sufficiently low enough to allow a route not exceeding 0.15 m from 2006, or the routes plotted do exceed the SIT threshold and are just schematic examples of the types of routes possible. On comparison with Fig 4.7 which shows the September multi-model–ensemble-mean mean SIT from the CMIP5 subset, neither the Raw or MAVRIC fields contain a path through the Arctic that doesn't exceed 0.15 m.

One explanation for the discrepancy between the multi-model means in Fig 4.7 and S&S is that different models were used, thereby providing a different multi-model mean. This is plausible as five of the seven GCMs S&S use (MIROC-ESM, ACCESS1.0, ACCESS1.3, GFDL-CM3 and HadGEM2-CC) are more open according to Stephenson and Smith (2015) than the GCMs used in this chapter. The second explanation is that the accessibility parameters used by S&S are different; their approach allows for grid cells above the SIT threshold to be navigable if the sea ice concentration is suitably low.

This risk is not allowed in the methodology presented in this chapter, as OW are particularly vulnerable to sea ice and navigation in border-line ice regimes would require dead-slow ship speeds, therefore those routes are likely slower than alternatives. The variation in the S&S routes (Figure 6.22A,C) is presumably from the fluctuating yearly multi-model means.

Figure 6.22 illustrates how the use of model means can be misleading for data sets with high variability. Early-century the NWP is never used in the S&S model-mean for PC6 vessels, whereas it is used for ~70% of years using the individual ensembles presented here. The model mean results from S&S also have the TSR opening mid-century; the results presented here suggest the TSR is already open to PC6 vessels for some Septembers (Figure 6.4 and Figure 6.22b).

Mid-century several differences remain. PC6 vessels on European routes in S&S all use an identical fastest TSR route via the North Pole. This route is also the most popular route in this study but some deviation in the central Arctic is seen. The TSR is also utilised for some OW vessels here, for both European and North American routes. The TSR is never available in the S&S model mean, though a follow-up study, Stephenson and Smith (2015), using the same models (with the addition of MIROC5 and MIROC-ESM-CHEM) suggests the TSR is accessible early-century in the individual models, ACCESS1.0, ACCESS1.3, GFDL-CM3, HADGEM2-CC, IPSL-CM5A-MR, MIROC-ESM-CHEM, none of which are assessed in this study due to the selection criteria (Ch. 6.2.1). The fact the TSR is open in these GCMs and not the multi-model means confirms that they simulated below average ice conditions, explaining some differences between this chapter's findings and S&S.

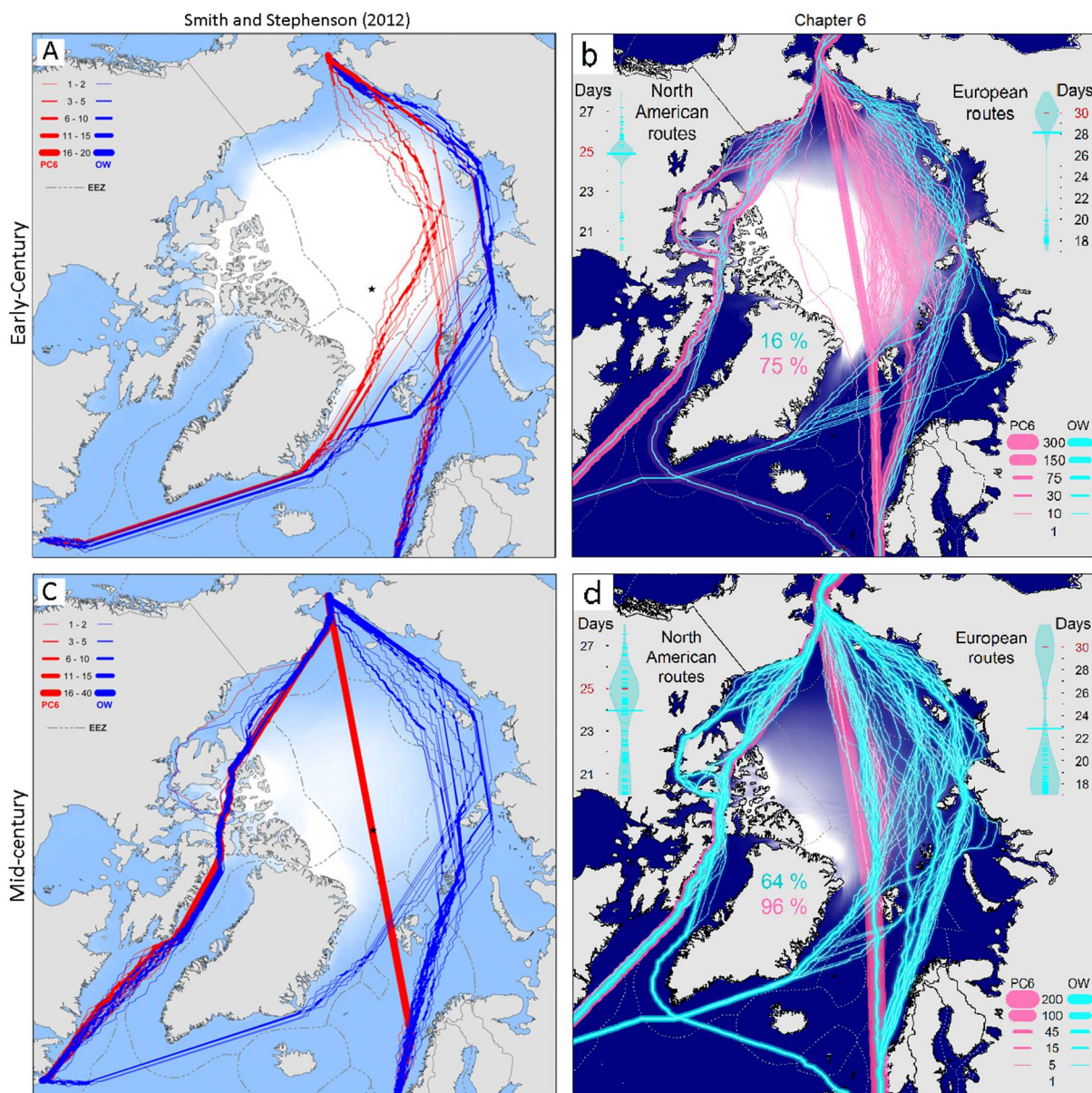


Figure 6.22 | Comparison with Smith and Stephenson (2013) (S&S). The S&S panels are “summary maps” generated by ensemble averaged data. Panel A is 2006 – 2015 from S&S, with RCP8.5 forcing, panel b is 1995 – 2015 historical and RCP8.5 forcings, from Figure 6.4b. Panel C (S&S) is 2040 – 2059 with RCP4.5 forcing, panel d is 2045 – 2060 with RCP4.5 forcing from Figure 6.5e. Note data and methods are not the same, see text.

European switch-transits (using the NWP) are never used in S&S, but this study suggests they can be utilised. The NWP is available mid-century but the longer southern version of the NWP is only utilised once. This is puzzling as the southern NWP, although longer, generally has favourable conditions compared to the northern NWP and should have comparable traffic early and mid-century as shown by Figure 6.5. There are two plausible reasons for the simulated lack of southern NWP usage in S&S.

Firstly, the conditions in the northern and southern NWP are the same or very similar, meaning that the northern and southern versions are open/closed simultaneously. This could be true as the representation of the Canadian Archipelago in some of the GCMs used by S&S maybe non-existent like in IPSL-CM5A-LR (which eliminated them from consideration in this chapter). Secondly, the entire length of the Parry Channel, which runs the whole length of the northern NWP (entering the Canadian Archipelago at Lancaster Sound and exiting at the M'Clure Strait, see Figure 6.3) may always produce very similar ice conditions in GCMs. Thus, the option of entering the Parry Channel to use the southern NWP coincides with the northern NWP being accessible, and so the northern route is preferred because it is shorter. Again, this is plausible with the limitations of GCMs in this region. This also implies that conditions in the Beaufort Sea near the M'Clure Strait and Amundsen Gulf are also very similar.

In addition to the careful selection of GCMs in this study, it is likely that the bias correction outlined in the previous chapter, and utilised here, has increased the realism of the Canadian Archipelago and thus transits through the NWP. This is possible as the PIOMAS reanalysis has a detailed depiction of the Canadian Archipelago including all the major channels and to a higher resolution than the CMIP5 GCMs used here. However, caution is still required when interpreting results for the NWP. The Canadian Archipelago ice in PIOMAS is more realistic because of the higher resolution and because it is constrained by the assimilation of observations. Ice in the "raw" GCMs can become stuck in these channels and pile up. SIT in excess of 50m is possible in some grid cells in this region in some GCMs.

6.5.2 Comparison with Stephenson and Smith (2015)

Stephenson and Smith (2015) extends the work of S&S by adding three GCMs (IPSL-CM5A-LR, MIROC5, and MIROC-ESM-CHEM) to the seven used in Smith and Stephenson (2013). These ten GCMs (*used here) are: ACCESS1-0, ACCESS1-3, CCSM4*, GFDL-CM3, HadGEM2-CC, IPSL-CM5A-LR, IPSL-CM5A-MR, MIROC5*, MIROC-ESM-CHEM, MPI-ESM-MR. Their GCM selection is based on the accuracy of the seasonal cycle and ice-loss trend as examined by Massonnet et al. (2012) and Liu et al. (2013). The selection methodology used here is based upon availability of multiple ensemble members to evaluate internal climate variability and a realistic depiction (resolution and land/sea mask) of the Arctic sea routes, discounting IPSL-CM5A-LR for lack of resolved Canadian Archipelago for example.

Direct comparison is between Stephenson and Smith (2015) and this chapter is possible as CCSM4 and MIROC5 are assessed in both. Stephenson and Smith (2015) do not provide statistics for September so success rates cannot be directly compared but qualitative trends can.

In both studies, CCSM4 shows relatively little accessibility early century for OW vessels. Early and mid-century Stephenson and Smith (2015) find transits are only possible using the NSR, but results presented in this chapter find there is an early-century bias towards the NSR but the NWP is still occasionally navigable. By mid-century, the share of transits between the NSR and NWP is approximately equal.

In both studies, MIROC5 also shows relatively little accessibility early century for OW vessels. Early-century Stephenson and Smith (2015) find transits are only possible using the NWP, whereas results presented in this chapter find there is an early-century preference towards the NWP, but the NSR is still navigable. Mid-century, Stephenson and Smith (2015) find that the NSR can occasionally be used, whereas results in this chapter suggest that access is a lot more common and the TSR even starts to be used.

Table 6.3 | Trans-Arctic PC6 season length (months) comparison

RCP	Stephenson and Smith (2015)		Ch. 6	
	RCP 4.5	RCP 8.5	RCP 4.5	RCP 8.5
Early-century	5.0	5.3	4.2	4.5
Mid-century	7.1	8.5	6.3	7.5

Stephenson and Smith (2015) find a 24 day longer shipping season for PC6 vessels early-century than the results presented here and a 24 – 30 day longer season by mid-century for RCP4.5 and RCP8.5 respectively. The relative change between the scenarios is more constant between the studies however; 9 days extra from RCP4.5 to RCP8.5 early-century and 36 – 42 days extra for mid-century.

As discussed previously the difference is likely due to the incorporation of more GCMs in S&S with a low sea ice bias and use of an algorithm, which is slightly less restrictive.

6.6 Discussion and Summary

6.6.1 Summary

This chapter assessed the potential for faster trade routes through the Arctic throughout the 21st century for normal Open Water (OW) vessels and ice-strengthened Polar Class 6 (PC6) vessels. By using a set of five calibrated GCMs, each with multiple ensemble members for three emission scenarios, the following questions have been answered:

1. *When will trans-Arctic shipping be possible?*

- Observations show that trans-Arctic shipping is already possible along the NSR using a combination of ice-strengthened vessels sometimes in convoy with Russian icebreakers. Projections from climate models show that accessibility will improve for all vessel classes through the century.
- For Open Water (OW) vessels, shipping is confined mainly to the summer/autumn months and is projected to extend into the winter for a RCP8.5 type scenario. Mid-century is identified as a transitional period for trans-Arctic OW shipping with accessibility increasing by up to 40% over 15 years. For OW vessels, internal variability is likely to be a significant factor throughout the century. The future emission scenario plays a pivotal role by late century with a reliable season of September – October in RCP2.6, August – November in RCP4.5, and July – December RCP8.5.
- For the ice strengthened Polar Class 6 (PC6) vessels transit potential is considerably higher with summer/autumn trans-Arctic voyages possible throughout the 21st century. The PC6 shipping season is projected to extend to include the winter months by mid-century, and include spring, becoming year round from mid-century in RCP8.5.

2. *What are the preferred routes to/from East Asia?*

- For OW vessels, the NSR and NWP are both intermittently available early-century, often using switch-transits when the only one of the NSR and NWP is available. The TSR starts to become open by mid-century but is the least open for the remainder for RCP2.6 and 4.5. Late-century under RCP8.5 conditions the TSR is comparable to the NSR.

- PC6 vessels prefer the NSR and NWP early-century and rarely need switch-transits. By mid-century PC6 vessels prefer the TSR instead of the NSR, and by late century for RCP4.5 and 8.5 the TSR has the longest and most reliable season.
3. *What are the time savings for open water vessels using trans-Arctic, opposed to conventional routes?*
- Utilising trans-Arctic routes when possible and using traditional European routes via Suez (30 days) otherwise, average journey times to East Asia can be dramatically reduced. Savings are achieved as Arctic routes become more available and more direct and ice-free through the century. In early-century, the average for all European (Arctic + Suez) voyages using open water vessels is 26 days, which becomes 20 days by mid-century and 17 days by late century under RCP8.5. Under RCP2.6 the journey times are 23 days by mid-century and 22 days by late century.
 - Savings are less striking for North America because the route via Panama only takes 25 days. Sailing the NWP from North America to East Asia takes 20–22 days depending on channel choice and ice conditions, and when the NWP is impassable using alternative Arctic routes via the NSR or TSR takes at least 24 days.

6.6.2 Discussion

The Arctic is in transition to a seasonally ice-free state, increasing economic opportunities to commercial shipping, with the opening of new and faster trans-Arctic routes and an extended shipping season. By utilising these Arctic routes when accessible, and using traditional European routes via Suez (30 days) otherwise, average journey times to East Asia can be dramatically reduced. Savings are achieved as Arctic routes become more available and more direct and ice-free through the century.

These reduced transit times could lead to significant savings from increased voyage turnover and lower costs, in addition to potentially reducing global shipping emissions. Despite these trends, interannual variability will remain a significant factor in route availability throughout the 21st century, motivating increased efforts in seasonal to interannual forecasting. In addition to the dramatic changes to sea ice, climate change is likely to modify other climatic hazards to shipping not assessed here such as fog, waves and icing; developing the full potential for trans-Arctic shipping will require knowledge of these along with comprehensive en-route infrastructure, providing incentives for substantial investment in Arctic regions. For a high emissions scenario, by late-century

trans-Arctic shipping is potentially commonplace, with a reliable season of 4–8 months. For a low emissions scenario, with global mean temperature stabilisation of less than 2 °C above pre-industrial, the frequency of open water vessel transits still has the potential to double by mid-century with a reliable season of 2–4 months. Companies wishing to utilise Arctic routes face choices such as whether to invest in technologically advanced ice-capable ships. These choices should consider the changing Arctic environment and the risks and opportunities this will offer. Crucially these results originate from corrected GCMs, with realistic mean SIT, spatial distribution, and interannual variability, so projections of future transit availability, route choices and frequency are likely to be more robust.

The results from this chapter are compared with previous work in this field. Although the data and methodologies are varied, there are some important messages. The most prominent difference in the methodology presented here is the use of calibrated sea ice thickness projections. For impact-based climate change studies bias correction is vital, as described by a special report from the IPCC (Seneviratne et al., 2012). By assessing years and ensemble members explicitly, and not in an ensemble or temporal-mean framework, the uncertainty in projections of Arctic shipping are also quantified.

The results presented here are projections and supply the general conditions expected for a particular time period and emission scenario. The results show that interannual variability is apparent throughout the 21st century, meaning that although generally accessibility increases, closed routes are always possible some years, even late-century. There is a distinct shipping season that extends through the 21st century, but there are always months where shipping is not practical or possible to the vessel classes assessed here. Forecasting the opening and closing of the open-water season is a vital need in the Arctic, for a range of applications (Eicken, 2013). With the potential for increased interest in using the faster routes described in this chapter, the need for accurate forecasts of the route openings will increase. Shipping companies operate on schedules that are far longer than the typical range of accurate weather forecasts so seasonal predictions are required. There may be an appetite for knowledge of ice conditions for next year too. The next chapter will examine the potential for GCMs to provide skilful predictions of the opening of Arctic sea routes on seasonal to interannual timescales.

References

- Aksenov, Y., Popova, E. E., Yool, A., Nurser, A. J. G., Williams, T. D., Bertino, L., and Bergh, J.: On the future navigability of Arctic sea routes: High-resolution projections of the Arctic Ocean and sea ice, *Mar. Policy*, doi: <http://dx.doi.org/10.1016/j.marpol.2015.12.027>, 2015.
- Arctic Logistics Information Office: http://www.arctic-lio.com/nsr_transits.
- Barnhart, K. R., Miller, C. R., Overeem, I., and Kay, J. E.: Mapping the future expansion of Arctic open water, *Nature Clim. Change*, doi: [10.1038/nclimate2848](https://doi.org/10.1038/nclimate2848), 2015.
- Canadian Coast Guard: http://www.ccg-gcc.gc.ca/eng/MCTS/Vtr_Arctic_Canada.
- Dijkstra, E. W.: A note on two problems in connexion with graphs, *Numer. Math.*, 1, 269-271, doi: [10.1007/bf01386390](https://doi.org/10.1007/bf01386390), 1959.
- Eicken, H.: Ocean science: Arctic sea ice needs better forecasts, *Nature*, 497, 431-433, doi: [10.1038/497431a](https://doi.org/10.1038/497431a), 2013.
- Gent, P. R., Danabasoglu, G., Donner, L. J., Holland, M. M., Hunke, E. C., Jayne, S. R., Lawrence, D. M., Neale, R. B., Rasch, P. J., and Vertenstein, M.: The community climate system model version 4, *J. Clim.*, 24, 4973-4991, doi: [10.1175/2011JCLI4083.1](https://doi.org/10.1175/2011JCLI4083.1), 2011.
- Hawkins, E., Tietsche, S., Day, J. J., Melia, N., Haines, K., and Keeley, S.: Aspects of designing and evaluating seasonal-to-interannual Arctic sea-ice prediction systems, *Q. J. R. Meteorolog. Soc.*, doi: [10.1002/qj.2643](https://doi.org/10.1002/qj.2643), 2015.
- Hulme, M.: 1.5 °C and climate research after the Paris Agreement, *Nature Clim. Change*, advance online publication, doi: [10.1038/nclimate2939](https://doi.org/10.1038/nclimate2939), 2016.
- International Maritime Organization (IMO): <http://www.imo.org/en/MediaCentre/HotTopics/polar/>.
- IPCC: *Climate Change 2013: The Physical Science Basis. Contribution of Working Group I to the Fifth Assessment Report of the Intergovernmental Panel on Climate Change*, Cambridge University Press, Cambridge, United Kingdom and New York, NY, USA, 2013.
- Jungclaus, J., Keenlyside, N., Botzet, M., Haak, H., Luo, J.-J., Latif, M., Marotzke, J., Mikolajewicz, U., and Roeckner, E.: Ocean circulation and tropical variability in the coupled model ECHAM5/MPI-OM, *J. Clim.*, 19, 3952-3972, doi: [10.1175/JCLI3827.1](https://doi.org/10.1175/JCLI3827.1), 2006.
- Khon, V. C., Mokhov, I. I., Latif, M., Semenov, V. A., and Park, W.: Perspectives of Northern Sea Route and Northwest Passage in the twenty-first century, *Clim. Change*, 100, 757-768, doi: [10.1007/s10584-009-9683-2](https://doi.org/10.1007/s10584-009-9683-2), 2010.
- Lasserre, F.: Case studies of shipping along Arctic routes. Analysis and profitability perspectives for the container sector, *Transp. Res. Part A Policy Pract.*, 66, 144-161, doi: <http://dx.doi.org/10.1016/j.tra.2014.05.005>, 2014.

- Liu, J., Song, M., Horton, R. M., and Hu, Y.: Reducing spread in climate model projections of a September ice-free Arctic, *Proc. Natl. Acad. Sci. U.S.A.*, doi: 10.1073/pnas.1219716110, 2013.
- Massonnet, F., Fichet, T., Goosse, H., Bitz, C. M., Philippon-Berthier, G., Holland, M. M., and Barriat, P. Y.: Constraining projections of summer Arctic sea ice, *Cryosphere*, 6, 1383-1394, doi: 10.5194/tc-6-1383-2012, 2012.
- Meehl, G. A., Washington, W. M., Arblaster, J. M., Hu, A., Teng, H., Kay, J. E., Gettelman, A., Lawrence, D. M., Sanderson, B. M., and Strand, W. G.: Climate change projections in CESM1 (CAM5) compared to CCSM4, *J. Clim.*, 26, 6287-6308, doi: 10.1175/JCLI-D-12-00572.1, 2013.
- Melia, N., Haines, K., and Hawkins, E.: Improved Arctic sea ice thickness projections using bias-corrected CMIP5 simulations, *Cryosphere*, 9, 2237-2251, doi: 10.5194/tc-9-2237-2015, 2015.
- Rogers, T., Walsh, J., Rupp, T., Brigham, L., and Sfraga, M.: Future Arctic marine access: analysis and evaluation of observations, models, and projections of sea ice, *Cryosphere*, 7, 321-332, doi: 10.5194/tc-7-321-2013, 2013.
- Seneviratne, S. I., Nicholls, N., Easterling, D., Goodess, C. M., Kanae, S., Kossin, J., Luo, Y., Marengo, J., McInnes, K., and Rahimi, M.: Changes in climate extremes and their impacts on the natural physical environment. In: *Managing the risks of extreme events and disasters to advance climate change adaptation*, edited by: Field, C. B., Barros, V., Stocker, T. F., Qin, D., Dokken, D. J., Ebi, K. L., Mastrandrea, M. D., Mach, K. J., Plattner, G. K., K., A. S., Tignor, M., and M., M. P., A Special Report of Working Groups I and II of the Intergovernmental Panel on Climate Change (IPCC), Cambridge University Press, Cambridge, UK, and New York, NY, USA, 109-230, 2012.
- Smith, L. C. and Stephenson, S. R.: New Trans-Arctic shipping routes navigable by midcentury, *Proc. Natl. Acad. Sci. U.S.A.*, 110, E1191–E1195, doi: 10.1073/pnas.1214212110, 2013.
- Stephenson, S. R. and Smith, L. C.: Influence of climate model variability on projected Arctic shipping futures, *Earth's Future*, 3, 331-343, doi: 10.1002/2015ef000317, 2015.
- Stephenson, S. R., Smith, L. C., Brigham, L. W., and Agnew, J. A.: Projected 21st-century changes to Arctic marine access, *Clim. Change*, 118, 885-899, doi: 10.1007/s10584-012-0685-0, 2013.
- Swart, N. C., Fyfe, J. C., Hawkins, E., Kay, J. E., and Jahn, A.: Influence of internal variability on Arctic sea-ice trends, *Nature Clim. Change*, 5, 86-89, doi: 10.1038/nclimate2483, 2015.
- Tan, X., Su, B., Riska, K., and Moan, T.: A six-degrees-of-freedom numerical model for level ice–ship interaction, *Cold Reg. Sci. Technol.*, 92, 1-16, doi: <http://dx.doi.org/10.1016/j.coldregions.2013.03.006>, 2013.
- Taylor, K. E., Stouffer, R. J., and Meehl, G. A.: An overview of CMIP5 and the experiment design, *Bull. Am. Meteorol. Soc.*, 93, 485-498, doi: 10.1175/Bams-D-11-00094.1, 2012.

The HadGEM2 Development Team, Martin, G. M., Bellouin, N., Collins, W. J., Culverwell, I. D., Halloran, P. R., Hardiman, S. C., Hinton, T. J., Jones, C. D., McDonald, R. E., McLaren, A. J., O'Connor, F. M., Roberts, M. J., Rodriguez, J. M., Woodward, S., Best, M. J., Books, M. E., Brown, A. R., Butchart, N., Dearden, C., Derbyshire, S. H., Dharssi, I., Doutriaux-Boucher, M., Edwards, J. M., Falloon, P. D., Gedney, N., Grey, L. J., Hewitt, H. T., Hobson, M., Huddleston, M. R., Huges, J., Ineson, S., Ingram, W. J., James, P. M., Johns, T. C., Johnson, C. E., Jones, A., Jones, C. P., Joshi, M. M., Keen, A. B., Liddicoat, S., Lock, A. P., Maidens, A. V., Manners, J. C., Milton, S. F., Rae, J. G. L., Ridley, J. K., Sellar, A., Senior, C. A., Totterdell, I. J., Verhoef, A., Vidale, P. L., and Wiltshire, A.: The HadGEM2 family of Met Office Unified Model climate configurations, *Geosci. Model Dev.*, 4, 723-757, doi: 10.5194/gmd-4-723-2011, 2011.

Tilling, R. L., Ridout, A., and Shepherd, A.: Near Real Time Arctic sea ice thickness and volume from CryoSat-2, *The Cryosphere Discuss.*, 2016, 1-15, doi: 10.5194/tc-2016-21, 2016.

Transport Canada: Arctic Ice Regime Shipping System (AIRSS) Standards, Transport Publication, 12259 E, 1998.

Van Etten, J.: *gdistance* Distances and Routes on Geographical Grids, R package, 2015.

Van Vuuren, D. P., Edmonds, J., Kainuma, M., Riahi, K., Thomson, A., Hibbard, K., Hurtt, G. C., Kram, T., Krey, V., and Lamarque, J.-F.: The representative concentration pathways: an overview, *Clim. Change*, 109, 5-31, doi: 10.1007/s10584-011-0148-z, 2011.

Vavrus, S. J., Holland, M. M., Jahn, A., Bailey, D. A., and Blazey, B. A.: Twenty-First-Century Arctic Climate Change in CCSM4, *J. Clim.*, 25, 2696-2710, doi: 10.1175/jcli-d-11-00220.1, 2012.

Walsh, J. E. and Zwally, H. J.: Multiyear sea ice in the Arctic: Model- and satellite-derived, *J. Geophys. Res. Oceans*, 95, 11613-11628, doi: 10.1029/JC095iC07p11613, 1990.

Watanabe, M., Suzuki, T., O'ishi, R., Komuro, Y., Watanabe, S., Emori, S., Takemura, T., Chikira, M., Ogura, T., and Sekiguchi, M.: Improved climate simulation by MIROC5: mean states, variability, and climate sensitivity, *J. Clim.*, 23, 6312-6335, doi: 10.1175/2010jcli3679.1, 2010.

Williams, P. D.: Transatlantic flight times and climate change, *Environ. Res. Lett.*, 11, 024008, doi: 10.1088/1748-9326/11/2/024008, 2016.

Zhang, J. and Rothrock, D.: Modeling global sea ice with a thickness and enthalpy distribution model in generalized curvilinear coordinates, *Mon. Weather Rev.*, 131, 845-861, doi: 10.1175/1520-0493(2003)131<0845:MGSIIWA>2.0.CO;2, 2003.

Chapter 7

**Seasonal to interannual predictability
of Arctic shipping routes**

Summary

With the combination of increasing shipping activity and highly variable sea routes, the need for better sea ice forecasts and the scope for seasonal predictions for the opening of Arctic sea routes are larger than ever. The potential predictability of the opening of Arctic sea routes is explored in the chapter using a ‘perfect model’ experiment, whereby the GCM ensemble divergence is analysed. The results from this provide an upper bound for the usefulness of GCMs in this respect.

Initial results indicate that predictions in years with anomalously high and low sea ice show the most skill; predicting years with marginal conditions is challenging. The simulations show that the opening and closing of the shipping routes are the hardest periods to predict. Predictions that are initialised closer to the forecast period show the strongest signal, which is expected as the ensemble will have dispersed less. However, there is evidence of a ‘predictability barrier’ around May, before which skill reduces dramatically. There are currently a few known limitations to the study. The relatively high levels of sea ice in the GCM HadGEM1.2 restricts the opening of sea routes so that only the NSR is open for a PC6 class vessel, limiting Intercomparison with alternative routes and vessel classes. The study would also benefit from developing an additional method for detecting a signal from the forecasts to aid the quantification of skill in the predictions. Despite this, the results presented show great promise for the use of GCMs to forecast the opening of the Arctic sea routes on seasonal to interannual timescales.

7.1 Introduction

Observations of Arctic sea ice continue to show declines in both extent and thickness, as discussed extensively in previous chapters. This raises the possibility of increased activity in the region for shipping, resource extraction, and tourism. The projections from Ch. 6 show that although potential for trans-Arctic shipping will become increasingly regular there remains substantial variability in routing options year-to-year. With the combination of increasing activity and highly variable sea routes, the need for better sea ice forecasts and the scope for seasonal predictions to manage these risks are larger than ever (Eicken, 2013).

The use of GCMs as seasonal to interannual prediction tools for sea ice conditions is an evolving field; initial studies show promise at producing skilful forecasts. However, the predictive skill of climatic variables is degraded by the chaotic nature of the climate system with increasing forecast lead-time. A common experiment is to predict retrospectively (hindcast) the September sea ice extent, where significant skill has been demonstrated, although substantial issues still remain (Chevallier et al., 2013; Merryfield et al., 2013; Sigmund et al., 2013; Wang et al., 2013; Guemas et al., 2014; Msadek et al., 2014). Other methods use a combination of standalone ice model simulations and empirical techniques (Schröder et al., 2014; Stroeve et al., 2014). The importance of the field was highlighted in early 2016 with a special issue on polar predictability published by the Quarterly Journal of the Royal Meteorological Society to assess the current state of knowledge and future research priorities (Bauer and Jung, 2016).

In a review study on Arctic sea-ice predictability and prediction on seasonal to decadal time-scales, Guemas et al. (2014) shows that these prediction systems show significant skill at predicting summer sea ice conditions, although they note that determining the source of forecast errors is problematic. Sea ice predictability is intrinsically bounded by inherent limits related to chaotic atmospheric variability (Holland et al., 2010; Blanchard-Wrigglesworth et al., 2011). In this fledgling area of research there is potential for vast improvements in forecast skill to be made, up to this fundamental limit, by finding and addressing the sources of forecast error. The current sources of error include an incomplete representation of physical processes (e.g. melt ponds (Schröder et al., 2014)), or inadequate knowledge of initial conditions, this has been

shown in idealised experiments using sea ice thickness, that is currently not assimilated in operational forecasts (Day et al., 2014a; Msadek et al., 2014; Massonnet et al., 2015).

Many logistical considerations of global shipping must be planned on seasonal timescales. For example, applications to sail on the NSR must be received between three and 24 weeks prior to departure (Northern Sea Route Information Office, 2016). This places a time range for operational pre-planning, including analysis of ice conditions, which is in the scope of long-range to seasonal forecasts. Improvements in forecasts at this time horizon might allow more informed pre-planning and decisions to be made about near-future voyages, which could be of great economic benefit to vessel operators. However, the predictive capability for Arctic sea-ice is likely to vary by location, so it is important to understand where the ships travel in order to understand whether relevant predictions could be provided. As an example, Figure 5.4 showed the total number of ships in each region for a single month in August 2011. Note that these data are for all ships, not just commercial. The majority of routes inside the Arctic are along the Eurasian coastlines on the NSR, at the sea ice edge between Spitzbergen and Greenland, and in the Labrador Sea and Canadian Archipelago. It is these regions where skilful predictions of sea-ice conditions would currently be most valuable for shipping considerations. However, as has been shown in Ch.6 and previous studies, these routes are likely to evolve as the sea ice continues to retreat.

It must be noted that current operational seasonal prediction systems, like the Met Office's GloSea5, typically use a horizontal resolution of 0.25° for their ocean model (MacLachlan et al., 2015); this is considerably higher than the 1° ocean resolution used in the CMIP3 generation of GCMs that the predictability studies were conducted. This is particularly important for forecasting Arctic sea ice and the intricacies of the shipping channels.

Many previous studies on the predictability of sea ice have only focussed on pan-Arctic quantities for assessing the skill of prediction systems. However, there is a demand for more regional predictions from users such as the shipping industry (Eicken, 2013).

This chapter will provide an insight into ongoing work to quantify the predictability of the opening of Arctic sea routes with a GCM.

The principal questions this chapter addresses are:

1. *How potentially skilful are GCMs as seasonal to interannual forecast tools for Arctic shipping?*
2. *How far in advance can predictions of Arctic sea route openings be made?*

7.2 Potential predictability experiments

To assess the prospects for a predictable shipping season using a GCM the ‘perfect-model’ approach to estimating predictability is used. The perfect-model approach involves producing a perturbed ensemble with tiny perturbations to their initial conditions, which is verified against the model itself rather than against observations. This method has the advantage over using observations, which contain a climate change signal that hinders analysis of the real world, in addition to problems arising from temporally and spatially sparse data.

Perfect model experiments have previously been used to understand modes of coupled climate variability such as the Atlantic Meridional Overturning Circulation (AMOC) (Griffies and Bryan, 1997; Pohlmann et al., 2004) and El Niño Southern Oscillation (ENSO) (Collins et al., 2002). The perfect model approach provides an upper bound for the predictive skill provided the system in question is governed by the same physical equations as the GCM (Hawkins et al., 2015), although this may not necessarily be the same upper limit in predictability for the real world (Eade et al., 2014; Shi et al., 2015).

The Arctic Predictability and Prediction on Seasonal-to-Interannual Timescales (APPOSITE) project follows a consistent protocol across many GCMs. The experimental protocol uses a ‘present day’ control simulation and ensemble predictions rather than a transient climate simulation. Simulations are initialised from ‘present day’ simulated ocean temperature and atmospheric states.

To examine the lead-time dependence of potential skill in predictions of ship route openings, the HadGEM1.2 GCM (Johns et al., 2006; Shaffrey et al., 2009) is used in a perturbed ensemble setup. Following an initial spin-up period a 250-year control run is simulated to sample the models mean state and the full range of climate variability. To examine the predictability of HadGEM1.2 a 16-member ensemble was initialised, each with a perturbation to the sea surface temperature field. This perturbation takes the form of a randomly generated spatially-uncorrelated Gaussian noise with a standard deviation of 10^{-4} K (Day et al., 2015). This perturbation is so small that it is equivalent to assuming perfect knowledge of the initial conditions. This methodology ensures that any differences henceforth are solely due to the chaotic nature of the simulated climate system. This process was applied to 10 start years during the control run to sample the range of high, low, and medium sea ice states; each ensemble was run for 3 years. Ensembles for the 10 start dates were initialised on the 1st of January, May, and July,

partly to target the May predictability barrier noted by Sigmond et al. (2013) in observations and Day et al. (2014b) in a selection of GCMs.

This chapter examines, with respect to the opening of the Arctic sea routes, the solutions from 16 ensemble members for all years and initialisation months. The predictions will be skilful until the ensemble becomes sufficiently divergent. Analysing these predictions from the different initialisation months will allow indicate how far in advance potentially skilful predictions can be made. By simulating and assessing the predictions out to 3-years in the future, the prospects for interannual predictions can also be assessed.

7.3 Predictability of the shipping season

The opening of the Northern Sea Route (NSR) for the upcoming season is predicted by HadGEM1.2 using the ‘alternative shipping algorithm’ from Ch. 6.4. Owing to the ‘present day’ forcings being from 1990, and the characteristic biases in the sea ice conditions simulated by HadGEM1.2 only the NSR is reliably open for a PC6 ice-strengthened class vessel, hence only results from this scenario can be presented.

7.3.1 1st July first season predictability

The July 1st predictions for a PC6 vessel sailing on the NSR are shown in Figure 7.1. The Y-axis shows the ensemble consensus: 0% denoting no ensemble members open, 100% — all ensemble members open. There is increased confidence that the routes will be closed in the 0 – 10% range and high confidence that the routes will be open in the 90 – 100% range. However, these exact thresholds are used for schematic purposes on the figures only rather than for any robust statistical reason. Outside of this range, the ensemble open consensus is more diverse, so there is lower confidence in any predictions.

To calculate the range expected by chance in any given year, the control run is treated as a very large ensemble, where each of the 250 years represents an individual ensemble member. The mean proportion of the control simulation that has an open NSR is then simply the percentage of years open on every day. The red region shows the open consensus percentage range possible by chance on any given day in the control run. The region was calculated using a binomial distribution about the daily probabilities with a confidence interval of 2σ . This is designed to represent the chance of randomly selecting 16 samples from the distribution given by the control simulation. If the ensemble prediction falls within this range then the forecast signal cannot be robustly determined, as the ensemble consensus cannot be separated from predictions expected by chance. If a prediction for an individual year falls outside this chance range, there is a signal, and more potential skill in those predictions.

The results in Figure 7.1 show that the most consistently difficult periods to predict are the opening and closing of the NSR, in August and November/December respectively. The control simulation indicates that average conditions peak in October with ~30% of years open. For predictions of the upcoming season, all start dates show a signal (defined by the ensemble consensus being outside of the 2σ chance region) for at least

some period in the season. This indicates that some level of potential predictability is available. This skill is higher for years when closed conditions are predicted, as the years 2180 and 2292 are never open for even a day in any of the 16 ensemble members. This enhanced skill for closed years is perhaps expected, as the mean chance of opening in the control simulation is only 30% maximum. There are four years (2202, 2230, 2304, and 2345) that show potential predictability that the NSR may become open.

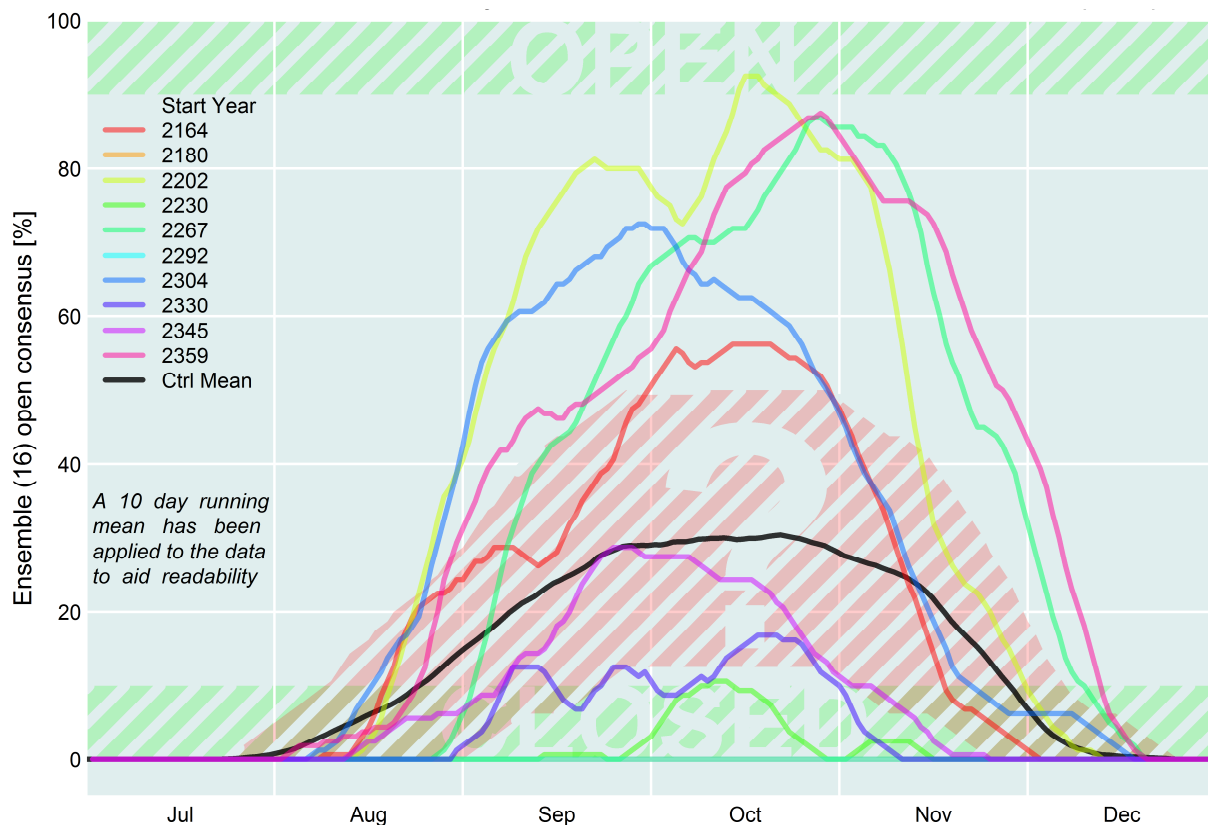


Figure 7.1 | Predictability from HadGEM1.2 initialised on July 1st for the opening of the Northern Sea Route (NSR) for Polar Class 6 (PC6) vessels for the current summer/autumn season. Each coloured line represents the ensemble consensus from the 16-member ensemble, 100% — all 16 members open, 0% — no members open. Each separate colour represents a separate start year in the control simulation (note absolute numerical value essentially arbitrary as control not transient simulation). The black line is the mean ‘openness’ from the 250 year control run, with the range by chance (2σ) represented by the red shading. The green shading schematically indicates regions of high confidence that NSR is open/closed. Note at 0% there is more than one start year.

The results indicate that the timing of the start of the shipping season may be harder to predict than the end for a July initialisation on the NSR. The reasoning for this is that more years are outside of the chance range at the end of the season than at the start.

This is potentially because the melt process governing the opening of sea routes is fundamentally different from the freezing processes governing the closing of sea routes. Generally, the opening of sea routes is expected to be difficult to predict due to the noise added to the initial conditions meaning each ensemble member will become open on slightly different days, as can be seen clearly by the progressive opening of 2345 (purple) in August. Despite the fact that for most years ensemble members first start to open in August there is no signal discernible from the chance distribution. There is slightly more of a signal apparent in the timing of the end of the season with some years closing outside of the range expected by chance.

7.3.2 1st July 3-year predictability

The first year results for the July 1st initialisation have been presented previously and show a marked improvement over predictions with a greater lead-time.

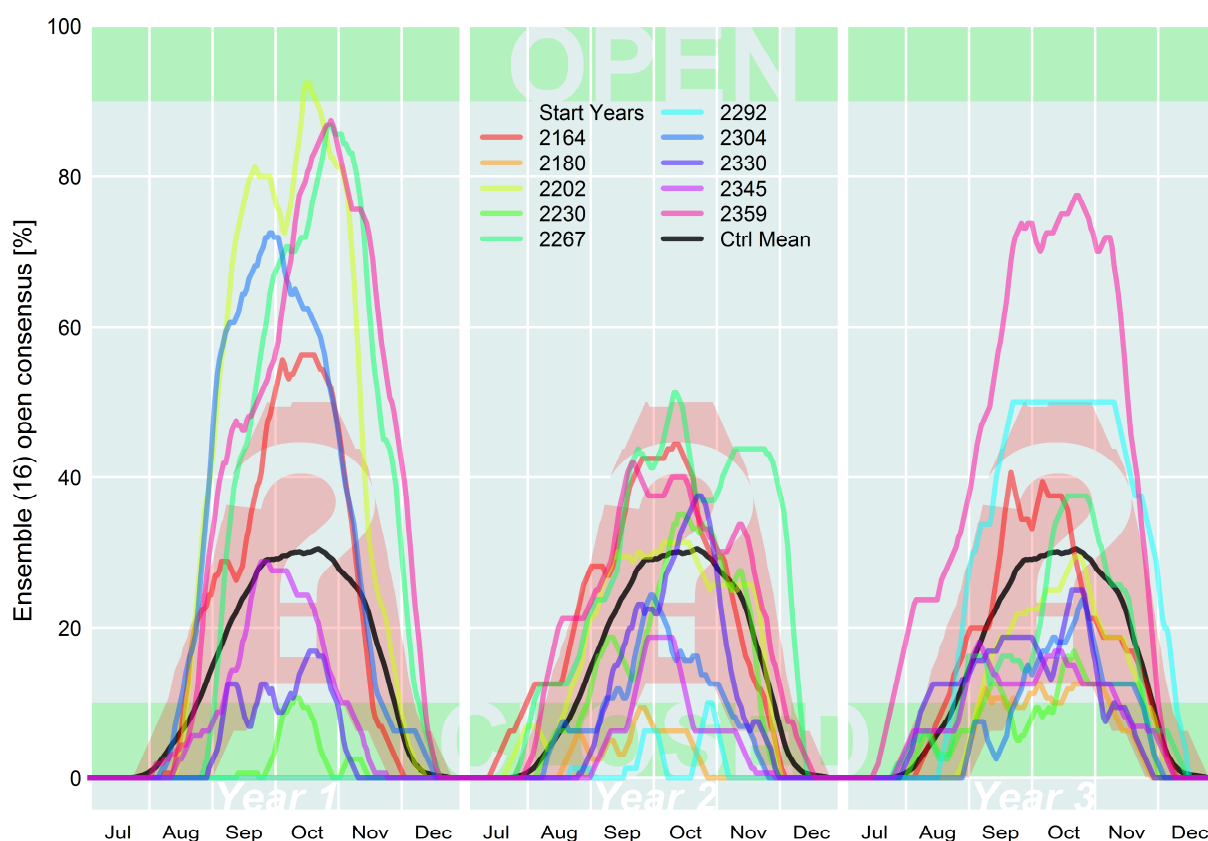


Figure 7.2 | Predictability for 3-years from HadGEM1.2 initialised on July 1st for the opening of the NSR for PC6 vessels. Details as Figure 7.1.

One might hope that some memory remains in the system so that some first year predictions might show repeated behaviour in the following years, although ensemble dispersion and hence a decline in skill is generally expected; one would not expect the

prospects for the second year to improve. Predictability for the second year shows a marked decline with no predictions of a navigable NSR remaining. However, two of the three years predicting a closed NSR remain closed although with a weakened signal. Predictability for the third year shows further reductions but with an interesting re-emergence of navigable conditions for 2359. This is equivalent to a closing of about 40%, or six ensemble members for the second year and then a reopening of these members in the third year. This does not mean that the third year is more predictable than the second year generally. Rather it suggests that the ice conditions are likely to be higher in the second year than the first and third year or merely by chance.

7.3.3 1st May 3-year predictability

The 1st May start date is included to target the May predictability barrier mentioned previously. The first year predictions show an improved signal for some years over that exhibited by the January initialisation Figure 7.3. Two years in particular are potentially skilful for the upcoming September and October as 2180 unanimously predicts closed conditions while about 80% of ensemble members in 2359 predict navigable conditions.

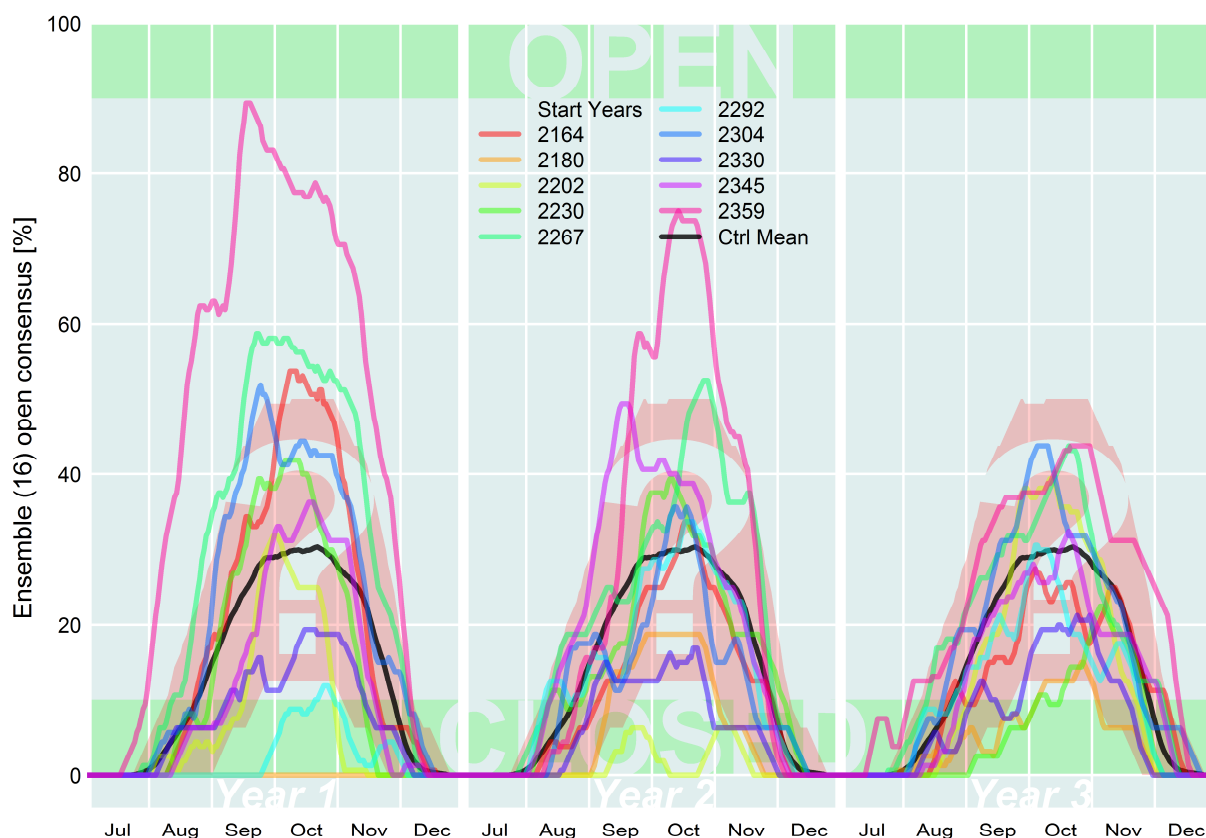


Figure 7.3 | Predictability for 3-years from HadGEM1.2 initialised on May 1st for the opening of the NSR for PC6 vessels. Details as Figure 7.1.

Predictability for the second year has decreased, although for 2359 a clear signal remains for a navigable October. However, the ensembles of the two most closed years (2180 and 2292) have both dispersed too much and are indistinguishable from climatological conditions. Interestingly an increase in signal is shown for 2202; it shows no signal for all but one month in the first year, but then displays a signal for 3 months in the second year. This increase is equivalent to one to four ensemble members that where open in the first year closing for the second year. This is plausible and illustrates that great care needs to be used when assigning any skill or confidence in predictability, as internal variability can affect interannual predictions. By the third year virtually no signal remains.

7.3.4 1st January 3-year predictability

A set of predictions were initialised on 1st January to examine if predictability is possible at longer lead times. There is virtually no signal for the 1st January predictions for the summer, with most years' ensemble predictions virtually indistinguishable from the control simulation distribution. This is even true for the initialisation years with high sea ice conditions, two of which (2180 and 2292) displayed 100% ensemble agreement that the NSR would be closed in the July initialisation for year 1. For the January initialisation, both years have at least one ensemble member open for the majority of the season. There is a weak signal for the 2359 low ice year, but due to the high background sea ice conditions in the control simulation the maximum consensus for 2359 is only about 60% implying low confidence. Likewise, there are some hints that some years are more likely to be closed e.g. 2180, but because of an intermittent increase in ensemble divergence, confidence in these predictions remains low.

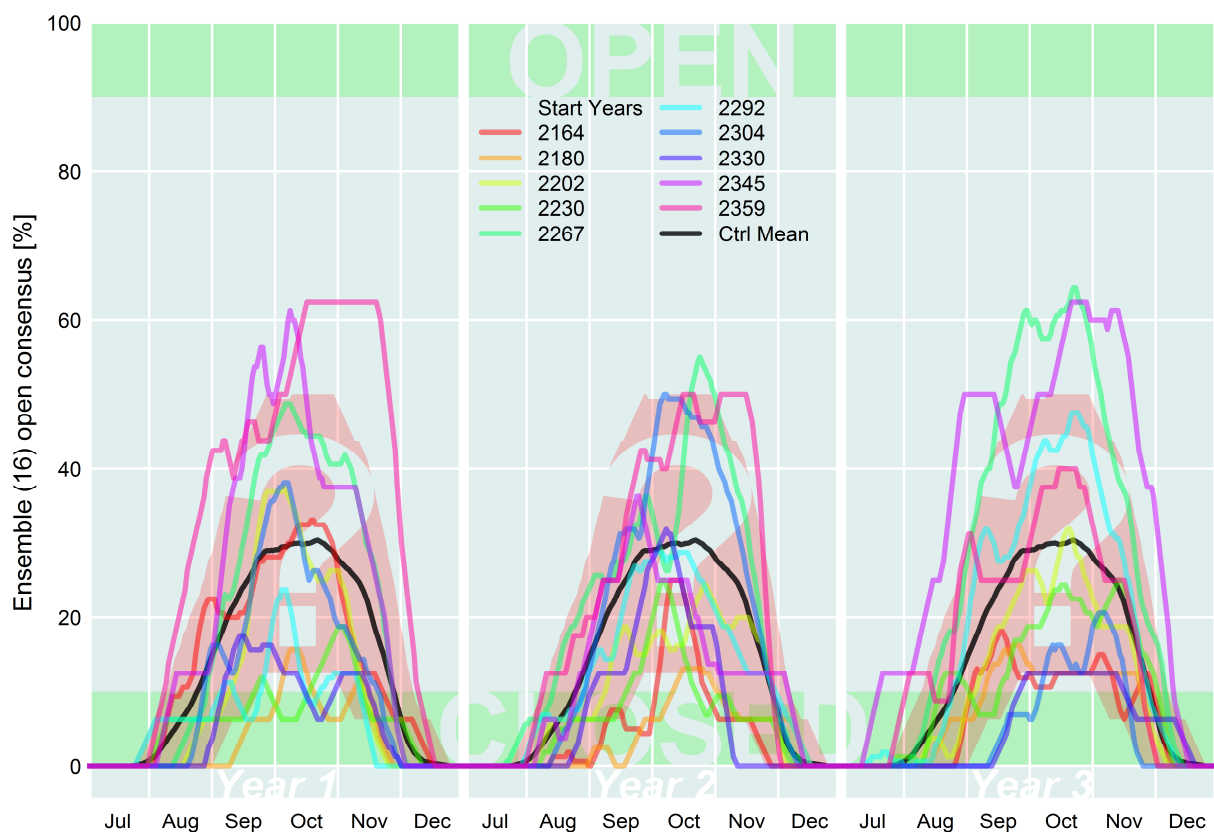


Figure 7.4 | Predictability for 3-years from HadGEM1.2 initialised on January 1st for the opening of the NSR for PC6 vessels. Details as Figure 7.1.

Indeed increasing ensemble divergence has led to even less signal being apparent, with the ensemble consensus hardly ever showing a signal beyond the range expected

coincidentally. The third year signal magnitude is essentially the same though perhaps with an increase in open consensus and a decrease in closed consensus. However, for a 2σ confidence interval there will still be $\sim 5\%$ signal of ensemble members or of years, by chance.

7.4 Lead time skill dependence

When predicting the following season, the ensemble consensus collapses towards climatology, with most skill remaining for those years with high levels of ice, and hence closed routes. It is encouraging to see that these high ice start years are also closed in the second year and hence there may be some available interannual memory in the system. By the third season, it is essentially impossible to decipher if the NSR is closed for the majority of start years.

A simple measure of potential predictability is to count the number of days that fall outside of the range expected by chance. Figure 7.5 shows the lead-time signal dependence for the opening of the NSR in HadGEM1.2. This measure reveals negligible potential predictability for forecasts initialised in January where year three actually has the largest signal.

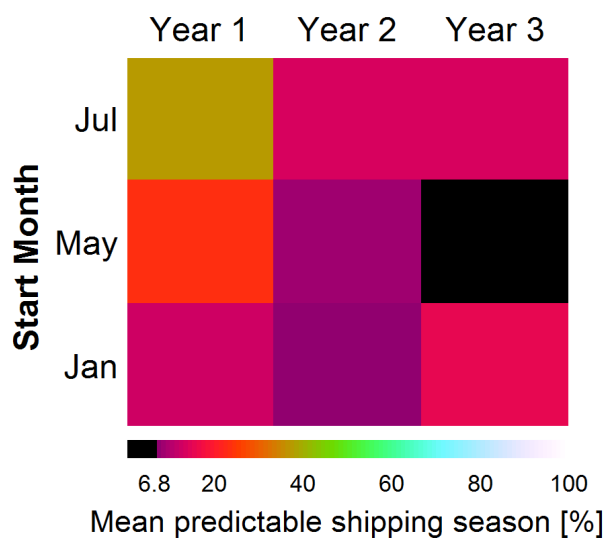


Figure 7.5 | HadGEM1.2 NSR opening for PC6 vessels start-date predictability dependence. Defined as the mean number of days outside the red region in Figure 7.2.

July has more predictability for the current season, and potentially some for future seasons. It should be noted however that this is the mean of the 10 start years and as shown in Figs. 7.1 – 7.2, and the skill for individual start years is highly state dependent, with more predictability for extreme high/low sea ice years. These initial results show that the May predictability barrier is also present when predicting the opening of sea routes. Potentially a June initialisation would provide much more skill, more similar to a July initialisation than May.

7.5 Conclusions and future work

The principal questions this chapter addressed are:

1. *How potentially skilful are GCMs as seasonal to interannual forecast tools for Arctic shipping?*

The results presented here show great promise for the use of GCMs to forecast the opening of the NSR and potentially all Arctic sea routes on seasonal to interannual timescales. Making reliable forecasts relies on the accurate simulation of the sea ice in the control simulation, specifically the sea ice mean, and variance. This also implies great scope for the application of the bias-correction methodology developed in Melia et al. (2015) discussed in Ch. 4. Initial results indicate that predictions in years with anomalously high and low sea ice show the most skill.

2. *How far in advance can predictions of Arctic sea route openings be made?*

Predictions that are initialised closer to the verification period show the strongest signal. Results from HadGEM1.2 strongly favour a July initialisation over January, with May initialisations also showing some potential. This is likely due to the reduced time for the ensemble to diverge. This indicates that there is a rapid increase in forecast skill during the melt season, before the onset of which little or no skill is apparent. This implies that there is sea ice information that becomes available during the melt season that the forecast uses which is obscured in the winter months. Potential predictability of the opening of the NSR exists for the current season, and although inter-annual forecasts may show some memory for specific case. Quantifying predictability at these longer lead-times is currently uncertain.

The major limitation with the methodology used here is that the detection of a signal, and the possibility of any skill, relies on the mean sea ice conditions in the control simulation. To illustrate this problem, imagine if the mean sea ice in the control simulation was lower so that the NSR was reliably open every year for a few months. Many of the ensemble predictions initialised would then also be open for these months but with the current metric one would not be able to ascertain if these predictions were robust, despite the 100% ensemble agreement. A similar problem would occur if the variance in the control simulation were higher, this would increase the range expected

by chance; this implies that a signal (as defined by the current metric) would be a far less common occurrence.

Even if the real world sea ice had the same characteristics as the HadGEM1.2 control simulation, there remains a limitation with the signal metric. The opening of a sea route in a particular year may contain a similar ensemble consensus as the climatology. The current skill metric will dismiss such years as not predictable. Operationally this is not too much of a problem, as a shipping company will assume that the opening date and season length is around the climatological mean unless a forecast contains enough skill to state otherwise. In this case, any robust forecast could only be for an anomalously open or closed season as these are the predictions that have the highest confidence and skill associated with them. Currently it is these high impact scenarios that contain the most predictive skill, a pleasing configuration. Despite this, from a theoretical perspective, more consideration is required to develop a more robust metric to measure the skill in seasonal to interannual predictions of Arctic sea route openings.

Another limitation with the current methodology is that the radiative forcing used is at 1990 levels. This results in the only route that reliably opens in HadGEM1.2 being the NSR for a PC6 vessel. In order to compare the effect of the different Arctic sea routes and ship classes, a future period control run would be needed. A relatively computationally efficient compromise would be to correct the data to sea ice levels projected in a future climate. This could be easily accomplished using the bias-correction methodology developed in Ch.4. Here the mean sea ice conditions for current and future periods can be used, from a combination of observations and bias-corrected GCM simulations.

The work presented in this chapter is ongoing, the methodology is planned to be extended to other GCMs. The APPOSITE calibration with other modelling centres means that GCM data from the predictability experiments exist for the:

- Canadian Centre for Climate Modelling and Analysis (CanCM4)
- ECHAM6-FESOM, run and developed by the Alfred Wegener Institute.
- EC-Earth consortium (EC-Earth2.3)
- Geophysical Fluid Dynamics Laboratory (GFDLCM3)
- Model for Interdisciplinary Research on Climate (MIROC5-2)

- Max-Planck-Institut for Meteorologie (MPI-ESM)

The multimodel data is available to download at the British Atmospheric Data Centre (Natural Environment Research Council (NERC) et al., 2015).

It is expected that due to the diligent design of the APPOSITE experiments, robust conclusions can be made about the effect of different GCMs on the predictability of the opening of the Arctic sea routes. It is hoped that this will improve understanding of seasonal to interannual predictions of Arctic sea route openings, a field that is likely to become increasingly important in the future.

References

- Bauer, P. and Jung, T.: Editorial for the Quarterly Journal's special issue on Polar Prediction, *Q. J. R. Meteorolog. Soc.*, 142, 537-538, doi: 10.1002/qj.2639, 2016.
- Blanchard-Wrigglesworth, E., Bitz, C. M., and Holland, M. M.: Influence of initial conditions and climate forcing on predicting Arctic sea ice, *Geophys. Res. Lett.*, 38, L18503, doi: 10.1029/2011gl048807, 2011.
- Chevallier, M., Salas y Mélia, D., Voltaire, A., Déqué, M., and Garric, G.: Seasonal Forecasts of the Pan-Arctic Sea Ice Extent Using a GCM-Based Seasonal Prediction System, *J. Clim.*, 26, 6092-6104, doi: 10.1175/jcli-d-12-00612.1, 2013.
- Collins, M., Frame, D., Sinha, B., and Wilson, C.: How far ahead could we predict El Niño?, *Geophys. Res. Lett.*, 29, 2002.
- Day, J. J., Hawkins, E., and Tietsche, S.: Will Arctic sea ice thickness initialization improve seasonal forecast skill?, *Geophys. Res. Lett.*, 41, 7566-7575, doi: 10.1002/2014gl061694, 2014a.
- Day, J. J., Tietsche, S., Collins, M., Goessling, H. F., Guemas, V., Guillory, A., Hurlin, W. J., Ishii, M., Keeley, S. P. E., Matei, D., Msadek, R., Sigmund, M., Tatebe, H., and Hawkins, E.: The Arctic Predictability and Prediction on Seasonal-to-Interannual TimeScales (APPOSITE) data set, *Geosci. Model Dev. Discuss.*, 2015, 8809-8833, doi: 10.5194/gmdd-8-8809-2015, 2015.
- Day, J. J., Tietsche, S., and Hawkins, E.: Pan-Arctic and Regional Sea Ice Predictability: Initialization Month Dependence, *J. Clim.*, doi: 10.1175/jcli-d-13-00614.1, 2014b.
- Eade, R., Smith, D., Scaife, A., Wallace, E., Dunstone, N., Hermanson, L., and Robinson, N.: Do seasonal-to-decadal climate predictions underestimate the predictability of the real world?, *Geophys. Res. Lett.*, 41, 5620-5628, doi: 10.1002/2014gl061146, 2014.
- Eicken, H.: Ocean science: Arctic sea ice needs better forecasts, *Nature*, 497, 431-433, doi: 10.1038/497431a, 2013.
- Griffies, M. S. and Bryan, K.: A predictability study of simulated North Atlantic multidecadal variability, *Clim. Dyn.*, 13, 459-487, doi: 10.1007/s003820050177, 1997.
- Guemas, V., Blanchard-Wrigglesworth, E., Chevallier, M., Day, J. J., Déqué, M., Doblas-Reyes, F. J., Fučkar, N. S., Germe, A., Hawkins, E., Keeley, S., Koenigk, T., Salas y Mélia, D., and Tietsche, S.: A review on Arctic sea-ice predictability and prediction on seasonal to decadal time-scales, *Q. J. R. Meteorolog. Soc.*, 142, 546-561, doi: 10.1002/qj.2401, 2014.
- Hawkins, E., Tietsche, S., Day, J. J., Melia, N., Haines, K., and Keeley, S.: Aspects of designing and evaluating seasonal-to-interannual Arctic sea-ice prediction systems, *Q. J. R. Meteorolog. Soc.*, doi: 10.1002/qj.2643, 2015.
- Holland, M. M., Bailey, D. A., and Vavrus, S.: Inherent sea ice predictability in the rapidly changing Arctic environment of the Community Climate System Model, version 3, *Clim. Dyn.*, 36, 1239-1253, doi: 10.1007/s00382-010-0792-4, 2010.

Johns, T. C., Durman, C. F., Banks, H. T., Roberts, M. J., McLaren, A. J., Ridley, J. K., Senior, C. A., Williams, K. D., Jones, A., Rickard, G. J., Cusack, S., Ingram, W. J., Crucifix, M., Sexton, D. M. H., Joshi, M. M., Dong, B. W., Spencer, H., Hill, R. S. R., Gregory, J. M., Keen, A. B., Pardaens, A. K., Lowe, J. A., Bodas-Salcedo, A., Stark, S., and Searl, Y.: The New Hadley Centre Climate Model (HadGEM1): Evaluation of Coupled Simulations, *J. Clim.*, 19, 1327-1353, doi: 10.1175/jcli3712.1, 2006.

MacLachlan, C., Arribas, A., Peterson, K. A., Maidens, A., Fereday, D., Scaife, A. A., Gordon, M., Vellinga, M., Williams, A., Comer, R. E., Camp, J., Xavier, P., and Madec, G.: Global Seasonal forecast system version 5 (GloSea5): a high-resolution seasonal forecast system, *Q. J. R. Meteorol. Soc.*, 141, 1072-1084, doi: 10.1002/qj.2396, 2015.

Massonnet, F., Fichet, T., and Goosse, H.: Prospects for improved seasonal Arctic sea ice predictions from multivariate data assimilation, *Ocean Modell.*, 88, 16-25, doi: <http://dx.doi.org/10.1016/j.ocemod.2014.12.013>, 2015.

Melia, N., Haines, K., and Hawkins, E.: Improved Arctic sea ice thickness projections using bias-corrected CMIP5 simulations, *Cryosphere*, 9, 2237-2251, doi: 10.5194/tc-9-2237-2015, 2015.

Merryfield, W. J., Lee, W. S., Wang, W., Chen, M., and Kumar, A.: Multi-system seasonal predictions of Arctic sea ice, *Geophys. Res. Lett.*, doi: 10.1002/grl.50317, 2013.

Msadek, R., Vecchi, G. A., Winton, M., and Gudgel, R. G.: Importance of initial conditions in seasonal predictions of Arctic sea ice extent, *Geophys. Res. Lett.*, 41, 5208-5215, doi: 10.1002/2014gl060799, 2014.

Natural Environment Research Council (NERC), Day, J. J., Hawkins, E., and Tietsche, S.: Collection of Multi-model Data from the Arctic Predictability and Prediction On Seasonal-to-Interannual Time-scales (APPOSITE) Project., NCAS British Atmospheric Data Centre, doi: 10.5285/45814db8-56cd-44f2-b3a4-92e41eaaff3f, 2015.

Northern Sea Route Information Office: How to Get a Permit, 2016, http://www.arctic-lio.com/nsr_howtogetpermit.

Pohlmann, H., Botzet, M., Latif, M., Roesch, A., Wild, M., and Tschuck, P.: Estimating the decadal predictability of a coupled AOGCM, *J. Clim.*, 17, 4463-4472, 2004.

Schröder, D., Feltham, D. L., Flocco, D., and Tsamados, M.: September Arctic sea-ice minimum predicted by spring melt-pond fraction, *Nature Clim. Change*, 4, 353-357, doi: 10.1038/nclimate2203, 2014.

Shaffrey, L. C., Stevens, I., Norton, W. A., Roberts, M. J., Vidale, P. L., Harle, J. D., Jrrar, A., Stevens, D. P., Woodage, M. J., Demory, M. E., Donners, J., Clark, D. B., Clayton, A., Cole, J. W., Wilson, S. S., Connolley, W. M., Davies, T. M., Iwi, A. M., Johns, T. C., King, J. C., New, A. L., Slingo, J. M., Slingo, A., Steenman-Clark, L., and Martin, G. M.: U.K. HiGEM: The New U.K. High-Resolution Global Environment Model—Model Description and Basic Evaluation, *J. Clim.*, 22, 1861-1896, doi: 10.1175/2008jcli2508.1, 2009.

Shi, W., Schaller, N., MacLeod, D., Palmer, T. N., and Weisheimer, A.: Impact of hindcast length on estimates of seasonal climate predictability, *Geophys. Res. Lett.*, 42, 1554-1559, doi: 10.1002/2014gl062829, 2015.

Sigmond, M., Fyfe, J. C., Flato, G. M., Kharin, V. V., and Merryfield, W. J.: Seasonal forecast skill of Arctic sea ice area in a dynamical forecast system, *Geophys. Res. Lett.*, 40, 529-534, doi: 10.1002/grl.50129, 2013.

Stroeve, J., Hamilton, L. C., Bitz, C. M., and Blanchard-Wrigglesworth, E.: Predicting September sea ice: Ensemble skill of the SEARCH Sea Ice Outlook 2008–2013, *Geophys. Res. Lett.*, 41, 2411-2418, doi: 10.1002/2014gl059388, 2014.

Wang, W., Chen, M., and Kumar, A.: Seasonal Prediction of Arctic Sea Ice Extent from a Coupled Dynamical Forecast System, *Mon. Weather Rev.*, 141, 1375-1394, doi: doi:10.1175/MWR-D-12-00057.1, 2013.

Chapter 8

Conclusions and future work

Satellite observations have revealed that the Arctic is undergoing rapid climate change. Projections from an international coalition of scientists using a suite of state of the art global climate models (GCMs) project this decline will continue through the 21st century. In recent years this reduction has opened up the once fabled Arctic sea routes, linking the Pacific and Atlantic Oceans. These new shipping routes across the top of the planet typically offer 40% distance reductions between East Asian and European ports compared to conventional routes via the Suez Canal. The projections of further reductions to Arctic sea ice and the increase in open Arctic water has led to speculation of increased use of these routes in the future.

This thesis aims to investigate the climatic potential for trans-Arctic shipping. Projections for Arctic shipping are needed to quantify when reliable transits may be possible under different greenhouse gas forcing scenarios, and to assess the uncertainties involved. Shipping in Arctic waters is a hazardous endeavour; with likely increases in shipping traffic in the future. Regional projections of shipping accessibility are important to assess the risks involved. Trans-continental shipping trade is a vital component of the global economy, savings in both transit time and monetary costs could have profound economic implications.

There have been many advances in quantifying the future of trans-Arctic shipping using climate models. However, all of these studies contain limitations to varying degrees, this thesis has addressed some of these limitations. The role of internal climate variability has often been overlooked. By using multiple ensemble members and explicitly analysing individual years, this thesis has quantified the uncertainty in projections of future shipping. Another common constraint on previous work arises from intrinsic biases in the sea ice that GCMs simulate. This thesis has produced a calibration technique to constrain these biases. Projections of Arctic shipping are made using these calibrated GCMs leading to more robust results.

The projections reveal that sea ice will be present during winter in the 21st century regardless of future greenhouse emission scenarios. This means that Arctic sea routes will continue to open and close annually. This, combined with increased shipping in the region highlights the need for improved seasonal predictions of conditions on the Arctic sea routes. Seasonal to interannual predictions of sea ice with GCMs show great promise to accurately predict Arctic sea ice. These predictions were explored with respect to sea route openings to examine how far in advance skilful predictions of the opening of Arctic sea routes can be made.

8.1 Summary of results

8.1.1 The Arctic early 20th century warming

In addition to the current warming period, a large-scale acceleration in Arctic temperatures occurred during the early part of the 20th century, as recorded by observations and literature from the era. This warming caused reductions in the Arctic sea ice that were observed by sailors and scientists at the time. Simulations from the Met Office earth system model, HadGEM2-ES, reproduce a large decline in sea ice around this period when the historical forcings are used. In Ch. 3, the possible cause of this decline in sea ice was investigated by using HadGEM2-ES to simulate the historical climate with individual forcing constituents isolated.

The individual forcing experiments revealed that both natural and anthropogenic greenhouse forcings were responsible for the decline 1915 – 1930, while changes to anthropogenic aerosols likely continued and maintained the anomaly during the 1930s and 1940s. However, the impact of all these forcings (natural, anthropogenic greenhouse gases, and aerosol) do not entirely account for the magnitude of the trend simulated when all these forcings are included together in the historical simulations. This implies that internal variability may have contributed.

The spatial signature of modelled ice loss indicates that separate forcings were responsible for distinct regional changes in the sea ice; it is likely that the complementary combination of these individual forcings resulted in the pattern of ice loss observed. The loss of sea ice in the central Arctic were predominantly caused by greenhouse gas forcings. Both greenhouse gas and natural forcing caused ice loss in the Canadian Archipelago. Ice loss in the Beaufort Sea was predominantly from Natural forcings. Forcings from anthropogenic aerosols accounted for ice loss in the Fram Strait and Russian Arctic seas. It is clear that future attribution work on the early 20th century warming should continue to use individual forcing simulations and focus on regional changes. For the effects of internal variability to be robustly quantified a larger ensemble than the four-member ensemble used here, is required. However data for the regional changes in the Arctic from the period are currently sparse, this highlights the importance of recovering observations from historical ships' logbooks (Brohan et al., 2009).

8.1.2 Improved Arctic sea ice thickness projections

Projections of Arctic sea ice thickness (SIT) have the potential to inform stakeholders about accessibility to the region, but are currently rather uncertain. The latest suite of CMIP5 GCMs produce a wide range of simulated SIT in the historical period (1979 – 2014) and exhibit various biases when compared with the Pan-Arctic Ice-Ocean Modelling and Assimilation System (PIOMAS) sea ice reanalysis. A new method to constrain such GCM simulations of SIT via a statistical bias correction technique called “MAVRIC” was published in Melia et al. (2015) and presented in Ch. 4.

The bias correction successfully constrains the spatial SIT distribution and temporal variability in the CMIP5 projections whilst retaining the climatic fluctuations from individual ensemble members. This was demonstrated in Figure 4.4 where the MAVRIC successfully corrects the SIT of CSIRO to known results from PIOMAS in a data denial experiment. The effect the MAVRIC is also illustrated spatially in Figure 4.6 where once calibrated the SIT fields of HadGEM2-ES and CSIRO are indistinguishable from PIOMAS.

The MAVRIC acts to reduce the spread in projections of SIT and reveals the significant contributions of climate internal variability in the first half of the century and of scenario uncertainty from mid-century onwards, as illustrated by Figure 4.9. The projected date of ice-free conditions in the Arctic under the RCP8.5 high emission scenario occurs in the 2050s (Figure 4.12), which is a decade earlier than without the bias correction and with significantly reduced ensemble spread. This bias correction methodology developed here could be similarly applied to other variables to reduce spread in climate projections more generally.

The development of this bias correction was a key calibration step required to allow the thesis goal of improved projections of Arctic shipping to proceed.

8.1.3 Faster 21st century shipping using trans-Arctic routes

With the MAVRIC of GCM sea ice cover now developed, the thesis proceeded in Ch.5 and Ch.6 to detail the shipping problem. Sea ice is the single biggest barrier to Arctic shipping, so reductions in sea ice thickness, and the increasing occurrence of open water, will reduce this primary hazard. The calibrated GCM sea ice projections are then utilised to quantify how faster Arctic shipping routes will become increasingly available in the 21st century.

By mid-century, for standard Open Water (OW) vessels, transit potential doubles with most years navigable irrespective of emissions scenario. The currently inaccessible Trans-polar Sea Route across the central Arctic also becomes accessible for the first time as illustrated by Figure 6.5. European routes to East Asia become 10 days faster on average than alternatives by mid-century and 13 days faster by late-century (Figure 6.6), while North American routes become 4 days faster (Figure 6.7). Future greenhouse-gas emissions play a significant role by late-century; the shipping season reaching 8 months in RCP8.5, double that of RCP2.6 (Figure 6.20), with substantial interannual variability (Figure 6.14). Moderately ice-strengthened vessels would enable fast and reliable trans-Arctic shipping, essentially year round, from mid-century (Figure 6.15).

Work from this chapter has been written into a paper draft which has been submitted for peer review.

8.1.4 Seasonal to interannual predictability of Arctic shipping routes

With the combination of increasing shipping activity and highly variable sea routes, the need for better sea ice forecasts and therefore the scope for seasonal predictions for the opening of Arctic sea routes, will become larger than ever. The potential predictability of the opening of Arctic sea routes was explored in Ch. 7 using a ‘perfect model’ experiment, whereby the divergence of an idealised GCM ensemble is analysed. The results from this type of study provide an upper bound for the usefulness of GCMs in this respect.

Initial results indicate that predictions in years with anomalously high and low sea ice show the most skill; predicting years with marginal conditions is more challenging. The simulations show that the opening and closing of the shipping routes are the hardest periods to predict. Predictions that are initialised closer to the forecast period show the strongest signal, which is expected as the ensembles will have dispersed less. However, there is evidence of a ‘predictability barrier’ around May, before which skill reduces dramatically as also noted by Day et al. (2014). There are currently a few known limitations with this study. The relatively high levels of sea ice in HadGEM1.2 restricts the opening of sea routes so that only the Northern Sea Route (NSR) along the Russian coast is open for an ice-strengthened Polar Class 6 (PC6) vessel, limiting intercomparison with alternative routes and vessel classes. These results do not make use of the bias correction methods developed earlier in this thesis, though this is planned as future work as discussed in Section 8.4.4.

The study would also benefit from analysing additional GCM simulations and developing an additional method for detecting a signal from the forecasts to aid the quantification of skill in the predictions. Despite this planned future work, the results presented in Ch. 7 show great promise for the use of GCMs to forecast the opening of the Arctic sea routes on seasonal to interannual timescales.

8.2 Conclusions

The principal questions this thesis addressed are:

1. *When will the Arctic display seasonally ice-free conditions?*

Using a sea ice volume metric and the ice-free criterion described in Ch. 4, calibrated GCMs with the high emissions (RCP8.5) scenario, project September ice-free conditions in the Arctic occurring in the 2050s, up to 10 years earlier than without the calibration, and with a considerably narrower range, e.g. excluding post-2085 dates. Under the medium emissions (RCP4.5) scenario, ice-free conditions are likely delayed to the end of the century, the low emissions (RCP2.6) scenario most likely avoids consistent September ice-free conditions altogether.

2. *When will reliable trans-Arctic shipping be possible?*

Observations show that trans-Arctic shipping is already possible along the NSR, often using a combination of ice-strengthened vessels in convoy with Russian icebreakers. Projections from GCMs show that accessibility will improve for all vessel classes through the 21st century.

For OW vessels, shipping is confined mainly to summer/autumn months and is projected to extend into the winter for an RCP8.5 type scenario. Mid-century is identified as a transitional period for trans-Arctic OW shipping, with accessible years increasing to 40% over 15 years. For OW vessels, internal variability is likely to be a significant factor throughout the century. Future emission scenarios play a pivotal role by late century with a reliable season of September – October in RCP2.6, August – November in RCP4.5, and July – December in RCP8.5.

For the ice strengthened PC6 vessels, transit potential is considerably higher with summer/autumn trans-Arctic voyages possible throughout the 21st century. The PC6

shipping season is projected to extend to include the winter months by mid-century, and include spring to become year round from mid-century in RCP8.5.

3. *How far in advance can predictions of Arctic sea route openings be made?*

Predictions that are initialised closer to the verification period show the strongest signal. Results from HadGEM1.2 strongly favour a July initialisation over January, with May initialisations also showing some potential. This is likely due to the reduced time for the ensemble to diverge. This indicates that there is a rapid increase in forecast skill during the melt season, before the onset of which little or no skill is apparent. This implies that there is sea ice information that becomes available during the melt season that the forecast uses which is not available in the winter months. Potential predictability of the opening of the NSR exists for a single season, and although interannual forecasts may show some memory for specific cases, quantifying predictability at these longer lead-times is currently challenging.

8.3 Will Arctic routes replace conventional routes?

The most common question I am asked in respect to this thesis topic is: “when will Arctic routes be open”? As illustrated by this thesis, the answer very much depends on how you define open. For example, the early 20th century warm period showed an open NSR and traffic peaked during the Cold War.

A linked question, which is sometimes assumed to be the same by non-specialists, is “will Arctic routes replace conventional routes, such as the Suez Canal”? The answers to this question depend primarily on non-climatic factors. Respected experts in the field of Arctic shipping answer a resounding “No!” to this speculation. In the near term this is very likely correct for a number of reasons. Container shipping from East Asia to Europe via the Suez Canal relies on strict schedules and part of the business model relies on calling into ports en route to exchange cargo. The current shipping season through the Arctic is too short and interannual variability too high to be advantageous for this type of shipping. The physical risks are also far greater, with the prevalence of damaging ice never too far from the shipping lanes. Currently, Arctic routes contain few ports that would be able to accommodate vessels in need of repair and the location of search and rescue sites means that help is often far away. The current cost of fees on the NSR is prohibitive to most business models, although as revealed earlier these are somewhat negotiable. In the near future, the current model of shipping via the Suez Canal is tried

and tested and any change in behaviour of the shipping companies would likely require substantial enticements.

For significant traffic on Arctic routes to develop there would likely require a number of factors to align. For some cargos, the dominant economic factor is the price of bunker fuel, as was shown this year (2016) when the price dropped so far that some ships shunned the Suez Canal route (and the transit costs associated with the Canal) and voyaged via the Cape of Good Hope. The price of bunker fuel would need to increase so that the fuel savings from Arctic routes became more significant. Because of the presence of winter ice throughout the 21st century, shipping companies would have to adjust to a dual route model, whereby Arctic routes are used when possible and traditional routes used when not. Alternatively, investments in ice class cargo ships like the PC6, would potentially enable year round trans-Arctic shipping. Newly innovated dual acting ships would make a wise investment for reliable trans-Arctic shipping. These ships have a traditional open water bow at one end and an ice-strengthened bow at the other, and their propulsion can be rotated 180° to allow navigation in both ice covered and open waters without the design limitations of single purpose ships. A renewing of the icebreaker fleet to maintain the routes and ports would also be required in the short to medium term when high ice years will be more frequent. Search and rescue sites and coverage must also improve in addition to extra ports with improved infrastructure.

Although there are many changes needed to accommodate a substantial increase in shipping, the increase in a niche shipping market using Arctic routes is plausible. This market would likely be shipping bulk cargos, which have far more flexible schedules than container shipping. This type of cargo shipping is already active on Arctic routes, transporting natural resources out of Arctic regions; it is this destination shipping that is likely to see the largest changes in the near term. This shipping sector is likely to increase in the future due to the increasing number and size of natural resource extraction projects, combined with permafrost melt making Arctic roads increasingly hazardous. Although Arctic routes have climatic hazards, the routes via Suez are not without their problems, such as the recent increase in piracy in the region. The Suez region is also not the most geo-politically stable, and a future event similar to the Suez Crisis, which closed the Suez Canal from October 1956 until March 1957, is not out of the question. If this were to happen again, shipping would be forced to use longer routes

via the Cape of Good Hope and Panama Canal; if conditions permit, would the far shorter Arctic routes see an increase in traffic too?

Notwithstanding these non-climatic factors, there are robust climatic changes, which would increase the potential use of Arctic shipping routes. By late-century, the opportunities for Open Water vessels are dependent on the magnitude of future anthropogenic emissions. If emissions continue to increase in a RCP8.5 style scenario then global shipping could realistically utilise Arctic routes and, with some adjustments to procedures, take advantage of the substantial distance saving they afford. If emissions are drastically reduced in a RCP2.6 style scenario, as is the wish of United Nations Paris targets, then Arctic shipping will increase but likely remain a niche, mostly destination shipping market.

The results from this thesis indicate that Arctic routes will not replace conventional routes for the majority of the 21st century. However, for some future climatic and economic scenarios they certainly can provide a useful supplement to the traditional canal routes. The projections in this thesis reveal that Arctic sea ice will be present in winter for the entire 21st century. This means that Arctic shipping routes will open and close annually. This enhances the need for further research in the field of seasonal Arctic climate predictions.

8.4 Potential for future work

8.4.1 The Arctic early 20th century warming

Although past studies and the analysis of simulations presented in this thesis have attempted to attribute the cause of the Arctic early 20th century warming, the conclusions are mixed and the period remains a bit of a mystery for climate science.

It is evident that GCM experiments, particularly individual forcing simulations, are the best tool to attribute the warming period. There are extra simulations that could be utilised which were not available for HadGEM2-ES including: (i) an ‘aerosol forcing only’ simulation, where only anthropogenic aerosols forcings vary, rather than being kept constant as in the HadGEM2-ES experiment used in Ch. 3; (ii) a ‘volcanic forcing only’ experiment would be very useful as volcanic eruptions are one of the leading causal hypotheses, and their effect cannot be fully quantified using the current range of

experiments; (iii) a ‘solar forcing only’ experiment could also be investigated although changes in solar forcings are less likely to be a significant contributor.

The sensitivity and climatic response to each of these individual forcings will likely be model dependent to some degree. It is hence important to repeat the analysis of these simulations with multiple GCMs. It is also abundantly clear that the current ensemble size of four in HadGEM2-ES is too small for the role of internal variability to be robustly quantified over a transient 30-year period. Ideally, a larger ensemble would be simulated with historical forcings to quantify the plausible range of internal variability during this period. Other GCMs have been used to perform larger ensembles (e.g. CSIRO Mk3.6, CanESM2) and these could be examined further.

8.4.2 Improved Arctic sea ice thickness projections

The bias-correction method developed in chapter 4 successfully uses observations to constrain the sea ice thickness produced by GCMs. The application of the technique will work on a broad range of other climate variables (e.g. snow depth and soil moisture content) and hence has a wide potential use for impact-based climate change studies that use GCMs.

By using the PIOMAS sea ice reanalysis to represent observations the MAVRIC technique successfully bias corrects the GCM simulated SIT to the SIT reanalysis of PIOMAS. The calibrated GCM projections, constrained with PIOMAS, will replicate the same biases of the PIOMAS reanalysis. To address this intrinsic limitations of PIOMAS the MAVRIC could be additionally performed using alternative realisations of PIOMAS, if these were able to be obtained. The MAVRIC could also be calibrated with satellite based SIT products, though these are not without their own inconsistencies and have limited spatial and temporal coverage.

There are some potential modifications, which would refine the technique. Developing and implementing a trend correction would further narrow the range of future projections. This was not attempted, as it is not clear how to accomplish this robustly. The rationale to keep the trend as prescribed by the different GCMs is because the response of the SIT to future warming is unknown, likely non-linear, and the GCMs are designed to give an estimate of this. It is also doubtful how well the current forced trend can be determined from 36 years of data given the high noise to signal ratio for trends, especially on grid point scales. It is also uncertain how much of the recent ice loss seen in the observations can be attributed to changes in external forcing as opposed to

internal variability. Great thought would need to be given on how to implement a trend correction so that the resulting projections are not too constrained due to overfitting.

The bias-correction technique substantially benefitted from the inclusion of a variance correction. This could have been taken further through the correction of some higher order moments; though with only 36 years of data it is questionable whether these higher order moments could be robustly quantified. This may improve the simulations at grid points in close proximity to land where variations in sea ice can be highly non-linear.

Sea ice thickness and sea ice concentration are two related variables. A multivariate bias-correction technique like Vrac and Friederichs (2014) could be developed that corrects the biases in both of these variables simultaneously by using co-varying information from both in observations.

8.4.3 Faster 21st century shipping using trans-Arctic routes

The obvious next steps for the shipping projections in Ch. 6 would be to include data from the refined bias-correction technique mentioned previously. The analysis should also repeat the study using CMIP6 GCMs, which will contain extra emission scenarios to fill the gaps between some of the RCPs (Meehl et al., 2014; O'Neill et al., 2015) and presumably more GCMs will have the required spatial resolution in the Canadian Archipelago region. The age of sea ice is an important variable for shipping. It was not assessed here as it was not a standard CMIP5 output variable, however it is a requested monthly variable for CMIP6.

In the meantime, further work could be carried out to explore the role of internal variability in projections of shipping accessibility. Here 15 ensemble members are assessed, three each from the five GCMs. However, the results are still somewhat model dependent. This study could be repeated with a large ensemble from a single GCM, such as the CESM-LE 30-member ensemble (Kay et al., 2015).

Sea ice varies on scales far smaller than the current grid scale of the CMIP5 GCMs; the use of high-resolution models should improve the realism of these simulations. Aksenov et al. (2015) use a high resolution eddy-permitting ocean model and suggest that variables additional to sea ice such as wind speed, wave height and ocean currents should also be assessed. Their study is a valuable addition to the literature and, with

the inclusion of appropriate bias-correction, would give an exciting insight into the future direction of research in this field.

8.4.4 Seasonal to interannual predictability of Arctic shipping routes

Chapter 7 on seasonal to interannual predictability of Arctic shipping routes is the subject of an ongoing research project. The details of future work for this topic are discussed in depth in Ch. 7 and so are only briefly repeated here. The immediate future direction for this topic is to repeat the analysis conducted with HadGEM1.2 for the six additional GCMs listed previously. An additional skill metric should be developed, as the current method for assigning skill to predictions has some limitations.

The bias correction technique should also be utilised here also to constrain the GCMs, as it is hoped that the predictability of all Arctic sea routes can be quantified. It will be fascinating to see what differences in predictability remain once the GCMs have been calibrated, and these results could lead to increased knowledge about the role that initialised GCMs could have in making sea ice predictions. The bias correction technique could also be used to calibrate the present day control run to some future climate, as simulated by GCM projections. This would enable the inherent changes in seasonal predictability into the future to be explored.

The current methodology for Ch. 7 to assess if a route is open uses the ‘fixed route algorithm’ outlined in Ch. 6. The ‘fastest route finding algorithm’ should also be tested, although a large difference should not be expected as results from the fixed route algorithm have been verified in Ch. 6.

The approach used here to test the ‘perfect model’ results could easily be used to test operational prediction systems such as the Met Office’s GloSea5. Here a hindcast set could be used where past forecasts can be verified against known results from observations. The hindcast testing of operational prediction systems will be a necessary step in quantifying the skill of seasonal forecasts of the opening of Arctic sea routes for the real world.

8.4.5 Summary

The experiments and results from this thesis have many implications for future work. The common factor throughout all the topics that this thesis covers is the crucial role of internal climate variability in climate predictions and climate change simulations. However, to robustly quantify the significance of internal variability in all these topics,

and many others beyond this thesis, requires larger ensembles. There is no correct answer to how many ensemble members are needed, though it is likely that some applications, like seasonal to inter-annual prediction, will need more than others, such as long term climate projections. It is hoped that the combination of improved understanding of the importance of internal climate variability, and increased computational resources, will motivate future simulations and predictions with GCMs to appropriately prioritise a larger number of ensemble members.

References

- Aksenov, Y., Popova, E. E., Yool, A., Nurser, A. J. G., Williams, T. D., Bertino, L., and Bergh, J.: On the future navigability of Arctic sea routes: High-resolution projections of the Arctic Ocean and sea ice, *Mar. Policy*, doi: <http://dx.doi.org/10.1016/j.marpol.2015.12.027>, 2015.
- Brohan, P., Allan, R., Freeman, J. E., Waple, A. M., Wheeler, D., Wilkinson, C., and Woodruff, S.: Marine Observations of Old Weather, *Bull. Am. Meteorol. Soc.*, 90, 219-230, doi: [doi:10.1175/2008BAMS2522.1](https://doi.org/10.1175/2008BAMS2522.1), 2009.
- Day, J. J., Tietsche, S., and Hawkins, E.: Pan-Arctic and Regional Sea Ice Predictability: Initialization Month Dependence, *J. Clim.*, doi: [10.1175/jcli-d-13-00614.1](https://doi.org/10.1175/jcli-d-13-00614.1), 2014.
- Kay, J., Deser, C., Phillips, A., Mai, A., Hannay, C., Strand, G., Arblaster, J., Bates, S., Danabasoglu, G., and Edwards, J.: The Community Earth System Model (CESM) large ensemble project: A community resource for studying climate change in the presence of internal climate variability, *Bull. Am. Meteorol. Soc.*, 96, 1333-1349, 2015.
- Meehl, G. A., Moss, R., Taylor, K. E., Eyring, V., Stouffer, R. J., Bony, S., and Stevens, B.: Climate model intercomparisons: preparing for the next phase, *Eos, Transactions American Geophysical Union*, 95, 77-78, 2014.
- Melia, N., Haines, K., and Hawkins, E.: Improved Arctic sea ice thickness projections using bias-corrected CMIP5 simulations, *Cryosphere*, 9, 2237-2251, doi: [10.5194/tc-9-2237-2015](https://doi.org/10.5194/tc-9-2237-2015), 2015.
- O'Neill, B., Tebaldi, C., and van Vuuren, D.: Scenario Model Intercomparison Project (ScenarioMIP) Application for CMIP6-Endorsed MIPs, 2015.
- Vrac, M. and Friederichs, P.: Multivariate—Intervariable, Spatial, and Temporal—Bias Correction, *J. Clim.*, 28, 218-237, doi: [10.1175/jcli-d-14-00059.1](https://doi.org/10.1175/jcli-d-14-00059.1), 2014.